Scaling in vehicle platoons

by

Ing. Ivo Herman

supervised by *Prof. Ing. Michael Šebek, DrSc.*,
co-supervised by *Ing. Zdeněk Hurák, Ph.D.*,

ČESKÉ
VYSOKÉ
UČENÍ
TECHNICKÉ
V PRAZE

Dissertation

Presented to the *Department of Control Engineering,*
Faculty of Electrical Engineering of
Czech Technical University in Prague
in Partial Fulfillment of the Requirements
for the Degree of

Doctor of Philosophy

in Ph.D. program
Electrical Engineering and Information Technology
in the branch of study
Control Engineering and Robotics

Czech Technical University in Prague,
May 2016

To Petra

Acknowledgements

Writing of this thesis would not have been possible if there were not great people around me. They were very inspiring for me both in academic and private life and I have much to learn from them.

I have spent wonderful four years at the Department of Control Engineering. I was lucky to have such advisors: prof. Michael Šebek and Zdeněk Hurák. They were always willing to help and give advices, but also gave me freedom to pursue research I liked. They also arranged for me everything to enable me fully concentrate on the research. I also appreciate that Martin Hromčík let me participate on an industrial project. Moreover, thanks to his sense of humor, the collaboration was more joy than hard work. I also thank to all my collaborators from abroad—prof. Peter Veerman, prof. Anders Ahlén and Dr. Steffi Knorn—for inspiring discussions and for all the work on the papers we submitted.

My deepest gratitude goes to my friend Dan Martinec for countless ideas we shared during the time of our Ph.D. studies. Working with Dan was a great pleasure for me and I am indebted to him for almost any achievement in this thesis. I am convinced that it was beneficial to both of us that we started our studies on a similar topic, which in the course of time evolved into two complementary directions. I have to mention Jirka Zemánek's inspiring creativity, which I always admired. I will never forget the fun we had with Pavel Otta and Štefan Knotek during our studies.

The greatest support I have received was from my girlfriend Petra. It was her love which made my studies such a great time. It was her who finally persuaded me to go to Prague for doctoral studies and she followed me here. At her side I enjoyed every day in Prague. Last but not least, I thank to my parents for their continuous care.

Declaration

This doctoral thesis is submitted in partial fulfillment of the requirements for the degree of doctor (Ph.D.). The work submitted in this dissertation is the result of my own investigation, except where otherwise stated. I declare that I worked out this thesis independently and I quoted all used sources of information in accord with Methodical instructions of CTU in Prague about ethical principles for writing academic thesis. Moreover I declare that it has not already been accepted for any degree and is also not being concurrently submitted for any other degree.

Czech Technical University in Prague
May 2016

Ivo Herman

Abstract

This thesis deals with analysis of scaling in autonomous vehicle platoons in which vehicles keep fixed distance to their neighbors. The vehicles are modelled as linear single-input single-output systems of arbitrary order. In order to control themselves, the vehicles use information from their nearest neighbors—their predecessor and successor. The states used for coupling are mainly position and velocity, but other states are allowed too. The errors to neighbors in these states can be weighted differently, hence the control law is asymmetric. Using the tools from distributed control, properties of platoons are analyzed. A comprehensive overview of the properties of platoons when identical asymmetry in all states is given. With the help of a newly derived product form of a transfer function in a network system, the steady-state gain, stability, string stability and particularly $\mathcal{H}_\infty$ norms are analyzed. The most important aspect specifying the scaling rate is the number of integrators in the open loop. For one integrator in the open loop the scaling of the $\mathcal{H}_\infty$ norm is quadratic for symmetric control and linear for asymmetric control. For two and more integrators the scaling is cubical for symmetric control and exponential for asymmetric. Since there is no good control for two integrators in the open loop with identical asymmetry, symmetric coupling in position and asymmetric in velocity is proposed. Such control is, at least for the cases analyzed in the thesis, superior to both completely symmetric and completely asymmetric control. It has similar convergence time as asymmetric control but it still keeps the bounded control effort as the symmetric control does.

Key words: vehicle platoons, distributed control, scaling, asymmetry, different asymmetries

Abstrakt

Tato práce se zabývá škálováním v distribuovaném řízení kolon vozidel. Vozidla jsou modelována jako lineární systémy libovolného řádu s jedním vstupem a jedním výstupem a mají za úkol držet konstantní vzdálenost ke svým sousedům. Vozidla pro své řízení využívají informace od svých nejbližších sousedů – od vozidla vepředu a vzadu. Nejčastěji jsou těmito informacemi poloha a rychlost sousedních vozidel, ale je možné použít i další stavy. Protože mohou být rozdíly v těchto stavech mezi sousedy váženy různě, řízení se nazývá asymetrické. Práce analyzuje asymetrické kolony vozidel pomocí nástrojů z teorie distribuovaného řízení a podává ucelený přehled vlastností těchto kolon. To platí hlavně pro situaci, kdy je asymetrie stejná pro všechny stavy. Na základě užitečné součinové formy pro libovolný přenos v koloně je odvozeno chování ustálených hodnot, stabilita, řetězová stabilita a zejména škálování $\mathcal{H}_\infty$ normy. Nejdůležitějším rozlišovacím znakem je počet integrátorů v otevřené smyčce vozidla. V případě, že má otevřená smyčka jen jeden integrátor, škálování $\mathcal{H}_\infty$ normy je kvadratické pro symetrické řízení a lineární pro asymetrické. Pro dva a více integrátorů se škálování zhorší na kubické pro symetrické řízení a exponenciální pro asymetrické. Jelikož není možné dosáhnout dobrého chování se dvěma integrátory s identickou asymetrií, je navrženo řízení se symetrickou vazbou v pozici a asymetrickou v rychlosti. Pro modely analyzované v této práci se chování takového řízení jeví jako kvalitativně nejlepší. Má podobný čas ustálení jako asymetrické řízení, ale zachovává si omezený akční zásah jako řízení symetrické.

Klíčová slova: kolony vozidel, distribuované řízení, škálování, asymetrie, rozdílné asymetrie

Goals of the thesis

The thesis is dedicated to investigation of properties of vehicle platoons which use local nearest-neighbor interactions. The goal is to concentrate on scenarios which have very limited requirements for communication, in particular asymmetric bidirectional control. The thesis has the following goals:

1. Study transfer functions in distributed control. The transfer functions might allow easy frequency-response analysis.
2. Analyse properties of asymmetric bidirectional control using the tools of distributed control theory.
3. Find conditions under which asymmetry/symmetry is beneficial and when not.
4. Derive scaling of the $\mathcal{H}_\infty$ norm as the number of vehicles in the platoon grows. Consider various transfer functions and general open-loop models.
5. Find conditions of string stability of platoons and requirements on the controller.
6. Investigate various asymmetries for different states and discuss its properties.

Notation

In general we denote matrices with capital letters and a particular element in a matrix A is denoted as a_{ij}. A^{T} stands for a transposition of a matrix.

All vectors are column vectors and are denoted with lowercase letters; the ith element of a vector v is v_i. Scalars are denoted by Greek letters. Identity matrix of size $n \times n$ is denoted as I_n (the subscript n is often omitted if the matrix size is clear from the context). The ith column in the identity matrix is the canonical-basis vector $\bar{e}_i = [0, \ldots, 1, \ldots, 0]^{\mathrm{T}}$ with 1 on the ith position. $\mathbf{1}$ is a vector of all ones. The symbol s used in transfer functions denotes the Laplace variable. Polynomials are denoted by lowercase letters and g_i is the coefficient at s^i in the polynomial $g(s)$ (the argument s is usually displayed for polynomials).

Often we will be interested in how some function depends asymptotically on N. We use the following symbols for asymptotic bounds.

- The function $f(N) = \mathcal{O}(g(N))$ if there exist $k > 0$ and $N_0 > 1$ such that $f(N) \leq k|g(N)|$ for all $N \geq N_0$.
- The function $f(N) = \Theta(g(N))$ if there exist $0 < k_1 < k_2$ and $N_0 > 1$ such that $k_1|g(N)| \leq f(N) \leq k_2|g(N)|$ for all $N \geq N_0$.
- The function $f(N) = \Omega(g(N))$ if there exist $k > 0$ and $N_0 > 1$ such that $f(N) \geq k|g(N)|$ for all $N \geq N_0$.

The meaning is the following (up to the constant factor): $\mathcal{O}$ states that $f(N)$ is bounded above by $g(N)$, Θ means that the function $f(N)$ is bounded above and below by $g(N)$ (it is of the same order) and Ω states that $f(N)$ is bounded below by $g(N)$.

Uppercase latin letters

A	state matrix or adjacency matrix, depending on the context
B	input matrix
C	output matrix
$\mathbb{C}$	set of complex numbers
D	feed-through matrix or generally a diagonal matrix, depending on the context
E	total measured transient error
$F_i(s)$	transfer function of the form $\frac{b(s)q(s)}{a(s)p(s)+\lambda_i b(s)q(s)}$. Appears after block diagonalization.
$\mathcal{F}_k^{i\to j}$	a set of spanning forests with k arcs. In this set there is a tree diverging from i and containing j
$G(s)$	transfer function of the vehicle or plant
$\mathcal{G}$	graph
I	identity matrix
$\Im\{a\}$	Imaginary part of a complex number a
K	state-feedback matrix
L	Laplacian matrix
$\bar{L}_{ij}$	reduced Laplacian where the rows and columns corresponding to the vertices on the path from i to j were removed
L_{p}	pinned Laplacian or Laplacian in which the row corresponding to the leader was removed
$\hat{L}$	Laplacian of a circular graph
L_y, L_v	Laplacians of a coupling in position and velocity
$M(s)$	open-loop transfer function of an individual agent
$M_{\mathrm{s}}(s)$	partial open-loop transfer function of an individual agent
N	number of agents
P	matrix solution of the Riccati equation in LQR control
Q	matrix weighting the state error in the Riccati equation
Q_k	matrix of diverging forests with k arcs
R	matrix weighting the control effort in LQR
$R(s)$	controller transfer function
$\mathbb{R}$	set of real numbers

$\Re\{a\}$	real part of a complex number a
$S_{ij}(s)$	a network part of the transfer function in the graph
$T(s)$	a transfer function, often a complementary sensitivity transfer function
$T_i(s)$	transfer function of a feedback system $T_i(s) = \frac{\lambda_i M(s)}{1+\lambda_i M(s)} = \frac{\lambda_i b(s) q(s)}{a(s)p(s)+\lambda_i b(s) q(s)}$
$T_{ij}(s)$	transfer function in the network system between the input of the controller of agent i and output of the agent j
$T_{\min}(s), T_{\max}(s)$	transfer function $T_i(s)$ where $\lambda_i = \lambda_{\min}$ and $\lambda_i = \lambda_{\max}$, respectively
$\mathbf{T}(s)$	transfer function matrix
V	matrix of eigenvectors of matrix L or L_{p}
$Z_{ij}(s)$	a biproper transfer function with a form $\frac{1+\gamma_i M(s)}{1+\lambda_j M(s)} = \frac{a(s)p(s)+\gamma_i b(s) q(s)}{a(s)p(s)+\lambda_i b(s) q(s)}$

List of lowercase letters

$a(s)$	denominator polynomial of the plant (vehicle)
$b(s)$	numerator polynomial of the plant (vehicle)
c	the index of the control node
d_{in}	disturbance acting at the input of the plant
d_{out}	disturbance acting at the output of the plant
e	input of the controller or the input to the open-loop model
$\bar{e}_i$	vector in a canonical basis $\bar{e} = [0, \ldots, 0, 1, 0, \ldots, 0]^T$ with 1 at ith position
$g(s)$	denominator polynomial in single-integrator dynamics
$h(s)$	numerator polynomial in single-integrator dynamics
$\jmath$	imaginary unit, $\jmath = \sqrt{-1}$
n	degree of the open-loop denominator, order of the open loop of the agent
o	the index of the output node
$p(s)$	denominator of the controller transfer function

$q(s)$	numerator of the controller transfer function
r	external signal for the regulation
s	Laplace variable
t	time
v	eigenvector of the matrix
v	velocity of a vehicle
w	general input of interest
x	state variable
$\tilde{x}$	local neighborhood error in states
y	position or the output used for coupling
$\tilde{y}$	local neighborhood error in outputs
z	output of interest
z	error in spacing in platoons

List of Greek uppercase letters

Δ_{ref}	reference distance
$\Theta(N)$	scaling of a given order
Λ	Jordan form of a matrix, usually of L or L_{p}

List of Greek lowercase letters

α	real part of the frequency response
β	imaginary part of the frequency response
γ	root of single-integrator numerator polynomial, eigenvalue of the reduced Laplacian $\bar{L}$
δ_{ij}	graph distance of the nodes i, j
ϵ	the level of asymmetry in proportional asymmetry = constant of bidirectionality
$\epsilon_{\max}$	the upper bound on the level of asymmetry
η	number of integrators in the open loop
θ	spatial frequency, frequency in the Fourier matrix

$\vartheta(\mathcal{F})$	weight of the set of spanning forests $\mathcal{F}$
$\vartheta(\mathcal{G}')$	weight of the subset $\mathcal{G}'$ of the graph $\mathcal{G}$
ϑ_{ij}	weight of the path in the graph between the nodes i and j
λ	eigenvalue of the Laplacian or pinned Laplacian
$\lambda_{\min}, \lambda_{\max}$	lower (upper) bound on eigenvalues of the Laplacian or pinned Laplacian
ν	eigenvalue of the overall network-control system
ρ	asymmetry when multiple Laplacians are used
σ	singular value
υ	order of the numerator of the open loop transfer function
χ	relative order of a transfer function
ψ_y, ψ_v	$\psi_y = 1 - 2\rho_y$, $\psi_v = 1 - 2\rho_v$
ω	angular frequency

Abbreviations

ACC	Adaptive cruise control
APAV	asymmetric coupling in position, asymmetric in velocity
APSV	asymmetric coupling in position, symmetric in velocity
CACC	Cooperative adaptive cruise control
CRHP	closed right-half plane
ORHP	open right-half plane
PF	predecessor following
SPSV	symmetric coupling in position, symmetric in velocity
SPAV	symmetric coupling in position, asymmetric in velocity
TF	transfer function
TFM	transfer function matrix

Contents

1 Introduction

It is well known that automatic cars are already driving in some countries. Although they are still in experimental use, there is no doubt that they will, sooner or later, replace human drivers on the roads. Now the autonomous car has to behave as if it was a human driver, e.g., it should keep the same safety distance from the car ahead as the human driver would do. However, when there will be more automatic cars on the road, all equipped with many sensors, a completely new driving behavior is achievable. Before we allow it, we first have to answer several questions. How should these cars interact? How should they react to the actions of nearby cars? What data the cars have to share among each other in order to guarantee safety and riding comfort?

Nowadays, dense traffic, especially around metropolitan areas, causes large traffic jams. So there is a great need to increase the road capacity. Commonly this is done by constructing new roads with more lanes. But there is a great promise with the advent of autonomous cars: the cars can travel together in chains with tight spacing. These chains are called *vehicle platoons*. Instead of driving with large safety distances between the cars required for human drivers, automatic control could (maybe?) allow very tight spacing, which would increase the capacity even qualitatively. In addition, the tight spacing also reduces a fuel consumption (this is achieved due to reduced drag coefficient). Hence, platooning is a very promising idea.

Although the automatic cars might appear in real-life traffic in far future, even the off-the-shelf driver assistance systems react to the state of the traffic and of the road. We have an emergency braking when an obstacle is detected, an adaptive cruise control is implemented not only in high-class vehicles and a lane-keeping assistant is also available. Imagine the following situation. A car equipped with the adaptive-cruise control and the emergency braking system is

travelling on a highway and the driver does not pay attention to the traffic. Suddenly, the car ahead of this car stops. How strong should the driver-assistance system brake? When should it brake? Is it even possible to avoid a crash? For one vehicle, this is probably guaranteed by the systems. But what happens when there are three such cars in a row? Is it still safe for the third one to rely on these systems? What if there are ten cars of this type?

All these examples should illustrate the following fact: it is not sufficient to design the control logic for a single car alone. It is the interaction among vehicles that must be taken into account. Then, the vehicles on the road become one large-scale dynamic system. The action of one car affects all the cars behind it and, possibly, also in front of it. In order to design a proper controller, the properties of this large dynamic system have to be analyzed and understood.

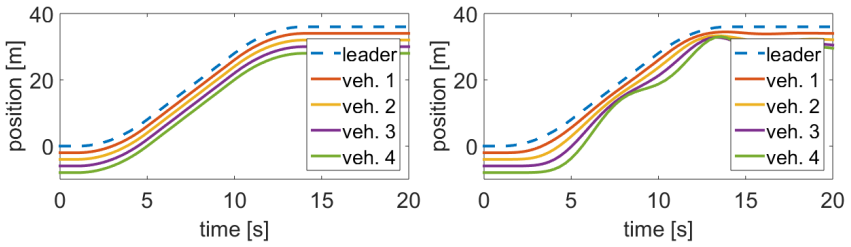

(a) Ideal response (b) Real response

Figure 1.1: Possible responses of a platoon.

The goal of platooning is that the whole platoon travels as one rigid body. An ideal response of a platoon is shown in Fig. 1.1a. All cars exactly copied the movement of the platoon leader (the vehicle in front of a platoon) and kept the safety distance from the car ahead. However, a “real" response of the simplest control algorithm is shown in Fig. 1.1b. This algorithm was designed to keep the desired distance (2m) to the car ahead—this strategy is called predecessor following. As can be seen, the cars crashed (the curves for positions of vehicles crossed each other). Note that the “real” response did not have any noise or other imperfections, the bad behavior results only from the dynamics of the cars. Roughly speaking, the cars were not able to accelerate and brake at the right time and with the right magnitude to keep the distance. The question now is: is this due to bad controller design or is there some limitation imposed by the dynamics of the cars? This thesis aims to answer this and similar questions.

The controller for each vehicle in a platoon should be designed to achieve the desired spacing of whole platoon as fast as possible but still having transient behavior convenient for the passengers. Since the platoons could be large, having a lot of vehicles, we are interested how the transient parameters change

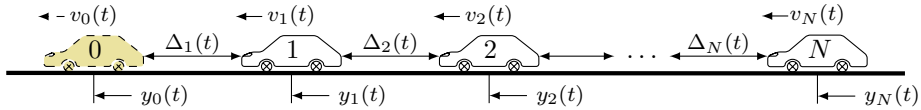

Figure 1.2: A schematic of the platoon. Index 0 corresponds to the leader, movement of which the platoon should track.

when more cars are added. Then, scalability becomes subject of investigation. A good scalability means that when more cars are added to the platoon, its performance (transient time, safety) is not deteriorated, or not that much. The scaling properties of the platoons will be the main topic of the thesis.

1.1 Thesis in a nutshell

In this section we will introduce the models and summarize the main results of the thesis. Note that the description here is just to get an overview of the content of the thesis, full details are given in the appropriate chapter of the thesis.

1.1.1 Platoon modelling

The platoon model is presented in its simplest form: as $N+1$ vehicles travelling in a line. The vehicles are indexed by $i, i = 0, 1, 2, \ldots, N$. The most important states of each vehicle are its position y_i, velocity v_i and distance to the predecessor $\Delta_i = y_{i-1} - y_i$. The vehicles should keep the distances equal to some reference distance Δ_{ref}, such that $\Delta_i \to \Delta_{\text{ref}}$ for all i. Assume also that there is a (virtual) independent leader travelling ahead of the platoon, having index 0. The leader serves as a reference for the platoon—the platoon should eventually travel with the speed of the leader. The platoon should also react to all changes of speed and position the leader. Such a platoon is depicted in Fig 1.2.

However, there might also be other states in the vehicle model. Those might be the vehicle's acceleration or additional states of the dynamic controller. The dynamic controller is designed to improve transient properties. Then, each vehicle is modelled as a linear, time invariant dynamic system of the nth order, given by its open-loop transfer function

$$M(s) = R(s)G(s) = \frac{b(s)q(s)}{a(s)p(s)}, \tag{1.1}$$

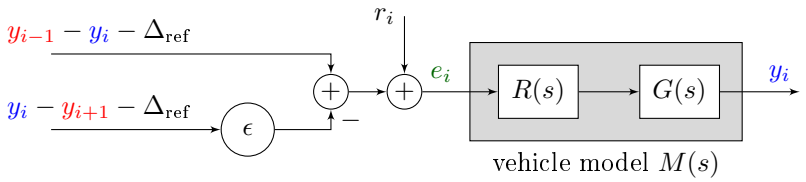

Figure 1.3: A schematic of the control loop. The model (1.1) is in grey rectangle, the control law e_i is from (1.2). In blue are the states of vehicle i, in red are the states of other vehicles, used for control.

where $R(s) = \frac{q(s)}{p(s)}$ and $G(s) = \frac{b(s)}{a(s)}$ are models of the controller and vehicle, respectively. Usually, the output is vehicle's position y_i and its derivative is velocity v_i. Such a model is shown in Fig. 1.3. The number η of poles of the transfer function $M(s)$ at the origin is called the *number of integrators in the open loop*. At least one integrator is necessary to allow the vehicles to travel with the leader's speed, hence $\eta \geq 1$.

Having the model, the goal of the designer is to design a controller for each vehicle. First, the set of states used for control has to be selected. It is definitely beneficial to decrease the communication burden by minimizing the global information needed. Thus, the cars use mainly the data measured by onboard sensors—the distances to the neighbors with indices $i-1$ and $i+1$. In the research, the following nearest-neighbor control law was used

$$e_i = \underbrace{(y_{i-1} - y_i - \Delta_{\text{ref}})}_{\text{front dist. err.}} - \epsilon \underbrace{(y_i - y_{i+1} - \Delta_{\text{ref}})}_{\text{rear dist. err.}} + r_i, \tag{1.2}$$

where r_i is an external input to the vehicle (for instance, a measurement noise). We call ϵ the *constant of bidirectionality* (or *constant of asymmetry*). ϵ weights the relative contribution of front spacing error $(y_{i-1} - y_i - \Delta_{\text{ref}})$ and rear spacing error $(y_i - y_{i+1} - \Delta_{\text{ref}})$. Note that due to dynamic controller, any derivative of the output y_i can be used for control. For example, relative velocity $v_{i-1} - v_i$ is also allowed.

The thesis is devoted to investigation of the scaling effects in platoons. That is, we quantify what happens with the performance when more vehicles are added to the platoon. The more vehicles in the platoon, the more effective the platooning is. Since the control theory allows to change the system order to almost any number by implementing a dynamic controller, the goal is to obtain a scaling characteristics which are independent of the model of individual vehicle. Similarly to computer science, which evaluates the complexity of algorithm as a function of the number of elements, here we derive the *scaling rules* as a function

of the *number of vehicles* N.

1.1.2 Proportional asymmetry

Since the vehicles use the measurements or estimations of their own states and the states of their neighbors, the suitable tools used for analysis are those of distributed control. Distributed-control theory has flourished in past years and we have many useful results both for analysis and controller design (see an overview in Chapter 2).

The majority of the results in this field rely on the fact that there is only one coupling rule for all derivatives of the output y_i: $y_i, v_i, \dot{v}_i, \ldots$. Here it means that ϵ is used for all states and we call it a proportional asymmetry. Then, a convenient block-diagonalization is possible and the network properties and vehicle model can be easily decoupled. There are three possible combinations:

- $\epsilon = 1$: this is called *symmetric bidirectional control*, as the vehicle pays the same attention to the front and rear spacing errors.
- $\epsilon = 0$: this is so called *predecessor following*—the vehicle only looks ahead. This is the strategy simplest to implement, since there is no need for backward sensors.
- $0 < \epsilon < 1$: this is so called *asymmetric bidirectional control*. The vehicle pays more attention to the front spacing errors. This should mimic a human driver, who also from time to time looks to the rear mirror, but watches more the situation ahead.

We used the $\mathcal{H}_\infty$ norm to measure the scaling. The $\mathcal{H}_\infty$ norm of a transfer function matrix $\mathbf{T}(s)$ is defined as

$$\|\mathbf{T}(s)\|_\infty = \sup_{\omega \in \mathbb{R}} \sigma_{\max}(\mathbf{T}(\jmath\omega)). \tag{1.3}$$

where $\sigma_{\max}(\cdot)$ is the maximal singular value. The $\mathcal{H}_\infty$ norm captures the worst-case amplification of the input signal. The greater the norm, the worse is the transient and the vehicles might crash. Hence, the norm should be as low as possible. In order to use this norm, it is necessary that the system is asymptotically stable, which is easy to achieve for proportional asymmetry.

For proportional asymmetry, a complete picture of scaling is obtained in this thesis. The scaling is summarized in Table 1.1. The table captures the scaling of the $\mathcal{H}_\infty$ norm of the whole platoon. The main distinguishing factor is the number of integrators η in the open loop. In order to track the leader and keep the desired spacing (fixed-distance policy), it is required that $\eta \geq 2$. If the leader's velocity measurement is available to each vehicle, it suffices to have

Control law	Number of integrators	
	$\eta = 1$	$\eta \geq 2$
Symmetric, $\epsilon = 1$	N^2	N^3
Asymmetric, $0 \leq \epsilon < 1$	N	c^N

Table 1.1: Scaling of the $\mathcal{H}_\infty$ norm for control law (1.2) with proportional asymmetry. The constant c is greater than one.

$\eta = 1$. The same holds when time-headway policy is used. As can be seen, the case with $\eta \geq 2$ has much worse scaling. The best scaling is achieved for asymmetric control with $\eta = 1$. On the other hand, when the leader's velocity is not available or fixed distance is used, the scaling for asymmetric control is the worst-possible—exponential in N. The response in this case would be catastrophic for large N. Symmetric control achieves polynomial scaling in both cases.

The most important fact is that the results hold for *arbitrary* vehicle model, hence the scaling presented is generic. The results emphasize the best achievable scaling given the communication topology. For instance, when $\eta = 2$ (required for tracking if fixed-distance is used and leader's velocity is not available), then there is *no linear controller* which would prevent exponential scaling with $0 \leq \epsilon < 1$. Thus, the table shows also inherent limitations of the platoon control. It can also be proved that with asymmetry, the transient time is much better than in symmetric bidirectional control. When there is one integrator, the response is good, while for two or more integrators the response might be very bad, so the cars might possibly crash.

For the controller design, a sufficient condition for systems with $\eta = 1$ to achieve linear scaling (asymmetric control) or quadratic (symmetric control), was obtained. The condition requires only single-vehicle model and the result holds for any N. Moreover, under some mild assumptions, we guarantee that it is possible to satisfy this condition and even the extreme case of asymmetric control—the predecessor following—can easily be used.

Proportional asymmetry is thoroughly analyzed in Chapter 4.

1.1.3 Different asymmetries for each state

From the discussion above it follows that there is no good fully distributed control when asymmetry in all states is identical. However, allowing different asymmetries for each state complicates the analysis a lot, since the matrices capturing the interconnection are not simultaneously diagonalizable. Then, overall platoon must be analyzed as one big system. That is why the results obtained are not general; they hold for one model only.

One of the first works in this field is our joint paper with prof. J.J.P. Veerman from Portland State University, USA. We considered a second-order vehicle model equipped with a PI controller, therefore the open loop was of the third order. Its model was

$$\dot{y}_i = v_i, \quad \dot{v}_i = c_i, \quad \dot{c}_i = -ac_i + e_i \tag{1.4}$$

with $a > 0$ and c_i being the controller state. The input to the controller is defined as

$$\begin{aligned} e_i = g_y \Big[(1-\rho_y) \underbrace{(y_{i-1} - y_i - \Delta_{\text{ref}})}_{\text{front dist. err.}} - \rho_y \underbrace{(y_i - y_{i+1} - \Delta_{\text{ref}})}_{\text{rear dist. err.}} \Big] \\ + g_v \Big[(1-\rho_v) \underbrace{(v_{i-1} - v_i)}_{\text{front vel. err.}} - \rho_v \underbrace{(v_i - v_{i+1})}_{\text{rear vel. err.}} \Big], \end{aligned} \tag{1.5}$$

where $\rho_y, \rho_v > 0$ are asymmetries used for coupling in position and velocity ($\rho_y = 0.5$ is symmetric coupling). The vehicles used only coupling in position and velocity. Note that a different asymmetry (ρ) was used than in proportional asymmetry (ϵ)—symmetry was achieved with $\epsilon = 1$, while for ρ it is for $\rho = 0.5$.

It was shown that in order to have a good scaling, the coupling in position must be symmetric ($\rho_y = 0.5$). Our system therefore had symmetric coupling in position, but to shorten the transient, we introduced asymmetry in velocity $\rho_v < 0.5$. Our results provide not only formulas describing the transients, but also a nonlinear optimization procedure for controller parameters tuning. This procedure is independent of the number of vehicles. The most distinctive feature, unlike many papers in distributed control, is that the procedure optimized not only the controller parameters, but also the asymmetry ρ_v (ρ_y was fixed to 0.5). Analysis of this third-order system is described in Chapter 5.

1.1.4 Practical applicability

Although the motivation for this thesis is a platoon of vehicles, honestly, I do not believe that the proposed fixed-distance methods are easily applicable in practice. The wave behavior (discussed later in the thesis) of any bidirectional string is such a limiting factor that the driver (or the passengers in automatic cars) will never accept permanent acceleration and deceleration of the vehicle. Moreover, the transients are too long. Only when the leader's velocity is available or time-headway strategy is used, the performance is satisfactory.

Hence, I believe that fixed-distance policy without communication can be used only as a backup solution when communication fails. In this case bidirectional control with symmetry in position and asymmetry in velocity should be used. Otherwise, at least the velocity of the leader should be communicated to every vehicle to achieve good performance.

I suggest that the results presented in the thesis should not be evaluated in terms of their immediate practical applicability, but rather as a theoretical research showing achievable limits for distributed control. I show what can happen when the system gets larger and larger, not how to design a particular controller for a real car.

1.2 Structure of the thesis

Chapter 2 deals with necessary mathematical preliminaries, especially the graph theory and the basics of distributed control. The main goals, models and approaches of distributed control are listed.

In Chapter 3 we derive a convenient product form of transfer functions in the consensus systems. This product form combines the graph properties and single-agent models in an explicit way.

The fourth chapter is devoted to platooning algorithms with nearest-neighbor interactions with proportional (or identical) asymmetry. Various types of scaling are derived. If there is one integrator in the open loop, a good scaling might be achieved, while for two integrators it becomes very difficult.

Since the results in Chapter 4 show that proportional asymmetry is bad for systems which have two integrators in the open loop, partial asymmetry is proposed in Chapter 5—there are different Laplacians for each state used for coupling. We discuss the necessity of symmetric coupling in the output state. In cooperation with prof. Peter Veerman, we analyze transients in the third-order system — a double integrator with a viscous friction controlled by a PI controller.

2 Distributed control overview

As we discussed in the introduction, results from distributed control are very useful in deriving scaling properties in platoons. In this chapter we will describe the current state of the art in distributed control. We will discuss the basic goals of distributed control and the ways how to achieve them.

First we show some mathematical preliminaries in graph theory which we will use throughout the thesis. Then we introduce the distributed control, the role of agents and their models. Stability, tracking and performance in distributed control is discussed. The effects of graph topology are highlighted.

Note that the list given here is neither intended to be complete, nor do we state all the technical details of the results presented. We just show it here in order to provide the results we will later rely on. A proper reference is always stated. Much more can be found in books dedicated to distributed control, such as [Lewis et al., 2014; Mesbahi and Egerstedt, 2010; Ren and Beard, 2008; Qu, 2009]

2.1 Graph theory

Only the basics of the graph theory necessary for the further development in the thesis will be described here. A thorough overview can be found in many books, for instance [Biggs, 1974; Godsil and Royle, 2001]. We will mainly concentrate on algebraic graph theory, which relates graph properties to properties of matrices associated with the graph.

The network-system interconnection (sharing of information) can be viewed as a *directed graph* (or digraph). The graph $\mathcal{G}$ has a vertex set $\mathcal{V}(\mathcal{G})$ and an arc

set $\mathcal{E}(\mathcal{G})$. The arc (or edge) $\epsilon(\nu_j, \nu_i)$ is oriented, which means that the ith agent receives information from the jth agent. A directed path π_{ij} from i to j of length $l(\pi_{ij})$ is a sequence of vertices and arcs $\nu_1, \epsilon_1, \nu_2, \epsilon_2, \dots \nu_{l+1}$, where each vertex and arc can be used only once. The length (number of arcs) of the shortest path between i and j is called the distance δ_{ij} of vertices. A cycle is a path with the first and last vertices identical.

An *adjacency matrix* A is a matrix whose entries a_{ij} are either zero if there is no arc from ν_j to ν_i or a positive number called weight if the arc is present. A graph is said to be *undirected* if for each a_{ij} there is a_{ji} such that $a_{ij} = a_{ji}$. That is, the pair of vertices i, j is connected by both the arc from i to j and the arc from j to i and the arcs have the same weight. In this case the adjacency matrix is symmetric. A graph is said to be a directed graph (a digraph) otherwise.

An undirected graph is said to be connected if there is a path from each vertex to any other vertex. A directed graph is said to be strongly connected if there is a directed path from each vertex to any other vertex. It is weakly connected if between all pairs i, j of vertices there is path from i to j or from j to i. This means that the vertex i can be accessible from j but the converse does not have to be true. A directed graph contains a directed spanning tree if there is a vertex (called a root) from which there is a directed path to every other vertex (there does not have to be a path from other vertices to the root).

We define the weight of the path as $\vartheta(\pi_{ij}) = \prod_{\epsilon(k,m)\in\pi_{ij}} a_{km}$. It is the product of weights of all arcs in the path. Similarly, we define the weight of a subset $\mathcal{G}'$ of a graph $\mathcal{G}$ as

$$\vartheta(\mathcal{G}') = \prod_{\epsilon(k,m)\in\mathcal{E}(\mathcal{G}')} a_{km}. \tag{2.1}$$

A *directed tree* is a subset of a graph without directed cycles. A diverging directed tree always has a path from one particular node called the root to each node in the tree. There is no directed path from the nodes in the diverging tree to the root and all the nodes except for the root have in-degree one. A forest $\bar{F}$ is a set of mutually disjoint trees. A *spanning forest* is a forest on all vertices of the graph (see [Chebotarev and Agaev, 2014] for an overview of directed trees). A diverging forest (out-forest) is a forest of diverging trees. Following the notation of [Chebotarev and Agaev, 2002] we denote $\mathcal{F}_k^{i\to j}$ the *set of all spanning diverging forests* with k arcs. Each spanning forest $\bar{F}_k^{i\to j}$ in this set must contain a tree with the root i which contains the node j. The weight of

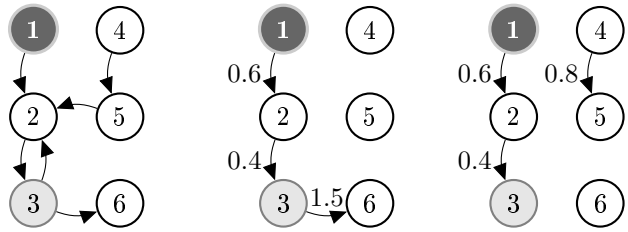

(a) Orig. graph (b) First forest (c) Second forest

Figure 2.1: Example of the set $\mathcal{F}_3^{1\to 3}$ of all spanning forests with three arcs with a tree diverging from the node 1 and containing 3. The weights of the two spanning forests are: (a) $\vartheta(\bar{F}_3^{1\to 3})_1 = 0.6 \cdot 0.4 \cdot 1.5 = 0.36$ and (b) $\vartheta(\bar{F}_3^{1\to 3})_2 = 0.6 \cdot 0.4 \cdot 0.8 = 0.192$. The weight of the set is $\vartheta(\mathcal{F}_3^{1\to 3}) = 0.192 + 0.36 = 0.552$.

this set is

$$\vartheta(\mathcal{F}_k^{i\to j}) = \sum_{\bar{F}_k^{i\to j} \in \mathcal{F}_k^{i\to j}} \vartheta(\bar{F}_k^{i\to j}), \tag{2.2}$$

with the sum taken over all spanning forests $\bar{F}_k^{i\to j}$ in the set $\mathcal{F}_k^{i\to j}$. This is illustrated in Fig. 2.1.

Let Q_k be a matrix of spanning out-forests of $\mathcal{G}$ which have k arcs. The (i,j)th element $(q^k)_{ij}$ of Q_k is given as

$$(q^k)_{ij} = \vartheta(\mathcal{F}_k^{j\to i}). \tag{2.3}$$

It is the weight of the set of all spanning out-forests $\mathcal{F}_k^{j\to i}$ with k arcs containing i and diverging from the root j.

2.1.1 Graph Laplacian

Let us denote $D = \mathrm{diag}\Big(\deg(\nu_i)\Big)$ the diagonal matrix of the sums of weights of the arcs incident to the vertex i where $\deg(\nu_i) = \sum_{j=1}^{N} a_{ij}$. Then the *Laplacian* matrix $L \in \mathbb{R}^{N\times N}$ of a directed graph is defined as

$$L = D - A. \tag{2.4}$$

Often we will refer to the so called reduced Laplacian (or grounded Laplacian [Pirani and Sundaram, 2014]), which is obtained from the original Laplacian

by deleting rows and columns corresponding to some vertices. The reduced Laplacian obtained by deleting rows and columns with indices in the set $\mathcal{S}$ is denoted by $\bar{L}_{\mathcal{S}}$.

For instance, for a directed graph with 5 nodes, we delete the third and the fourth rows and columns of L to get $\bar{L} = L_{3,4}$ as

$$L = \begin{bmatrix} 2 & -1 & 0 & 0 & -1 \\ -1 & 3 & -1 & -1 & 0 \\ 0 & -1 & 2 & -1 & 0 \\ 0 & 0 & -1 & 1 & -0 \\ -1 & 0 & 0 & -1 & 2 \end{bmatrix} \Longrightarrow L_{3,4} = \begin{bmatrix} 2 & -1 & -1 \\ -1 & 3 & 0 \\ -1 & 0 & 2 \end{bmatrix}. \tag{2.5}$$

We denote the eigenvalues of the Laplacian as λ_i, $i = 1, \ldots, N$.

Lemma 2.1. *The Laplacian L in (2.4) has the following properties:*

1. *The Laplacian is a singular M-Matrix. [Horn and Johnson, 1999].*
2. *All the eigenvalues have non-negative real part, i.e. $\Re\{\lambda_i\} \geq 0$, $\forall i$.*
3. *All the eigenvalues lie in the circle centered at $\max\{\deg(\nu_i)\}$ and has a radius $\max\{\deg(\nu_i)\}$. This follows from Gershgorin theorem [Horn and Johnson, 1990]*
4. *There is always a zero eigenvalue of the Laplacian, i.e., $\lambda_1 = 0$ with the corresponding eigenvector $\mathbf{1}$ of all ones, i.e., $L\mathbf{1} = 0$. This is a consequence of the construction of the Laplacian (zero sum in the row).*

We will list separately additional properties of the Laplacian for directed and undirected graphs.

Undirected graphs

The Laplacian of the undirected graph has the following properties:

1. It is a symmetric matrix, i.e., $L = L^{\mathrm{T}}$.
2. It has only real eigenvalues. We order them as $\lambda_1 \leq \lambda_2 \leq \ldots \leq \lambda_N$ and $\lambda_1 = 0$.

3. The second smallest eigenvalue $\lambda_2 > 0$ if and only if the graph is connected.

The second smallest eigenvalue λ_2 has a special meaning. It captures so called "algebraic connectivity" of the graph. The larger this eigenvalue is, the larger is the connectivity (roughly speaking the more paths there are among vertices) of the graph. This property was discovered by a Czech mathematician Miroslav Fiedler [Fiedler, 1973] and hence the eigenvalue λ_2 is called a "Fiedler eigenvalue".

The eigenvalues of the reduced Laplacian interlace those of the original Laplacian.

Lemma 2.2 ([Horn and Johnson, 1990, Thm. 4.3.15]). *Let $\bar{L}$ be a principal $r \times r, 0 < r < n$ submatrix of L ($L = L^{\mathrm{T}}$) and $\mu_1 \leq \mu_2 \leq \ldots \leq \mu_r$ be the eigenvalues of $\bar{L}$. Then for each $1 \leq k \leq r$ we have*

$$\lambda_k < \mu_k \leq \lambda_{k+n-r}. \tag{2.6}$$

This result is known as the Cauchy Interlacing Theorem.

Directed graphs

The Laplacian of the directed graph has these properties:

1. The zero eigenvalue is simple (i.e, $\Re\{\lambda_i\} > 0$) if and only if the graph contains a directed spanning tree [Lewis et al., 2014, Thm. 2.1].

The location of the eigenvalues is in [Agaev and Chebotarev, 2005] given more precisely than just by Gershgorin's disks. For other properties of the Laplacians we refer the reader to the books [Mesbahi and Egerstedt, 2010; Qu, 2009; Lewis et al., 2014].

Pinned Laplacian

Often the multi-agent system is required to track some reference and this reference agent is not considered to be part of the graph, but the system interacts with it. Let G be a diagonal matrix consisting of the weights of the coupling ρ_i with the reference, i.e., $G = \mathrm{diag}[\rho_1, \rho_2, \ldots, \rho_N]$. Then the pinned Laplacian is given as follows

$$L_{\mathrm{p}} = L + G. \tag{2.7}$$

As the following two lemmas indicate, using pinning, we can get rid of the eigenvalue at zero.

Lemma 2.3 ([Li et al., 2010, Lem. 5]). *Suppose that the directed graph $\mathcal{G}$ has a directed spanning tree with the root r and the root has access to the reference, i.e., $\rho_r \neq 0$. Then all eigenvalues λ_i of the pinned Laplacian L_p have positive real part.*

Lemma 2.4 ([Qu, 2009, Cor. 4.33]). *Let G be a diagonal matrix with all elements non-negative and at least one positive element. Then if L is irreducible matrix, then $L + G$ is non-singular.*

Irreducible Laplacian corresponds to a strongly connected graph.

Other useful results

In the thesis we will use a version of Lemma 3.1 in [Briegel et al., 2011]. Here we provide a different proof, as the original proof is valid only for commuting matrices and unweighted graphs.

Lemma 2.5. *For the elements of the powers of Laplacian holds*

$$(-L^m)_{ij} = \begin{cases} 0, & \text{for } m < \delta_{ji}, \\ \vartheta(\mathcal{F}_m^{j\to i}) & \text{for } m = \delta_{ji}. \end{cases} \tag{2.8}$$

Proof. We will use the result [Chebotarev and Agaev, 2002, Proposition 8], which shows

$$(-L)^m = \sum_{k=0}^{m} \alpha_k Q_{m-k}, \tag{2.9}$$

with $\alpha_k \in \mathbb{R}$ being a constant. Since $(q^{m-k})_{ij}$ is the weight of $\mathcal{F}_{m-k}^{j\to i}$, the minimal number of arcs for any forest in the set to exist is the distance δ_{ji} from the node i to the node i. Hence, for $m < \delta_{ji}$, (i,j)th element of all Q_{m-k} is zero and therefore $(-L^m)_{ij}$ is also zero. For $m = \delta_{ji}$ the element $(-L^m)_{ij}$ is the sum of the weights of all shortest paths. □

2.2 Distributed control

The description of distributed control in this chapter is by no means complete and it is not intended to be complete. We just want to provide the necessary basics which will be referred to later in the thesis.

The majority of practically important network systems are nonlinear systems (oscillators, robot formations, etc.). Moreover, the controller is usually implemented on a computer, so it operates in discrete time. However, in whole thesis we work only with linear continuous-time models. We decided to take this limitation because scaling is a difficult problem even for such simplified models. And many nonlinear systems can be exactly linearized using a feedback linearization.

Moreover, to keep the analysis simple, we will work only with homogeneous systems, i.e., systems, in which all the agents are identical (have identical models). Whenever heterogeneity is allowed, it will be stated explicitly.

2.2.1 Consensus

A typical task solved in distributed control is to synchronize the agents or to reach a consensus on some value. The main approach how to reach it is that the agent tries to minimize the error between its own value and the values of its neighbors. Let us consider the consensus first. Suppose that the agent has only one state $x_i \in \mathbb{R}$ with dynamics

$$\dot{x}_i = e_i. \tag{2.10}$$

We will refer to this model as a *single-integrator system*. We have a set of N agents, each having some (different) initial value. The agents should finally agree on some value. Define the *local neighborhood error* of one agent to its neighbors as

$$\tilde{x}_i = \sum_{j \in \mathcal{N}_i} a_{ij}(x_j - x_i), \tag{2.11}$$

where $\mathcal{N}_i$ is a set of the neighbors of agent i and a_{ij} is the weight of the arc from j to i. This error is the input to the agent, that is, $e_i = \tilde{x}_i$. The overall system of N agents coupled together can be written using the Laplacian L in (2.4) as

$$\dot{x} = -Lx, \tag{2.12}$$

where $x = [x_1, x_2, \ldots, x_N]^{\mathrm{T}} \in \mathbb{R}^N$. Since the Laplacian has nonnegative eigenvalues, the system (2.12) is stable. If there is a directed spanning tree, the agents will, as the time $t \to \infty$, reach consensus, i.e., $x_1 = x_2 = \ldots = x_N = \bar{x}$. The

properties of the final value $\bar{x}$ as a function of the graph properties are discussed in [Olfati-Saber et al., 2007].

Even when there is not a directed spanning tree, the parts in the graph will synchronize. This is captured by the term Forest consensus in [Chebotarev and Agaev, 2014].

There can be also an exogenous input to each agent to drive the consensus system to some desired state. Then, the control input of an agent has a form $e_i = \tilde{x}_i + r_i$ with r_i being some exogenous input. This input can be for instance a desired value, a noise or another controller input. The overall system then is

$$\dot{x} = -Lx + r \tag{2.13}$$

with $r = [r_1, r_2, \ldots, r_N]^{\mathrm{T}} \in \mathbb{R}^N$.

For the case when the external input is a white noise we have a lot of results on the effect of the topology, e.g., [Zelazo and Mesbahi, 2011].

2.2.2 Synchronization (or higher-order consensus)

Another typical task is a synchronization of agents or any other physical devices. Typical examples are synchronization of pendulums, oscillators or generators in electric power grids. Keeping a specified shape in formation of mobile robots also needs some kind of synchronization. Unlike in a simple consensus, here the agents converge to some trajectory, not to a single value.

Usually, in this case the model of an agent is of higher order with a state vector $x_i \in \mathbb{R}^n$, input $e_i \in \mathbb{R}^m$ and output $y_i \in \mathbb{R}^p$. The model is

$$\begin{aligned} \dot{x}_i &= Ax_i + Be_i \\ y_i &= Cx, \end{aligned} \tag{2.14}$$

where $A \in \mathbb{R}^{n\times n}, B \in \mathbb{R}^{n\times m}$ and $C \in \mathbb{R}^{p\times n}$. We do not allow a direct feed-through of the input to the output, since this would cause problems when connecting agents together. We call the model (2.14) *open-loop model* of the agent. The input to this open-loop model is again given as a local neighborhood error in states plus some external input

$$e_i = K\tilde{x}_i + r_i, \tag{2.15}$$

where the matrix $K \in \mathbb{R}^{m\times n}$ is a feedback gain matrix. The local neighborhood

error is defined as

$$\tilde{x}_i = \sum_{j \in \mathcal{N}_i} a_{ij}(x_j - x_i), \tag{2.16}$$

where a_{ij} is the weight of the arc from j to i. Using such inputs, the overall network system can be written

$$\begin{aligned} \dot{x} &= (I_N \otimes A)x - (L \otimes BK)x + (I_N \otimes B)r \\ y &= (I_N \otimes C)x. \end{aligned} \tag{2.17}$$

The overall state vector is $x = [x_1^{\mathrm{T}}, x_2^{\mathrm{T}}, \ldots, x_N^{\mathrm{T}}]^{\mathrm{T}}$, the external input vector is $r = [r_1^{\mathrm{T}}, r_2^{\mathrm{T}}, \ldots, r_N^{\mathrm{T}}]^{\mathrm{T}}$ and the output vector is $y = [y_1^{\mathrm{T}}, y_2^{\mathrm{T}}, \ldots, y_N^{\mathrm{T}}]^{\mathrm{T}}$. $\otimes$ denotes the Kronecker product. We will refer to (2.17) as the *overall network system model*.

The goal of the synchronization is to make all the states converge to the same trajectory (usually nonzero), that is, as time goes to infinity ($t \to \infty$), $x_1(t) = x_2(t) = \ldots = x_N(t)$. For instance, all agents will eventually be travelling with the same velocity or all oscillators will have the same phase and frequency.

In many cases only the outputs are used for synchronization. Then, instead of the matrix K in (2.17) we have a matrix C, so the system has a form

$$\begin{aligned} \dot{x} &= (I_N \otimes A)x - (L \otimes BC)x + (I_N \otimes B)r \\ y &= (I_N \otimes C)x. \end{aligned} \tag{2.18}$$

2.2.3 More general model

The model (2.17) is a standard model used in the literature, see [Zhang et al., 2011; Fax and Murray, 2004; Olfati-Saber et al., 2007; Hengster-Movric and Lewis, 2014] and many, many more. The information about the states of the neighbors is usually obtained by communication or a direct measurement of the states relative to the neighbors. Once the agent obtains the states from its neighbors, it can weight each state differently. The local neighborhood error (2.16) in the kth state then might be

$$\tilde{x}_{i,k} = \sum_{j \in \mathcal{N}_i} a_{ij,k}(x_{j,k} - x_{i,k}), \tag{2.19}$$

where $x_{i,k}$ is the kth element in the state vector of the agent i and $a_{ij,k}$ is the weight of the arc from j to i for the state k. The total local neighborhood error of the ith agent is then given as $\tilde{x}_i = [\tilde{x}_{i,1}, \tilde{x}_{i,2}, \ldots \tilde{x}_{i,n}]^{\mathrm{T}}$. Such a local error then

yields an overall network model

$$\begin{aligned} \dot{x} &= (I_N \otimes A)x - \sum_{k=1}^{n} \left[(L_k \otimes B(g\,\bar{e}_k^{\mathrm{T}}))x \right] + (I_N \otimes B)r \\ y &= (I_N \otimes C)x. \end{aligned} \tag{2.20}$$

where $g = [g_1, g_2, \ldots, g_m]^{\mathrm{T}} \in \mathbb{R}^m$ is a weighting vector and $\bar{e}_k$ is the kth canonical vector (kth column in identity matrix I_n). Note that from implementation point of view this control input is not more difficult than (2.17). The only difference is that instead of using one Laplacian for all states, in this case each state can have its own Laplacian. When $L_1 = k_2 L_2 = \ldots = k_n L_n$ with some real constants $k_2, \ldots, k_n$, the system (2.20) simplifies to (2.17).

Nevertheless, there is a major drawback. It is very hard to analyze the system (2.20). Such a system has to be analyzed as a whole, the analysis cannot be split into part for local dynamics and part coming from interconnection (see next subsections). In the following two chapters of the thesis, we will work with identical Laplacians for all states. Only in the Chapter 5 different Laplacians will be allowed. The price is that the analysis can be done for a particular system only. No results for a class of systems are available so far.

Example

As an example, take a double integrator with a model

$$\begin{bmatrix} \dot{\hat{x}}_i \\ \dot{v}_i \end{bmatrix} = \underbrace{\begin{bmatrix} 0 & 1 \\ 0 & 0 \end{bmatrix}}_{A} \underbrace{\begin{bmatrix} \hat{x}_i \\ v_i \end{bmatrix}}_{x_i} + \underbrace{\begin{bmatrix} 0 \\ 1 \end{bmatrix}}_{B} e_i, \quad y_i = \underbrace{\begin{bmatrix} 1 & 0 \end{bmatrix}}_{C} \begin{bmatrix} \hat{x}_i \\ v_i \end{bmatrix}. \tag{2.21}$$

where $\hat{x}_i$ is position and v_i is velocity of the ith agent. The Laplacians for position and velocity are given as follows

$$L_x = \begin{bmatrix} 2 & -1.5 & 0 & -0.5 \\ 0 & 1 & -1 & 0 \\ -0.2 & 0 & 0.2 & 0 \\ 0 & -2 & 0 & 2 \end{bmatrix}, \; L_v = \begin{bmatrix} 1.1 & -1 & 0 & -0.1 \\ 0 & 0.5 & -0.5 & 0 \\ -0.2 & 0 & 0.2 & 0 \\ 0 & -1 & 0 & 1 \end{bmatrix}. \tag{2.22}$$

Note that both Laplacians used the same set of neighbors (although the information about the velocity of the fourth agent is almost ignored by the first agent), just the weights are different. The weighted directed graphs for position and

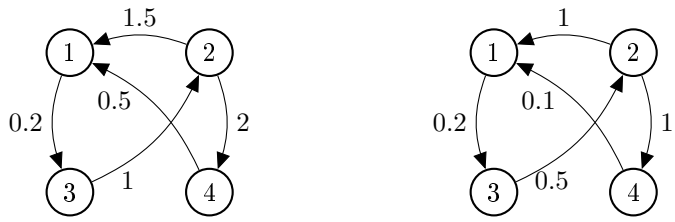

Figure 2.2: Example of Laplacians for coupling in (a) position and (b) velocity.

velocity are illustrated in Fig. 2.2. The overall formation model is

$$\begin{aligned} \dot{x} &= (I_N \otimes A)x - (L_x \otimes Bg_x\bar{e}_1^{\mathrm{T}})x - (L_v \otimes Bg_v\bar{e}_2^{\mathrm{T}})x + (I_N \otimes B)r \\ y &= (I_N \otimes C)x. \end{aligned} \tag{2.23}$$

2.2.4 Pinning control

It is often a task for a distributed system to synchronize to some given value or for a formation to reach some given position. In this case a (virtual) leader has to be present in the system. Such a leader serves as a reference value for the rest of the network system. The local neighborhood error for the kth state of the ith agent is

$$\tilde{x}_{i,k} = \sum_{j \in \mathcal{N}_i} a_{ij,k}(x_{j,k} - x_{i,k}) + \rho_{i,k}(x_{0,k} - x_{j,k}), \tag{2.24}$$

where $\rho_{i,k}$ is the weight of the coupling between the leader and the ith agent, $x_{0,k}$ is the kth state of the leader having index 0. That is, the agent synchronizes not only to its neighbors, but also to the leader. The weight $\rho_{i,k}$ is usually nonzero only for a small number of agents—the agents which are neighbors of the leader. The states of the leader evolve independently of the network. We say that the leader pins to the ith agent if $\rho_{i,k} \neq 0$.

In vector form, the local neighborhood error for synchronization of the kth state reads

$$\tilde{x}_{\mathrm{a},k} = -L_k x_{\mathrm{a},k} - G_k x_{\mathrm{a},k} + G_k x_{0,k} \tag{2.25}$$

with $G_k = \mathrm{diag}[\rho_{1,k}, \rho_{2,k}, \ldots, \rho_{N,k}]$ and $x_{\mathrm{a},k} = [x_{1,k}, x_{2,k}, \ldots, x_{N,k}]^{\mathrm{T}}$. When the leader is assumed as an external input and not part of the network system, it

cannot influence its stability. Then, assuming that $x_{0,k} = 0$ for all k,

$$\tilde{x}_{\mathrm{a},k} = -(L_k + G_k)x_{\mathrm{a},k} = -L_{\mathrm{p}}x_{\mathrm{a},k}. \tag{2.26}$$

We will denote the coupling matrix $L_{\mathrm{p}} = L_k + G_k$ and called it a *pinned Laplacian*. As follows from Lemma 2.3, if the graph corresponding to L has directed spanning tree and the leader pins to the root of this tree, then L_{p} is a non-singular matrix. We will use the pinning control scheme whenever we want to analyze a performance of the network with respect to external inputs. It is beneficial because the pinned network does not have an eigenvalue at zero.

Whenever the result holds both for pinned Laplacian and for a standard singular Laplacian, we will, with a slight abuse of notation, use the notation L for both of them.

2.3 Stability

For a single-integrator system stability is very easy—the state matrix is just $-L$, which is a semi-stable matrix (it has an eigenvalue at zero and other eigenvalues have positive real part).

When a more complicated model of an agent is used, stability as a necessary condition of synchronization becomes an issue. A major step in the stability analysis of a homogeneous system was done in [Fax and Murray, 2004, Thm. 1] or even earlier in [Wu and Chua, 1995]. We will here repeat the analysis, because we will later need some of the results.

Consider the system (2.17), which uses only one Laplacian. Instead of the Schur decomposition used in [Fax and Murray, 2004], we will use the Jordan form of L, since it reveals better the internal structure of the system. The state transformation is

$$x = (V \otimes I_N)\hat{x}, \tag{2.27}$$

where $\Lambda = V^{-1}LV$ is the Jordan form of L. The matrix $V = [v_1, \ldots, v_N]$ is formed by (generalized) eigenvectors of L and v_{ji} is the jth element of the vector v_i. The system (2.17) using the new states $\hat{x}$ has a block diagonal form

$$\begin{aligned} \dot{\hat{x}} &= [I_N \otimes A - \Lambda \otimes BK]\,\hat{x} + (V^{-1} \otimes B)r, \\ y &= (V \otimes C)\hat{x}. \end{aligned} \tag{2.28}$$

Consider a block in this block diagonal form (2.28). If this block is of size one,

it has the form

$$\dot{\hat{x}}_i = [A - \lambda_i BK]\,\hat{x}_i + B\bar{e}_i^{\mathrm{T}} V^{-1} r, \quad \hat{y}_i = C\hat{x}_i. \tag{2.29}$$

This equation can be viewed as an output feedback system with a feedback gain λ_i and output $\hat{y}_i$. A more thorough discussion of the structure of the diagonal block is shown in the next chapter.

In this section we are interested in stability of the system (2.17), which is equivalent to the stability of (2.28). Since this is a block diagonal system, we require that each diagonal block in (2.28) is stable.

Lemma 2.6 ([Fax and Murray, 2004]). *The overall network system (2.17) is stable if and only if the matrix*

$$A - \lambda_i BK \tag{2.30}$$

is stable for all eigenvalues λ_i of the Laplacian L.

This Lemma allows us to analyse the stability of multiple single-agent closed loops (2.30) ($A - \lambda_i BK$ is a matrix of a closed loop of an agent) in order to assess stability of the overall network model (2.17). Note that the eigenvalues λ_i can be complex, hence we analyze stability of complex matrices.

Remark 2.7. *If pinning control is not used, there is always a zero eigenvalue λ_1 of the Laplacian matrix. Then $A - \lambda_1 BK = A$ and there is always a block in (2.28) corresponding to the open-loop model. Thus, if the open-loop of an agent is unstable or has eigenvalues on the stability boundary, the overall system will be unstable or on the stability boundary, respectively. This corresponds to the "rigid drift" of the system—the agents might synchronize, but together their states will change their values (oscillate, etc.). Sometimes the fact the that the agents synchronize, but together they drift somewhere, is called cooperative stability.*

2.3.1 Synchronization region

There are many convenient approaches how to stabilize the system (2.17) using the property in Lemma 2.6. One of those very easy to implement and design is a so-called "synchronization region approach" described in [Li et al., 2010; Zhang et al., 2011] for continuous-time systems, [Hengster-Movric et al., 2012] for discrete-time systems and later extended to time-delay systems [Hengster-Movric et al., 2015b] and output feedback [Hengster-Movric et al., 2015a]. The approach is based on first designing the matrix K using LQR (or LMI) approach (as for a single agent) and then setting the coupling gain sufficiently high. This moves all the eigenvalues of the overall system to the left-half plane. Synchronization

region approach was later proved as inversely optimal [Hengster-Movric and Lewis, 2014], provided the Laplacian is not a defective matrix.

The basic idea is the following (taken from [Zhang et al., 2011]). Each agent uses a relative state feedback with a feedback matrix K. The control input is given as

$$e_i = cK \sum_{j \in \mathcal{N}_i} a_{ij}(x_j - x_i), \tag{2.31}$$

which is very similar to (2.15) with external signal $r = 0 \, \forall i$ and weighted error as in (2.16). The only difference is the presence of the coupling gain $c > 0$.

The main idea is to design the matrix K using an LQR design for individual agent, hence

$$K = R^{-1} B^{\mathrm{T}} P, \tag{2.32}$$

where the matrix $P = P^{\mathrm{T}} > 0$, $P \in \mathbb{R}^{n \times n}$ satisfies the Riccati equation

$$0 = A^{\mathrm{T}} P + PA + Q - PBR^{-1} B^{\mathrm{T}} P, \tag{2.33}$$

where $Q = Q^{\mathrm{T}} \geq 0$, $Q \in \mathbb{R}^{n \times n}$ is a matrix weighting the error in the state and $R = R^{\mathrm{T}} > 0$, $R \in \mathbb{R}^{m \times m}$ is the matrix weighting the control input in the standard LQR control design (see [Lewis and Syrmos, 1995]). We restate here the main result of the paper [Zhang et al., 2011].

Lemma 2.8 ([Zhang et al., 2011, Thm. 1])**.** *Let the matrix K be designed as in (2.32), satisfying (2.33). Then the control (2.31) cooperatively stabilizes the system (2.17) if the coupling gain satisfies*

$$c \geq \frac{1}{2 \min_i \Re\{\lambda_i\}}, \tag{2.34}$$

where λ_i is a nonzero eigenvalue of L or L_{p}.

Similar ideas were used in the works of [Li et al., 2010], where an LMI criterion was used to design the controller. Later even some performance measures were introduced in [Li et al., 2011]. Another LMI criterion was used for an easy controller design in [Massioni and Verhaegen, 2009].

An approach based on passifiability of agents was proposed in [Fradkov and Junussov, 2011]. Although completely different from the LQR design, the ideas and results as well are very similar. Again, only the gain (the same for each agent) has to be adjusted when the communication topology changes. This adjustment is inversely proportional to the real part of the smallest eigenvalue of

the Laplacian. The papers [Fradkov and Junussov, 2011] and [Zhang et al., 2011] both achieve unbounded synchronization region, though by different approaches. The relation between these two approaches remains an open question.

Adaptive control approaches

In the synchronization region approach, the network designer had to set the coupling gain c sufficiently large. However, this required to know the graph topology beforehand and as such it was a centralized information. That is why a number of completely decentralized approaches were proposed.

Usually, the coupling gains c_i of individual agents are different. They should grow until the system reaches synchrony. This is an approach used in the work [Li et al., 2013a] for consensus in undirected graphs and in [Li et al., 2013b] for tracking a leader in undirected graphs. In directed graphs consensus can be reached adaptively [Li et al., 2015] using a similar controller. A neural network controller was used in [Zhang et al., 2012]. An adaptive control for passifiable system is presented in [Junussov, 2014].

The main drawback of the controllers is that the coupling gain can only grow. Hence, when the system is subject to a noise, the gains will grow without a bound.

2.3.2 Passivity

Passivity is a property of many real physical systems. Such systems can only store or dissipate energy. Electrical circuits without sources, mechanical systems (such as mass-spring models) or hydraulic systems are all passive systems.

Passivity often allows to consider heterogeneous networks. For instance, a synchronization of passive agents is proved in [Chopra and Spong, 2006]. The synchronization is realized using the outputs, to which the agents are passive. This, for instance, disapproves its use to mass-spring-damper models, where the coupling is using distances, but the system is not passive when positions are the output.

An important paper dealing with synchronization of passive systems is [Arcak, 2007]. In this paper a consensus of systems being passive from the input to the derivative of the output ("velocity") is considered. Hence, the system does not have to be passive from the input to the output, but the output state is still used for synchronization. A simple mechanical example of such a system is a mass-spring-damper network. Each mass is a passive system from the input

force to its velocity (not to position — there is no energy stored in the position of the mass), but the coupling between masses is not only realized by relative velocities (dampers among masses), but also through relative positions (springs). Still, since this system has no energy sources, it must be passive.

2.4 Performance and controller design

So far we spoke only about stability, which is just a necessary condition for a reasonable performance. However, it is often only stability which can be guaranteed by current state-of-the-art approaches.

2.4.1 Inverse optimality

LQR control usually leads to a centralized controller [Bamieh et al., 2002; Jovanovic, 2010]. For a class of distributed control problems inverse optimality was proved [Hengster-Movric and Lewis, 2014]. Inverse optimality in the LQ sense means that the designed control law is optimal to some LQ criterion. That is, the optimality can be checked after the controller is designed. The main condition of [Hengster-Movric and Lewis, 2014] is that the local controller (2.32) was designed according to Lemma 2.8. Since we will use this result, we state here.

Lemma 2.9 ([Hengster-Movric and Lewis, 2014, Thm. 2])**.** *Suppose that there exist matrices* $P_1 = P_1^{\mathrm{T}} \geq 0$ *and* $P_2 = P_2^{\mathrm{T}} > 0$ *such that*

$$P_1 = cR_1L, \tag{2.35}$$
$$A^{\mathrm{T}}P_2 + P_2A + Q_2 - P_2BR_2^{-1}B^{\mathrm{T}}P_2 = 0, \tag{2.36}$$

for some $R_1 = R_1^{\mathrm{T}} > 0$, $R_2 = R_2^{\mathrm{T}} > 0$, $Q_2 = Q_2^{\mathrm{T}} > 0$ *and a coupling gain* $c > 0$. *Define the feedback matrix* $K_2 = R_2^{-1}B^{\mathrm{T}}P_2$. *Then the control* $u = -cL \otimes K_2$ *is optimal with respect to the cost function* $\int_0^\infty x^{\mathrm{T}}\overline{Q}x + u^{\mathrm{T}}\overline{R}u\,\mathrm{d}t$ *with matrices*

$$\overline{Q} = c^2(L \otimes K_2)^{\mathrm{T}}(R_1 \otimes R_2)(L \otimes K_2) - cR_1L \otimes (A^{\mathrm{T}}P_2 + P_2A), \tag{2.37}$$
$$\overline{R} = R_1 \otimes R_2. \tag{2.38}$$

The coupling gain c *must be selected such that* $\overline{Q} > 0$.

The condition (2.35) can be satisfied when the Laplacian L is not a defective[1] matrix [Hengster-Movric and Lewis, 2014, Thm. 4] and has real eigenvalues.

We will present a simplifying result, which gives a design condition on c, which

[1] Defective matrix is a matrix which has eigenvalues with different algebraic and geometric multiplicity [Horn and Johnson, 1990, Def. 1.4.4].

we will use later in the thesis. Note that this result appears for the first time in this thesis (was submitted as [Herman, 2016a]). It holds for a pinned Laplacian.

Theorem 2.10. *Assume that the Laplacian L_{p} is non-singular, non-defective and has only real eigenvalues, i.e., $LV = V\Lambda$, Λ is real and diagonal and Λ^{-1} exists. Let $\lambda_{\min} > 0$ be the smallest eigenvalue of L_{p}, i.e., $\lambda_{\min} \leq \lambda_i \, \forall i$. Then the local static-state feedback control law $u = -cL_{\mathrm{p}} \otimes K_2$, $c \geq \frac{1}{\lambda_{\min}}$ is the optimal control law with respect to the performance criterion*

$$J(x,u) = \int_0^\infty x^{\mathrm{T}} \overline{Q} x + u^{\mathrm{T}} \overline{R} u \, \mathrm{d}t \tag{2.39}$$

with

$$\overline{Q} = c^2 (L_{\mathrm{p}} \otimes K_2)^{\mathrm{T}} (R_1 \otimes R_2)(L_{\mathrm{p}} \otimes K_2) - cR_1 L_{\mathrm{p}} \otimes (A^{\mathrm{T}} P_2 + P_2 A^{\mathrm{T}}), \tag{2.40}$$

$$\overline{R} = R_1 \otimes R_2, \tag{2.41}$$

$$R_1 = (V^{-1})^{\mathrm{T}} V^{-1}, \tag{2.42}$$

for some $R_2 = R_2^{\mathrm{T}} > 0, Q_2 \geq 0$ and $K_2 = R_2^{-1} B^{\mathrm{T}} P_2$ with $P_2 > 0$ satisfying (2.36).

Proof. We need to satisfy the conditions in Lemma 2.9. First we show that the matrix $P_1 = cR_1 L_{\mathrm{p}}$ in Lemma 2.9 is symmetric and positive definite. When we plug for R_1 equation (2.42), we get

$$P_1 = cR_1 L_{\mathrm{p}} = c(V^{-1})^{\mathrm{T}} V^{-1} L_{\mathrm{p}} = c(V^{-1})^{\mathrm{T}} \Lambda V^{-1}. \tag{2.43}$$

Since $\Lambda > 0$ (the eigenvalues of L_{p} are positive), it follows that $P_1 = P_1^{\mathrm{T}} > 0$.

Next we show that $\overline{Q}$ in (2.40) is positive semi-definite for a fixed c. Rewrite it as

$$\begin{aligned} \overline{Q} &= c \left[cL_{\mathrm{p}}^{\mathrm{T}} R_1 L_{\mathrm{p}} \otimes K_2^{\mathrm{T}} R_2 K_2 - R_1 L_{\mathrm{p}} \otimes (A^{\mathrm{T}} P_2 + P_2 A^{\mathrm{T}}) \right] \\ &= c \left[cL_{\mathrm{p}}^{\mathrm{T}} R_1 L_{\mathrm{p}} \otimes K_2^{\mathrm{T}} R_2 K_2 + R_1 L_{\mathrm{p}} \otimes (Q_2 - K_2^{\mathrm{T}} R_2 K_2) \right] \\ &= c \left[\left(cL_{\mathrm{p}}^{\mathrm{T}} - I \right) R_1 L_{\mathrm{p}} \otimes K_2^{\mathrm{T}} R_2 K_2 + R_1 L_{\mathrm{p}} \otimes Q_2 \right] \end{aligned} \tag{2.44}$$

Note that $R_1 L_{\mathrm{p}} \otimes Q_2 \geq 0$ since $Q_2 \geq 0$ and $R_1 L_{\mathrm{p}} > 0$, as follows from (2.43). Also $K_2^{\mathrm{T}} R_2 K_2 \geq 0$. It follows that if $\left(cL_{\mathrm{p}}^{\mathrm{T}} - I \right) R_1 L_{\mathrm{p}} > 0$, then $\overline{Q} \geq 0$.

Consider the matrix $H = V^{\mathrm{T}} \left(cL_{\mathrm{p}}^{\mathrm{T}} - I \right) R_1 L_{\mathrm{p}} V$. Since V is non-singular, it follows from [Horn and Johnson, 1990, Obsv. 7.1.6] that if $H > 0$, then $\tilde{H} = (V^{-1})^{\mathrm{T}} V^{\mathrm{T}} \left(cL_{\mathrm{p}}^{\mathrm{T}} - I \right) R_1 L_{\mathrm{p}} V V^{-1} = \left(cL_{\mathrm{p}}^{\mathrm{T}} - I \right) R_1 L_{\mathrm{p}} > 0$. Thus, we will test

positive definiteness of the matrix $H = V^{\mathrm{T}}\left(cL_{\mathrm{p}}^{\mathrm{T}} - I\right) R_1 L_{\mathrm{p}} V$. So we have:

$$\begin{aligned} H &= V^{\mathrm{T}}\left(cL_{\mathrm{p}}^{\mathrm{T}} - I\right) R_1 L_{\mathrm{p}} V = cV^{\mathrm{T}} L_{\mathrm{p}}^{\mathrm{T}} R_1 L_{\mathrm{p}} V - V^{\mathrm{T}} R_1 L_{\mathrm{p}} V \\ &= cV^{\mathrm{T}} L_{\mathrm{p}}^{\mathrm{T}} (V^{-1})^{\mathrm{T}} V^{-1} L_{\mathrm{p}} V - V^{\mathrm{T}} (V^{-1})^{\mathrm{T}} V^{-1} L_{\mathrm{p}} V \\ &= c(V^{-1} L_{\mathrm{p}} V)^{\mathrm{T}} V^{-1} L_{\mathrm{p}} V - (V^{-1} V)^{\mathrm{T}} V^{-1} L_{\mathrm{p}} V \\ &= c\Lambda^2 - \Lambda = \Lambda(c\Lambda - I). \end{aligned} \tag{2.45}$$

The matrix $\Lambda = \mathrm{diag}[\lambda_1, \lambda_2, \ldots, \lambda_N]$ and recall that $0 < \lambda_{\min} \leq \lambda_i$, $\forall i$. It follows that $\Lambda > 0$ and if $(c\Lambda - I) > 0$, then also $\overline{Q} \geq 0$. We take $c = \frac{1}{\lambda_{\min}}$ to guarantee that $\overline{Q} \geq 0$.

We have satisfied all requirements of Lemma 2.9, hence our control law $u = -cL_{\mathrm{p}} \otimes K_2$ is optimal with respect to (2.39). □

Comparing this result with the results on synchronization region (Lemma 2.8), we see that the condition is stricter: instead of $\frac{1}{2\lambda_{\min}}$ in (2.34) we have now $\frac{1}{\lambda_{\min}}$. But by this restriction we guarantee optimal performance.

Using a synchronization region, $\mathcal{H}_2$ and $\mathcal{H}_\infty$ optimal controller can be designed [Li et al., 2011]. For path graphs inverse optimality was derived in [Jovanovic, 2010] and [Jovanović et al., 2008].

2.4.2 Tracking

One of the requirements, especially in formation control, is the ability of all agents to track some reference signal. This reference signal comes often in a form of a leader, which should drive the formation to a given state. For instance, in vehicular platoons the cars should eventually travel with the same speed as the leader does and keep desired spacing.

The papers [Wieland et al., 2011] and [Lunze, 2012] state that the necessary condition for synchronization of agents to a given trajectory is that all agents satisfy the *Internal Model Principle*. Both papers consider heterogeneous agents. Our description will follow that of [Lunze, 2012].

The model of the reference signal can be defined as an output of the (virtual) system

$$\Sigma_s : \begin{cases} \dot{x}_s = A_s x_s \\ y_s = C_s x_s \end{cases} \tag{2.46}$$

Let Σ_1, Σ_2 be models of two agents. Their intersection $\Sigma_1 \cap \Sigma_2$ is a system $\Sigma_\cap$

such that for both systems there exists a transformation T_i achieving

$$T_i^{-1} A_i T_i = \begin{bmatrix} A_\cap & 0 \\ 0 & A_{pi} \end{bmatrix}, \quad C_i T_i = (C_\cap \quad C_{pi}). \tag{2.47}$$

The matrix $A_\cap$ must be the same for both systems. Hence, the intersection of the models is $\Sigma_1 \cap \Sigma_2 = \Sigma_\cap$. For linear agents the Internal Model Principle might be restated as follows.

Lemma 2.11 ([Lunze, 2012, Thm. 2])**.** *If the agents synchronize, then* $\cap_{i=1}^N \Sigma_i \neq 0$*. If they synchronize to the leader, then* $\cap_{i=1}^N \Sigma_i = \Sigma_s$*.*

Note that the description here is not complete and for brevity it does not show all the assumptions and technical details, which can be found in [Lunze, 2012].

2.5 Effects of a graph topology

A very important research field is the effect of the graph topology on various performance measures. The speed of the consensus algorithms was shown to be related to the second smallest eigenvalue λ_2 of the Laplacian—the Fiedler eigenvalue —and hence to the algebraic connectivity [Olfati-Saber et al., 2007].

When an external input is considered, the authors investigate, for instance, the effect of the location of the input node on the speed of convergence. It was shown in [Shi et al., 2014] that the the synchronization is the faster the shorter is the maximum distance to some other node from the input nodes. A selection of the best input node is described in [Fitch and Leonard, 2013]. The best nodes are quantified based on information centrality.

The effect of noise acting at various nodes is also subject of research. This is usually captured using $\mathcal{H}_2$ norm of the system. The paper [Zelazo and Mesbahi, 2011] shows that the $\mathcal{H}_2$ norm of the system does not depend on the choice of the spanning trees (but the $\mathcal{H}_\infty$ norm does). The effect of the network size on the LQ-like performance was analyzed in [Lovisari et al., 2013]. This paper used the effect of noise in analysis.

Coherence

The effect of noise on the rigidity of the formation as a function of graph dimension was analyzed in [Bamieh et al., 2012]. The term *coherence* was used to capture that the formation moves as a rigid body. It was shown—both for

single and double integrator models—that the effect of noise in linear communication structure grows polynomially in N, it is better for 2D lattices and the best for a 3D graph. The coherence is improved when some absolute state feedback is used (for instance, absolute friction or absolute position measurement). In one-dimensional formation an accordion-like motion was observed.

For double integrator models the effect of noise is bounded for formation of arbitrary size if the graph has-three dimensional topology for absolute velocity and relative position feedback. For relative position and velocity feedback it requires five dimensions. In general, the graph dimension to bound the effect of noise is $2\eta+1$, where η is the number of integrators in the agent model [Bamieh, 2014].

Later on, some of the results were generalized to fractal graphs [Patterson and Bamieh, 2014]. The authors concluded that fractal dimension does not capture the dimension of the graph and the measure of the dimension of a general graph is still unknown.

The most important fact is that for low-dimensional graphs, a local relative feedback cannot suppress large-scale disturbances. It is the graph topology which imposes a limitation on the achievable performance.

2.6 Wave-based description

So far we discussed approaches for analysis which described the system as a whole. This is done using state-space methods or in the frequency domain. However, in such description the global performance measure can be good, while locally the system does not exhibit satisfactory behavior. As an example, consider a large graph where only a few agents amplify the signal. Locally, at these agents, the behavior is bad—they amplify the disturbance as it propagates through them. This amplification does not play any important role in the $\mathcal{H}_2$ norm of overall system. Hence, from the system perspective, the performance is satisfactory, while locally it is not. Local description also plays an important role in understanding how an agent influences its neighbors.

The local description shown here follows the so called *wave-based approach*. The application of wave-based approach to distributed control was a work of my colleague Dan Martinec, so many details about it (except for the publications cited here) can be found in his dissertation.

The concept of travelling waves in lumped systems was originated in the work of William O'Connor [O'Connor, 2007], where wave-absorber was designed for one-dimensional mass-spring system. The author continued in his research in

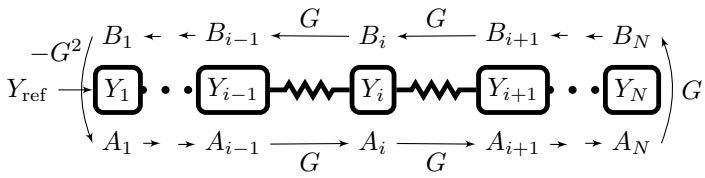

Figure 2.3: Schematics of waves A, B in a path graph

[O'Connor and McKeown, 2008; O'Connor, 2011]. Similar ideas are known in the control of PDEs with the name Absolute Vibration Suppression [Sirota and Halevi, 2014] or [Sirota and Halevi, 2015]. The work [Martinec et al., 2014] generalized the travelling-wave concept to homogeneous agents with arbitrary models connected a path graph-topology. The motivation was to shorten transients in long vehicular platoons. Heterogeneity was allowed in [Martinec et al., 2016a] and general graphs were considered in [Martinec et al., 2015].

The description shown here is valid only for homogeneous path graph. The details can be found in [Martinec et al., 2014, 2016a]. The main idea of the wave approach is to separate the (Laplace transform of the) output $Y_i(s)$ (e.g., the position) of the ith agent into two parts: $A_i(s)$ and $B_i(s)$, which correspond to wave travelling from the left and from the right, respectively (see Fig. 2.3). The wave propagates from $A_i(s)$ to the agent A_{i+1} through the *wave transfer function* G having a form

$$G(s) = \frac{A_{i+1}(s)}{A_i(s)} = \frac{\alpha}{2} - \frac{1}{2}\sqrt{\alpha^2 - 4} \tag{2.48}$$

with $\alpha = 2 + \frac{1}{M(s)}$ with $M(s)$ being the open-loop of an agent. The transfer function from agent $i+1$ to agent i is again $\frac{B_i(s)}{B_{i+1}(s)} = G(s)$. It is clear that $G(s)$ is an irrational transfer function. The transfer function (2.48) holds in this simple form only in a homogeneous path graph.

The transfer function $G(s)$ has several interesting properties [Martinec et al., 2016a]: it is a stable transfer function if and only if the infinitely long path graph is stable; its $\mathcal{H}_\infty$ norm is equal to one, i.e., $\|G(s)\|_\infty = 1$; its steady-state gain is one, i.e., $|G(0)| = 1$; and it has neither poles nor zeros.

Knowledge of $G(s)$ allows us to describe the reflection on the terminal nodes of the graph. There is no reflection when the wave propagates between identical agents, it reflects only at the graph ends. Once the reflection is known, we can design a wave-absorber to cancel the reflection. This qualitatively improves the transient speed [Martinec et al., 2014]—the settling time scales linearly in N.

In heterogeneous path-graph systems there are reflections even between agents—those that do not have the same models [Martinec et al., 2016a]. As with the reflection at the ends of the path graph, we can design a wave absorber at the boundary between agents, such that nothing reflects back. The investigation of the wave transfer function and the reflection at the boundaries gives us local behavior of the system.

In general graphs a wave reflection occurs at any agent, unless the agent has only two neighbors [Martinec et al., 2015].

2.6.1 Impedance matching

Zdeněk Hurák has been working on the interpretation of the wave phenomena in chains of dynamical systems within the framework of impedance matching and scattering description [Hurák, 2015]. These powerful concepts are well mastered in electrical engineering for characterization of interconnected systems, namely two-port networks. Exploiting analogy among physical domains, some insight can also be obtained for vehicular platooning. In particular, he shows that the wave absorbing controller attached to the first or the last vehicle in a symmetric platoon can be actually viewed as a reflectionless impedance matching, which for LCR ladder circuits also leads to an irrational impedance. Moreover, he discusses that extensions to chains (platoons) with asymmetric coupling are only possible due to presence of active elements. Since this multiport framework exhibits a genuine focus on power interactions among neighbors, the methodology has a close connections with $\mathcal{H}_\infty$-optimal control and, even more appropriately, integral quadratic constraints (IQC) popular in control theory.

3 Transfer functions in network systems

In this chapter we deal with transfer functions between any input in the network system and any state in the system, taken as an output. We present a convenient product form a transfer function, which reveals the structure of poles and zeros. Our results in this chapter hold for a system of identical SISO systems with higher order dynamics, where agents use output feedback. The content of this chapter is submitted as [Herman et al., 2016c] and preliminary results were presented as [Herman et al., 2014b].

Unlike path graphs in the subsequent two chapters, in this chapter we consider arbitrary graphs. Thus, the results here are not limited to platoons and hold for arbitrary distributed system of identical agents.

3.1 Related work

The research in the field of the structure of the transfer functions in consensus systems was originated by the work [Briegel et al., 2011], which considered undirected networks and single-integrator agents. Some basic relations between the structure of the network and the location of transfer-function zeros were stated in the paper. Some of the results of [Briegel et al., 2011] were extended and rediscovered in [Abad Torres and Roy, 2013, 2014]. In these papers some results on the relation of zeros of single-integrator dynamics and paths in the graph were discovered. The paper [Abad Torres and Roy, 2014] and its journal version [Abad Torres and Roy, 2015] discovered that even stable single-integrator networks can have CRHP (closed right half-plane) zeros, if the path between vertices satisfies some properties. Zeros of the overall transfer function matrix of discrete-time systems are analyzed in [Zamani et al., 2015].

3.2 Agent and network model

We consider a network system consisting of N identical agents which exchange information about their outputs (either using a communication or measurements). All are modelled as SISO systems, where dynamic controllers are used. Each agent is governed locally, therefore no central controller is used.

The plant model $G(s)$ (the model of an agent without the controller) is given as a transfer function of an arbitrary order

$$G(s) = \frac{b(s)}{a(s)}. \tag{3.1}$$

The output of the ith plant is denoted as y_i. The plant model is driven by the output of the dynamic controller $R(s)$. The controller is generally given as a transfer function

$$R(s) = \frac{q(s)}{p(s)}. \tag{3.2}$$

The input to the controller is denoted as e_i and is given in (3.5). As the plant and the controller are connected in series, the agent model is described by the *scalar* open-loop transfer function of order n

$$M(s) = G(s)R(s) = \frac{b(s)q(s)}{a(s)p(s)}. \tag{3.3}$$

The relative degree (the difference between the degree n of the denominator and the degree υ of the numerator) of $M(s)$ is denoted as $\chi = n - \upsilon$.

Definition 3.1 (Number of integrators in the open loop)**.** *Let the open-loop model be factored as* $M(s) = 1/s^{\eta}\, M_{\mathrm{s}}(s)$ *with* $M_{\mathrm{s}}(0) < \infty$*. Then* $\eta \in \mathbb{N}_0$ *is the number of integrators in the open loop.*

The number η is also known as a *type number* of the system and it is also the number of eigenvalues of the feedback matrix A at the origin. For instance, the model $M(s) = \frac{1}{s(s+a)}$ is a system with one integrator in the open loop and $M(s) = \frac{s+1}{s^2(s+b)}$ has $\eta = 2$. We call the well-known cases with $M_{\mathrm{s}}(s) = 1$ a single-integrator system ($M(s) = 1/s$) for $\eta = 1$ and a double-integrator system ($M(s) = 1/s^2$) for $\eta = 2$, respectively.

The neighbor of an agent i is defined as an agent j from which the agent i can obtain information about its output y_j, that is, there exists an arc $\epsilon(\nu_j, \nu_i)$ with weight a_{ij} in the graph $\mathcal{G}$. The local neighborhood error of the ith agent is

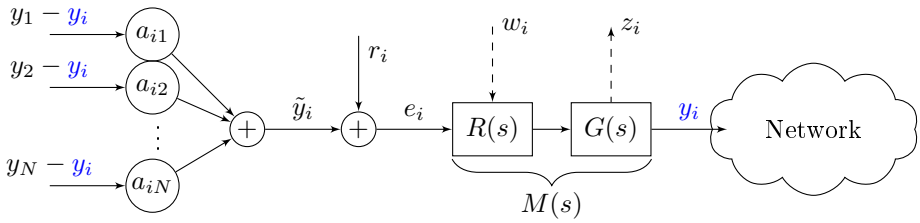

Figure 3.1: Agent interconnection. The input w_i and the output z_i are general signals discussed in Sec. 3.4

defined as

$$\tilde{y}_i = \sum_{j \in \mathcal{N}(i)} a_{ij}(y_j - y_i), \tag{3.4}$$

where $\mathcal{N}(i)$ denotes the set of neighbors of the ith agent. Unlike (2.16), here only the agents' outputs are used.

Apart from the local neighborhood error $\tilde{y}_i$, an exogenous input r_i can be acting at the input of the controller. The total input to the controller thus is

$$e_i = \tilde{y}_i + r_i = \left(\sum_{j \in \mathcal{N}(i)} a_{ij}(y_j - y_i) \right) + r_i. \tag{3.5}$$

The input r_i can be, for instance, the sum of reference values or some other external signal such as error in measurement, disturbance etc. We treat r_i as a general signal. The interconnection is depicted in Fig. 3.1.

3.2.1 Problem statement

The stacked vector of all inputs to the open loops is

$$e(s) = -Ly(s) + r(s), \tag{3.6}$$

with $e = [e_1, \ldots, e_N]^{\mathrm{T}}$, $y = [y_1, \ldots, y_N]^{\mathrm{T}}$ and $r = [r_1, \ldots, r_N]^{\mathrm{T}}$. The matrix L is the graph Laplacian in (2.4)[1]. Now we can write the model of the overall

[1] In this section we assume that the zero eigenvalue of the Laplacian is always present ($\lambda_1 = 0$). Pinning control is discussed in Sec. 3.4.

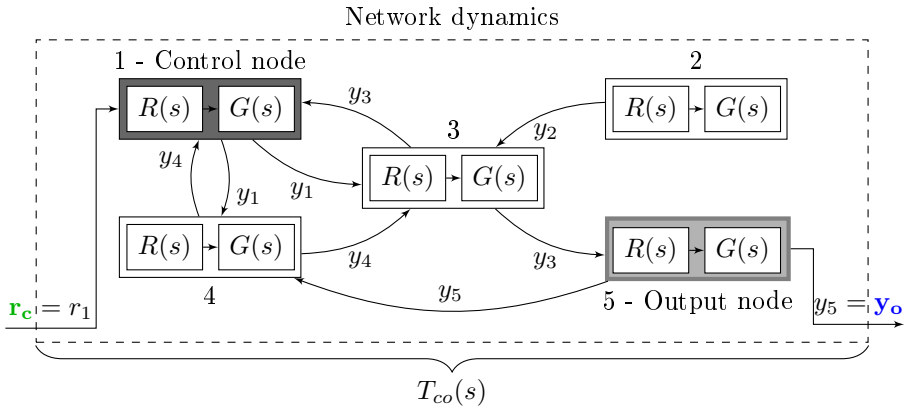

Figure 3.2: A set of agents sharing information about their outputs (arrows). We are interested how an external input at the agent c (in this case $c = 1$) affects the output of some other vehicle with index o (in this case $o = 5$). This is captured by the transfer function $T_{co}(s) = \frac{y_o(s)}{r_c(s)}$, which in this case is $= T_{15}(s) = \frac{y_5(s)}{r_1(s)}$.

network system as

$$y(s) = M(s)e(s) = M(s)\left[-Ly(s) + r(s)\right]. \tag{3.7}$$

We are interested in how an exogenous input acting at one selected agent affects the output of another agent. We assume that there is only one input r_c, acting at the input of the agent with index c. That is, the input vector equals $r = [0, \ldots, 0, r_c, 0, \ldots, 0]^{\mathrm{T}} = \bar{e}_c r_c$, where $\bar{e}_c$ is the cth canonical vector. We will call the agent with index c a *control agent*.

The output of interest is the output y_o of the agent with index o, i.e., the output vector is $y = [0, \ldots, 0, y_o, 0, \ldots, 0]^{\mathrm{T}} = \bar{e}_o y_o$. We call the agent with index o an *output agent*. The indices c and o can be arbitrary. We will use the statement "from c to o" with the meaning of "from the input r_c acting at the agent c to the output y_o of the agent o". The setup is schematically depicted in Fig. 3.2.

Define a transfer function $T_{co}(s)$ as

$$T_{co}(s) = \frac{y_o(s)}{r_c(s)}. \tag{3.8}$$

Consider the transfer function $T_{co}(s)$ for a network of SISO agents connected by a directed graph. We study the structure of $T_{co}(s)$ and analyze how does

$T_{co}(s)$ depend on the open loop model $M(s)$, the choice of agents c and o and the interconnection Laplacian L.

3.2.2 Block diagonalization

As was shown in the introduction to distributed control in Sec. 2.3, the system with one Laplacian can be easily block diagonalized using the eigenvectors of the Laplacian. We will show here how to do it using polynomial description for SISO systems. We can block diagonalize the system (3.7) using the transformation $y = V\hat{y}$. The matrix $V = [v_{ij}]$ is a matrix of (generalized) eigenvectors of the Laplacian, i. e. $LV = V\Lambda$ with Λ being the Jordan form of L. With such a transform, the model has a form

$$V\hat{y}(s) = M(s)\left[-LV\hat{y}(s) + r(s)\right]. \tag{3.9}$$

Note that $M(s)$ is a scalar transfer function. Separating $\hat{y}$ on the left-hand side using $\Lambda = V^{-1}LV$ yields

$$\left[I + \Lambda M(s)\right]\hat{y}(s) = M(s)V^{-1}r(s). \tag{3.10}$$

We can define the transformed input to the system $\hat{r}(s) = V^{-1}r(s)$. Since $M(s)$ is a scalar transfer function, (3.10) is a block diagonal system, where each block has a size of a Jordan block corresponding to the eigenvalue λ_i of L. If the Jordan block for the eigenvalue λ_i has a size 1, then it can be written using a transfer function

$$F_i(s) = \frac{\hat{y}_i(s)}{\hat{r}_i(s)} = \frac{M(s)}{1 + \lambda_i M(s)} = \frac{b(s)q(s)}{a(s)p(s) + \lambda_i b(s)q(s)}. \tag{3.11}$$

$F_i(s)$ is an output feedback system with a feedback gain λ_i. We will also later use a system $T_i(s) = \lambda_i F_i(s) = \frac{\lambda_i b(s)q(s)}{a(s)p(s)+\lambda_i b(s)q(s)}$. Such a transfer function is a complementary sensitivity function for an open loop $\lambda_i M(s)$. Although these two transfer functions $T_i(s)$ and $F_i(s)$ are very similar to each other, we decided to introduce different notation since they will be used many times throughout the thesis.

If, on the other hand, the block in (3.10) corresponds to a Jordan block of size 2, then its output can be written as the output of a series connection of identical blocks, such as

$$\begin{aligned}\hat{y}_i(s) &= \frac{M(s)}{1 + \lambda_i M(s)}\left(\hat{r}_i(s) + \frac{M(s)}{1 + \lambda_i M(s)}\hat{r}_{i+1}(s)\right) \\ &= F_i(s)\Big(\hat{r}_i(s) + F_i(s)\hat{r}_{i+1}(s)\Big) = F_i(s)\hat{r}_i(s) + F_i^2(s)\hat{r}_{i+1}(s).\end{aligned} \tag{3.12}$$

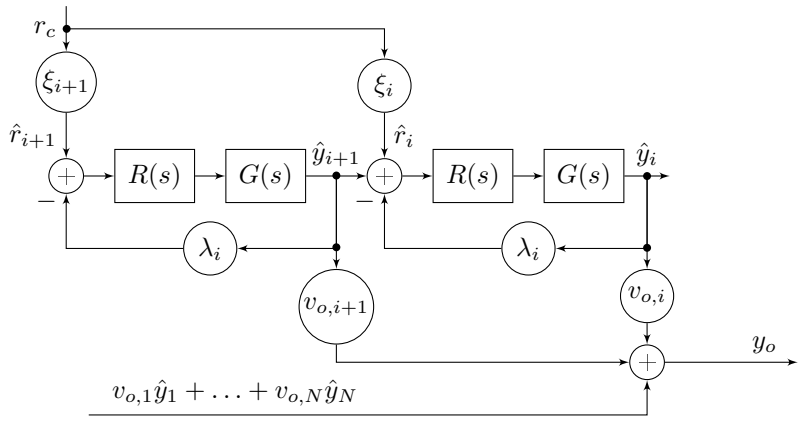

Figure 3.3: One diagonal block for the case of Jordan block of size 2. The eigenvalue λ_i acts as a gain in the feedback. Only one closed loop is present if the Jordan block has a size one.

This easily generalizes to larger Jordan blocks. The structure is shown in Fig. 3.3.

For simplicity, the derivations throughout this section will be shown only for the case where all Jordan block in Λ are simple—the eigenvalues λ_i have the same algebraic and geometric multiplicity. All the proofs can be conducted the same way for blocks of larger size and all the results remain valid.

If the eigenvalue λ_i is simple, the input to the ith diagonal block in (3.10) is the ith element of $\hat{r}$ and equals $\hat{r}_i = \bar{e}_i^T V^{-1} \bar{e}_c r_c = \xi_i r_c$ with $\xi_i = \bar{e}_i^T V^{-1} \bar{e}_c = (V^{-1})_{ic}$. Thus, the input r_c enters the block $F_i(s)$ through the gain ξ_i and from (3.11) $\hat{y}_i(s) = F_i(s)\xi_i r_c(s)$. The output of the ith agent can be obtained using the outputs of the blocks as $y_i(s) = \sum_{j=1}^{N} v_{ij}\hat{y}_j(s)$. By setting $\hat{y}_j(s) = F_i(s)\xi_i r_c(s)$ in the previous equation, the output of the output node is

$$y_o(s) = \left[\sum_{i=1}^{N} v_{oi}\xi_i F_i(s)\right] r_c(s) = T_{co}(s) r_c(s). \tag{3.13}$$

This also expresses the transfer function $T_{co}(s)$ in (3.8).

3.3 Transfer functions in graphs

In this section we derive the structure of the transfer function $T_{co}(s)$ between the input r_c of the control node and output of the output node y_o.

3.3.1 Single integrator dynamics

Before investigating the general case with higher-order dynamics, let us discuss a standard single-integrator case. We will later relate it to the higher-order dynamics. For the single single-integrator case $M(s) = \frac{1}{s}$ and the state-space description of the network system is

$$\dot{x} = -Lx + \bar{e}_c r_c, \quad y_o = \bar{e}_o^{\mathrm{T}} x. \tag{3.14}$$

Let the single-integrator transfer function from r_c to y_o be a fraction of two polynomials as

$$T_{co}(s) = \frac{y_o(s)}{r_c(s)} = \frac{h(s)}{g(s)}. \tag{3.15}$$

From the state-space description, the transfer function can be obtained as $T_{co}(s) = \bar{e}_o^{\mathrm{T}}(sI + L)^{-1}\bar{e}_c$. The denominator polynomial $g(s)$ is given as

$$g(s) = \det(sI_N + L) = s^N + g_{N-1}s^{N-1} + \ldots + g_1 s + g_0. \tag{3.16}$$

$g(s)$ is a characteristic polynomial of $-L$. The roots of g (i. e., the poles of $T_{co}(s)$ for single-integrator dynamics) are $-\lambda_i$, the eigenvalues of $-L$. The coefficient $g_0 = 0$ because there is always a zero eigenvalue of $-L$. If the zero eigenvalue is simple, it is known that the coefficients are

$$g_{N-1} = \sum_{i=1}^{N} \lambda_i, \quad g_{N-2} = \sum_{i=1, j=1, i\neq j}^{N} \lambda_i \lambda_j, \quad \ldots, \quad g_1 = \prod_{i=2}^{N} \lambda_i. \tag{3.17}$$

The other terms g_k are sums of all products of k eigenvalues.

The numerator polynomial is given as $h(s) = h_{N_n} s^{N_n} + \ldots + h_1 s + h_0$. It was shown in [Briegel et al., 2011; Abad Torres and Roy, 2013] that $N_n = N - \delta_{co} - 1$ with δ_{co} being the distance of nodes c, o. We denote the roots of $h(s)$ as $-\gamma_i$, so

$$h(s) = h_{N_n}(s + \gamma_1)(s + \gamma_2)\ldots(s + \gamma_{N_n}). \tag{3.18}$$

The coefficients of $g(s)$ and $h(s)$ have a graph-theoretic representation. For the

denominator polynomial $g(s)$ they are given by [Chebotarev and Agaev, 2002, Proposition 2] as $g_i = \vartheta(\mathcal{F}_{N-i})$, which is the weight of the set of all diverging forests in the graph with $N-i$ arcs[2]. This also explains why $g_0 = 0$ — there is no spanning forest with N arcs (there has to be a cycle in N arcs).

The numerator polynomial can be calculated as

$$h(s) = \bar{e}_o^{\mathrm{T}} \operatorname{adj}(sI + L)\, \bar{e}_c, \tag{3.19}$$

which is the o,cth cofactor of $(sI + L)$. It is shown in [Chebotarev and Agaev, 2002, Proposition 3] that

$$\operatorname{adj}(sI + L) = \sum_{i=0}^{N} Q_i s^{N-i-1}. \tag{3.20}$$

Lemma 3.2. *The coefficients h_i are given as $h_i = \vartheta(\mathcal{F}^{c\to o}_{N-i-1})$.*

Proof. The polynomial $h(s)$ equals the o,c element of $\operatorname{adj}(sI + L)$ (3.19). The coefficient at s^i in $h(s)$ is by (3.20) equal to the o,c element of matrix Q_{N-i-1}, i.e., $h_i = q_{oc}^{N-i-1}$. By (2.3) this element also must be equal to $\vartheta(\mathcal{F}^{c\to o}_{N-i-1})$. □

This indicates that the coefficients h_i are given as the weights of the set of all spanning diverging forests with $N-i-1$ arcs which contain o and diverge from c. In the case of unweighted graph the weight reduces to the number of such out-forests.

While the coefficients in the denominator polynomial correspond to all diverging forests with the given number of arcs, the numerator polynomial takes only those spanning out-forests containing the control and the output nodes.

3.3.2 Higher order dynamics

Now let us go back to higher-order systems. We have the definition of $-\gamma_i$ as the roots of $h(s)$ in (3.18), so we can state the main theorem of this chapter. It relates the single-integrator systems to the higher-order dynamics.

[2] Please see Section 2.1 for the notation in graph theory

Theorem 3.3. *The transfer function $T_{co}(s)$ can be written as*

$$T_{co}(s) = \frac{y_o(s)}{r_{c(s)}} = \vartheta_{co} \frac{[b(s)q(s)]^{1+\delta_{co}} \prod_{i=1}^{N-1-\delta_{co}} \Big(a(s)p(s) + \gamma_i b(s)q(s)\Big)}{\prod_{i=1}^{N} \Big(a(s)p(s) + \lambda_i b(s)q(s)\Big)}, \quad (3.21)$$

where $\vartheta_{co} = h_{N-\delta_{co}-1}$ is the sum of weights of all shortest paths from c to o, δ_{co} is the distance from c to o and the gains $-\gamma_i$ defined in (3.18) are the roots of $h(s)$.

The proof can be found in Sec. 3.8.1. It is clear that the roots $-\gamma_i$ of the numerator polynomial $h(s)$ in single-integrator dynamics have the same role as the roots $-\lambda_i$ of the denominator polynomial $g(s)$. As can be seen, the structure of the terms in the numerator and the denominator of (3.21) is $a(s)p(s) + k\, b(s)q(s)$, where $k = \lambda_i$ in the denominator and $k = \gamma_i$ in the numerator. In addition, such structure is the same as the structure of the characteristic polynomial of an output-feedback system with the open loop $M(s) = k\,\frac{b(s)q(s)}{a(s)p(s)}$ with the gain $k = \lambda_i$ or $k = \gamma_i$.

If both γ_i and λ_i are real, the poles and zeros of (3.21) lie on the root-locus curve (see Fig. 3.7 for an example).

Definition 3.4 (Root-locus curve)**.** *The root-locus curve is defined as a location of roots of $a(s)p(s) + k\, b(s)q(s)$ as a function of $k \in (0, \infty)$.*

Note that both the terms in the numerator and denominator of (3.21) have the form of the root-locus curve.

A particular case of the product form (3.21) was shown in [Lin et al., 2012a, Prop. 3], where the authors considered single integrators ($M(s) = 1/s$) and unidirectional interaction.

The product form in (3.21) can be written also as

$$T_{co}(s) = \vartheta_{co} \prod_{i=1}^{N-\delta_{co}-1} Z_{ii}(s) \prod_{j=N-\delta_{co}}^{N} \frac{1}{\lambda_j} \prod_{j=N-\delta_{co}}^{N} T_j(s), \quad (3.22)$$

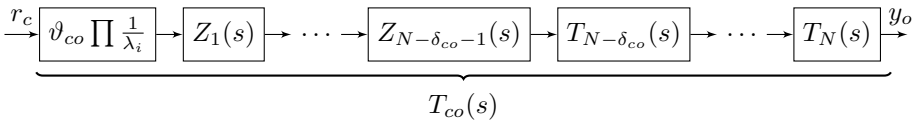

Figure 3.4: Series form of the transfer function $T_{co}(s)$. The product is $\prod_{i=N-\delta_{co}}^{N} \frac{1}{\lambda_i}$ and we used shorthand notation $Z_i(s) = Z_{ii}(s)$.

with

$$Z_{ii}(s) = \frac{a(s)p(s) + \gamma_i b(s)q(s)}{a(s)p(s) + \lambda_i b(s)q(s)}, \tag{3.23}$$

$$T_j(s) = \frac{\lambda_j b(s)q(s)}{a(s)p(s) + \lambda_j b(s)q(s)}. \tag{3.24}$$

All eigenvalues λ_i must be used, so $N - \delta_{co} - 1$ of them go to $Z_{ii}(s)$ and the remaining $\delta_{co} + 1$ to $T_j(s)$. The transfer functions $Z_{ii}(s)$ are biproper and the numerator differs from the denominator only in the multiplication factor γ_i. The transfer functions $T_j(s)$ are standard output feedback systems in (3.11).

The network system (3.7) of identical agents with arbitrary interconnection was transformed in equation (3.22) to a series connection (product of transfer functions) of non-identical (but structured) subsystems. In many cases, such as in determining a frequency response, the series connection is much easier to analyze, see Chapter 4. The series connection is illustrated in Fig. 3.4.

As the numerator of the open loop $b(s)q(s)$ is present for $\delta_{co}+1$ times in (3.21), we have the following corollary.

Corollary 3.5. *The transfer function $T_{co}(s)$ has $\delta_{co} + 1$ multiple zeros at the locations of the zeros of the open loop, i. e. roots of $b(s)q(s) = 0$.*

These zeros can be partly chosen by the designer of the network, since he can choose the controller numerator $q(s)$ freely. On the contrary, the zeros of $Z_{ii}(s)$ are given by the interconnection matrix in the same way as the poles are.

A relative degree comes immediately from Theorem 3.3.

Corollary 3.6. *Let χ be the relative degree of $M(s)$. Then the relative degree χ_{co} of $T_{co}(s)$ is $\chi_{co} = (\delta_{co} + 1)\chi$.*

Proof. There is $N - \delta_{co} - 1$ blocks of type $Z_{ii}(s)$ in (3.21), which have relative

degree 0. Then there is $\delta_{co}+1$ terms $T_i(s)$ which have relative degree χ. Hence, $\chi_{co} = (\delta_{co}+1)\chi$. □

The relative degree strongly affects the transients. The transfer functions $Z_{ii}(s)$ have relative order 0, so the input gets directly to the output. The $\delta_{co}+1$ terms $T_j(s)$ slow down the transient. Quite clearly, the further the control and observer nodes are from each other, the slower the transient will be.

Another immediate result is the steady-state value.

Corollary 3.7. *For at least one integrator in the open loop ($\eta \geq 1$), the steady-state gain of any transfer function in the network system is*

$$T_{co}(0) = \vartheta_{co} \frac{\prod_{i=1}^{N-1-\delta_{co}} \gamma_i}{\prod_{i=1}^{N} \lambda_i}. \tag{3.25}$$

Proof. For at least one integrator in the open loop, $a(0)p(0) = 0$. After plugging this to (3.21), the result follows. □

At least one integrator in the open loop is a common requirement to allow an uncontrolled network system to have a nonzero equilibrium.

The most important fact following from the Corollary 3.7 is that the steady-state gain *does not depend* on the open-loop model, as long as there is at least one integrator in $M(s)$. To change the steady-state value, the interconnection structure must be modified.

We will discuss two cases. First, assume that $\gamma_i \neq 0$, $\forall i$. Then the eigenvalue $\lambda_1 = 0$ of the Laplacian in the denominator makes the steady-state gain infinite. This happens when there is no independent leader in the network system and it is a result of the "rigid drift" of the network system.

If, on the other hand, there is $\gamma_1 = 0$, the eigenvalue at the origin $\lambda_1 = 0$ will be cancelled. As a result, the steady-state value is bounded. The presence of $\gamma_1 = 0$ is usually caused by the presence of an independent leader in the system. Such a leader cannot be controlled from the network system, hence the zero eigenvalue will be uncontrollable, causing the pole-zero cancellation. If pinning control is used, the steady-state gain is again finite, because the Laplacian is non-singular (see Sec. 3.4.1)

3.4 General transfer functions

In the previous section we analyzed properties of a transfer function from the input of the controller of agent c to the output of the agent o. However, we might also be interested in a transfer function from a general input w_c at the control node to a general output z_o of the output node. In this section we show that the general transfer function has two parts: an open-loop part and a network part.

If pinning control is not used, there is always at least one zero eigenvalue of L, therefore in (3.21) $a(s)p(s)+\lambda_1 b(s)q(s) = a(s)p(s)$, which is the denominator of the open loop $M(s)$. Also at least one numerator polynomial of the open loop $b(s)q(s)$ is present in $T_{co}(s)$ in (3.21). Then the transfer function in (3.21) can be written as

$$\begin{aligned} T_{co}(s) &= \vartheta_{co} M(s) \frac{\Big(b(s)q(s)\Big)^{\delta_{co}} \prod_{j=1}^{N_n} \Big(a(s)p(s)+\gamma_j b(s)q(s)\Big)}{\prod_{i=2}^{N} \Big(a(s)p(s)+\lambda_i b(s)q(s)\Big)} \\ &= M(s) S_{co}(s), \end{aligned} \tag{3.26}$$

where

$$S_{co}(s) = \vartheta_{co} \frac{\Big(b(s)q(s)\Big)^{\delta_{co}} \prod_{j=1}^{N_n} \Big(a(s)p(s)+\gamma_j b(s)q(s)\Big)}{\prod_{i=2}^{N} \Big(a(s)p(s)+\lambda_i b(s)q(s)\Big)} \tag{3.27}$$

is the network part of $T_{co}(s)$ and $M(s)$ is the open-loop.

Motivated by this factorization, we will now show a general transfer function. Let $M_{\mathrm{s}}(s)$ be the transfer function in open loop of one agent from the desired input w_i (e. g. a reference or a disturbance) to the desired output z_i of same agent, i. e., $M_{\mathrm{s}}(s) = z_i(s)/w_i(s)$.

Theorem 3.8. *The transfer function $T_{wz,co}(s)$ from the input of the control agent w_c to the output z_o of the output agent is given as*

$$T_{wz,co}(s) = \frac{z_o(s)}{w_c(s)} = M_{\mathrm{s}}(s)\, S_{co}(s). \tag{3.28}$$

Proof. Consider first that the control and the output nodes are collocated ($c = o$). Then by changing the input from r_c to w_c and the output from y_o to z_o we just change the direct branch of the transfer function $T_{cc}(s)$. The direct branch is then $M_{\mathrm{s}}(s)$ instead of $M(s)$. The network (feedback) part S_{cc} in (3.27) remains

unchanged. That is,

$$\frac{z_c(s)}{w_c(s)} = M_{\mathrm{s}}(s)S_{cc}(s). \tag{3.29}$$

Consider now that c and o are not collocated. Define two transfer functions of a single agent:

$$M_1(s) = \frac{y_i(s)}{w_i(s)}, \quad M_2(s) = \frac{z_i(s)}{r_i(s)}. \tag{3.30}$$

Note that $\frac{M_1(s)M_2(s)}{M(s)} = \frac{[y_i(s)/w_i(s)]\,[z_i(s)/r_i(s)]}{y_i(s)/r_i(s)} = M_{\mathrm{s}}(s)$.

The transfer function from $y_c(s)$ to $y_o(s)$ using the input $r_c(s)$ is

$$\frac{y_o(s)}{y_c(s)} = \frac{r_c(s)M(s)S_{co}(s)}{r_c(s)M(s)S_{cc}(s)} = \frac{S_{co}(s)}{S_{cc}(s)}. \tag{3.31}$$

From (3.29) we get $y_c(s) = M_1(s)S_{cc}w_c(s)$. Plugging this to (3.31) gives

$$y_o(s) = \frac{S_{co}(s)}{S_{cc}(s)}M_1(s)S_{cc}(s)w_c(s) = M_1(s)S_{co}(s)w_c(s). \tag{3.32}$$

Similarly, the transfer function from $z_o(s)$ to $y_o(s)$ is

$$\frac{y_o(s)}{z_o(s)} = \frac{r_o(s)M(s)S_{oo}(s)}{r_o(s)M_2(s)S_{oo}(s)} = \frac{M(s)}{M_2(s)}, \tag{3.33}$$

therefore $y_o(s) = M(s)/M_2(s)z_o(s)$. Plugging this to (3.32) and separating $z_o(s)$ yields

$$z_o(s) = \frac{M_1(s)M_2(s)}{M(s)}S_{co}(s)w_c(s) = M_{\mathrm{s}}(s)S_{co}(s)w_c(s). \tag{3.34}$$

The transfer function $T_{\mathrm{wz},co}(s)$ follows. □

The general structure is shown in Fig. 3.5. It follows that each transfer function in the network system is given by two parts:

1. the network part $S_{co}(s)$, which is the same for all transfer functions with the same c and o nodes and is given by the interconnection,
2. the open-loop part $M_{\mathrm{s}}(s)$, which depends on the inputs and outputs of interest.

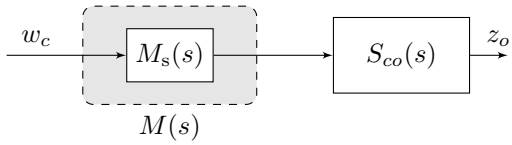

Figure 3.5: Two parts of transfer functions between c and o for general input and output.

3.4.1 Pinning control

The results in previous section holds for the case when $\lambda_1 = 0$. When pinning control scheme is used, we get rid of this eigenvalue. Assume that the original system with pinning had $N-1$ agents. In order to use the result of Theorem 3.8, we have to incorporate the leader into the network system by modifying the Laplacian with pinning as follows

$$L = \begin{bmatrix} 0 & 0 \\ v & L_{\mathrm{p}} \end{bmatrix}, \tag{3.35}$$

where $v = [\rho_1, \rho_2, \ldots, \rho_{N-1}]^{\mathrm{T}}$ captures the interconnection with the leader. It is shown in Lemma 4.6 that the nonzero eigenvalues of L and L_{p} are the same. Since the leader is independent of the network system, it is also not controllable from the system. Therefore, the zero gain $\lambda_1 = \gamma_1 = 0$ will be both in the numerator and in the denominator. The transfer function with Laplacian in (3.35) is

$$\begin{aligned} T_{co}(s) &= M_{\mathrm{s}}(s) S_{co}(s) \\ &= M_{\mathrm{s}}(s) \frac{[b(s)q(s)]^{\delta_{co}} \prod_{i=1}^{N-\delta_{co}-1} \Big(a(s)p(s) + \gamma_i b(s)q(s)\Big)}{\prod_{j=2}^{N} \Big(a(s)p(s) + \lambda_j b(s)q(s)\Big)} \\ &= M_{\mathrm{s}}(s)a(s)p(s) \frac{[b(s)q(s)]^{\delta_{co}} \prod_{i=2}^{N-\delta_{co}-1} \Big(a(s)p(s) + \gamma_i b(s)q(s)\Big)}{\prod_{j=2}^{N} \Big(a(s)p(s) + \lambda_j b(s)q(s)\Big)} \\ &= M_{\mathrm{s}}(s)a(s)p(s)\overline{S_{co}}(s), \end{aligned} \tag{3.36}$$

where $\overline{S_{co}}(s)$ is feedback part of the transfer function when L is used. Thus, in pinning control, the equation (3.28) changes to (3.36).

3.4.2 Disturbances

First we analyze an input disturbance $d_{\text{in}c}$, acting at the input of the plant. The modified open-loop transfer function is $M_{\text{s}}(s) = G(s)$. Then the transfer function is

$$T_{\text{in},co}(s) = \frac{y_o(s)}{d_{\text{in}\,c}(s)} = G(s)S_{co}(s). \tag{3.37}$$

It is clear that $T_{co}(s)$ and $T_{\text{in},co}(s)$ differ only in the presence of transfer function of the controller and $T_{co}(s) = R(s)T_{\text{in},co}(s)$.

The output disturbance d_{out} changes the output of the plant of the jth agent as $y_j = \bar{y}_j + d_{\text{out}\,j}$, where $\bar{y}_i$ is the output of the agent without disturbance. In this case $M_{\text{s}}(s) = 1$, so the transfer function for output disturbance is

$$T_{\text{out},co}(s) = \frac{y_o(s)}{d_{\text{out}\,c}(s)} = S_{co}(s). \tag{3.38}$$

3.4.3 State-space model

So far we have discussed the situation when the vehicle and controller model are given as SISO transfer functions. However, the output-feedback control is less common in the distributed control literature than static-state feedback based on the relative error to the neighbors (see Section 2.2.2). Let us now convert the state-space description to transfer functions, using the fact that agents under consideration are SISO systems. Assume that there is only one input to the network system r_c and one output y_o. The closed-loop system then using the model in (2.17) is

$$\begin{aligned} \dot{x} &= (I \otimes A - L \otimes BK)x + (\bar{e}_c \otimes B)r_c \\ y_o &= (\bar{e}_o \otimes C)x. \end{aligned} \tag{3.39}$$

Corollary 3.9. *The transfer function from the input $r_c(s)$ to the output $y_o(s)$ in the system (3.39) is*

$$T_{co}(s) = \vartheta_{co} M_{\text{s}}(s)\, \frac{[b(s)]^{\delta_{co}} \prod_{i=1}^{N-1-\delta_{co}} \Big(a(s) + \gamma_i b(s)\Big)}{\prod_{i=2}^{N} \Big(a(s) + \lambda_i b(s)\Big)}, \tag{3.40}$$

where the transfer function $M_{\text{s}} = \frac{c(s)}{a(s)} = C(sI - A)^{-1}B$ and the polynomials

$a(s)$, $b(s)$ are defined as $M(s) = \frac{b(s)}{a(s)} = K(sI - A)^{-1}B$.

Proof. Assume that $R(s) = 1$ or that the controller model is already included in the matrices A, B, C, K. Then for a SISO agent model the transfer function in the system

$$\begin{aligned} \dot{x} &= (I \otimes A - L \otimes BK)x + (\bar{e}_c \otimes B)r_c \\ y_o &= (\bar{e}_o \otimes K)x. \end{aligned} \tag{3.41}$$

is given by (3.21), because it has the same form as (2.18) for which the product form was derived. Notice that the system (3.41) differs from the system of interest (2.17) only in the output equation. Hence, the poles of the open-loop will not change. This means that we can use Theorem 3.8. □

3.5 Relations to a single-integrator case

In this section we provide some results for the single-integrator case. They easily generalize to higher-order dynamics, because of the fact that γ_i, the gain in the closed loop in (3.21), is the same as the zero in the single-integrator dynamics. Let us denote $\bar{L}^k_{i:j}$ as a matrix which is obtained from L by deleting the rows and columns corresponding to the vertices on the kth path from vertex i to j.

The simplest case is when the controller node and observer nodes are collocated, i.e. $c = o$. Then, as shown in [Briegel et al., 2011; Abad Torres and Roy, 2014; Herman et al., 2014b], the zeros are given as eigenvalues of $\bar{L}^1_{c:c}$ and the numerator polynomial is

$$h(s) = \det(sI + \bar{L}^1_{c:c}). \tag{3.42}$$

The spectrum of this reduced Laplacian (also known as a grounded Laplacian) is discussed in [Pirani and Sundaram, 2014, 2015].

The next theorem was independently discovered in [Abad Torres and Roy, 2013] using purely algebraic techniques. Here we provide a graph-theoretic proof, shown in Sec. 3.8.2.

Theorem 3.10. *If there is only one path between the control node and the output node, then*

$$h(s) = \vartheta_{co} \det\left(sI + \bar{L}^1_{c:o}\right). \tag{3.43}$$

The roots $-\gamma_i$ of $h(s)$ are the eigenvalues of $-\bar{L}^1_{c:o}$.

The theorem allows to find γ_i directly from the submatrix of the Laplacian. The real part of γ_i is positive, since the matrix $\bar{L}^1_{c:o}$ is still an M-matrix [Horn and Johnson, 1999]. In addition, if L is a symmetric matrix and the conditions in Theorem 3.10 hold, then γ_i interlace with λ_i due to the Cauchy interlacing theorem (Lem. 2.2).

The second theorem is an extension of the previous one.

Theorem 3.11. *Let $p(\mathcal{G})_{c,o}$ be the number of paths from the node c to the node o. Then the numerator polynomial $h(s)$ in (3.15) is given as a sum of characteristic polynomials of $\bar{L}^i_{c:o}$ corresponding to the individual paths π^i_{co}, i. e.*

$$h(s) = \sum_{i=1}^{p(\mathcal{G})_{c,o}} \vartheta(\pi^i_{co}) \det(sI + \bar{L}^i_{c:o}), \tag{3.44}$$

Proof. Since there are $p(\mathcal{G})_{c,o}$ paths between the nodes, there are also $p(\mathcal{G})_{c,o}$ basic trees diverging from c and containing o (they can have different lengths). For each of the paths Theorem 3.10 must hold. Let us denote the weight of spanning forests with $N-\delta^k_{co}-1-i$ arcs corresponding to the path k with length δ^k_{co} as h^k_i. Since the paths are distinct, also the spanning forests corresponding to the paths will be distinct and the total weight of the set $\mathcal{F}^{i\to j}_k$ is the sum of the weights of the individual forests, corresponding to each of the path. Then each coefficient in $h(s)$ is a sum of the weights of the trees corresponding to each path, i. e.

$$h_i = \sum_{k=1}^{p(\mathcal{G})_{c,o}} h^k_i. \tag{3.45}$$

Equation (3.44) then follows from (3.45) using Theorem 3.10. □

3.5.1 Multiple control nodes

Instead of one control node c we can have a set $\mathcal{S}_c = \{c_1, c_2, \ldots, c_{N_c}\}$ of N_c control nodes to which the same signal is fed (for instance, the leader connected to more agents). Then the numerator polynomial is simply given as a sum of polynomials for individual control nodes.

Lemma 3.12. *The polynomial $h(s)$ for the set of control nodes $\mathcal{S}_c$ is equal to $h(s) = \sum_{i=1}^{N_c} h_i(s)$, where $h_i(s)$ is the polynomial when the input is fed only to the ith agent.*

Table 3.1: Controllable subspaces for some typical undirected graphs with N vertices.

Graph	c node	$\max_i d_{ci}$	Dim. of ctrb. subs.
Star graph	central	1	2
Path graph	end node	$N-1$	N
Path graph	central node	$N/2$	$N/2+1$

Proof. The proof can be obtained using the same arguments of mutually exclusive forests as in the proof for Theorem 3.11. □

Suppose that $c_n \in \mathcal{S}_c$ is the node in $\mathcal{S}_c$ with the shortest distance to the output node. Then the relative degree of the transfer function $T_{co}(s)$ between $\mathcal{S}_c$ and o with agents having higher order-dynamics is $\chi_{co} = (\delta_{c_n o} + 1)\chi$. This follows since the degree of the sum of polynomials is the degree of the polynomial of the highest degree.

3.5.2 Minimal dimension of a controllable subspace

From equation (3.21) it follows that if the single-integrator case is uncontrollable, so are all the systems with higher order dynamics (we use an output feedback). The following result is an extension of [Zhang et al., 2014, Thm. 2] to directed graphs.

Theorem 3.13. *Let* $\max_i d_{ci}$ *be the maximal distance to some of the other nodes from the control node* c*. Then for the dimension of the controllable subspace* $\operatorname{rank}(\mathcal{C})$ *of single integrator dynamics holds* $\operatorname{rank}(\mathcal{C}) \geq \max_i d_{ci} + 1$.

Proof. Let us denote the furthest node from c as f and the distance of f from c as $d_f = \max_i d_{ci}$. Let L_c^i denote the cth column in L^i. Let the vertices on the shortest path from c to f be labeled as $\nu_0, \ldots, \nu_{d_f}$ and the distance of ν_i from c as δ_i. By Lemma 2.5 the ν_ith element in L_c^j is zero for all $j < d_i$ and is nonzero for $j \geq d_i$. Therefore, $L_c^{d_i}$ is linearly independent of L_c^j for $j < d_i$ and $d_i = 0, \ldots, d_f$. Consequently, all columns $[L_c^0, L_c^1, \ldots, L_c^{d_f}]$ must be linearly independent.

The controllability criterion matrix is defined as $\mathcal{C} = [L_c^0, L_c^1, \ldots, L_c^N]$. By previous development we know that at least $L_c^0, \ldots L_c^{d_f}$ are linearly independent, hence $\operatorname{rank}(\mathcal{C}) \geq d_f + 1$. □

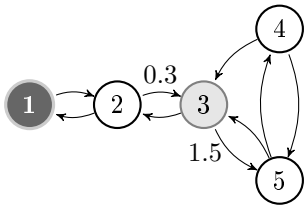

Figure 3.6: Directed graph used in the example. Control node is $c = 1$, output node is $o = 3$. The arcs without a weight shown have a weight one.

Of course, the controllable subspace can be much greater than indicated by this theorem and our result can be very conservative. The bound is achieved for some graphs and control nodes, as shown in Table 3.1. Some further discussion of the tightness of the bound is in [Zhang et al., 2014, Remark 2]. Theorem 3.13 gives a strong structural controllability, since it does not depend on the weights of the arcs. By any choice of the nonzero weights of arcs, the controllable subspace cannot have smaller dimension than $\max_i d_{ci} + 1$. Structural controllability is described, e.g., in [Chapman and Mesbahi, 2013; Clark et al., 2014].

Surprisingly, the more distant node exists in a graph, the greater the guaranteed dimension of the controllable subspace. On the other hand, it was shown in [Shi et al., 2014] that the transient time grows with the maximal distance from the control node. Similarly, at least for a path graph it follows from [Fitch and Leonard, 2013] that the external input should be applied to the agent where it minimizes the maximal distance. This is also confirmed by the relative degree in Corollary 3.6—the higher the degree, the slower is the information propagation. However, in this case the node has the smallest guaranteed dimension of the controllable subspace. An optimization procedure for the trade-off between performance and controllability is presented in [Clark et al., 2014].

3.6 Illustrative example

Consider a directed and weighted graph with five nodes shown in Fig. 3.6. The plant is $G(s) = 1/s$, the controller is $R(s) = (s + 1)/s$ (a PI controller applied to a single integrator). The open-loop model is $M(s) = \frac{s+1}{s^2}$. Let us choose the control node $c = 1$ and the output node $o = 3$. The transfer function is

$$T_{13}(s) = 0.3\frac{(s+1)^3 \prod_{i=1}^{2}(s^2 + \gamma_i s + \gamma_i)}{\prod_{i=1}^{5}(s^2 + \lambda_i s + \lambda_i)}. \tag{3.46}$$

with $\lambda = \{0, 0.39, 2, 2.72, 3.69\}$ and $\gamma = \{0.5, 3\}$. As indicated by (3.21), the terms in the numerator and the denominator products have the structure of $a(s)p(s) + kb(s)q(s)$. Moreover, since the distance between the nodes 1 and 3 is 2, there is also $(s+1)^{2+1}$ in the numerator, as follows from Corollary 3.5. The weight of the path from the node 1 to 3 is 0.3 (the product of the weights of the arcs). The gains λ_i can be obtained as the eigenvalues of the Laplacian matrix

$$L = \begin{bmatrix} 1 & -1 & 0 & 0 & 0 \\ -1 & 2 & -1 & 0 & 0 \\ 0 & -0.3 & 2.3 & -1 & -1 \\ 0 & 0 & 0 & 1 & -1 \\ 0 & 0 & -1.5 & -1 & 2.5 \end{bmatrix}. \tag{3.47}$$

The gains γ_i in the numerator can be obtained as the negatives of the roots of the polynomial $h(s) = s^2 + 3.5s + 1.5$. Since there is only one path between c and o, we can use Theorem 3.10 to calculate the polynomial $h(s)$. It equals the characteristic polynomial of a matrix $\bar{L}^1_{(1:3)}$, obtained from L by deleting the rows and columns with indices $1, 2, 3$ of the vertices on the path from 1 to 3. The polynomial is given as

$$h(s) = \det\left(sI_2 + \begin{bmatrix} 1 & -1 \\ -1 & 2.5 \end{bmatrix} \right) = s^2 + 3.5s + 1.5. \tag{3.48}$$

As both γ_i and λ_i are real in this example, the poles and zeros must lie on the root-locus curve for $M(s) = (s+1)/s^2$, as shown in Fig. 3.7. The minimal dimension of the controllable subspace is by Theorem 3.13 equal to five ($\delta_{14}+1 = 4+1$), hence, the system is controllable from the node 1.

The transfer function $T_{\mathrm{wz},13}(s)$ from the input disturbance $d_{\mathrm{in}1}$ of agent 1 to the output y_3 is

$$T_{\mathrm{in},13}(s) = \frac{y_3(s)}{d_{\mathrm{in}1}(s)} = 0.3\frac{1}{s}\frac{(s+1)^2\prod_{i=1}^{2}(s^2+\gamma_i s+\gamma_i)}{\prod_{i=2}^{5}(s^2+\lambda_i s+\lambda_i)}. \tag{3.49}$$

The structure is the same as predicted in Theorem 3.8, since $M_{\mathrm{s}}(s) = G(s) = 1/s$. The network part remains unchanged.

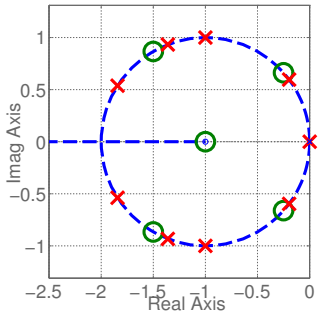

Figure 3.7: Poles (crosses) and zeros (circles) of $T_{13}(s)$ in the graph in Fig. 3.6. The root-locus curve for $M = (s+1)/s^2$ is dashed.

3.7 Conclusion

In this chapter we considered transfer functions between two nodes in an arbitrary network system of identical SISO agents with an output coupling. Using the algebraic properties of forests in the graph, both numerator and denominator of the transfer function were derived in a simple form of a product of closed-loop polynomials with non-unit feedback gain. The transfer function for general input and output consists of two parts: the feedback part (fixed for a given pair of nodes) and the open-loop part.

The gains in the denominator and numerator polynomials are the roots of polynomials in the single-integrator system. If there is only one path between the control and output nodes, the numerator gains are given as eigenvalues of the principal submatrix of the Laplacian. Finally, it is shown that the minimal dimension of the controllable subspace grows with the maximal distance from the control node.

Although it is hard to tell any transient properties from the location of poles and zeros — there are simply too many of them — still the product form can serve as an analytical tool. For instance, it may help in the analysis of the scaling in distributed control designs, as will be illustrated in the next chapter.

3.8 Appendix

3.8.1 Proof of Theorem 3.3

Before the proof, we need the following technical lemma.

Lemma 3.14. *Let $(L^k)_{oc}$ be the o,c element of L^k. Then*

$$\sum_{i=1}^{N} \xi_i v_{oi} \lambda_i^k = (L^k)_{oc}, \tag{3.50}$$

Proof. Since $\xi_i = \bar{e}_i^T V^{-1} \bar{e}_c$ and $v_{oi} = \bar{e}_o^T V \bar{e}_i$, we get

$$\begin{aligned}\sum_{i=1}^{N} v_{o,i} \lambda_i^k \xi_i &= \sum_{i=1}^{N} \bar{e}_o^T V \bar{e}_i \lambda_i^k \bar{e}_i^T V^{-1} \bar{e}_c \\ &= \bar{e}_o^T V \left(\sum_{i=1}^{N} \bar{e}_i \lambda_i^k \bar{e}_i^T \right) V^{-1} \bar{e}_c = \bar{e}_o^T V \Lambda^k V^{-1} \bar{e}_c \\ &= \bar{e}_o^T L^k \bar{e}_c = (L^k)_{oc}. \end{aligned} \tag{3.51}$$

This holds also for Jordan blocks in Λ larger than one. □

Proof of Theorem 3.3. Let us denote the numerator of the open loop in (3.3) as $\phi(s) = b(s)q(s)$ and the denominator as $\psi(s) = a(s)p(s)$. Note that the development here shows the case with simple Jordan blocks, although the proof remains valid for the case with larger blocks. The transfer function $T_{co}(s)$ can be obtained from (3.13) by using a common denominator as

$$T_{co}(s) = \frac{n(s)}{d(s)} = \sum_{i=1}^{N} \xi_i v_{oi} \frac{b(s)q(s)}{a(s)p(s) + \lambda_i b(s)q(s)} \tag{3.52}$$

$$= \frac{\sum_{i=1}^{N} \left(\xi_i v_{oi}\, \phi(s) \prod_{j=1, j\neq i}^{N} [\psi(s) + \lambda_j \phi(s)] \right)}{\prod_{i=1}^{N} [\psi(s) + \lambda_i \phi(s)]}$$

$$= \frac{\sum_{i=1}^{N} \xi_i v_{oi}\, \tau_i(s)}{\prod_{i=1}^{N} [\psi(s) + \lambda_i \phi(s)]}, \tag{3.53}$$

with $\tau_i(s) = \phi(s) \prod_{j=1, j\neq i}^{N} [\psi(s) + \lambda_j \phi(s)]$. Note that the polynomials in single-integrator dynamics are $h(s), g(s)$, while in higher-order dynamics they are $n(s), d(s)$. The denominator of (3.53) is the denominator in Theorem 3.3.

Having the denominator, we have to find the numerator $n(s)$. The polynomial

$\tau_i(s)$ in (3.53) can be expanded in terms of powers of $\phi(s)$ and $\psi(s)$ as

$$\begin{aligned}\tau_i(s)= \phi(s) \prod_{j=1,j\neq i}^{N} [\psi(s)+\lambda_j\phi(s)] = \psi^{N-1}(s)\phi(s) \\ +\psi^{N-2}(s)\phi^2(s)\left[\sum_{j=1,j\neq i}^{N}\lambda_j\right] + \psi^{N-3}(s)\phi^3(s)\left[\sum_{j=1,k=1,k\neq i\neq j}^{N}\lambda_j\lambda_k\right] \\ +\ldots+\psi^1(s)\phi^{N-1}(s)\left[\sum_{j=1,j\neq i}^{N}\left(\prod_{k=1,k\neq i\neq j}^{N}\lambda_k\right)\right]+\phi^N(s)\left[\prod_{j=1,j\neq i}^{N}\lambda_j\right].\end{aligned} \tag{3.54}$$

Let us denote the the coefficients at the terms $\psi^j(s)\phi^{N-j}(s)$ in $\tau_i(s)$ as $\bar{\tau}_i^j$. They are given as a sum of all products of $N-j-1$ eigenvalues. Then the polynomial $\tau_i(s)$ can be written as

$$\tau_i(s) = \psi^{N-1}(s)\phi(s)+\bar{\tau}_i^{N-2}\psi^{N-2}(s)\phi^2(s)+\ldots+\bar{\tau}_i^1\psi(s)\phi^{N-1}(s)+\bar{\tau}_i^0\phi^N(s). \tag{3.55}$$

The coefficients $\bar{\tau}_i^j$ can be simplified. Let us start with

$$\bar{\tau}_i^{N-2} = \sum_{j=1,j\neq i}^{N}\lambda_j = g_{N-1}-\lambda_i, \tag{3.56}$$

since the coefficient g_{N-1} of $g(s)$ is by (3.17) $g_{N-1} = \sum_{i=1}^{N}\lambda_i$. Similarly, the second coefficient is using (3.17)

$$\bar{\tau}_i^{N-3} = \sum_{j=1,k=1,k\neq i\neq j}^{N}\lambda_j\lambda_k = g_{N-2}-\lambda_i(g_{N-1}-\lambda_i). \tag{3.57}$$

For the last coefficient we get

$$\bar{\tau}_i^0 = \prod_{j=1,j\neq i}^{N}\lambda_j = g_1-\lambda_i(g_2-\lambda_i(g_3-\lambda_i(\ldots))). \tag{3.58}$$

Knowing the coefficients $\bar{\tau}_j^i$, the numerator polynomial $n(s)$ can be using (3.53)

written as

$$\begin{aligned} n(s) = \sum_{i=1}^{N} \xi_i v_{oi} \tau_i(s) &= \psi^{N-1}\phi \left(\sum_{i=1}^{N} \xi_i v_{oi} \right) \\ &+ \psi^{N-2}\phi^2 \left(\sum_{i=1}^{N} \xi_i v_{oi}\, \bar{\tau}_i^{N-2} \right) + \dots \\ &+ \psi\phi^{N-1} \left(\sum_{i=1}^{N} \xi_i v_{oi}\, \bar{\tau}_i^{1} \right) + \phi^N \left(\sum_{i=1}^{N} \xi_i v_{oi}\, \bar{\tau}_i^{0} \right). \end{aligned} \tag{3.59}$$

The coefficients $\bar{h}_i$ of individual powers of $\psi^i\phi^{N-i}$ in $n(s)$ can be simplified using Lemma 3.14 and the formulas for $\bar{\tau}_j^i$ (3.56-3.58). The first two read

$$\bar{h}_{N-1} = \sum_{i=1}^{N} \xi_i v_{oi} = (L^0)_{oc}, \tag{3.60}$$

$$\begin{aligned} \bar{h}_{N-2} = \sum_{i=1}^{N} \xi_i v_{oi}\, \bar{\tau}_i^{N-2} &= g_{N-1} \left(\sum_{i=1}^{N} \xi_i v_{oi} \right) - \sum_{i=1}^{N} \xi_i v_{oi} \lambda_i \\ &= g_{N-1}(L^0)_{oc} - (L^1)_{oc}. \end{aligned} \tag{3.61}$$

Using the same ideas, the other coefficients $\bar{h}_i$ are

$$\bar{h}_{N-3} = g_{N-2}(L^0)_{oc} - g_{N-1}(L^1)_{oc} + (L^2)_{oc}, \tag{3.62}$$

$$\vdots$$

$$\bar{h}_0 = g_1(L^0)_{oc} - g_2(L^1)_{oc} + \dots + (L^{N-1})_{oc}. \tag{3.63}$$

The general form is now apparent,

$$\bar{h}_i = \sum_{j=0}^{N-i-1} g_{i+j+1}(-L)^j_{oc}. \tag{3.64}$$

Using the coefficients $\bar{h}_i$ in (3.60)-(3.63), the numerator $n(s)$ in (3.59) equals

$$\begin{aligned} n(s) = \phi(s) \Big(&\bar{h}_{N-1}\psi(s)^{N-1} + \bar{h}_{N-2}\psi^{N-2}(s)\phi(s) \\ &+ \bar{h}_{N-3}\psi^{N-3}(s)\phi^2(s) + \dots + \bar{h}_0\phi^{N-1}(s) \Big). \end{aligned} \tag{3.65}$$

Now we show that the coefficients $\bar{h}_i$ in (3.65) are equal to the coefficients h_i of the numerator polynomial $h(s)$ in the single integrator dynamics, i.e., $\bar{h}_i = h_i, \forall\, i$.

To see this, Corollary 4 in [Chebotarev and Agaev, 2002] gives us a relation

$$\mathrm{adj}(sI + L) = \sum_{k=0}^{N-1} \left(\sum_{j=0}^{N-k-1} g_i s^{N-j-1} \right) (-L^k/s^k). \tag{3.66}$$

The coefficient matrix Γ_i at s^i in (3.66) is then defined as

$$\Gamma_i = \sum_{j=0}^{N-i-1} g_{i+j+1}(-L)^j. \tag{3.67}$$

Taking as an element of interest the o, cth element in $\mathrm{adj}(sI+L)$, we see by (3.64) that the coefficients $(\Gamma_i)_{oc} = \bar{h}_i$. Moreover, since by (3.19) $\mathrm{adj}(sI+L)_{oc}$ is equal to the numerator polynomial in single-integrator dynamics, we get $h_i = \bar{h}_i$, $\forall i$.

All the coefficients h_i are functions of the powers of the Laplacian. Using Lemma 2.5, it is clear that $h_i = 0$ for $i > N - \delta_{co}$, since all $(L^j)_{oc}$ for $j = 0, 1, \ldots, \delta_{co} - 1$ are zeros. Then in (3.18), $N_n = N - \delta_{co} - 1$ also for directed weighted graphs. This result allows us to rewrite (3.65) as

$$\begin{aligned} n(s) = \phi^{1+\delta_{co}}(s) \Big(& h_{N-\delta_{co}-1} \psi^{N-1-\delta_{co}}(s) \\ & + h_{N-\delta_{co}-2} \psi^{N-2-\delta_{co}}(s)\phi(s) + \ldots + h_0 \phi^{N-1-\delta_{co}}(s) \Big). \end{aligned} \tag{3.68}$$

Previous equation can be factored into a product

$$n(s) = h_{N-\delta_{co}-1} \phi^{1+\delta_{co}}(s) \prod_{i=1}^{N-1-\delta_{co}} \Big(\psi(s) + \gamma_i \phi(s) \Big), \tag{3.69}$$

where the scalars $-\gamma_i$ are the roots of the polynomial $h(s)$ defined in (3.18). They are thus the zeros of the transfer function for the single integrator dynamics.

Note that $\bar{h}_{N-\delta_{co}-1} = h_{N-\delta_{co}-1} = \vartheta_{co}$ by Lemma 3.2. Then we get the numerator as

$$n(s) = \vartheta_{co}\, \phi^{1+\delta_{co}}(s) \prod_{i=1}^{N-1-\delta_{co}} \Big(a(s)p(s) + \gamma_i b(s) q(s) \Big). \tag{3.70}$$

Now in (3.70) and (3.53) we have both the numerator $n(s)$ and the denominator

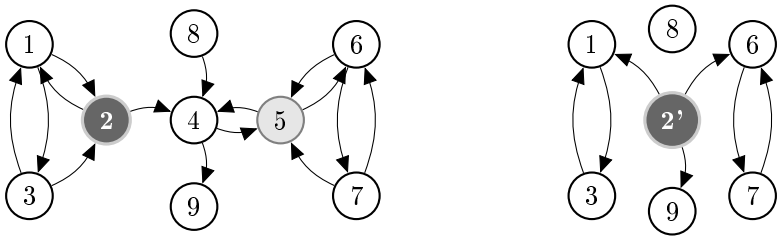

(a) Before reduction

(b) After reduction

Figure 3.8: Graph reduction without changing $h(s)$. The control node is the node 2, output node is 5.

$d(s)$ of (3.21), which concludes the proof. □

3.8.2 Proof of Theorem 3.10

Proof. Recall that by (3.19) $h(s)$ equals (o,c) cofactor of $(sI+L)$. By Lemma 3.2 coefficients h_i of $h(s)$ are the weights of the set of all spanning diverging forests with the root c and containing o having $N-i-1$ arcs, therefore $h_i = 0$ for $i \geq N - \delta_{co}$. In addition, the path from c to o must be present in every spanning forest with more than δ_{co} arcs.

The proof will be shown in several steps of modifying the original graph $\mathcal{G}$ and constructing a new one $\mathcal{G}'$ with the preserved polynomial $h(s)$.

1. Remove all the arcs converging to the path π_{co} from c to o. They cannot be part of any forest diverging from c and containing o.

2. Since by the assumption there is only one path between c and o, the path π_{co} is present in each forest in Lemma 3.2 and the weight $\vartheta_{co} = \vartheta(\pi_{co})$ of the path must be present in all coefficients h_i. We can write

$$h(s) = \vartheta_{co}\bar{h}(s) = \vartheta_{co}\Big(s^{N-1-\delta_{co}} + \mu_{N-2-\delta_{co}}s^{N-2-\delta_{co}} + \ldots + \mu_0\Big). \tag{3.71}$$

   This factoring acts as removing the arcs on the path from the graph.

3. Now we want to find a matrix of which $\bar{h}(s)$ is a characteristic polynomial. By factoring the weight of the path, we identified (created one from many) the vertices on the path into only one new vertex c'. All arcs connected to the path are now connected to the new vertex c'. The control and

output nodes were collocated. Denote such a new graph as $\mathcal{G}^{'}$ with the number of vertices $N(\mathcal{G}') = N - \delta_{co}$. The process of such graph reduction is illustrated in Fig. 3.8.

4. The coefficients μ_i in (3.71) are the weights of the set of all spanning forests in the reduced graph $\mathcal{G}^{'}$, diverging from c' with $N(\mathcal{G}') - i - 1$ arcs. Then, by (3.19-3.20), the polynomial $\bar{h}(s)$ equals the (c', c') cofactor of $(sI_{N-\delta_{co}} + \bar{L}^1_{c:o-1})$. Since the output and control nodes are collocated in the modified graph $\mathcal{G}'$, we can use (3.42) to remove also the node c' from the graph.

In step 3 we deleted all nodes on the path except for the node c. In the last step we were also able to eliminate the control node, so the polynomial $h(s)$ can be calculated as

$$h(s) = \vartheta_{co} \det(sI + \bar{L}^1_{c:o}). \tag{3.72}$$

□

4 Vehicle platoons with proportional asymmetry

In this chapter we give a comprehensive overview of achievable limits and scaling in vehicle platoons described by one special type of bidirectional control law—so called proportional asymmetry. We analyze both symmetric and asymmetric interactions between vehicles, but we restrict ourselves to identical asymmetry used for coupling in all states. It follows from the discussion that for at least two integrators in the open loop this type of asymmetry is not a good solution for platoons. On the other hand, with one integrator the system is very scalable and fast. The findings of this chapter are summarized in Tables 4.2 and 4.3. We show the table also here for convenience.

Property	Symmetric		Asymmetric, $\epsilon < 1$	
	$\eta = 1$	$\eta = 2$	$\eta = 1$	$\eta \geq 2$
Steady-state gain of TF	N	N	bounded	bounded
$\mathcal{H}_\infty$ norm of TF	N	N^2	bounded	ζ^N
$\mathcal{H}_\infty$ norm of TFM	N^2	N^3	N	ζ^N

Table 4.1: Basic properties of various control laws with proportional asymmetry. TF stands for transfer function between the input of one vehicle and output of another, TFM is a transfer function matrix of the overall platoon. η is the number of integrators in the open loop and ϵ is the level of asymmetry—$\epsilon < 1$ means stronger weight towards the vehicle's predecessor. In symmetric control for more than two integrators the platoon becomes asymptotically unstable.

The most important fact is that the scaling results presented in this chapter are generic, that is, they do not (except for some very mild assumptions) depend

on the particular model of the vehicle. The main distinguishing factor is the number of integrators in the open loop. Thus, the results here show the basic properties imposed by the communication topology—the inherent limitations of the topology.

The results of this chapter were published as [Herman et al., 2015b], [Herman et al., 2016b] (conditionally accepted), preliminary results were presented in [Herman et al., 2014a] and some of the result are submitted as [Herman, 2016a,b].

The chapter is structured as follows. First we provide some introduction to vehicle platoons and state the goals of platooning (Sec. 4.1). Afterwards in Section 4.3, the model and the basic quantities for bidirectional control are derived. Then we show results for symmetric bidirectional control (Sec. 4.4) and in the next section asymmetric control is discussed (Sec. 4.5). Subsequently, in Section 4.6, we discuss when and under what conditions it is possible to design a string-stable controller. The transients of individual architectures are compared in Section 4.7. In Section 4.8 we discuss some properties of time-headway spacing policy. Open problems are briefly mentioned in Section 4.9. At the end of the chapter we provide proofs for some results (Sec. 4.11).

4.1 Introduction to platooning

Vehicle platoons are chains of automatically controlled vehicles which travel with a tight spacing. As discussed in the introduction, they are supposed to be the future of the highway traffic. There are still many practical challenges related to the application in everyday traffic, but several successful tests have been already conducted.

Vehicle platoons are just a part of Automated Highway Systems (AHS), which include also intelligent highway infrastructure, communication between vehicles and infrastructure and among vehicles, traffic planning, routing etc [Horowitz and Varaiya, 2000]. The goal of AHS is to increase capacity of the highways and safety of traffic at the same time. One of the assumptions is that the cars will drive automatically on highways.

There are two types of roles in the platoon: one vehicle serves as a platoon leader and the others are just followers. The leader should "command" the platoon because it sees (or can measure) what happens ahead of the platoon. If there is any obstacle, it should either go around (avoid it) or stop, if there is another platoon ahead, it should slow down etc. The goal of the other vehicles is just to keep the prescribed distances or time gaps to some selected vehicles. There are several possible choices of the vehicles used for control:

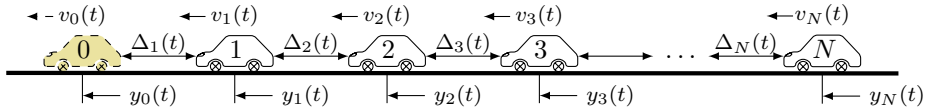

Figure 4.1: A schematic of the platoon. 0 denotes the leader, movement of which the platoon should track. y_i is position of the ith vehicle, v_i is its velocity and Δ_i is the distance between vehicle $i-1$ and i.

- Just the car ahead. This is called *predecessor following*.
- The nearest cars ahead and behind. This is known as *bidirectional control with nearest-neighbor interaction*.
- Several cars ahead and behind. This is known as *k-nearest neighbor interaction*.
- The leader (or possible also some neighbors). We will call it *leader following*.

Also any combination of these choices is possible. A schematic of a platoon is shown in Fig. 4.1.

There are several aspects of platoon control, each of which must be solved before platooning can be applied in real traffic:

- Joining the platoon. This involves questions such as when should a car join a travelling platoon, where should it join and how this action affects the performance of the platoon.
- Longitudinal control. Since the vehicles are supposed be travelling with very tight spacing (up to 2 meters [Horowitz and Varaiya, 2000]), the control of the inter-vehicle distance must be very precise and must guarantee safety. Moreover, since every vehicle is subject to noise (e.g., measurement errors, disturbances caused by road surface etc.), the control algorithm must guarantee that these disturbances would not be amplified in the platoon.
- Lateral control. Each car must be able to stay within a lane and also follow the lane changing manoeuvre (or obstacle avoidance) of the leading vehicle. As with the longitudinal control, disturbances must be attenuated, while the leader's movement must be followed.
- Leaving the platoon. If the car wants to take an exit from the highway, it must leave the platoon. The platoon must be able to fill the gap caused by the leaving vehicle and again, it should do it in a smooth way.

From all these aspects we will in this thesis describe only the *longitudinal control*.

4.1.1 Experimental platoons

Before giving details of the particular algorithms used for platooning, we describe real experimental platforms. One the world's first experimental platoons appeared as a result of the Californian PATH project (Partnership for Advanced Transportation Technology). The first results were published in early 90's [Chang et al., 1991b,a] for a platoon with two cars. Control challenges and opportunities were stated in [Varaiya, 1993; Hedrick et al., 1994]. Experiments done for a general public with a platoon of 8 cars were described in [Rajamani et al., 2000]. Comparison of theoretical achievable performance with a practical implementation are discussed in [Rajamani and Shladover, 2001]. It was shown that with the off-the-shelf technologies at that time the minimum achievable gap between autonomously controlled vehicles is 1 second (corresponding to a spacing of 30 m). Nevertheless, when a high degree of cooperation is used, the achievable distance is 6.5 m with high accuracy. Recent experimental results for a platoon of 4 vehicles using communication are presented in [Milanés et al., 2014].

The European counterpart of the PATH project is the project SARTRE (Safe Road Trains for the Environment) which was realized by a consortium of international academic institutions and industrial companies. They developed a platoon of cars and trucks which achieved tight spacing. The experiments using 5 standard cars equipped with standard sensors proved that tight spacing is achievable [Chan et al., 2012] and was kept even for changes in leader's acceleration. A traffic-flow improvement was proved by simulations [Kotte et al., 2012]. Good behavior was again achieved thanks to inter-vehicle communication. Some other description is available at [Coelingh and Solyom, 2012].

There are also other groups at companies or in academia which have their own platoons. We can name TU Eindhoven's platoon [Naus et al., 2010b] or Scania autonomous cooperative trucks in cooperation with KTH in Stockholm [Alam et al., 2015]. Saving of fuel due to platooning was experimentally proved in [Alam et al., 2010]. For an overview of platooning projects see [Bergenhem et al., 2012].

Several truck manufacturers (DAF, Daimler, Iveco, MAN, Scania and Volvo) participated recently in the European Truck Platooning Challenge [ETPC, 2016]. The six platoons arrived successfully to Netherlands from different locations. However, each manufacturer used its own communication system and its own control policy, so there is still a long journey to a practical use.

4.2 Platoon control algorithms

We decided to discuss practical platoon experiments before stating the control algorithms to motivate the following classification:

- algorithms without communication,
- algorithms with communication.

As follows from [Rajamani and Shladover, 2001], when there is no communication, the performance will be lower compared to cooperative control. On the other hand, if everything needed for control is measured using on-board sensors, the vehicle does not have to rely on the communication infrastructure. The communication can have time delays, can be disturbed or even denied by an intruder. In the worst-case, algorithms without communication can be applied as a backup solution when communication fails.

4.2.1 String stability

There is one important requirement which every strategy has to satisfy. It is called *string stability*. Loosely speaking, it means that when there is a disturbance acting at a vehicle, this disturbance should not amplify as it propagates along the platoon. There are several definitions in the literature and several criteria to evaluate it.

One of the definitions is based on l_p norm [Swaroop and Hedrick, 1996], which works even for nonlinear system. Other one is based on l_1 norm which captures that the peak in the amplitude should not grow in the platoon. In general, this norm is hard to calculate. However, if the system is linear and has positive impulse response, its l_1 norm is equal to its $\mathcal{H}_\infty$ norm [Eyre et al., 1998]. This motivates one of the most commonly used string stability definition.

Definition 4.1 ($\mathcal{H}_\infty$ string stability)**.** *Let $T_{ij}(s)$ be a transfer function in the formation from disturbance at vehicle i to the position of vehicle j The platoon is $\mathcal{H}_\infty$-string stable if $\|T_{ij}(s)\|_\infty \leq 1$.*

Note that this definition guarantees attenuation of the disturbance only if $T_{ij}(s)$ has positive impulse response. Nevertheless, it is often used even without guaranteeing this (see for instance [Milanés et al., 2014]).

A thorough list of definitions is presented in [Ploeg et al., 2014]. A weaker criterion of string stability is used in [Knorn et al., 2015]. Since it might be hard to achieve bounded change in the position of the vehicles, we might want to relax it to bounded *inter-vehicular distance*. This was named weak string stability.

4.2.2 Algorithms with communication

Almost all platoon control approaches realized in practice rely on communication. There is a good reason for it. With no-communication scenarios it seems that there is no string-stable strategy with a good performance.

The most commonly implemented is so called *Cooperative Automatic Cruise Control* (CACC). In this scenario the vehicle communicates its own control effort to its follower. The follower then adds it to its own control effort calculated from the predecessor-following strategy in a feed-forward manner. Then the follower sends this summed effort to its own follower. This repeats till the end of the platoon. If the communication is fast enough, CACC allows the platoon to move as a rigid block. The communication range does not have to be limited to only one nearest vehicle. The distance to the predecessor does not have to be constant, in order to achieve string stability a small time headway can be added [Öncü et al., 2012; Ploeg et al., 2015]. This strategy was used in PATH project [Milanés et al., 2014], SARTRE [Coelingh and Solyom, 2012], in Eindhoven [Naus et al., 2010a] and by Scania [Alam et al., 2015]. The effects of communication delay was analyzed in [Öncü et al., 2012] and graceful degradation to ACC when there are communication problems was proposed in [Ploeg et al., 2015].

Another common control law is based on the information from the platoon leader. In its simplest form the leader shares its velocity with all the other vehicles. They use this velocity as their desired velocity and try to keep it. Sometimes this communicated velocity is called a desired velocity. Such control was used in [Barooah et al., 2009; Hao and Barooah, 2012; Lin et al., 2012b]. Since keeping the leader's velocity is achieved using local controller, two integrators are no longer necessary and one integrator will suffice to keep both distance and velocity (see Section 4.6). As we will see, allowing for only one integrator improves the transient a lot. This strategy requires only broadcasting the leader's velocity, which is much easier than complete inter-vehicular communication.

In some papers also sharing of the leader's position is considered [Sebek and Hurak, 2011; Hedrick et al., 1994].

Effect of the communication delay is considered in [Peters et al., 2013]. [Jia and Ngoduy, 2016] analyses even inter-platoon communication and the proves stability for the case when information about the leader is delayed due to the communication network. The proposed IEEE 802.11p was considered as a communication medium.

4.2.3 Algorithms without communication

The current technology allows the vehicle to measure its own acceleration (accelerometer), velocity (tachometer), distance to the car ahead (lidar or radar) and possibly distance to the car behind. Also relative velocity measurement can be included (again using radar). Having these measurement, several algorithms can be implemented:

- time-headway spacing policy.
- predecessor following,
- symmetric bidirectional control,
- asymmetric bidirectional control,

The control laws for particular strategies will be illustrated using a standard double-integrator model

$$\begin{aligned} \dot{y}_i &= v_i, \\ \dot{v}_i &= e_i, \end{aligned} \tag{4.1}$$

where y_i is position of the ith vehicle, v_i is velocity of the ith vehicle and e_i is the input based on the particular control strategy. This model captures the open loop of the system—the controller is assumed to be just $R(s) = 1$. Double integrator captures the essence of the dynamics of a vehicle and thanks to its simplicity it is also the most widely studied model.

Time headway

Time headway spacing policy increases distance to the car ahead with increasing speed of the vehicle. Hence, the platoon length increases as well. On the other hand, string stability can be achieved for sufficiently large time gap [Middleton and Braslavsky, 2010] and this is the strategy used by human drivers. It is included in almost every microscopic traffic-flow models [Treiber and Kesting, 2013]. In fact, the current Adaptive Cruise Control (ACC) devices in cars use time-headway policy [Treiber and Kesting, 2013]. These systems might overcome the limitations of human drivers, but since the distance between vehicles grows with velocity, its effect on the road capacity is lower than what might be achievable for fixed-distance policy. The simplest control law for double-integrator model (4.1) is

$$e_i = y_{i-1} - y_i - (\underbrace{\Delta_{\min} + T_{\mathrm{h}} v_i}_{\text{desired distance}}), \tag{4.2}$$

where T_{h} is the desired time gap to the preceding vehicle. The desired distance is therefore a function of the self-velocity v_i. The model (4.1) can be rewritten

as

$$\begin{aligned} \dot{y}_i &= v_i \\ \dot{v}_i &= -T_\mathrm{h} v_i + \varepsilon_i, \end{aligned} \tag{4.3}$$

with $\varepsilon_i = y_{i-1} - y_i - \Delta_{\min}$ is the spacing error to the predecessor. The open-loop model (4.3) is in transfer-function form given as $M(s) = \frac{1}{s(s+T_\mathrm{h})}$, which has only one integrator in the open loop (see Def. 3.1). For this simple model the time-headway policy removes one integrator from the open loop. As we will see, systems with only one integrator in the open loop can behave well. Of course, in real systems the control law might be more complicated. As discussed before, a small time headway is often added to CACC control to guarantee string stability. In this thesis we mainly deal with fixed-distance spacing policy, but a short discussion of time headway is in Section 4.8.

Predecessor following

Predecessor following (PF) is the easiest strategy to implement. The vehicle measures the distance (and possibly relative velocity) only to the car ahead. Then the model of the double integrator with the control law becomes,

$$\begin{aligned} \dot{y}_i &= v_i \\ \dot{v}_i &= k_y(y_{i-1} - y_i - \Delta_{\mathrm{ref}}) + k_v(v_{i-1} - v_i), \end{aligned} \tag{4.4}$$

with gains $k_y > 0, k_v \geq 0$ weighting the distance and relative velocity to the predecessor. In general, there might be nonlinear functions of the distance and relative velocity (and possibly other states). Unlike in time-headway policy, the desired distance Δ_{ref} is fixed for any velocity of the vehicle.

Before designing a controller for the predecessor following strategy, we first have to know the model structure. One of the required properties of a platoon is that all vehicles are able to track the movement of the leader. Assume that the leader starts from zero velocity and after a while it travels with a constant velocity v_0 (for instance, it is travelling on a free highway). For the rest of the platoon this causes a ramp (linearly growing) input which they have to track (the position of the leader grows linearly with the slope v_0). That is, all vehicles have to be able to track a linearly growing signal.

Lemma 4.2. *In order to track the leader moving with a constant velocity v_0, in every fixed-distance spacing policy each car has to have at least two integrators in the open-loop, i.e, $\eta \geq 2$.*

This follows from the internal model principle—Lemma 2.11, since the model of the reference signal is $\frac{1}{s^2}$—there are two integrators. The same result was also

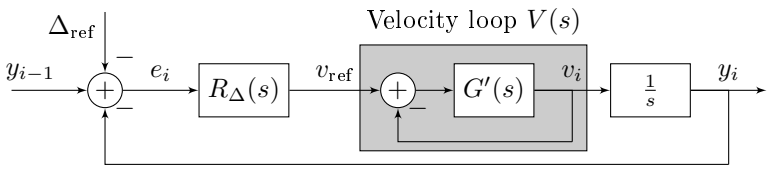

Figure 4.2: A cascade controller structure. $G'(s)$ is an arbitrary transfer function from the velocity error to velocity. It might be for instance a velocity controller combined with the vehicle model with velocity as the output.

proved in [Barooah and Hespanha, 2005], [Yadlapalli et al., 2006]. The result does not hold only for predecessor following, but for any fixed-distance scenario.

Except for the internal model principle, the necessity of having two integrators in the open loop can be intuitively explained using the diagram in Fig. 4.2. It shows a standard cascade control, which might be implemented in an adaptive cruise control (ACC) system. The distance controller $R_\Delta(s)$ produces a reference velocity v_{ref} for the velocity control loop $V(s)$. The velocity v_i is then integrated to position y_i. The input to the distance controller is the standard spacing error $e_i = y_{i-1} - y_i - \Delta_{\text{ref}}$. We want the vehicle to travel with the leader's velocity, hence in the steady state it should hold $v_{\text{ref}} = v_0$. If there is no integrator in the controller $R_\Delta(s)$, then in the steady state the controller acts just as a gain. Hence, $v_{\text{ref}} = R_\Delta(0)e$ and in order to make the vehicle travel with the leader's velocity, we require that the there is some nonzero spacing error e. The vehicle then cannot keep the reference distance Δ_{ref} to the car ahead. The spacing error even grows with the leader's velocity and the control strategy behaves as a time headway. On the other hand, if the controller contains an integrator, then to keep v_{ref} constant, it requires that $e = 0$ and the spacing error is zero. Therefore, the desired distance is kept. In this case there are two integrators in the open loop (one in the controller and one from velocity to position).

The following result disapproves string stability of predecessor following.

Lemma 4.3 ([Seiler et al., 2004, Thm. 1])**.** *Let η be the number of integrators in the open-loop of a single agent, i.e., $M(s) = \frac{1}{s^\eta} M'(s)$ with $M'(0) < \infty$. Then for the closed loop $T(s) = M(s)/(1+M(s))$ holds: if $\eta \geq 2$, then $\|T(s)\|_\infty > 1$.*

The transfer function in predecessor following between two neighboring vehicles is $\frac{y_{i+1}(s)}{y_i(s)} = T(s)$. The cars are connected in series, hence $\frac{y_{i+k}(s)}{y_i(s)} = T^k(s)$. Since the open loops must contain two integrators to track the leader, $\|T(s)\|_\infty \geq 1$, making the platoon string unstable. In fact, the norm grows exponentially in the graph distance.

Bidirectional control

In bidirectional control the distance (and possibly other states, typically velocity) to the car *ahead* and to the car *behind* are used. Although this is more complicated than to implement predecessor following strategy, it offers a couple of advantages from the practical point of view. The car can detect that a misbehaving vehicle is approaching it from behind and accelerate to avoid a crash. Moreover, bidirectional strategy mimics a real driver, who also looks to the rear-view mirror from time to time. The input generally is

$$e_i = f(x_{i-1} - x_i, x_i - x_{i+1}), \tag{4.5}$$

where f is some (possibly nonlinear) function and x_i is the state vector of the ith vehicle; typically at least position y and velocity v is considered. Nevertheless, bidirectional control is much harder to analyze, since instead of a single vehicle (in PF), whole platoon must be taken in consideration for analysis and design.

We can distinguish between symmetric and asymmetric bidirectional control law. In *symmetric bidirectional control*, the same weight is given to the front spacing error (and, possibly, error in other states, e.g., velocity) as it is to the rear one. Hence, the input to the model (4.1) has a form

$$e_i = k_y(y_{i-1} - y_i - \Delta_{\text{ref}}) - k_y(y_i - y_{i+1} - \Delta_{\text{ref}}) + k_v(v_{i-1} - v_i) - k_v(v_i - v_{i-1}), \tag{4.6}$$

where k_p, k_v are some constants and Δ_{ref} is the reference distance. Hence, the front spacing error $(y_{i-1} - y_i - \Delta_{\text{ref}})$ has the same weight k_p as the rear spacing error $(y_i - y_{i+1} - \Delta_{\text{ref}})$. The same symmetry holds for velocity (and possibly other states used for coupling).

Symmetric control was often analyzed in the literature. For instance, [Veerman et al., 2007; Hao and Barooah, 2013] proved linear scaling of the norm of the movement of the the last vehicle as a result of the movement of the leader. Effect of noise and the number of integrators was investigated in [Barooah and Hespanha, 2005]. Weak string stability of the model having integral action was proved in [Knorn et al., 2014]. The effect of measurement noise was considered in [Knorn et al., 2015]. The main disadvantage of symmetric control is a very long transient.

In *asymmetric bidirectional control*, the front and rear spacing errors are processed differently, hence the input to the model (4.1) is

$$e_i = f_1(y_{i-1} - y_i) - f_2(y_i - y_{i+1} - \Delta_{\text{ref}}) + g_1(v_{i-1} - v_i) - g_2(v_i - v_{i-1}), \tag{4.7}$$

f_1, f_2 are functions of distance and g_2, g_3 are functions of velocity. They might be nonlinear functions but the important fact is that front and rear errors are

processed differently. Note that the predecessor following is a special (extreme) case of asymmetric bidirectional control where $f_2 = 0, g_2 = 0$.

Asymmetric control was first proposed to shorten the transients in the platoon in [Barooah et al., 2009], later generalized to higher-order lattices in [Hao et al., 2011]. Uniform bound on eigenvalues was shown in [Hao and Barooah, 2012]. The fact that for the double-integrator model the $\mathcal{H}_\infty$ norm scales exponentially in N was emphasized in [Tangerman et al., 2012].

Another type of asymmetry is when there is different coupling in relative position and in relative velocity. Analysis of this kind of systems is even more complicated, since the system is not block diagonalizable using the approach in Lemma 2.6. It was first numerically shown in [Hao et al., 2012] that when the platoon uses symmetric coupling in position and asymmetric in velocity, scaling can be improved. The paper [Cantos and Veerman, 2014] shows faster transients in platoons with that type of asymmetry. The derivations are based on the analogy between circular and path systems. Wave properties of the circular system were analyzed in [Cantos et al., 2014]. Both [Hao et al., 2012] and [Cantos and Veerman, 2014] considered double-integrator systems.

For double-integrator systems (4.1), the model for asymmetric control can have a form

$$\begin{aligned} \dot{y}_i &= v_i \\ \dot{v}_i &= k_y(y_{i-1} - y_i - \Delta_{\text{ref}}) - k_y\epsilon_y(y_i - y_{i+1} - \Delta_{\text{ref}}) \\ &\quad + k_v(v_{i-1} - v_i) - k_v\epsilon_v(v_i - v_{i+1}), \end{aligned} \tag{4.8}$$

where $\epsilon_y > 0, \epsilon_v > 0$ are the constants of asymmetry. Such a model was considered in [Tangerman et al., 2012] with $\epsilon_y = \epsilon_v$ and in [Cantos and Veerman, 2014] for $\epsilon_y \neq \epsilon_v$.

In papers [Barooah et al., 2009; Lin et al., 2012b], a modified version of the control law (4.8) appeared. It used the desired velocity v_{ref}, to which each car regulates its own velocity. The overall double-integrator model is

$$\begin{aligned} \dot{y}_i &= v_i \\ \dot{v}_i &= k_y(y_{i-1} - y_i - \Delta_{\text{ref}}) - k_y\epsilon_y(y_i - y_{i+1} - \Delta_{\text{ref}}) + b(v_{\text{ref}} - v_i), \end{aligned} \tag{4.9}$$

where $b > 0$. The derivative of velocity can be also formulated as $\dot{v}_i = -bv_i + \varepsilon_i + bv_{\text{ref}}$ where $\varepsilon = k_y(y_{i-1} - y_i - \Delta_{\text{ref}}) - k_y\epsilon_y(y_i - y_{i+1} - \Delta_{\text{ref}})$ is external (coupling) input. Again, as was the case with time-headway policy, the open loop model is $M = \frac{1}{s(s+b)}$ and it has only one integrator in the open loop. The self-velocity feedback removed one integrator from the open loop. The reference velocity is usually the velocity with which the platoon should travel. Hence, it is the leader's velocity ($v_{\text{ref}} = v_0$) and this solution requires permanent communication. The

formation topology then changed to partially centralized. Nevertheless, having only one integrator in the open loop is very plausible from the transient point of view.

For the case with k-nearest neighbor interaction we do not have that many results. [Middleton and Braslavsky, 2010] shows that having more neighbors does not qualitatively improve performance for symmetric interactions, but quantitatively it can. When symmetric interaction in position and asymmetric in velocity is used, several interesting phenomena can be observed [Herbrych et al., 2015]. For instance, a reflectionless wave can emerge as a result of partial asymmetry.

In this thesis nearest-neighbor bidirectional control will be the main subject of interest. We will generalize some of the results discussed above.

4.3 Vehicle and platoon modelling for bidirectional control with proportional asymmetry

As was mentioned before, we will describe the platoons with bidirectional control. We will only use linear models and linear control laws. Moreover, in this section we will restrict ourselves to what we call *proportional asymmetry* (see below).

Consider $N+1$ *identical* vehicles indexed as $i = 0, 1, 2, \ldots, N$, with $i = 0$ corresponding to the platoon leader. As stated above, the leader drives independently of the platoon and its behavior is not affected by the rest of the platoon. The vehicles have identical transfer functions

$$G(s) = \frac{b(s)}{a(s)} \tag{4.10}$$

of an arbitrary type and order with positions y_i as the outputs. The vehicles are supposed to travel in one lane on the highway, so the output is just one-dimensional—the coordinate of their position.

The input to the vehicle is produced by a dynamic controller

$$R(s) = \frac{q(s)}{p(s)}. \tag{4.11}$$

Again, we do not impose any limitation on the transfer function. The vehicle model and the controller are connected in series, so the nth order open-loop model is

$$M(s) = R(s)G(s) = \frac{b(s)q(s)}{a(s)p(s)}. \tag{4.12}$$

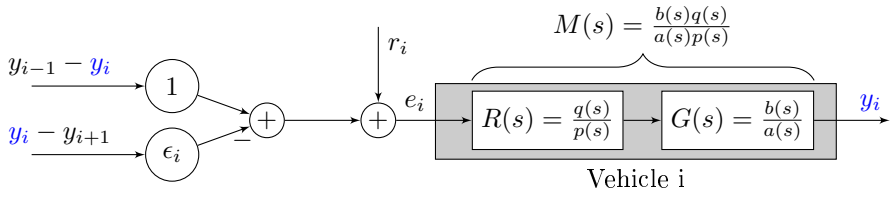

Figure 4.3: Vehicle interconnection in a platoon using (4.13).

We require that the open loop is a proper transfer function. The number of integrators in the open loop is again denoted as η (see Def. 3.1).

The input to the open loop is a weighted combination of the front spacing error $y_{i-1} - y_i$, rear spacing error $y_i - y_{i+1}$ and external reference r_i as

$$e_i = (y_{i-1} - y_i) - \epsilon_i(y_i - y_{i+1}) + r_i. \tag{4.13}$$

We call the non-negative weight ϵ_i of the rear spacing error the *constant of bidirectionality* (in our papers it was also called the *constant of asymmetry*). If $\epsilon_i = 1$ for all $i \geq 1$, the control law becomes symmetric bidirectional control. If $\epsilon_i = 0$, we have predecessor following. The control law is illustrated in Fig. 4.3. The general external input r_i can represent, for instance, a disturbance acting at the input of the controller or a reference such as the reference distance Δ_{ref}, in which case $r_i = -\Delta_{\text{ref}} + \epsilon_i\Delta_{\text{ref}}$ and the distances $y_{i-1} - y_i$ are regulated to Δ_{ref}. The leader's control input is just r_0 and the controller of the trailing vehicle has the input $e_N = (y_{N-1} - y_N) + r_N$.

Remark 4.4. *Note that although the regulation error (4.13) is a combination of just the spacing errors, the control law can also use the relative velocity or other derivatives of the spacing errors. The reason is that any dynamic controller is allowed. For instance, when the controller is of a PD type $R(s) = k_v s + k_p$, it produces as its output $k_p(y_{i-1} - y_i) - k_p\epsilon_i(y_i - y_{i+1}) + k_v(v_{i-1} - v_i) - \epsilon_i(v_i - v_{i+1}) + r_i + \dot{r}_i$—both relative positions and velocities are used. This control law is similar to (4.8).*

Definition 4.5 (Proportional asymmetry)**.** *The control law with the dynamic controller (4.11), the vehicle (4.10) and the input (4.13) is called bidirectional control with proportional asymmetry.*

Proportional asymmetry means that the asymmetry between front and rear errors is identical for all derivatives of the spacing error and the rear spacing error is weighted just proportionally (with constant ϵ_i) to the front error. There are also other and more general types of asymmetry. For instance, the rear spacing error can have a completely different controller. We do not discuss these cases

in this chapter.

4.3.1 Laplacian properties

The inputs to the open loops in (4.13) are given in a vector form as

$$e = -Ly + r \tag{4.14}$$

with $e = [e_0, e_1, \ldots, e_N]^{\mathrm{T}}, y = [y_0, y_1, \ldots, y_N]^{\mathrm{T}}$ and $r = [r_0, r_1, \ldots, r_N]^{\mathrm{T}}$. The matrix $L = [l_{ij}] \in \mathbb{R}^{N+1 \times N+1}$ is the Laplacian of a path graph, which describes the communication structure of the platoon. L has the following structure

$$L = \begin{bmatrix} 0 & 0 & 0 & 0 & \ldots & 0 \\ -1 & 1+\epsilon_1 & -\epsilon_1 & 0 & \ldots & 0 \\ 0 & -1 & 1+\epsilon_2 & -\epsilon_2 & \ldots & 0 \\ \vdots & \vdots & \vdots & \vdots & \ddots & \vdots \\ 0 & \ldots & -1 & 1+\epsilon_{N-2} & -\epsilon_{N-2} & 0 \\ 0 & \ldots & 0 & -1 & 1+\epsilon_{N-1} & -\epsilon_{N-1} \\ 0 & 0 & \ldots & 0 & -1 & 1 \end{bmatrix}. \tag{4.15}$$

It is a non-symmetric tridiagonal matrix. Next we state some useful properties of L.

Lemma 4.6. *Laplacian L in (4.15) and its eigenvalues λ_i, $i = 0, 1, \ldots, N$ have the following properties:*

a) *The eigenvalues λ_i are all real and $\lambda_i \geq 0$.*
b) *With the eigenvalues ordered as $\lambda_0 \leq \lambda_1 \leq \ldots \leq \lambda_N$, the smallest eigenvalue $\lambda_0 = 0$ and this eigenvalue is simple.*
c) *The eigenvalues are upper-bounded by $\lambda_{\max}$, that is, $\lambda_i \leq \lambda_{\max} = 2\max(l_{ii})$.*
d) *Let $L_{\mathrm{p}} \in \mathbb{R}^{N \times N}$ be the matrix obtained from L by deleting the first row and the first column (both correspond to the leader). Then $\lambda_i(L) = \lambda_i(L_{\mathrm{p}})$ for all $\lambda_i \neq 0$. Thus, the matrix L_{p} is non-singular.*
e) *Let $L_k \in \mathbb{R}^{N-1 \times N-1}$ be a matrix obtained from L_{p} by deleting the kth row and column. Let the eigenvalues of L_k, $1 \leq k \leq N$, be $\mu_1 < \mu_2 < \ldots < \mu_{N-1}$. Then*

$$\lambda_{j+2} \geq \mu_j \geq \lambda_j,\ j = 1, 2, \ldots, N-1. \tag{4.16}$$

Proof. a) The fact that the eigenvalues are real follows from the fact that the Laplacian is similar to a symmetric matrix [Fallat and Johnson, 2011, Lem.

0.1.1]. If $\epsilon_i > 0$ for $i = 1, \ldots, N$, then the eigenvalues are also simple [Fallat and Johnson, 2011, Lem. 0.1.1]. The fact $\lambda_i \geq 0$ follows from Lemma 2.1.

b) Since the eigenvalues are real, we can order them. The graph contains a directed spanning tree (rooted at the leader), so the zero eigenvalue is simple.

c) This follows from Gershgorin's theorem. All Gershgorin's circles are centered at l_{ii} and have a radius l_{ii}, so to get the upper bound on eigenvalues, we take the largest diagonal element $\max(l_{ii})$ as the center.

d) Combining the property that the first row of L is zero and one of the eigenvalues is zero, similarity transformation reveals the eigenstructure described in the lemma. It is also a consequence of the pinning control.

f) This follows from [Fallat and Johnson, 2011, Thm. 5.5.6], which gives conditions of interlacing for totally nonnegative matrices. L_p is similar to a totally nonnegative matrix [Fallat and Johnson, 2011, pages 6,7]. Both L_p and L_k can be transformed to totally nonnegative matrices using similarity transform with signature matrices $S = \mathrm{diag}[1, -1, \ldots, 1, -1]$. The results are $|L_\mathrm{p}|$ and $|L_k|$ with the absolute values taken element-wise. Since $|L_k|$ is a principal submatrix of $|L_\mathrm{p}|$, interlacing occurs. Since L_p is similar to $|L_\mathrm{p}|$ and L_k to $|L_k|$, the eigenvalues of L_k and L_p interlace as well. □

Applying e) successively, the same result is obtained for arbitrary principal submatrix.

In the literature the authors often work with non-sigular Laplacian as in d). This scheme, where the leader is not part of the formation, is called a *pinning control*. In our case the leader pins only to the vehicle with index 1 and the weight is $\rho_1 = 1$. We will use this convention often. For convenience, the pinned Laplacian has a form

$$L_\mathrm{p} = \begin{bmatrix} 1+\epsilon_1 & -\epsilon_1 & 0 & \ldots & 0 \\ -1 & 1+\epsilon_2 & -\epsilon_2 & \ldots & 0 \\ \vdots & \vdots & \vdots & \ddots & \vdots \\ 0 & \ldots & -1 & 1+\epsilon_{N-1} & -\epsilon_{N-1} \\ 0 & \ldots & 0 & -1 & 1 \end{bmatrix}. \tag{4.17}$$

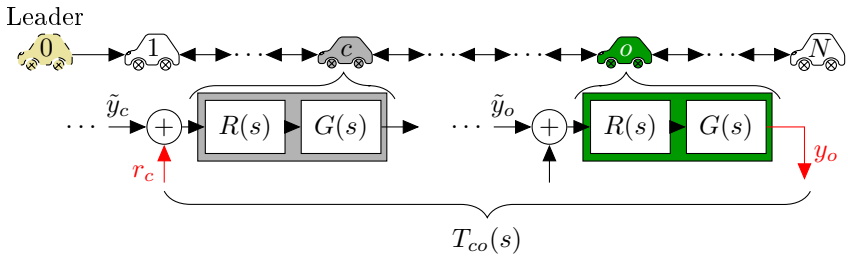

Figure 4.4: Block diagram showing the transfer function $T_{co}(s)$.

4.3.2 Transfer functions

In this chapter we will consider transfer functions in the pinned platoon, i.e., in which the leader is excluded from the formation and the pinned Laplacian is L_{p} in (4.17). The reason is that whenever there is the zero eigenvalue of the Laplacian, the $\mathcal{H}_\infty$ norm of any transfer function is infinity [Li et al., 2011], due to the rigid drift of the formation. The pinning from the leader "keeps" the formation in place and does not allow the vehicles to get arbitrarily far away from the leader, provided that the pinned system is stable.

We are interested in how the vector of external inputs r (acting at the inputs of the controller) affects the vector of positions y of vehicles. This is in general described by a transfer function matrix

$$y(s) = \mathbf{T}(s)r(s). \tag{4.18}$$

The (o,c)th element of matrix $\mathbf{T}(s) \in \mathbb{R}^{N\times N}$ is denoted by $T_{co}(s) = \frac{y_o(s)}{r_c(s)}$, $c = 1,\dots,N, o = 1,\dots,N$. The transfer function $T_{co}(s)$ therefore describes the effect of the external input r_c acting at a vehicle indexed c (called a *control vehicle*) on the position y_o of the vehicle with an index o (called an *output vehicle*)—see Fig. 4.4. We will be interested in how the properties of $T_{co}(s)$ scale with a growing number N of vehicles and the distance δ_{co} in a graph. We use the statement "from c to o" with the meaning of "from the input r_c of the vehicle c to the output y_o of the vehicle o". The indices c and o can be chosen arbitrarily. Note that due to bidirectional architecture, for any selection of c, o the transfer function $T_{co}(s)$ depends on the whole formation.

Since the graph of a platoon is a path graph, there is only one directed path from the node c to the node o. This path is a sequence of edges with the weights $\vartheta_{i,j}$. The weight of the path is $\vartheta_{co} = \prod_{j=c}^{o} \vartheta_{j,j+1}$. Since in our case $\vartheta_{i,i+1} = 1$

and $\vartheta_{i+1,i} = \epsilon_i$, we have

$$\vartheta_{co} = \begin{cases} 1 & \text{for } c \leq o, \\ \prod_{i=o}^{c-1} \epsilon_i & \text{for } c > o. \end{cases} \tag{4.19}$$

The number of edges on the directed path from a node c to a node o is called the graph distance between c and o and we denote it δ_{co}. We will use the product form of $T_{co}(s)$ that we derived in Theorem 3.3.

$$T_{co}(s) = \vartheta_{co} \frac{[b(s)q(s)]^{\delta_{co}+1} \prod_{i=1}^{N-\delta_{co}-1} [a(s)p(s) + \gamma_i b(s)q(s)]}{\prod_{i=1}^{N} [a(s)p(s) + \lambda_j b(s)q(s)]}, \tag{4.20}$$

where λ_j is the jth eigenvalue of L_{p}. The coefficients $\gamma_i \in \mathbb{R}$, $\gamma_i \leq \gamma_{i+1}$, are the eigenvalues of the matrix $\bar{L}_{co} \in \mathbb{R}^{N-\delta_{co}-1 \times N-\delta_{co}-1}$ that is obtained from L_{p} by deleting all the rows and columns corresponding to the nodes on the path from c to o, see Theorem 3.10. Note that $\bar{L}_{co}$ is a principal submatrix of L_{p}, hence interlacing in the sense of Lemma 4.6 e) holds. For instance, for a formation with $c = 2$, $o = 3$ and $N = 4$, we delete the third and the fourth rows and columns of

$$L_{\mathrm{p}} = \begin{bmatrix} 1+\epsilon_1 & -\epsilon_1 & 0 & 0 \\ -1 & 1+\epsilon_2 & -\epsilon_2 & 0 \\ 0 & -1 & 1+\epsilon_3 & -\epsilon_3 \\ 0 & 0 & -1 & 1 \end{bmatrix}, \tag{4.21}$$

from which we get the reduced Laplacian

$$\bar{L}_{co} = \bar{L}_{2,3} = \begin{bmatrix} 1+\epsilon_1 & 0 \\ 0 & 1 \end{bmatrix} \tag{4.22}$$

with the eigenvalues $\gamma_i = [1, 1+\epsilon_1]$.

Since we work with the pinned Laplacian L_{p}, the leader is not considered to be part of the platoon. To obtain the transfer function from the leader's input, we can multiply the transfer function $T_{co}(s)$ with the open loop transfer function $M(s)$ (the eigenvalue corresponding to the leader is $\lambda_0 = 0$).

Assumption 4.7. *The system (4.20) is asymptotically stable for all N.*

It follows from (4.20) that the polynomial $a(s)p(s)+\lambda_j b(s)q(s)$ must be stable for any $\lambda_j \in [\lambda_{\min}, \lambda_{\max}]$, $\lambda_j \in \mathbb{R}$ (similarly to [Fax and Murray, 2004]), where $\lambda_{\min}$ is the lower bound on eigenvalues of $L_{\rm p}$. Note that $a(s)p(s)+\lambda_j b(s)q(s)$ is a standard form for the denominator in the root-locus theory for the system $\lambda_j M(s)$ with the gain λ_j—see the discussion after Theorem 3.3 and Definition 3.4. Thus, we just need to stabilize the single-agent system $\lambda_j M(s)$ for a bounded interval of the real gain $\lambda_j \in [\lambda_{\min}, \lambda_{\max}]$. If $\lambda_{\min} \geq \varepsilon > 0$, we can stabilize even a formation of unstable agents. From (4.16) it follows that also $\gamma_i \in [\lambda_{\min}, \lambda_{\max}]$, $\forall i$, so if the system is asymptotically stable, all its zeros are in the left half-plane too.

We can rewrite the transfer function (4.20) into a more convenient form. Similarly to (3.22), we define two types of transfer functions

$$T_j(s) = \frac{\lambda_j b(s)q(s)}{a(s)p(s)+\lambda_j b(s)q(s)},\; Z_{ij}(s) = \frac{a(s)p(s)+\gamma_i b(s)q(s)}{a(s)p(s)+\lambda_j b(s)q(s)}. \tag{4.23}$$

From the product in (4.20), we can form $\delta_{co}+1$ transfer functions of type $T_j(s)$ and $N-\delta_{co}-1$ of type $Z_{ij}(s)$. So the transfer function can be written as

$$T_{co}(s) = T_{co}(0) \prod_{i=1, j\in\mathcal{J}}^{N-\delta_{co}-1} \frac{\lambda_j}{\gamma_i} Z_{ij}(s) \prod_{j=1, j\notin\mathcal{J}}^{N} T_j(s), \tag{4.24}$$

where the set $\mathcal{J}$ is the set of indices j used for eigenvalues λ_j which are in $Z_{ij}(s)$. The term $T_{co}(0) = \vartheta_{co} \frac{\prod_{i=1}^{N-\delta_{co}-1}\gamma_i}{\prod_{j=1}^{N}\lambda_j}$ is the steady-state gain. Recall also that in the previous chapter we used transfer functions $F_j(s) = \frac{1}{\lambda_j}T_j(s) = \frac{b(s)q(s)}{a(s)p(s)+\lambda_j b(s)q(s)}$.

The next technical Lemma is proved in Section 4.11.1.

Lemma 4.8. *Let $\lambda_j M(\jmath\omega_0) = \alpha_j + \jmath\beta_j$ for some frequency $\omega_0 > 0$, $\alpha_j, \beta_j \in \mathbb{R}$, $\jmath = \sqrt{-1}$. Then for $\lambda_i > 0, \lambda_j > 0, \gamma_i > 0$ it holds*

a) *If $|T_i(\jmath\omega_0)| > 1$ and $\lambda_j \geq \lambda_i$, then $|T_j(\jmath\omega_0)| > 1$ and $\alpha_j < -1/2$.*
b) *If $|T_i(\jmath\omega_0)| \leq 1$ and $\lambda_j \leq \lambda_i$, then $|T_j(\jmath\omega_0)| \leq 1$ and $\alpha_j \geq -1/2$.*
c) $|Z_{ij}(\jmath\omega_0)| \geq |Z_{ij}(0)|$ *for* $\{\alpha_j \leq -1$ *and* $\gamma_i \geq \lambda_j\}$.
d) $|Z_{ij}(\jmath\omega_0)| \geq |Z_{ij}(0)|$ *for* $\{-1 < \alpha_j \leq -\frac{1}{2}$ *and* $\gamma_i \leq \lambda_j\}$.
e) $|Z_{ij}(\jmath\omega_0)| \leq |Z_{ij}(0)|$ *for* $\{\alpha_j > -\frac{1}{2}$ *and* $\gamma_i \geq \lambda_j\}$.

The most important result following from a) is the relation between the closed-

loop and open-loop frequency response. Namely,

$$\Re\{\lambda_j M(\jmath\omega_0)\} < -\frac{1}{2} \quad \Longleftrightarrow \quad \left|\frac{\lambda_j M(\jmath\omega_0)}{1+\lambda_j M(\jmath\omega_0)}\right| > 1. \tag{4.25}$$

In words, in order to have the magnitude frequency response of the closed loop greater than 1, it is necessary and sufficient that the real part of the open-loop frequency response is less than $-\frac{1}{2}$ on the same frequency. We will use this fact many times throughout this chapter.

4.3.3 Steady-state gain of transfer functions

First we study one of the important control-related characteristic of a transfer function in a platoon—its steady-state gain $T_{co}(0)$. We assume that there is at least one integrator in the open-loop to enable the vehicles to track the leader's constant velocity or position. With $\eta \geq 1$ we get $a(0)p(0) = 0$. After excluding the leader, the steady-state gain follows from (4.20) as

$$T_{co}(0) = \vartheta_{co}\frac{[b(0)q(0)]^{\delta_{co}+1}\prod_{i=1}^{N-\delta_{co}-1}[\gamma_i b(0)q(0)]}{\prod_{j=1}^{N}[\lambda_j b(0)q(0)]} = \vartheta_{co}\frac{\prod_{i=1}^{N-\delta_{co}-1}\gamma_i}{\prod_{j=1}^{N}\lambda_j}. \tag{4.26}$$

As follows from Lemma 3.7, the steady-state gain does not depend on the dynamic model of an individual agent, it is only a function of the structure of the network (λ_j and γ_i are both related to L_{p}). We can now apply the previous result to get the steady-state gain of the transfer function $T_{co}(s)$ in vehicular platoons.

Theorem 4.9. *The steady-state gain $|T_{co}(0)|$ in platoon with the pinned Laplacian (4.17) is given by*

$$T_{co}(0) = \begin{cases} \vartheta_{co}\left(1+\sum_{i=1}^{c-1}\prod_{j=1}^{i}\epsilon_{c-j}\right) & \text{for } c \leq o, \\ \vartheta_{co}\left(1+\sum_{i=1}^{o-1}\prod_{j=1}^{i}\epsilon_{o-j}\right) & \text{for } o < c. \end{cases} \tag{4.27}$$

The proof is in Section 4.11.2. Note that for $c \leq o$, the steady-state gain does not depend on o as $\vartheta_{co} = 1$ for $c \leq o$.

A change in the distances may be even more relevant to platoon control.

Corollary 4.10. *Let $\Delta_i = y_{i-1} - y_i$ be the intervehicular distance. Then the*

steady-state gain of the transfer function $T_{\Delta,o}(s) = \frac{\Delta_o(s)}{r_c(s)}$ *equals*

$$|T_{\Delta,o}(0)| = \begin{cases} 0 & \text{for } o \geq c, \\ \prod_{i=o}^{c-1} \epsilon_i & \text{for } o < c. \end{cases} \tag{4.28}$$

Proof. The transfer function $T_{\Delta,o}(s)$ can be calculated as $T_{\Delta,o}(s) = \frac{\Delta_o(s)}{r_c} = \frac{y_{o-1}(s)-y_o(s)}{r_c} = \frac{(T_{c,o-1}(s)-T_{c,o}(s))r_c(s)}{r_c} = T_{c,o-1}(s) - T_{c,o}(s)$. For $o \geq c$ we have $T_{\Delta,o}(0) = T_{c,o-1}(0) - T_{c,o}(0) = 0$ since by (4.27) for $o \geq c$ the steady-state gain does not depend on o.

For $o < c$ we get the result by plugging (4.19) and (4.27) into $T_{\Delta,o}(0) = T_{c,o-1}(0) - T_{c,o}(0)$. We get

$$\begin{aligned} T_{\Delta,o}(0) &= \vartheta_{c,o-1}\left(1 + \sum_{i=1}^{o-2}\prod_{j=1}^{i}\epsilon_{o-j}\right) - \vartheta_{c,o}\left(1 + \sum_{i=1}^{o-1}\prod_{j=1}^{i}\epsilon_{o-j}\right) \\ &= \epsilon_{o-1}\epsilon_o \dots \epsilon_{c-1}\Big(1 + \epsilon_{o-2} + \epsilon_{o-2}\epsilon_{o-3} + \dots + \epsilon_{o-2}\epsilon_{o-3}\dots\epsilon_1\Big) \\ &\quad -\epsilon_o\epsilon_{o+1}\dots\epsilon_{c-1}\Big(1 + \epsilon_{o-1} + \epsilon_{o-1}\epsilon_{o-2} + \dots + \epsilon_{o-1}\epsilon_{o-2}\dots\epsilon_1\Big) \\ &= -\epsilon_o\epsilon_{o+1}\dots\epsilon_{c-1} = -\prod_{i=o}^{c-1}\epsilon_i. \end{aligned} \tag{4.29}$$

In the result we use absolute value, so $|T_{\Delta,o}(0)| = \prod_{i=o}^{c-1}\epsilon_i$. □

4.4 Symmetric bidirectional control

Having the necessary results for general proportional bidirectional control, we can specialize them to particular systems. We start with symmetric bidirectional control, which is in the literature analyzed more often than its asymmetric counterpart. Since the front and rear spacing error are weighted equally, the constant of bidirectionality $\epsilon_i = 1$ for all vehicles. The controller input (4.13) has a form

$$e_i = (y_{i-1} - y_i) - (y_i - y_{i+1}) + r_i \tag{4.30}$$

and the Laplacians are

$$L = \begin{bmatrix} 0 & 0 & 0 & 0 & \dots & 0 \\ -1 & 2 & -1 & 0 & \dots & 0 \\ 0 & -1 & 2 & -1 & \dots & 0 \\ \vdots & \vdots & \vdots & \vdots & \ddots & \vdots \\ 0 & \dots & 0 & -1 & 2 & -1 \\ 0 & \dots & 0 & 0 & -1 & 1 \end{bmatrix}, \quad L_{\mathrm{p}} = \begin{bmatrix} 2 & -1 & 0 & \dots & 0 \\ -1 & 2 & -1 & \dots & 0 \\ \vdots & \vdots & \vdots & \ddots & \vdots \\ 0 & \dots & -1 & 2 & -1 \\ 0 & \dots & 0 & -1 & 1 \end{bmatrix}. \tag{4.31}$$

Lemma 4.11. *The eigenvalues λ_i of L in (4.31) have the following properties.*

a) *The eigenvalues are given as*

$$\begin{aligned} \lambda_0 &= 0 \\ \lambda_i &= 2\left(1 - \cos\left(\frac{(2i-1)\pi}{2N+1}\right)\right) = 4\sin^2\left(\frac{(2i-1)\pi}{4N+2}\right), \quad i = 1, 2, \dots, N. \end{aligned} \tag{4.32}$$

b) *The eigenvalues are bounded as*

$$\frac{4(2i-1)^2}{(2N+1)^2} \leq \lambda_i \leq \frac{(2i-1)^2\pi^2}{4N^2}. \tag{4.33}$$

Further, assume that $i \ll N$. Then λ_i approaches zero as N grows with a quadratic rate, $\lambda_i \approx \frac{4\pi^2(2i-1)^2}{16N^2+16N+4} = \Theta\left(\frac{1}{N^2}\right)$. Specifically, the smallest nonzero eigenvalue $\lambda_1 = \Theta(\frac{1}{N^2})$.

c) *The reduced Laplacian L_{p} is a symmetric and positive definite matrix.*

d) *Let L_k be a matrix obtained from L_{p} by deleting kth row and column, $1 \leq k \leq N$. Let the eigenvalues of L_k be $\gamma_1 \leq \gamma_2 \leq \dots \leq \gamma_{N-1}$. Then*

$$\lambda_j \leq \gamma_j \leq \lambda_{j+1}, \; j = 1, 2, \dots, N-1. \tag{4.34}$$

Proof. a) The proof is in [Herman et al., 2013]. We just had to modify the result to our numbering of vehicles.

b) From (4.32) using $\sin x \leq x$ for $x \in (0, \pi/2)$ we get $\lambda_i \leq 4\left(\frac{(2i-1)\pi}{4N+2}\right)^2 \leq \frac{(2i-1)^2\pi^2}{4N^2}$. The lower bound follows from (4.32) using $\sin x \geq 2x/\pi$ (Jordan inequality [Özban, 2006]) as $\lambda_i \geq 4\left(\frac{2}{\pi}\frac{(2i-1)\pi}{4N+2}\right)^2 = \frac{4(2i-1)^2}{(2N+1)^2}$. The approximation

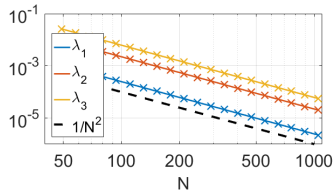

Figure 4.5: The smallest three nonzero eigenvalues $\lambda_1, \lambda_2, \lambda_3$ of the Laplacian matrix (4.31) for various N in logarithmic coordinates. The crosses indicate the approximation by (4.35). The quadratic decay rate is apparent.

can obtained using small angle argument $\sin x \approx x$ for x small as

$$\lambda_i = 4\sin^2\left(\frac{\pi(2i-1)}{4N+2}\right) \approx 4\left(\frac{\pi(2i-1)}{4N+2}\right)^2 = \frac{4\pi^2(2i-1)^2}{16N^2+16N+4} = \Theta\left(\frac{1}{N^2}\right), \tag{4.35}$$

since $\lambda_i < \frac{\pi^2(2i-1)^2}{4N^2}$ and $\lambda_i > \frac{\pi^2(2i-1)^2}{12N^2}$. The quadratic approach was also shown in [Barooah et al., 2009]. So the eigenvalues are bounded as $\lambda_{\min} = 0 \leq \lambda_i \leq 4 = \lambda_{\max}$.

c) The eigenvalues of L_{p} in (4.32) are positive and the matrix is symmetric, hence it is also positive definite.

d) Note that we work with reduced Laplacian $L_{\mathrm{p}} \in \mathbb{R}^{N\times N}$, whose smallest eigenvalue is λ_1. Since this matrix is symmetric and positive definite, Cauchy Interlacing Theorem holds (Lem. 2.2). The interlacing property (4.34) is stricter than that of a general Laplacian of a path graph (4.16). □

The approach of the three smallest eigenvalues to zero is shown in Fig 4.5.

4.4.1 Stability

As all the eigenvalues of the Laplacian are real, the poles of the overall formation lie on the root-locus curve (Definition 3.4). The location of poles for a particular system is shown in Fig. 4.6. The pole with the smallest real part of $T_{co}(s)$ will approach the origin because $a(s)p + \lambda_1 b(s)q(s) \to a(s)p$ as $\lambda_1 \to 0$. Recall that we assume at least one integrator in the open loop, hence there is at least one pole at the origin in $a(s)p(s)$.

Lemma 4.12. *The overall formation is unstable for sufficiently large N, if*

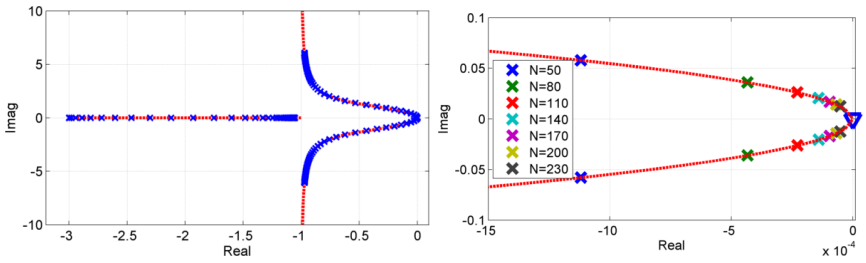

(a) (b)

Figure 4.6: The figure shows poles of a transfer function $T_{co}(s)$ for $R(s) = 10\frac{s+1}{s}$ and $G(s) = \frac{1}{s^2+3s}$. This a PI controller applied to the double integrator with friction. Fig. 4.6a shows all poles for $N = 50$. The red curve is the root-locus curve for $M(s) = 10\frac{s+1}{s^2(s+3)}$. Fig. 4.6b shows the location of the smallest nonzero pole as a function of N. The triangle shows two poles at the origin, which are present for each N.

a) *the open loop $M(s)$ contains more than two integrators, i.e, $\eta > 2$, or*
b) *the open loop is unstable.*

Proof. It is clear that since the eigenvalues are bounded as $\lambda_i \in [0, 4]$, the root-locus curve of $a(s)p(s) + \lambda_i b(s)q(s)$ must not enter the right-half plane for any $\lambda_i \in [0, 4]$. If $\eta \geq 3$, then in the open loop there are three poles at the origin. Root-locus theory [Dorf and Bishop, 2008, pp. 418] tells us that the tangents to the loci of poles at breakaway point are equally spaced over 360°. Thus, for $\eta \geq 3$ the angle is at most 120°, hence at least one branch leaves to the right half-plane. Since the gain λ_i can be arbitrarily close to zero (for N large enough), the poles of the formation will eventually be in the right-half plane. The same argument that as λ_i goes to zero, the poles of $a(s)p(s) + \lambda_i b(s)q(s)$ go to the poles of $a(s)p(s)$ shows instability when the open loop itself is unstable. □

The same result about instability of more than two integrators was shown in [Barooah and Hespanha, 2005].

The fact that the eigenvalues of the formation approach the imaginary axis makes the overall system very slow and the transients take very long time to settle. A response to the step in leader's position is shown in Fig. 4.7. As can be seen, there is a standing-wave pattern. According to [Martinec et al., 2014], the movement of the leader causes a wave, which propagates in the formation and reflects on both ends. The sum of the incident and reflected wave causes the standing-wave pattern. The propagation of the wave is seen from Fig. 4.8. The reflections are the reason for very long transients. Thus, when the wave-absorber

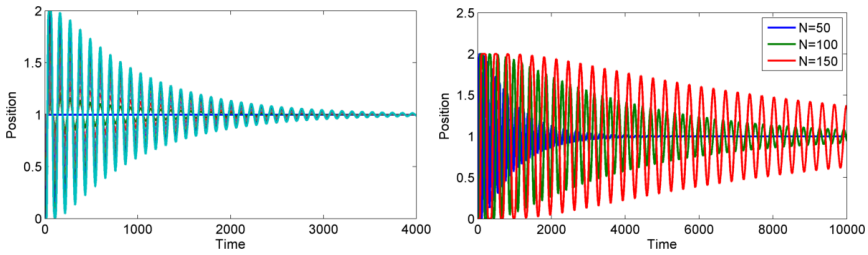

(a) (b)

Figure 4.7: The figure shows response to the step in leader's position for vehicles with $T_{co}(s)$ for $R(s) = 10\frac{s+1}{s}$ and $G(s) = \frac{1}{s^2+3s}$. Fig. 4.7a shows transients of all agents for $N = 50$, while Fig. 4.7b shows response of the last vehicle for various N. The response with more agents is much slower.

is implemented at either of the platoon end, the transient is qualitatively shorten [Martinec et al., 2014].

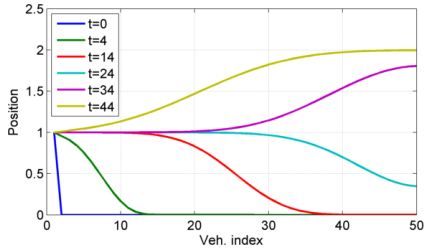

Figure 4.8: Propagation of wave in a symmetric bidirectional system with models $R(s) = 10\frac{s+1}{s}$ and $G(s) = \frac{1}{s^2+3s}$. As time grows, the wave gets closer to the platoon end. There it reflects in phase and travels back.

4.4.2 Performance measures

As symmetric control was investigated many times, much is known about its performance. For instance, the response of such platoon to white noise grows without bound with the platoon size [Barooah and Hespanha, 2005], which shows some kind of string instability. A similar claim was established for a circular system in [Bamieh et al., 2012]. The effect of nonlinear coupling is discussed in [Hao and Barooah, 2013].

The series of papers using port-Hamiltonian approach analyzed scaling of the effect of disturbance on the system energy. [Knorn et al., 2014] shows that for a system with integral control the effect of the disturbance is bounded re-

gardless of the number of vehicles. [Knorn et al., 2015] discusses the effect of measurement errors on the distances between vehicles. If the vehicle open-loop is passive from the controller input to the derivative of the output (velocity), then the network is passive [Arcak, 2007]. For instance, the bidirectional platoon of double-integrator vehicles is a passive system, as also follows from [Knorn et al., 2014].

First we can derive the steady-state gain of the transfer function $T_{co}(s)$ and $T_{\Delta,co}(s)$.

Corollary 4.13. *The steady-state gains of symmetric control are*

$$|T_{co}(0)| = \begin{cases} c & \text{for } o \geq c, \\ o & \text{for } o < c. \end{cases} \tag{4.36}$$

$$|T_{\Delta,co}(0)| = \begin{cases} 0 & \text{for } o \geq c, \\ 1 & \text{for } o < c. \end{cases} \tag{4.37}$$

The proof is just by direct calculations from (4.27) using the fact that $\epsilon_i = 1$, $\forall i$. Hence, the steady-state gain of the transfer function $T_{co}(0)$ grows linearly with the index of the control node (and, in turn, can grow with N). This means that it is not bounded in N. The distances change by 1 for each car ahead of the control node, while they remain unchanged for the vehicles behind. Since the control node and $c-1$ vehicles ahead of it increased their distances by 1, the vehicle changed its position by c. Thus, the steady-state gains to positions and distances are in agreement. Examples of the steady-state gain are in Fig. 4.15.

4.4.3 $\mathcal{H}_\infty$ norm of transfer functions

All results in this section are valid for symmetric control with pinned Laplacian defined in (4.31). As a tool for analysis of scaling we will use the $\mathcal{H}_\infty$ norm. It is defined as

Definition 4.14 ([Zhou et al., 1996, p. 100]). *The $\mathcal{H}_\infty$ norm of a transfer function matrix $G(s)$ which is analytic for $\Re\{s\} > 0$ is defined as*

$$\|G(s)\|_\infty := \sup_{\Re\{s\}>0} \sigma_{\max}[G(s)] = \sup_{\omega\in\mathbb{R}} \sigma_{\max}[G(\jmath\omega)], \tag{4.38}$$

where $\sigma_{\max}(\cdot)$ is the largest singular value.

When we consider a simple transfer function, the definition reduces to $\|G(s)\|_\infty = \sup_{\omega\in\mathbb{R}} |G(\jmath\omega)|$.

First we show a couple of auxiliary results, which will be needed later in this chapter. First we investigate the $\mathcal{H}_\infty$ norm of the the system $T_1(s) = \lambda_1 F_1(s)$, corresponding to the smallest eigenvalue λ_1 of the Laplacian.

Lemma 4.15. *Suppose that $M(s)$ contains neither pole nor zero in the closed right half-plane (CRHP), except for two poles at the origin, i.e., $\eta = 2$. Let $T_1(s) = \frac{\lambda_1 M(s)}{1+\lambda_1 M(s)}$, where λ_1 in (4.32) is the smallest eigenvalue of L_p. Then for N large, the norm $\|T_1(s)\|_\infty$ grows linearly with N, i.e., $\|T_1(s)\|_\infty = \Theta(N)$.*

The proof is in the Section 4.11.3. Recall that $\Theta(N)$ means scaling in the order of N, that is, $k_1 N \leq \|T_1(s)\|_\infty \leq k_2 N$ (see page xi for details). The result means that the peak in the magnitude frequency response of a closed loop corresponding to the smallest nonzero eigenvalue of the Laplacian grows linearly with the number of vehicles in the platoon. The result holds for any open-loop model satisfying the conditions in the lemma.

Nevertheless, for one integrator in the open loop, we can prove that the norm is bounded. First we need the following result, proved in Sec. 4.11.4.

Lemma 4.16. *Suppose that $M(s)$ contains neither pole nor zero in CRHP, except for one pole at the origin, i.e., $\eta = 1$. Then there exists $\kappa_0 > 0$ such that for a system $T_\kappa(s) = \frac{\kappa M(s)}{1+\kappa M(s)}$ holds $\|T_\kappa(s)\|_\infty = 1$ for any $0 < \kappa \leq \kappa_0$.*

From this we can easily derive the boundedness of $\mathcal{H}_\infty$ norm of $T_i(s)$ for a vehicle having one integrator in the open loop.

Lemma 4.17. *Suppose that $M(s)$ contains neither pole nor zero in CRHP, except for one pole at the origin. Then there exists a ξ, $1 \leq \xi < \infty$ such that $\|T_i(s)\|_\infty \leq \xi$ for any $0 < \lambda_i \leq 4$.*

Proof. Fix κ_0 as in Lemma 4.16. Consider an interval $\lambda_i \in [\kappa_0, 4]$ where 4 is the upper bound on eigenvalues of L_p. Since this interval is bounded and $T_i(s)$ does not have any pole on the imaginary axis (follows from Assumption 4.7), then also the frequency response of $T_i(s)$ is bounded. That is, there exists $\lambda_m \in [\kappa_0, 4]$ such that $\|T_m(s)\|_\infty = \xi \geq \|T_i(s)\|_\infty$ for all $\lambda_i \in [\kappa_0, 4]$. Recall that for $\lambda_i \leq \kappa_0$ we have $\|T_i(s)\|_\infty = 1$. Hence, for all $\lambda_i \in (0, 4]$ $\|T_i(s)\| \leq \xi$. □

Having the result on $\mathcal{H}_\infty$ norm of $T_1(s)$ (Lemma 4.15), we can generalize the results of [Hao and Barooah, 2013; Veerman et al., 2007] for transfer function $T_{1N}(s) = y_N(s)/r_1(s)$. This is the transfer function from the input of the first

vehicle behind the leader to the last vehicle in the platoon. As N grows, also the graph distance between vehicles $c = 1$ and $o = N$ grows.

Theorem 4.18. *Suppose that $M(s)$ contains neither pole nor zero in the closed right half-plane (CRHP), except for two poles at the origin, i.e., $\eta = 2$. Then the norm of the transfer function $\|T_{1N}(s)\|_\infty$ for any $M(s)$ scales linearly in N, i.e., $\|T_{1N}(s)\|_\infty = \Theta(N)$.*

The proof is in Sec. 4.11.5.

However, there is a transfer function which scales quadratically with N. Let $T_{NN}(s) = \frac{y_N(s)}{r_N(s)}$ be the transfer function from the input of the last vehicle to its output.

Theorem 4.19. *Suppose that $M(s)$ contains neither pole nor zero in the closed right half-plane (CRHP), except for two poles at the origin, i.e., $\eta = 2$. Then the norm of the transfer function $\|T_{NN}(s)\|_\infty$ for any $M(s)$ scales quadratically in N, i.e., $\|T_{NN}(s)\|_\infty = \Theta\left(N^2\right)$.*

The proof is in Sec. 4.11.6. This is basically a consequence of the linear scaling of the peak in $T_1(j\omega)$ and the linear scaling of $T_{NN}(0)$ as N grows. Despite the fact that the graph distance between the input and output is zero (both are at the last agent), the scaling is quite bad—quadratic.

Linear and quadratic scaling is illustrated in Fig. 4.9. It is apparent that whenever the index the control node grows with N, the scaling is quadratic, while it remains linear when the index is fixed. This is a consequence of the linear growth of the steady-state gain with c.

It is also interesting to compare transfer functions between agents with different distances. We can show that with $\eta = 2$, $\|T_{1N}\|_\infty \geq \|T_{1,o}\|_\infty$ for any o. The reason is the presence of terms $Z_{ij}(s)$ in the product form (3.22). The zeros of $Z_{ij}(s)$ will interlace on the root-locus curve with the poles. The reason for interlacing is Lemma 4.11 d). Hence, the effect of pole causing increase of the magnitude frequency response will be mitigated by a nearby zero. Only the transfer function $T_{1N}(s)$ does not have any block $Z_{ij}(s)$, so its $\mathcal{H}_\infty$ norm must be the largest of all. This is illustrated in Fig. 4.10.

4.4.4 $\mathcal{H}_\infty$ norm of the transfer function matrix

When we work with the reduced Laplacian L_p, we get rid of the eigenvalue at zero. For a system with symmetric and non-singular Laplacian L_p, calculation of the $\mathcal{H}_\infty$ norm of the transfer function matrix becomes an easy task.

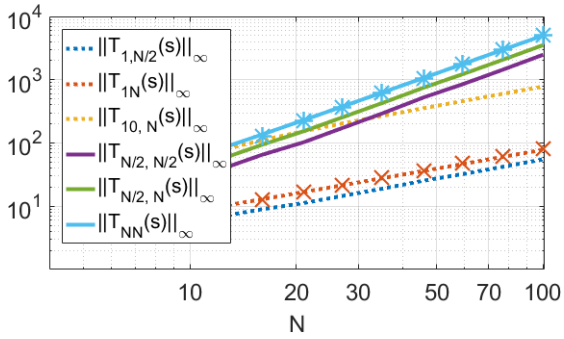

Figure 4.9: The norms of several transfer functions in logarithmic scale with N growing. The models is $R(s) = \frac{6.9s^3+33s^2+49s+23}{s^3+4.5s^2+4.5s}$, $G(s) = \frac{1}{s(s+3)}$. The crosses correspond to $0.8N$ and asterisks to $0.6N^2$. It is clear that $\|T_{NN}(s)\|_\infty$ scales quadratically, while $\|T_{1N}(s)\|_\infty$ only linearly. The norm was calculated using *norm* function in Matlab.

Let $\mathbf{T}(s)$ be the transfer function matrix from the input vector $r(s)$ to the position vector $y(s)$, i.e., $y(s) = \mathbf{T}(s)r(s)$. Its $\mathcal{H}_\infty$ norm is defined as $\|\mathbf{T}(s)\|_\infty = \sup_{\omega\in\mathbb{R}}\sigma_{\max}(\mathbf{T}(\jmath\omega))$ (Def. 4.14).

Lemma 4.20. *The $\mathcal{H}_\infty$ norm of the transfer function matrix $\mathbf{T}(s)$ is*

$$\|\mathbf{T}(s)\|_\infty = \max_i \left\| \frac{b(s)q(s)}{a(s)p(s)+\lambda_i b(s)q(s)} \right\|_\infty = \max_i \|F_i(s)\|_\infty. \tag{4.39}$$

The proof is in Sec. 4.11.7. Since for any transfer function $\|T(s)\|_\infty \geq |T(0)|$, we have a simple corollary for any model of vehicle.

Corollary 4.21. *Assume that $\eta \geq 1$ in $M(s)$. Then the norm $\|\mathbf{T}(s)\|_\infty$ scales at least quadratically with N, i.e. for some $c > 0$,*

$$\|\mathbf{T}(s)\|_\infty \geq \left| \frac{b(0)q(0)}{a(0)p(0)+\lambda_1 b(0)q(0)} \right| \geq cN^2. \tag{4.40}$$

Proof. From (4.39) we have

$$\|\mathbf{T}(s)\|_\infty = \max_i \|F_i(s)\|_\infty \geq \|F_1(s)\|_\infty \geq |F_1(0)| \geq \frac{1}{\lambda_1}. \tag{4.41}$$

and since $\lambda_1 = \Theta\left(\frac{1}{N^2}\right)$, the result follows. □

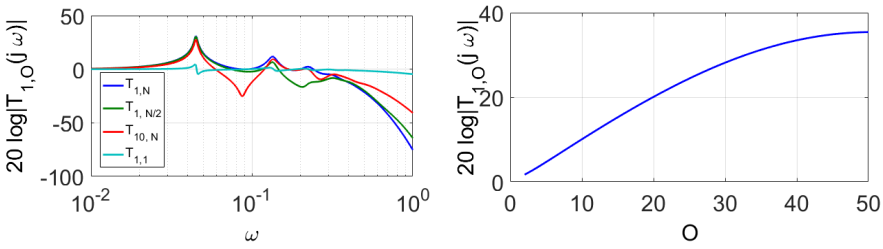

(a) (b)

Figure 4.10: a) The magnitude frequency responses of $T_{1,o}(s)$—the control node is fixed $c = 1$ and output node o varies. The effect of complex zeros is especially seen in $T_{1,1}(s)$, where the response goes up and down based on poles and zeros. b) shows $\|T_{1,o}(s)\|_\infty$ as a function of o. It grows with distance δ_{1o}. In both cases the model is $R(s) = \frac{s+1}{s}$, $G(s) = \frac{10}{s^2+5s}$.

This result holds for any open-loop model with at least one integrator.

Now we can use Lemmas 4.15 and 4.17 the derive scaling of the $\mathcal{H}_\infty$ norms of the transfer function matrix.

Theorem 4.22. *Suppose that $M(s)$ has neither poles nor zeros in CRHP, except for η poles at the origin. Then the norm $\|\mathbf{T}(s)\|_\infty$ scales with N as*

$$\|\mathbf{T}(s)\|_\infty = \begin{cases} \Theta\left(N^2\right) & \text{for } \eta = 1, \\ \Theta\left(N^3\right) & \text{for } \eta = 2 \end{cases} \tag{4.42}$$

and for $\eta \geq 3$ the system becomes unstable for N large enough.

The proof is in Section 4.11.8. Again, this result holds for any symmetric vehicle platoon having one or two integrators, respectively, and the result does not depend on the open-loop model. The scaling of $\mathcal{H}_\infty$ norm of the transfer function matrix is shown in Fig. 4.11. The system with one integrator in the open-loop scales quadratically, while the system with two integrators scales even cubically. For one integrator, the quadratic growth is a consequence of the quadratic growth of the steady-state gain in Corollary 4.21 and boundedness of the blocks $T_i(s)$—Lemma 4.17. For two integrators, the quadratic scaling of the steady-state gain is combined with linear growth of the norm of $T_1(s)$.

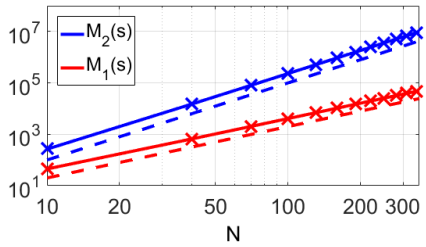

Figure 4.11: The norm $\|\mathbf{T}(s)\|_\infty$ as a function of N for different models $M_1(s) = 10\frac{s+1}{s^3+5s^2+6s}$ with $\eta = 1$ and $M_2(s) = 10\frac{s+1}{s^3+5s^2}$ with $\eta = 2$. The solid line is the norm calculated in Matlab using the *norm* function in Control System Toolbox. The crosses correspond to the norm obtained by (4.39) and dashed line is $0.1N^3$ (blue) and $0.2N^2$ (red). It is clear that platoon with one integrator scales quadratically and with two integrators cubically (Theorem 4.22).

4.5 Asymmetric bidirectional control

As we discussed in the previous section, the transients in symmetric bidirectional control are very long, because the smallest eigenvalue of the Laplacian approaches zero quadratically fact (Lemma 4.11). To improve the convergence time, proportional asymmetry was first proposed in [Barooah et al., 2009]. It was shown in the paper that the least-stable eigenvalue of the platoon converges to zero slower than it does in symmetric control. Later this was generalized to multidimensional systems in [Hao et al., 2011]. For double integrator system the same authors show in [Hao and Barooah, 2012] that asymmetry even achieves a uniform bound on eigenvalues. We will generalize it in this section to any open-loop model and varying asymmetry along the platoon.

A uniform bound on eigenvalues might seem as a very good solution for platoons, since the convergence time is improved. However, [Tangerman et al., 2012] shows that for the double-integrator model the $\mathcal{H}_\infty$ norm of the transfer function from the leader's position to the last vehicle grows exponentially with N. So the uniform bound on eigenvalues must be paid for by very bad scaling in frequency domain. This result will be extended to any model of the vehicle having at least two integrators in the open loop and also to any transfer function in the formation. Moreover, we discuss the behavior of systems with only one integrator in the open loop and show, how to design a string-stable controller.

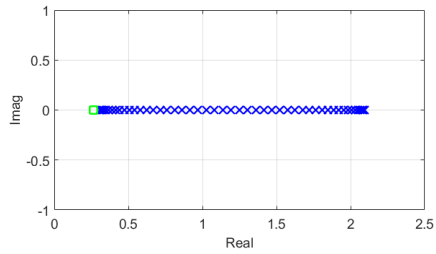

Figure 4.12: The eigenvalues λ_i of the Laplacian matrix L_p. $\epsilon_i = 0.2, N = 50$. The green square shows the bound (4.44).

4.5.1 Laplacian properties

Let us first show the asymmetric pinned Laplacian again for convenience.

$$L_\mathrm{p} = \begin{bmatrix} 1+\epsilon_1 & -\epsilon_1 & 0 & \dots & 0 \\ -1 & 1+\epsilon_2 & -\epsilon_2 & \dots & 0 \\ \vdots & \vdots & \vdots & \ddots & \vdots \\ \dots & 0 & -1 & 1+\epsilon_{N-1} & -\epsilon_{N-1} \\ 0 & \dots & 0 & -1 & 1 \end{bmatrix}. \tag{4.43}$$

We can add to the properties in Lemma 4.6 a very important one. We prove that Laplacian of asymmetric control with forward asymmetry ($\epsilon_i < 1$ for all $i \geq 1$) achieves a uniform bound on eigenvalues.

Definition 4.23 (Uniform boundedness)**.** *The eigenvalues λ_i of a matrix $L_\mathrm{p} \in \mathbb{R}^{N\times N}$ are uniformly bounded from zero if there exists a constant $\lambda_{\min} > 0$ such that $\lambda_i \geq \lambda_{\min}$ for $i = 1, \dots, N$ and $\lambda_{\min}$ does not depend on N.*

We now state uniform boundedness of asymmetric bidirectional control.

Theorem 4.24. *If there is $\epsilon_{\max} < 1$ such that $\epsilon_i \leq \epsilon_{\max} \forall i$ and $\forall N$, then the eigenvalues of the pinned Laplacian L_p in (4.43) are uniformly bounded from zero with a bound*

$$\lambda_{\min} \geq \frac{(1-\epsilon_{\max})^2}{2+2\epsilon_{\max}}. \tag{4.44}$$

The proof is in Sec. 4.11.9. This theorem states that if all cars have larger weight

to the front spacing error, then uniform bound on eigenvalues is achieved. The eigenvalues of L_{p} are illustrated in Fig. 4.12. When all the cars use the same constant of bidirectionality $\epsilon_i = \epsilon$, $\forall i$, we can find even a closed-form expression for the eigenvalues [Herman et al., 2013].

$$\lambda_i = 1 + \epsilon - 2\sqrt{\epsilon}\cos\theta_i, \tag{4.45}$$

where θ_i is the ith solution of $\sin(N\theta_i) - \sqrt{\frac{1}{\epsilon}}\sin((N+1)\theta_i) = 0$. The uniform bound of course holds also for this case as $\lambda_i \geq (1-\epsilon)^2$. A similar claim was done in [da Fonseca and Veerman, 2009; Tangerman et al., 2012]. In this case we can also calculate the eigenvectors as

$$w_{i,k} = \left(\sqrt{\frac{1}{\epsilon}}\right)^k \sin(\theta_i k). \tag{4.46}$$

This exponential scaling of eigenvectors is the first sign that certain properties of asymmetric distributed control need not scale well.

The opposite case where the constants of bidirectionality are greater than one was for a special case of identical values analyzed in [Tangerman et al., 2012]. It was shown there that apart from one eigenvalue very close to zero, the others are uniformly bounded as well.

4.5.2 Stability and steady-state gains

In the introduction we stated that asymptotic stability is a necessary condition for string stability. Let us now investigate stability with asymmetric control.

Lemma 4.25. *Suppose that the eigenvalues λ_i of the pinned Laplacian are uniformly bounded. Then the eigenvalues ν_i of the platoon are uniformly bounded from the origin, that is, for any N,*

$$|\nu_i| \geq \xi > 0, \forall\, i \tag{4.47}$$

for some constant ξ depending on the open-loop model $M(s)$ and $\lambda_{\min}$.

Proof. The proof is a direct consequence of the product form in (3.21), or in general, of the block diagonalization from the paper [Fax and Murray, 2004]. The eigenvalues ν are given as roots of $a(s)p(s) + \lambda_i b(s)q(s)$. Since the eigenvalues of the Laplacian are real and non-negative, we can use root-locus theory. In root locus, the poles of the closed-loop polynomial start at the poles of the open loop (for gain equal to zero) and they go to zeros of the open loop as the gain increases. In our case the "gain" $\lambda_i \geq \lambda_{\min} > 0$, so the poles of the

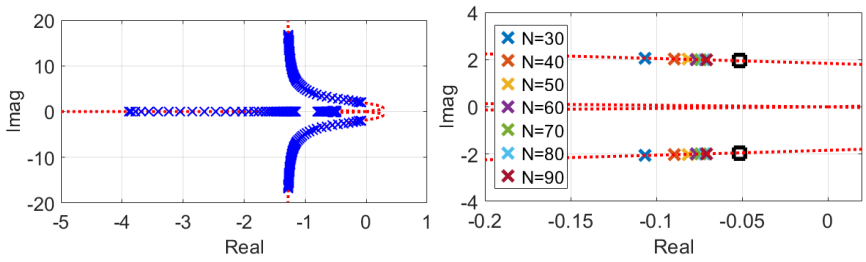

(a) (b)

Figure 4.13: The figure shows the eigenvalues of the formation with $N = 50$, $R(s) = \frac{s^2+1.4s+0.45}{s^2}$ and $G(s) = \frac{100s+100}{s^3+5s^2}$. This system has 4 integrators in the open loop. Fig. 4.13a shows all eigenvalues. The dashed curve is the root-locus curve for $M(s)$ and it is apparent that it enters the right half-plane. Fig. 4.13b shows location of the smallest nonzero pole as a function of N. The black squares show the bound on eigenvalues ν_i.

formation cannot get arbitrarily close to the poles of the open loop. The most important open-loop poles are the η poles at the origin. It follows that ν cannot get arbitrarily close to the origin, the distance is lower bounded by the smallest root of $a(s)p(s) + \lambda_{\min} b(s)q(s)$. □

This result generalizes the result of [Hao and Barooah, 2012; Tangerman et al., 2012] from the double-integrator system.

Unlike in symmetric bidirectional control, vehicles in asymmetric platoon can have more than two integrators in the open loop. Although the root-locus plot of the roots at the origin will enter the right half-plane, thanks to the bound on eigenvalues $\lambda_{\min}$, the eigenvalues of the formation still can remain in the left half-plane. To achieve that, we have to guarantee that the root-locus curve lies in the left half-plane for $\lambda_i \in [\lambda_{\min}, \lambda_{\max}]$. Therefore, for the gain lower than $\lambda_{\min}$ the root locus can be in right half-plane, for larger gain it cannot. An example of a four-integrator system is shown in Fig. 4.13.

When the pinning control scheme is assumed (the leader is excluded from the formation), we can stabilize even a formation of unstable systems. Again, this is achieved thanks to the bound. An example is shown in Fig. 4.14.

Steady-state gain

As in the section on symmetric control, we start with analysis of the steady-state gain.

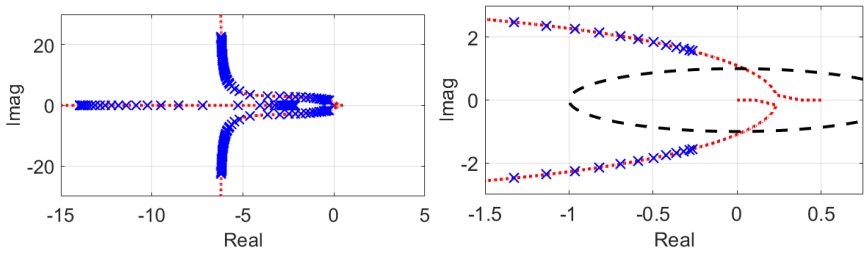

(a) (b)

Figure 4.14: The figure shows the eigenvalues of the formation with $N = 80$, $R(s) = 200\frac{s+1}{s+15}$ and $G(s) = \frac{1}{s^2-0.5s}$. This system has unstable open loop (pole at 0.5). Fig. 4.14a shows all eigenvalues. The dotted curve is the root-locus curve for $M(s)$ and it is apparent that it starts in the right half-plane. Fig. 4.14b shows a detail of the poles the near imaginary axis. The black ellipse is the unit circle $e^{\jmath\phi}$. The absolute value of the eigenvalues is bounded as $|\nu| \geq 1$.

Corollary 4.26. *If there is a maximal asymmetry $\epsilon_{\max}$ such that $\epsilon_i \leq \epsilon_{\max} < 1\ \forall i$, then the steady-state gain is upper bounded as $T_{co}(0) \leq \frac{1}{1-\epsilon_{\max}}$. This holds for all N and for all c, o.*

Proof. We can bound the product in (4.27) as $\prod_{j=1}^{i} \epsilon_{c-j} \leq \epsilon_{\max}^i$. Then the bound on $T_{co}(0)$ is $T_{co}(0) \leq \vartheta_{co}\left(1 + \sum_{i=1}^{c-1} \epsilon_{\max}^i\right) \leq \vartheta_{co}\frac{1}{1-\epsilon_{\max}}$, since $\sum_{i=0}^{\infty} \epsilon_{\max}^i = \frac{1}{1-\epsilon_{\max}}$. The same holds for $\vartheta_{co}\left(1 + \sum_{i=1}^{o-1}\prod_{j=1}^{i} \epsilon_{o-j}\right) \leq \vartheta_{co}\frac{1}{1-\epsilon_{\max}}$. If $c \leq o$, then all the weights are 1 and $\vartheta_{co} = 1$. If $c > o$, then $\vartheta_{co} = \prod_{i=c-1}^{o} \epsilon_i \leq \epsilon_{\max}^{\delta_{co}} < 1$. Therefore, $T_{co}(0) \leq \vartheta_{co}\frac{1}{1-\epsilon_{\max}} \leq \frac{1}{1-\epsilon_{\max}}$. □

The bound on $T_{co}(0)$ for the predecessor-following control strategy is one (note $\epsilon_{\max} = 0$), which is the minimum amidst all control strategies. The steady-state gains for a fixed control node and a varying output node for several strategies are in Fig. 4.15a, while the gain from c to c is in Fig. 4.15b. Although the gain grows with c, for a fixed c, it does not grow with the number N of agents. As follows from Corollary 4.10, in asymmetric control with $\epsilon_i \leq \epsilon_{\max} < 1 \forall i$ the change in distance will be less than one since $\prod_{i=o}^{c-1} \epsilon_i < 1$.

4.5.3 Inverse optimality

We have seen that asymmetric platoons have uniform bound on eigenvalues and that they have bounded steady-state gain. In this section we prove an additional useful property. We prove that a local static state feedback with

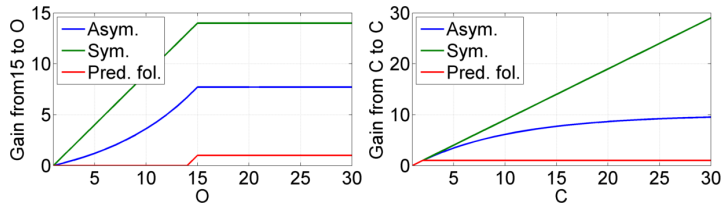

(a) Fixed $c = 15$, varying o. (b) Varying c and o, $o = c$.

Figure 4.15: Steady-state gains for different choices of c and o and for asymmetry $\epsilon = 0.9$.

a fixed coupling gain of the controller is an optimal controller for asymmetric platoons for any platoon size. In other words, one fixed controller is an optimal distributed controller for the platoon. We will rely on the results presented in section 2.4.1.

Similarly to Lemma 2.9 we need to define a couple of matrices. In this section the open loop (the vehicle model with the dynamic controller) of the vehicle is given in a state-space form with matrices A, B, C. We work here with pinned Laplacian L_{p} in order to get rid of the eigenvalue at zero. The platoon has a model

$$\begin{aligned} \dot{x} &= (I \otimes A - L_{\mathrm{p}} \otimes BK)x + (I \otimes B)r \\ y &= (I \otimes C)x. \end{aligned} \tag{4.48}$$

Let V be the matrix of eigenvectors of L_{p} such that $V^{-1}L_{\mathrm{p}}V = \Lambda$ with Λ being a diagonal matrix.

Corollary 4.27. *Consider L_{p} in (4.43) with $\epsilon \leq \epsilon_{\max} < 1$ for all N. Further let the matrices Q_2, R_2, K_2 be given as in Theorem 2.10. Then the local state-feedback control law $u = cL_{\mathrm{p}} \otimes K_2$ with $c \geq \frac{2+2\epsilon_{\max}}{(1-\epsilon_{\max})^2}$ is the optimal control law with respect to (2.39) for all N.*

Proof. Recall the properties of the pinned Laplacian: the eigenvalues are real, positive and bounded from below as $\lambda_i \geq \lambda_{\min} \geq \frac{(1-\epsilon_{\max})^2}{2+2\epsilon_{\max}}$ for all $i \geq 1$. These properties satisfy the conditions in Theorem 2.10 and the result follows. □

The theorem can be explained as follows. When a static state-feedback matrix K_2 is calculated, it suffices to take a fixed gain for any platoon size to achieve optimality. Hence, it is not necessary to increase the gain with the platoon size.

Inverse optimality might seem as a very good result, but there is at least one important caveat. The eigenvectors of the Laplacian L_{p} are exponentially weighted

with growing index, similarly to (4.46). Then the matrix $R_1 = (V^{-1})^{\mathrm{T}} V^{-1}$ has very large entries in the top-left corner and very low entries in the bottom-right corner. It follows from (2.40) that the resulting criterion (2.39) almost ignores the contribution of the agents at the end of the platoon. The reason will become apparent in the next subsection.

The result on inverse optimality is for the state-space description. To obtain a transfer function $T_{co}(s)$ for this system, one can use Corollary 3.9.

4.5.4 Exponential growth

So far all the properties of asymmetric control seemed to be beneficial. It is inversely optimal for any number of vehicles, its steady-state gain is bounded regardless of the number of vehicles and the eigenvalues do not approach zero for any N. However, there is a price to pay—exponential scaling of the $\mathcal{H}_\infty$ norm.

Let $T_{\min}(s)$ be the transfer function of the closed-loop system with $\lambda_{\min}$ acting as a proportional gain ($\lambda_{\min} > 0$ is the lower bound on $\lambda_i, i \geq 1$)

$$T_{\min}(s) = \frac{\lambda_{\min} b(s) q(s)}{a(s) p(s) + \lambda_{\min} b(s) q(s)}. \tag{4.49}$$

Note that $|T_j(0)| = 1$ for any j due to at least one integrator in the open loop, hence $\|T_j(s)\|_\infty \geq 1$.

It was proven in [Tangerman et al., 2012] that the magnitude of the response of the last vehicle grows exponentially in N when asymmetric control is used. However, the analysis was done only for one transfer function in the platoon and one input—the movement of the leader. Moreover, only the double-integrator model of the vehicle was considered. The next theorem, proven in Appendix 4.11.10, extends the exponential scaling to an arbitrary transfer function in a finite platoon and arbitrary dynamics of the vehicle. The test involves only the closed-loop $T_{\min}(s)$ of an individual agent.

Theorem 4.28. *If $\|T_{\min}(s)\|_\infty > 1$ and the eigenvalues of L_{p} are uniformly bounded from zero, then there are two real constants $\xi > 0$ and $\zeta > 1$ depending only on $\lambda_{\min}, \lambda_{\max}$ and $M(s)$, such that it holds $\|T_{co}(s)\|_\infty > \zeta^{\delta_{co}+1}\ T_{co}(0)\ \xi^2$. That is, the norm $\|T_{co}(s)\|_\infty$ grows exponentially with the graph distance δ_{co}.*

Note that the theorem does not assume that the control is asymmetric and neither it assumes any type of the open-loop dynamics. The sufficient conditions are only the uniform boundedness and the norm of individual agent's closed loop greater than one.

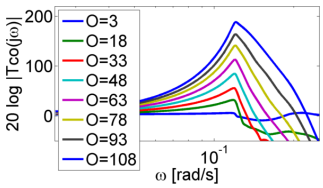

(a) $c = 3$, $o \geq c$, $\epsilon_i \in [0.4, 0.6]$

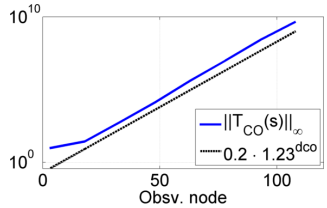

(b) $\|T_{co}(s)\|_\infty$ for a), $c = 3$

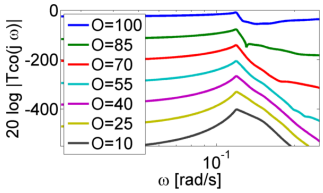

(c) $c = 105$, $o \leq c$, $\epsilon_i \in [0.4, 0.6]$

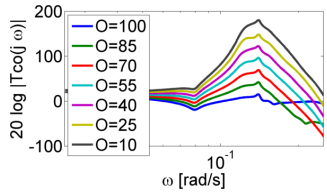

(d) $c = 105$, $c \geq o$, $\epsilon_i \in [1.4, 1.6]$

Figure 4.16: Scaling of $|T_{co}(\jmath\omega)|$ as a function of c kept fixed and o varying with $N = 110$. The model is a PI controller $R(s) = \frac{s+1}{s}$ designed for a vehicle model $G(s) = \frac{1}{s^2+5s}$, hence $\eta = 2$ and the vehicle can track the leader moving with constant velocity. ϵ_i were randomly generated in the given range. Fig. 4.16b shows $\|T_{co}(s)\|_\infty$ for the pairs c, o used in a) in semilogarithmic coordinates. It is clear that the norm scales exponentially.

The effect of the input r_c applied at the control node gets exponentially amplified with the graph distance between c and o. In other words, if the control node is kept fixed, its effect on position y_o of the o node is the larger the larger is the distance between the two nodes. Hence, we have string instability even for a finite platoon.

Figure 4.16 shows scaling for a third-order model with varying asymmetry in a given range. If $c \leq o$, then $\|T_{co}(s)\|_\infty \gg 1$ for large δ_{co} (Fig. 4.16a). In Fig. 4.16b we show how $\|T_{co}(s)\|_\infty$ changes with a graph distance—$c = 3$ is kept fixed and o is varied, so that δ_{co} grows with growing o. If $o < c$, then $T_{co}(0)$ given in (4.27) might decrease faster than $\zeta^{\delta_{co}}$ grows and the norm might be less than one (Fig. 4.16c). A step response of the platoon is shown in Fig. 4.17. Front asymmetry ($\epsilon_i < 1$) has very large oscillations and rear asymmetry ($\epsilon_i > 1$) has very long transients.

Note that even when static state feedback is used, the proof for Theorem 4.28 holds. Define the transfer function

$$T^K_{\min}(s) = \lambda_{\min} K_2 (sI - (A - \lambda_{\min} B K_2))^{-1} B. \tag{4.50}$$

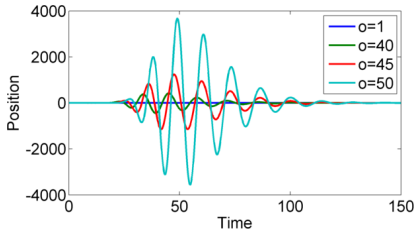

(a) $N = 50, \epsilon_i = 0.5\,\forall i, c = 1, o$ varying

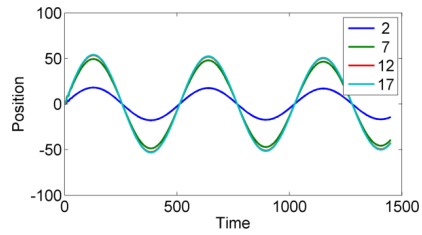

(b) $N = 20, \epsilon_i = 1.5\,\forall i, c = 20, o$ varying.

Figure 4.17: a) A response of the platoon to step in the leader's position. $R(s) = \frac{s+1}{s}, G(s) = \frac{1}{s^2+5s}$. The system has two integrators in the open loop, so exponential scaling with distance occurs. Large oscillations are a consequence of exponential scaling with distance. b) response to step in input of the last agent for $N = 20$ and rear coupling stronger than front. The response is very slow due to presence of an eigenvalue very close to zero [Tangerman et al., 2012].

.

Corollary 4.29. *Consider transfer functions* $T_{co}(s) = \frac{y_o(s)}{r_c(s)}$ *in system (4.48). If* $\|T^K_{\min}(s)\|_\infty > 1$ *and the eigenvalues of* L_p *are uniformly bounded from zero, then* $\|T_{co}(s)\|_\infty \geq \zeta^{\delta_{co}} T_{co}(0)\xi^2$, *where* $\zeta > 1, \xi > 0$ *depend on the open-loop model.*

Proof. Corollary 3.9 gave us the transfer function $T_{co}(s)$ for a system where $\lambda_1 = 0$. Since in the proof of Theorem 4.28 we excluded the leader from the formation, we have to use the formula (3.36) to obtain the transfer function. It reads

$$T_{co}(s) = M_\mathrm{s}(s)a(s)p(s)\overline{S_{co}}(s) = \frac{c(s)}{a(s)}a(s)\overline{S_{co}}(s) = c(s)\overline{S_{co}}(s) \tag{4.51}$$

with $M_\mathrm{s}(s) = \frac{c(s)}{a(s)} = C(sI - A)^{-1}B$ and

$$\overline{S_{co}}(s) = \frac{[b(s)]^{\delta_{co}} \prod_{i=1}^{N-\delta_{co}-1} \Big(a(s) + \gamma_i b(s)\Big)}{\prod_{j=1}^{N} \Big(a(s) + \lambda_j b(s)\Big)}. \tag{4.52}$$

The rest of the proof is identical to the proof of Theorem 4.28. We can form $T_j(s) = \frac{\lambda_j b(s)}{a(s)+\lambda_j b(s)}$ and $Z_{ij}(s) = \frac{a(s)+\gamma_i b(s)}{a(s)+\lambda_j b(s)}$ from (4.51) the same way as in the proof of Thm. 4.28. By this we form $N-\delta_{co}-1$ terms $Z_{ij}(s)$ and δ_{co} terms $T_j(s)$. The only remaining term is $\frac{c(s)}{a(s)+\lambda_\mathrm{r} c(s)}$, where λ_r is an eigenvalue which was used

in neither in $Z_{ij}(s)$ nor $T_j(s)$. The magnitude frequency response of this transfer function is bounded, hence it does not change the exponential scaling. □

The interpretation of this corollary is the following: no matter if the control uses a static state or dynamic feedback, if the single-agent transfer function has the $\mathcal{H}_\infty$ norm greater than 1, exponential scaling occurs for a system with uniformly bounded eigenvalues.

Particular systems

Two integrators in the open loop are necessary for tracking of the leader moving with a constant velocity (Lemma 4.2). However, for at least two integrators in the open-loop we have $\|T_{\min}(s)\|_\infty > 1$ (Lemma 4.3).

Now we state several special cases of the previous theorem. We are aware that some of the them are immediate corollaries of the others, but we want all the cases to be clearly stated.

Corollary 4.30. *The exponential scaling in sense of Theorem 4.28 occurs if either of the following holds.*

a) $\eta = 1$, $\|T_{\min}(s)\|_\infty > 1$ *and the eigenvalues of the Laplacian are uniformly bounded.*

b) $\eta = 1$, $\|T^K_{\min}(s)\|_\infty > 1$ *and the eigenvalues of the Laplacian are uniformly bounded.*

c) $\eta \geq 2$ *and the eigenvalues of the Laplacian are uniformly bounded.*

d) $\eta \geq 2$ *and the control is asymmetric with* $\epsilon_i \leq \epsilon_{\max} < 1$, $\forall i$.

e) $\eta \geq 2$ *and the control is predecessor following with* $\epsilon_i = 0$, $\forall i$.

f) the open-loop model $M(s)$ *is unstable.*

Proof. Parts a)-e) are immediate consequences of Theorem 4.28, 4.24 and Lemma 4.3. Statement a) is almost a restatement of Theorem 4.28. b) follows from Corollary 4.29. Statement c) follows due to norm of system with two integrators—Lemma 4.3. d) follows from c) because asymmetric control achieves a uniform bound on eigenvalues, see Theorem 4.24. In e) predecessor following has uniform bound as well, so exponential scaling occurs.

Note that in f) although not explicitly stated, uniform boundedness is necessary for asymptotic stability of the platoon (see discussion in Sec. 4.5.2). We will

use Nyquist criterion of stability. In order to stabilize an unstable system, the frequency response of open loop $M(s)$ must encircle the point -1 p times in counter-clockwise direction. That means that there exists a frequency ω_0 for which $\Re\{\lambda_i M(\jmath\omega_0)\} < -\frac{1}{2}$ for each λ_i. Hence, by Lemma 4.8 a) for all closed loops holds $|T_i(\jmath\omega)| > 1$. This satisfies the condition in Theorem 4.28. □

For instance, if the vehicle model contains two integrators in the open loop, there is no controller which would prevent exponential scaling. Thus, we cannot have a good behavior with a uniform bound and two integrators. The same holds for a platoon of unstable agents. The price for stability is the exponential scaling on the $\mathcal{H}_\infty$ norm. The main results of [Seiler et al., 2004; Tangerman et al., 2012] are special cases of Theorem 4.28, since asymmetric Laplacian with $\epsilon_i \leq \epsilon_{\max} < 1$ has uniformly bounded eigenvalues.

Moreover, even though the controller in asymmetric platoon is a static state feedback and it is inversely optimal, if the vehicle model contains two or more integrators, exponential scaling is unavoidable. This means that one of the best possible controllers (optimal) still cannot circumvent bad properties of the communication topology. Nevertheless, even a platoon with only one integrator in the open loop can exhibit exponential scaling.

We have not yet discussed the effect of unstable zeros of the open loop. When the open loop is stable but has zeros in the right half-plane, for $\eta = 1$ the closed loop $T_{\min}(s)$ can usually be tuned such that $\|T_{\min}(s)\|_\infty = 1$. However, the standard limitations hold, i.e., the system response will be very slow and the vehicles might exhibit undershoot—see Fig. 4.18.

Also note that for $\eta \geq 2$, the norm $\|\mathbf{T}(s)\|_\infty$ of the transfer function matrix also scales at least exponentially (all the transfer functions in the platoon do so). Note that the proof of Lemma 4.20 should not be used for asymmetric bidirectional control, since the asymmetric Laplacian does not have a unitary matrix of eigenvectors. In this case $\|\mathbf{T}(s)\|_\infty$ can be upper bounded by $\|\mathbf{T}(s)\|_\infty \leq \frac{\sigma_{\max}(V)}{\sigma_{\min}(V)} \max_i \|F_i(s)\|_\infty$ with V being the matrix of eigenvectors of L_{p}, which might be a very conservative bound. In the next section we will see that the norm can grow much better than indicated by this upper bound.

4.6 Design of a string stable controller

We have extensively discussed scaling in platoons which are comprised of vehicles having two integrators in the open loop. In symmetric control the scaling of individual transfer functions is linear or quadratic, while scaling of the transfer function matrix is cubic. When asymmetry is introduced, everything gets even

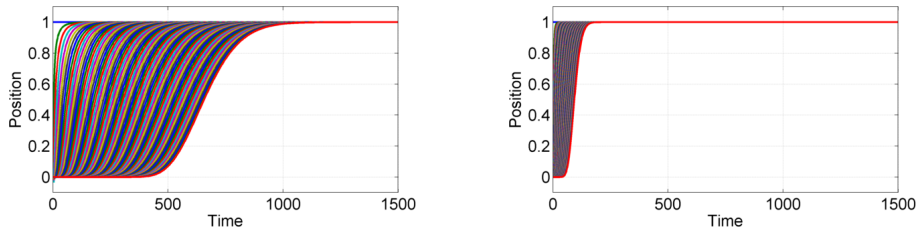

(a) $R(s) = -1.4\frac{s+1}{s+2}, G(s) = \frac{s-1}{s(s+3)}$ (b) $R(s) = 10\frac{s+1}{s+2}, G(s) = \frac{s+1}{s(s+3)}$.

Figure 4.18: a) Response of the platoon with open loop containing CRHP zero. It is clear that the response is slow and the system even exhibits undershoot. The gain of the controller is the maximum for which stability is achieved. b) If, on the other hand, there is no CRHP zero, the gain can be much higher and the response is faster. In both cases, $N = 80$.

worse and the scaling becomes exponential. Hence, having two integrators in the open loop means very bad transients when the platoon gets large. Nevertheless, two integrators are necessary to enable vehicles track the leader's movement (Lemma 4.2).

Thus, so far we have discussed situations in which the system scales badly. In this section we provide a test for string stability. One of the most common string stability conditions in vehicular platoons is $\left\| \frac{y_i(s)}{y_{i-1}(s)} \right\|_\infty \leq 1 \quad \forall i$, used e.g., in [Milanés et al., 2014] (see [Ploeg et al., 2014] for other definitions). In other words, the effect of disturbance at one vehicle must be attenuated when propagated along the platoon. However, in a bidirectional platoon the signal can propagate in both directions.

Definition 4.31 (Bidirectional string stability)**.** *The bidirectional platoon is string-stable if for an input r_c acting at any vehicle c the output y_o at a vehicle o satisfies*

$$\left\| \frac{y_o(s)}{y_{o-1}(s)} \right\|_\infty \leq 1 \quad \forall o \geq c; \qquad \left\| \frac{y_{o-1}(s)}{y_o(s)} \right\|_\infty \leq 1 \quad \forall o < c. \tag{4.53}$$

Similarly to (4.49), for the upper bound on eigenvalues $\lambda_{\max}$ let

$$T_{\max}(s) = \frac{\lambda_{\max} b(s)q(s)}{a(s)p(s) + \lambda_{\max} b(s)q(s)} \tag{4.54}$$

be the corresponding closed loop. We can now state a very simple sufficient condition for the bidirectional string stability, again involving only a norm of the closed loop of an individual agent.

Theorem 4.32. *If* $\|T_{\max}(s)\|_\infty = 1$*, then* $\|T_{co}(s)\|_\infty = |T_{co}(0)|$ *and the platoon is bidirectionally string stable.*

The first part states that the $\mathcal{H}_\infty$ norm of $T_{co}(s)$ equals the steady-state gain of the transfer function (which is only a function of the interconnection structure). If $\lambda_{\max}$ does not depend on N, the bidirectional string stability holds for all N, all ϵ_i and for an arbitrary transfer function.

Note that due to Lemma 4.16, for $\eta = 1$ there almost always exists a controller which satisfies the condition of $\|T_{\max}(s)\|_\infty = 1$. It is just necessary to scale the gain of the controller such that the real part of the open-loop frequency response $\lambda_{\max} M(\jmath\omega)$ is greater than $-\frac{1}{2}$.

The condition $\|T_{\max}(s)\|_\infty = 1$ provides a simple way how to tune a SISO controller for a vehicle model $G(s)$ in a platoon of arbitrary size. As follows from the previous discussion, both for symmetric and asymmetric control, there must be at most one integrator in the open loop to achieve $\|T_{\max}(s)\|_\infty = 1$. Systems with one integrator are appeared in the literature on distributed platoon control [Barooah et al., 2009; Lin et al., 2012b], despite the fact that they cannot track the leader's position. This is usually overcome using leader's velocity as the reference velocity. However, this is a *centralized information* and the leader's velocity needs to be broadcast perpetually, which requires a communications infrastructure. The control law is shown in (4.9).

It remains to show how the norm of the transfer function matrix $\mathbf{T}(s)$ scales.

Theorem 4.33. *Suppose that* $\|T_{\max}(s)\|_\infty = 1$ *and* $\epsilon_i \leq \epsilon_{\max} < 1$*. Then the norm* $\|\mathbf{T}(s)\|_\infty$ *scales linearly with* N*, i.e.* $\|\mathbf{T}(s)\|_\infty = \Theta(N)$*.*

The proof is in Sec. 4.11.12. Linear scaling is the best among the cases discussed in this thesis. It is achieved only when there is one integrator in the open loop and with asymmetric control. Linear sclaling is confirmed in Fig. 4.19. Thus, asymmetry for one integrator in the open loop is a very good solution, while for two integrators it is the worst solution—the scaling is exponential.

4.6.1 Design of a predecessor following controller

For a platoon with uniformly bounded eigenvalues it follows from Theorem 4.28 that $\|T_{\min}\|_\infty = 1$ is necessary for string stability. Denote a standard closed loop $T(s) = M(s)/(1 + M(s))$.

Lemma 4.34. *If the model of the vehicle* $G(s)$ *has neither poles nor zeros in CRHP, except for at most one pole at the origin, then there always exists a predecessor following controller* ($\epsilon = 0$) *achieving* $\|T(s)\|_\infty = 1$*.*

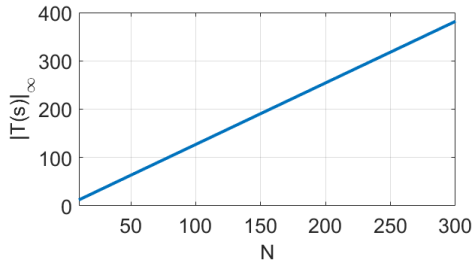

Figure 4.19: Scaling of $\|\mathbf{T}(s)\|_\infty$ for $M(s) = \frac{10(s+1)}{s^3+5s^2+8s}$. This system has $\eta = 1$ and the scaling is linear. Calculated using the *norm* function in Matlab.

This can proved as follows. Since the vehicle model $G(s)$ satisfies the conditions in Lemma 4.16, it is always possible to achieve $\|T(s)\|_\infty = 1$ just by decreasing the gain. The controller can then be designed just to improve the transient.

In addition to that, the controller should be designed to make the closed loop achieve a positive impulse response. Together with $\mathcal{H}_\infty$ norm equal to one, this guarantees string stability for predecessor following in $\mathcal{L}_1$ norm [Eyre et al., 1998]. The necessary conditions for positive impulse response are dominant real pole and no real zero right from this pole [Darbha, 2003]. Besides of string stability, positive impulse response guarantees monotone step response, so the car will not be required to go backwards when there is a larger gap than required. In general, vehicles in platoons should never be required to go backwards. However, it is still not known if we can always guarantee an existence of a controller which has both $\|T(s)\|_\infty = 1$ and positive impulse response for any $G(s)$ having neither poles nor zeros in CRHP.

Although in general we cannot guarantee better transients of predecessor following (PF) compared to asymmetric bidirectional control, we believe that PF offers many advantages:

1) simple architecture—no need for a backward sensor,
2) developed theory for a closed-loop controller design (e. g., $\mathcal{H}_\infty$ approach),
3) handling of heterogeneity—controller for each car can be easily designed separately,
4) faster convergence time for the same maximal control effort—with the same controller the PF has a larger spectral gap (larger $\lambda_{\min}$)

The performance could then be compared by simulations. Note that bidirectional architecture might still be needed in some applications, e.g., for safety reasons

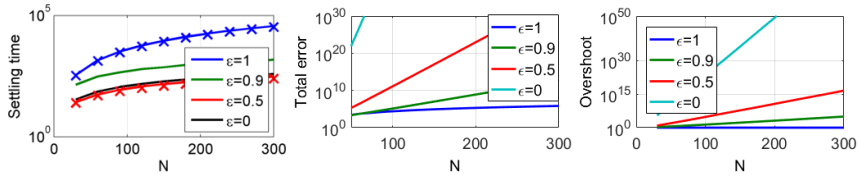

(a) Settling time (b) Total error (c) Max. overshoot

Figure 4.20: Characteristics of response to leader's step in position for different constants of bidirectionality as a function of N. Notice semilogarithmic coordinates. In Fig. 4.20a the crosses are $0.37N^2$ (blue) and $0.81N$ (red). Then it is apparent that symmetric control scales quadratically and asymmetric linearly. In Fig. 4.20b asymmetric control laws scale exponentially, while symmetric only quadratically. In Fig. 4.20c asymmetric control has exponential scaling, while symmetric remains bounded at 1.

(if the vehicle from behind approaches too quickly, the car should accelerate in order to prevent crash).

4.7 Architecture comparison

Here we compare the control architectures discussed so far. In Fig. 4.20 we compare several characteristics of the control law scaling. Namely, transient time, l_2 norm of the error (total error) and overshoot. We assumed for simplicity $\Delta_{\text{ref}} = 0$. The transient time t_0 is defined as the smallest time for which for all i holds $|y_0(t) - y_i(t)| < 0.03$, $\forall t > t_0$. The total error is calculated as $E = \sum_{i=1}^{N} \int_0^\infty (y_0 - y_i)^2 \mathrm{d}t$.

Transient of asymmetric platoon with two integrators in the open loop have already been shown in Fig. 4.17a. For only one integrator in the open loop we show it in Fig. 4.21. The vehicle model is $G(s) = \frac{1}{s(s+0.5)}$. In the top row we show the response of the systems with controller $R_1(s) = 1$. Exactly the same open-loop system was used in [Barooah et al., 2009]. It is clear that if the controller is not designed properly, for larger asymmetries exponential scaling occurs. Indeed, the case with $\epsilon_i = 0.1$ satisfies the conditions for Theorem 4.28.

In the bottom row we show the response of the system in which the controller $R_2(s) = \frac{2.4s+1}{0.05s+1}$ is designed such that is satisfies the conditions in Theorem 4.32. It is apparent that the transient for $\epsilon_i = 0.9$ takes the same time as it did with $R_1(s)$. When the constant of bidirectionality is decreased, it does not start oscillating as the previous controller did. Moreover, the transient is much better. Note that a platoon with such open-loop could not be analyzed by any of the

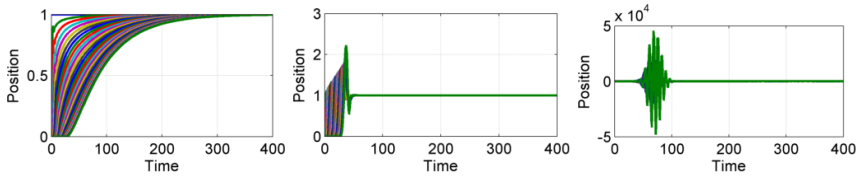

(a) $R_1(s), \epsilon = 0.9$ (b) $R_1(s), \epsilon = 0.5$ (c) $R_1(s), \epsilon = 0.1$

(d) $R_2(s), \epsilon = 0.9$ (e) $R_2(s), \epsilon = 0.5$ (f) $R_2(s), \epsilon = 0.1$

Figure 4.21: Comparison of different levels of asymmetry for a static controller (top row) and dynamic controller (bottom row), $N = 30$.

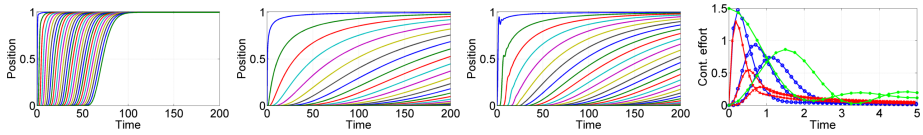

(a) Pred.fol., $R_2(s)$ (b) $R_2(s), \epsilon = 0.9$ (c) $R_3(s), \epsilon = 0.9$ (d) Control effort

Figure 4.22: Responses to leader's step in position for different architectures for $N = 150$. Notice oscillations in the position of the second vehicle in Fig. 4.22c. In 4.22d: blue - predecessor following for $R_2(s)$, red - asymmetric control with $R_2(s)$, green - asymmetric control with $R_3(s)$ for the first three vehicles.

approaches in literature so far. This illustrates that the conditions of Theorem 4.32 should be taken into account when designing the controller.

It is clear that one should not expect for a certain asymmetry that the transient will be good for another one, unless the conditions in Theorem 4.32 are satisfied. For constant of bidirectionality close to one we can achieve similar responses, while for small ϵ_i the responses are much better for the controller taking into account Theorem 4.32.

The comparison of predecessor following and asymmetric architectures is in Fig. 4.22. We use $R_2(s)$ and $R_3(s) = 1.5 = 1.5 \cdot R_1(s)$ defined above. We increased the gain of the static controller in order to have the same control effort for all control architectures. Note that $R_2(s)$ achieves $\|T(s)\|_\infty = 1$ for predecessor following (PF). In addition to that, it also has a positive impulse response. It is apparent from Fig. 4.22 that for the same maximal control effort, the PF achieves the

Property	Symmetric		Asymmetric, $\epsilon_i \leq \epsilon_{\max} < 1$	
	$\eta = 1$	$\eta = 2$	$\eta = 1$	$\eta \geq 2$
$\lvert T_{co}(0)\rvert$	N [4.13]	N [4.13]	bounded[4.26]	bounded[4.26]
$\lVert T_{co}(s)\rVert_\infty$	N [4.32, 4.13]	N^2[4.19]	bounded[4.26, 4.32]	ζ^N [4.28]
$\lVert \mathbf{T}(s)\rVert_\infty$	N^2[4.22]	N^3[4.22]	N [4.33]	ζ^N [4.28]

Table 4.2: Scaling properties of various control laws with proportional asymmetry. In brackets we show the corresponding Lemma, Theorem or Corollary. We consider the best case possible, that is, the controller is properly tuned. Mainly, for systems with one integrator, we assume that conditions in Theorem 4.32 are satisfied. The constant $\zeta > 1$. For $\eta > 2$ the symmetric control becomes asymptotically unstable—Lemma 4.12.

best transient response among the cases shown. Moreover, examining closely the response of $R_1(s)$ in Fig. 4.21a and $R_1(s)$ in Fig. 4.22c one sees that the positions oscillate when converging to the desired state while the response with $R_2(s)$ is monotone.

4.7.1 Complete list of properties

A comprehensive overview of the properties of individual control scenarios discussed so far is shown in Table 4.2. The scaling shown there is the best possible, hence, for control with one integrator, we assume that the conditions in Theorem 4.32 are satisfied. In Table 4.3 we discuss general properties of symmetric and asymmetric distributed control.

Once again we remark that the results are very general and they do not depend on particular model of the vehicle. Only the number of integrators matter, not the particular open-loop model. We therefore show the inherent limitations of the communication topology and of the requirements on the vehicles. For instance, when no communication is allowed and when the topology is asymmetric, exponential scaling must occur and there is no linear controller to prevent it. On the other hand, when the leader's velocity is communicated, performance can be very good.

Control law	Symmetric	Asymmetric, $\epsilon_i \leq \epsilon_{\max} < 1$
Advantages	Easy analysis	Bounded steady-state gain
	Worst scaling of N^3	Can stabilize unstable $M(s)$
		Bounded transient time
		Inversely optimal for a fixed gain
		Good scaling for $\eta = 1$
Disadvantages	Very slow transients	Large peaks and control effort for unstable $M(s)$ and $\eta \geq 2$
	Unstable for $\eta \geq 3$ and unstable $M(s)$	Exponential scaling of $\mathcal{H}_\infty$ norm for $\eta \geq 2$ and for unstable $M(s)$.

Table 4.3: General properties of symmetric and asymmetric control

4.8 Time-headway spacing policy

Having the fixed-distance approaches completely analyzed, we can investigate the effect of the time headway. This section should give some reasons why time headway can behave well. The discussion here is not intended to be complete, it should just illustrate the key facts.

Time-headway spacing policy increases the desired distance with velocity of the vehicle, that is

$$\Delta_{\text{ref}} = \Delta_{\min} + v_i T_{\text{h}}, \tag{4.55}$$

where T_{h} is the headway constant and $\Delta_{\min}$ is the minimal distance which the vehicle should keep from its predecessor. The term $v_i T_{\text{h}}$ states that the vehicle, travelling with v_i, passes the current location of the vehicle ahead in T_{h} seconds. This is similar to the recommendation to human drivers: they should keep the gap equivalent to 2 seconds.

Assume that the controller input (4.13) is changed to

$$\bar{e}_i = (y_{i-1} - y_i - \Delta_{\min} - v_i T_{\text{h}}) - \epsilon(y_i - y_{i+1} - \Delta_{\min} - v_i T_{\text{h}}) + \bar{r}_i. \tag{4.56}$$

We set in this section that all cars have the same asymmetry $\epsilon_i = \epsilon \, \forall i$. Factor the vehicle transfer function as $G(s) = G'(s)\frac{1}{s}$. $G'(s)$ is the transfer function

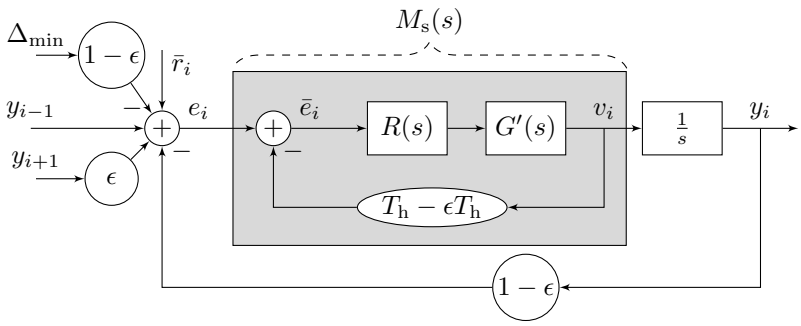

Figure 4.23: Schematic of bidirectional control with time-headway policy.

from controller output to velocity v_i. Define another control

$$e_i = (y_{i-1} - y_i) - \epsilon(y_i - y_{i+1}) + r_i. \tag{4.57}$$

where $r_i = -\Delta_{\min} + \epsilon\Delta_{\min} + \bar{r}_i$. Then $\bar{e}_i = e_i - (T_h - \epsilon T_h)v_i$. This control law can be schematically depicted as in Fig. 4.23. We can view the velocity feedback loop as a transfer function

$$M_s(s) = \frac{R(s)G'(s)}{1 + T_h(1-\epsilon)R(s)G'(s)}. \tag{4.58}$$

The open loop then is $M_h(s) = \frac{y_i(s)}{\varepsilon_i(s)} = \frac{1}{s}M_s(s)$. If neither $R(s)$ nor $G(s)$ have poles on the positive real axis, then $M_s(s)$ does not have a pole at origin. Thus, it contains no integrator. It follows that the open loop $M_h(s)$ has only one integrator (from velocity to position), hence $\eta = 1$. Note that the input e_i to the open loop $M_h(s)$ is identical to the original control signal in bidirectional control with fixed distance (4.13).

Remark 4.35. *Note that neither of the theorems in this chapter can be directly applied to analysis of time headway, except for when predecessor following is used. The reason is that the velocity feedback from the time headway in $M_s(s)$ corresponds to the constant of bidirectionality ϵ_i. Since the last vehicle has no follower, the feedback gain is $\epsilon_N = 1$, while for the others it is $1 - \epsilon$. Hence, in order to have homogeneous platoon, we set the control law of the last agent to*

$$e_N = (1-\epsilon)(y_{N-1} - y_N) + r_N, \tag{4.59}$$

By this we changed the last row of the Laplacian, but we achieved homogeneous platoon. Then only the steady-state gain of transfer function (Theorem 4.9) is different, but the results on string stability remain valid (Theorem 4.32). For predecessor following all the results in this chapter hold without change, because

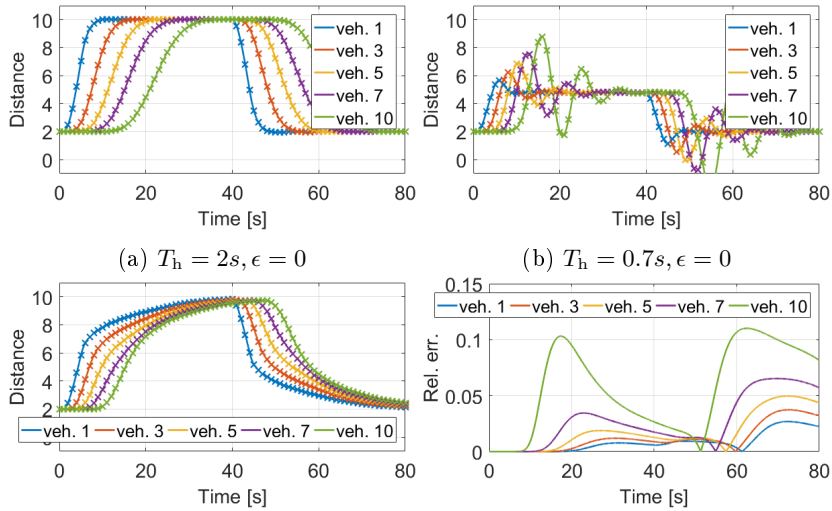

(a) $T_{\mathrm{h}} = 2s, \epsilon = 0$ (b) $T_{\mathrm{h}} = 0.7s, \epsilon = 0$

(c) $T_{\mathrm{h}} = 2s, \epsilon = 0.8$ (d) $T_{\mathrm{h}} = 2s, \epsilon = 0.8$

Figure 4.24: Responses of platoon with $N = 10$ using different time headways for model $M(s) = \frac{2s+2}{s^3+2s}$. The leader's acceleration was $a(t) = 1, t \in [1, 5], a(t) = -1, t \in [41, 45]$ and $a(t) = 0$ otherwise. The crosses are for system with $M_{\mathrm{h}}(s) = \frac{2s+2}{s(s^2+2s+(1-\epsilon)T_{\mathrm{h}}(2s+2))}$ with $\eta = 1$. a), b): response of predecessor following, c) response of asymmetric bidirectional control with $\epsilon = 0.8$. Fig. d) shows relative error to original system when the last vehicle has modified control law (4.59).

the gain for all vehicles is one.

The simulations are in Fig. 4.24. The top row shows results for predecessor following. It follows from the figure that the single-integrator approximation with fixed distance (using $M_{\mathrm{h}}(s) = \frac{2s+2}{s(s^2+2s+(1-\epsilon)T(2s+2))}$) is identical to the original system with time headway. When the time headway was sufficiently large, the response was string stable, while it was string unstable for lower value of T_{h}. String stability can be decided from the norm of closed loop $T(s) = \frac{M_{\mathrm{h}}(s)}{1+M_{\mathrm{h}}(s)}$: for $T_{\mathrm{h}} = 2s$ we get $\|T_{\min}(s)\|_\infty = 1$, while string instability for the second case ($T_{\mathrm{h}} = 0.7s$) follows from $\|T_{\min}(s)\|_\infty = 1.18$. When asymmetric control is used, as expected, the response is a bit slower. Fig. 4.24d shows how different the response of the platoon is when we change the control law of the last agent to (4.59). The error is about 10%, which is tolerable. Moreover, it will get lower when the number of agents increases. For predecessor following the error will be zero.

We have shown that using time-headway spacing policy, we get rid of one inte-

grator in the open loop, so only one integrator remains. Then, as follows from Theorem 4.32 and Lemma 4.16, bidirectional string stability is achievable. This is in agreement with [Middleton and Braslavsky, 2010], where string stability with sufficiently large time headway is also proved.

4.8.1 Model for a real traffic

It is well known that when human drivers are driving a car on the road, no string instability is seen if the conditions are good. We will analyze a reason why it is so. As a model, we will use so called Intelligent Driver Model (IDM), presented in [Treiber and Kesting, 2013, pp. 188]. The model used for individual vehicle is

$$\begin{aligned} \dot{y}_i &= v_i \\ \dot{v}_i &= a\left[1 - \left(\frac{v}{v_{\text{free}}}\right)^{\delta} - \left(\frac{\Delta^*(v, v_i - v_{i-1})}{y_{i-1} - y_{x_i}}\right)^2\right], \end{aligned} \tag{4.60}$$

where v_{free} is the velocity which the driver would use when travelling on an empty road (freeway velocity), $a > 0$ is a acceleration constant and $\delta > 0$. The desired distance $\Delta^*(v, v_i - v_{i-1})$ is defined as

$$\Delta^*(v, v_i - v_{i-1}) = \Delta_{\min} + \max\left(0, v_i T_{\text{h}} + \frac{v_i(v_i - v_{i-1})}{2\sqrt{ab}}\right), \tag{4.61}$$

where $\Delta_{\min}$ is a minimal distance to the car ahead, T_{h} is a desired time headway from the vehicle ahead and b is a comfortable deceleration which the driver wants to take.

Since we are interested in autonomous platooning, the freeway velocity v_{free} makes no sense or can be set sufficiently high, so $\left(\frac{v}{v_{\text{free}}}\right)^{\delta} \to 0$. Further, assume steady-state conditions, in which $y_{i-1} - y_i = \Delta_{\min} + v_i T_{\text{h}}$ and $v_i = v_{i-1}$, so $\Delta^*(v, v_i - v_{i-1}) = \Delta_{\min} + v_i T_{\text{h}} + \frac{v_i(v_i - v_{i-1})}{2\sqrt{ab}} = \Delta_{\min} + v_i T_{\text{h}}$. In order to investigate string stability, we will linearize the system (4.60) at this steady-state equilibrium. Denote

$$f(\cdot) = \frac{\Delta^*(v, v_i - v_{i-1})}{y_{i-1} - y_i} = \frac{\Delta_{\min} + v_i T_{\text{h}} + \frac{v_i(v_i - v_{i-1})}{2\sqrt{ab}}}{y_{i-1} - y_i} \tag{4.62}$$

such that $\dot{v}_i = g(\cdot) = a - af^2(\cdot)$. The linearized model is

$$\begin{aligned}\Delta\dot{y}_i &= \Delta v_i \\ \Delta\dot{v}_i &= \frac{\partial g(\cdot)}{\partial y_{i-1}}\Delta y_{i-1} + \frac{\partial g(\cdot)}{\partial y_i}\Delta y_i + \frac{\partial g(\cdot)}{\partial v_{i-1}}\Delta v_{i-1} + \frac{\partial g(\cdot)}{\partial v_i}\Delta v_i\end{aligned} \tag{4.63}$$

with $\Delta y_{i-1}, \Delta y_i, \Delta v_{i-1}, \Delta v_i$ are the deviations in positions and velocity from the steady-state. The partial derivatives are

$$\frac{\partial g(\cdot)}{\partial y_{i-1}} = 2af(\cdot)\frac{\Delta_{\min} + v_i T_{\mathrm{h}} + \frac{v_i(v_i - v_{i-1})}{2\sqrt{ab}}}{(y_{i-1} - y_i)^2}, \tag{4.64}$$

$$\frac{\partial g(\cdot)}{\partial y_i} = -2af(\cdot)\frac{\Delta_{\min} + v_i T_{\mathrm{h}} + \frac{v_i(v_i - v_{i-1})}{2\sqrt{ab}}}{(y_{i-1} - y_i)^2}, \tag{4.65}$$

$$\frac{\partial g(\cdot)}{\partial v_{i-1}} = -2af(\cdot)\frac{\frac{v_i}{2\sqrt{ab}}}{y_{i-1} - y_i}, \tag{4.66}$$

$$\frac{\partial g(\cdot)}{\partial v_i} = 2af(\cdot)\frac{T_{\mathrm{h}} + \frac{2v_i - v_{i-1}}{2\sqrt{ab}}}{y_{i-1} - y_i}. \tag{4.67}$$

We evaluate the partial derivatives at equilibrium $v_i = v_{i-1} = \bar{v}, y_{i-1} - y_i = \Delta_{\min} + \bar{v}T_{\mathrm{h}}$. Note that $f(\cdot) = 1$ in equilibrium and denote $\psi = \frac{2a}{\Delta_{\min} + \bar{v}T_{\mathrm{h}}}$. Then the linearized model (4.63) is

$$\begin{aligned}\Delta\dot{y}_i &= \Delta v_i \\ \Delta\dot{v}_i &= \psi\left[\underbrace{(\Delta y_{i-1} - \Delta y_i)}_{\text{distance err.}} + \frac{\bar{v}}{2\sqrt{ab}}\underbrace{(\Delta v_{i-1} - \Delta v_i)}_{\text{velocity err.}} - \underbrace{T_{\mathrm{h}}\Delta v_i}_{\text{absolute vel. feedback}}\right].\end{aligned} \tag{4.68}$$

The linearized model consists of two parts: a standard predecessor following part (distance and velocity errors) and a negative absolute velocity feedback. Due to the latter term the model has only one integrator in the open loop. To see this, consider the standard regulation error $\Delta\tilde{y}_i = (\Delta y_{i-1} - \Delta y_i)$. Then, the model (4.68) can be written as a transfer function from $\Delta\tilde{y}_i$ to Δy_i as

$$M_{\mathrm{h}}(s) = \frac{\Delta y_i(s)}{\Delta\tilde{y}_i(s)} = \psi\frac{\frac{\bar{v}}{2\sqrt{ab}}s + 1}{s(s + \psi T_{\mathrm{h}})}. \tag{4.69}$$

This is a PD controller applied to second order model with damping ψT_{h}. That means, similarly to (4.58), that the time headway acts as a damping in the system. As follows from Table 4.2, this system can be tuned such it is string stable. To conclude, the tools used in this chapter can also be used to describe models of the real traffic. Consequently, the case with fixed distance is the hardest to achieve, as it requires two integrators in the open loop.

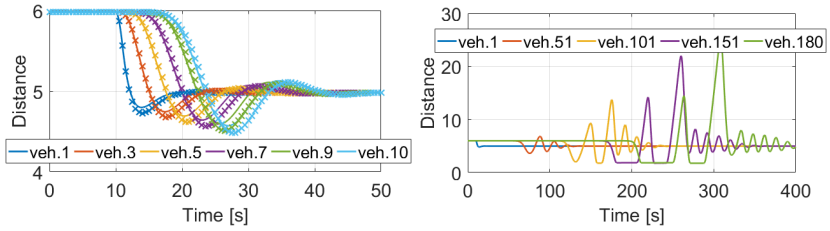

(a) $N = 10$ (b) $N = 180$

Figure 4.25: Response of the IDM model with parameters from [Treiber and Kesting, 2013, pp. 190]. The platoon initially travelled with velocity $v_i = 4$, hence $\Delta_i = 6$ and at time $t = 10$ the leader decelerated for $1s$ with deceleration $1m/s^2$ (speed dropped from 4 to 3). In a) the crosses show response of the linearized system (4.68). The match is satisfactory and string instability is apparent. For $N = 180$ (b) the cars did not undershoot the minimal distance due to nonlinear terms.

Note that for typical parameters given in [Treiber and Kesting, 2013, pp. 190] ($a = 1, b = 1.5, v_{\text{free}} = 120km/h, \Delta_{\min} = 2, \delta = 4, T_{\text{h}} = 1$), the linearized model has its norm $\left\| \frac{M_{\text{h}}(s)}{1+M_{\text{h}}(s)} \right\|_\infty = 1.02$, which means that the system is string unstable. Indeed, this is confirmed in Fig. 4.25a. Looking at the simulation results, it is apparent the response of the vehicles is growing with the distance from the leader. But when the distance gets too small, the nonlinear effects take place and the response of the platoon will be better. The main fact is that the cars do not crash, as follows from Fig. 4.25b. The reason is that the cars are not allowed to go backwards. Anyway, the response is still very oscillatory. For $T_{\text{h}} = 2$ the $\mathcal{H}_\infty$ norm is equal to one.

4.9 Open problems

The most important limitations of the results in this chapter is that they are derived for homogeneous platoons. In practice, every platoon is heterogeneous. Hence, it could be interesting to see how the results here change when the vehicles are not identical. There are some works on robust control of networked systems, such as [Trentelman et al., 2013; Li et al., 2012], which might allow to analyze properties of heterogeneous platoons.

The results in this chapter might also be generalized to other graphs. Quite logically, when the communication topology is a strongly connected tree, asymmetric towards the leader, then exponential scaling is expected. It is also interesting to investigate the properties of platoons where the vehicle uses data not only from

the nearest neighbors, but also from other vehicles nearby. As stated in [Middleton and Braslavsky, 2010], this should change the behavior only quantitatively, not qualitatively. But there is no proof yet.

Everything derived in this section was done using linear control law and linear models of the vehicles. At least the maximal braking and acceleration force is limited for every real vehicle, so a static nonlinearity is always present. Moreover, a nonlinear control law which might improve transients and scalability can be used instead of (4.13). However, analysis would be very complicated and the results would hold probably only for particular models, such as in [Hao and Barooah, 2013].

4.10 Conclusion

We investigated asymmetric control of vehicle platoons where only one Laplacian is used. We say that this control strategy uses proportional asymmetry. First we analyzed scaling of steady-state gain of the platoon. It was proved that it grows without bound with N for a symmetric bidirectional control scheme, while it stays bounded in a presence of asymmetry. We proved that for more than one integrator in the open loop, the asymmetric bidirectional control is not scalable, because $\mathcal{H}_\infty$ norm of any transfer function grows exponentially with the graph distance. This happens despite that fact that the controller was designed to be LQR optimal. The norm of the transfer function matrix with asymmetric control and one integrator in the open loop scales linearly, which is the best among the cases discussed in this thesis. For symmetric architecture, the norm of the transfer function matrix scales quadratically with N for one integrator in the open loop, while for two integrators in the open loop it scales even cubically.

If we allow the vehicles to know the leader's velocity (which requires communications), only one integrator in the open loop can be present. Then we provide a simple design method for tuning the controller to achieve bidirectional string stability. In this case a string-stable predecessor following controller can always be designed. Such controller has much simpler implementation and can achieve faster transients than asymmetric bidirectional control with the same maximal control effort.

The properties of individual control strategies are summarized in Tables 4.2 and 4.3. We conclude that for symmetric interaction everything scales polynomially, while for asymmetric control boundedness is achievable, but also exponential scaling can occur. Time headway acts as a damping, so it can have a good scaling, because it has only one integrator in the open loop.

4.11 Appendix

In this section we provide the proofs which were too long to be shown in the main body of the text. Majority of the proofs here are an exercise in frequency responses combined with the product form of a transfer function.

4.11.1 Proof of Lemma 4.8

Proof. Proof of a): Recall that $\lambda_i M(\jmath\omega_0) = \alpha + \jmath\beta$ (with $\sqrt{-1} = \jmath$) is the value of the frequency response of the scaled open loop. Then the squared modulus of the frequency response of the closed loop $|T_i(\jmath\omega_0)|$ is

$$|T_i(\jmath\omega_0)|^2 = \left|\frac{\lambda_i M(\jmath\omega_0)}{1+\lambda_i M(\jmath\omega_0)}\right|^2 = \frac{\alpha^2+\beta^2}{(\alpha+1)^2+\beta^2}. \tag{4.70}$$

Note that by assumption the magnitude $|T_i(\jmath\omega_0)| > 1$. From (4.70) we have

$$\frac{\alpha^2+\beta^2}{(\alpha+1)^2+\beta^2} > 1 \Rightarrow \alpha < -\frac{1}{2}. \tag{4.71}$$

We write $\lambda_j = \kappa_j\lambda_i$ with gain $\kappa_j \in \langle 1, \frac{\lambda_{\max}}{i}\rangle$. The corresponding closed loop transfer function is $T_j(s) = \frac{\kappa_j\lambda_i M(s)}{1+\kappa_j\lambda_i M(s)}$ with $\kappa_j = \frac{\lambda_j}{\lambda_i}$. The value of $\lambda_i M(\jmath\omega_0)$ is still written as $\alpha + \jmath\beta$. The squared modulus of the closed-loop frequency response at ω_0 is

$$|T_j(\jmath\omega_0)|^2 = \left|\frac{\kappa_j\lambda_i M(\jmath\omega_0)}{1+\kappa_j\lambda_i M(\jmath\omega_0)}\right|^2 = 1 - \frac{2\kappa_j\alpha+1}{(\kappa_j\alpha+1)^2+\kappa_j^2\beta^2}. \tag{4.72}$$

Since $\alpha < -\frac{1}{2}$, κ_j is real and greater than 1 and the denominator is positive, the sign of the fraction must be negative and (4.72) is greater than 1. This proves the statement.

Proof of b) follows from a). Suppose that $|T_j(\jmath\omega_0)| > 1$ for $\lambda_j < \lambda_i$. Then by a) also $|T_i(\jmath\omega_0)| > 1$, which contradicts the assumption $|T_i(\jmath\omega)| \leq 1$. Hence, $|T_j(\jmath\omega_0)| \leq 1$.

Proof of statements c)-e): The transfer function $Z_{ij}(s)$ can be written as $Z_{ij}(s) = \frac{1+\gamma_i M(s)}{1+\lambda_j M(s)}$. Its squared modulus at ω_0 is using $\kappa_{ij} = \frac{\gamma_i}{\lambda_j}$ given as

$$|Z_{ij}(\jmath\omega_0)|^2 = \left|\frac{1+\kappa_{ij}(\alpha_j+\jmath\beta_j)}{1+(\alpha_j+\jmath\beta_j)}\right|^2 = \kappa_{ij}^2\left[1+\frac{\left(\frac{1}{\kappa_{ij}}-1\right)\left(2\alpha_j+1+\frac{1}{\kappa_{ij}}\right)}{(\alpha_j+1)^2+\beta_j^2}\right]. \tag{4.73}$$

Denote the numerator $m_{ij} = \left(\frac{1}{\kappa_{ij}} - 1\right)\left(2\alpha_j + 1 + \frac{1}{\kappa_{ij}}\right)$. The square of the steady-state gain is $|Z_{ij}(0)|^2 = \kappa_{ij}^2$. If $m_{ij} > 0$, then $|Z_{ij}(\jmath\omega_0)|^2 > |Z_{ij}(0)|^2 = \kappa_{ij}^2$ since $(\alpha_j+1)^2+\beta_j^2 > 0$. If $m_{ij} \leq 0$, then $|Z_{ij}(\jmath\omega_0)|^2 \leq |Z_{ij}(0)|^2$. Let us analyze the statements in the Lemma.

c) If $\alpha_j \leq -1$ and $\gamma_i \geq \lambda_j$, then $\left(\frac{1}{\kappa_{ij}} - 1\right) \leq 0$ and also $\left(2\alpha_j + 1 + \frac{1}{\kappa_{ij}}\right) \leq 0$, hence $m_{ij} \geq 0$ which proves the statement c).

d) If $-1 < \alpha_j \leq -\frac{1}{2}$ and $\gamma_i \leq \lambda_j$, so $\kappa_{ij} \leq 1$, then $\left(\frac{1}{\kappa_{ij}} - 1\right) \geq 0$ and also $\left(2\alpha_j + 1 + \frac{1}{\kappa_{ij}}\right) \geq 0$, $m_{ij} > 0$ and d) is proved.

e) If $\alpha_j > -\frac{1}{2}$ and $\gamma_i \geq \lambda_j$, then $\left(\frac{1}{\kappa_{ij}} - 1\right) \leq 0$ and $\left(2\alpha_j + 1 + \frac{1}{\kappa_{ij}}\right) \geq 0$, hence $m_{ij} \leq 0$ and e) is proved. □

4.11.2 Proof of Theorem 4.9

Proof. As stated before, we will work with $L_\mathrm{p} = [l_{ij}]$. We begin by calculating the product in the denominator of (4.26). The product of all λ_i's equals $\det L_\mathrm{p}$. Note that the pinned Laplacian is nonsingluar. The recursive rule to calculate the determinant of a tridiagonal matrix is

$D_n = l_{n,n}D_{n-1} - l_{n,n+1}l_{n+1,n}D_{n-2}$, [Horn and Johnson, 1990, Lem. 0.9.10] where D_n is the determinant of the submatrix of size n. We begin from bottom right corner of L_p. Then $D_1 = 1$ (the bottom right element) and $D_2 = 1$. Then D_3 can be calculated as $D_3 = (1+\epsilon_{N-2})D_2 - \epsilon_{N-2}D_1 = 1$. By induction, the determinant of L_p is $\det L_\mathrm{p} = \prod_{j=1}^{N} \lambda_j = 1$ for any size of L_p.

Now we calculate the product in the numerator of (4.26). It equals the determinant of $\bar{L}_{co}$. Suppose that $c \leq o$. If $o < c$, then the indices c and o are swapped and only the weight of the path is different. The matrix $\bar{L}_{co}$ reads $\bar{L}_{co} = \mathrm{diag}(L_1, L_2)$ with

$$L_1 = \begin{bmatrix} 1+\epsilon_1 & -\epsilon_1 & 0 & .. & 0 \\ -1 & 1+\epsilon_2 & -\epsilon_2 & \dots & 0 \\ \vdots & \vdots & \vdots & \ddots & \vdots \\ 0 & \dots & 0 & -1 & 1+\epsilon_{c-1} \end{bmatrix}. \tag{4.74}$$

The matrix L_2 has the same structure as L_p, hence $\det L_2 = 1$. The dimensions are $L_1 \in \mathbb{R}^{(c-1)\times(c-1)}$ and $L_2 \in \mathbb{R}^{(N-o)\times(N-o)}$.

The determinant of L_1 of size $n \times n$ can be recursively calculated as $\det L_{1,n} = (1+\epsilon_n)\det L_{1,n-1} - \epsilon_n \det L_{1,n-2}$. Let us start from the bottom right corner again. Then $\det L_{1,1} = 1 + \epsilon_{c-1}$ and $\det L_{1,2} = 1 + \epsilon_{c-1} + \epsilon_{c-1}\epsilon_{c-2}$. The determinant

$$\begin{aligned}\det L_{1,3} &= (1+\epsilon_{c-3})\det L_{1,2} - \epsilon_{c-3}\det L_{1,1} \\ &= 1 + \epsilon_{c-1} + \epsilon_{c-1}\epsilon_{c-2} + \epsilon_{c-1}\epsilon_{c-2}\epsilon_{c-3}. \end{aligned} \tag{4.75}$$

The pattern is now apparent and the determinant of L_1 is

$$\det L_1 = 1 + \sum_{i=1}^{c-1}\prod_{j=1}^{i}\epsilon_{c-j}. \tag{4.76}$$

The sum goes from 1 to $c-1$ because the vehicle c is part of the path from c to o, so $c-1$ vehicles remain. Since $\det L_\mathrm{p} = \det L_1 \det L_2$, the steady state gain is then $T_{co}(0) = \vartheta_{co}\frac{\det L_1 \det L_2}{\det L_\mathrm{p}} = \vartheta_{co}\left(1 + \sum_{i=1}^{c-1}\prod_{j=1}^{i}\epsilon_{c-j}\right)$. □

4.11.3 Proof of Lemma 4.15

Proof. We will show the proof in two steps. First, we show that we are interested in low frequencies and then we introduce an approximate system and prove its linear scaling. Note that we use the system $T_1(s) = \lambda_1 \frac{b(s)q(s)}{a(s)p(s)+\lambda_1 b(s)q(s)}$, so it is a multiple of the diagonal block and $T_1(0) = 1$.

First we show that we are interested in low frequencies. Fix $\kappa > 0$. Then let ξ be $\xi = \max_{\lambda_i \in [\kappa,4]} \left\| \lambda_i \frac{b(s)q(s)}{a(s)p(s)+\lambda_i b(s)q(s)} \right\|_\infty$. Since the poles do not lie on the imaginary axis and the interval of gains is bounded, ξ is bounded from above. If we can show that with λ_1 decaying to zero (and with $\lambda_1 < \kappa$) the $\mathcal{H}_\infty$ norm of $T_1(s)$ grows without bound, it will sooner or later exceed ξ. Let us do that.

We know from (4.35) that $\lambda_1 \to 0$ quadratically fast in N. Hence, the gain in the closed loop gets to zero, making the bandwidth of $T_1(s)$ very small and decaying to zero. Therefore, we are interested in low-frequency behavior, so ω is small.

Let the open loop be written as

$$M(s) = \frac{d_m s^m + d_{m-1}s^{m-1} + \ldots + d_1 s + d_0}{s^2(c_{n-2}s^{n-2}c_{n-3}s^{n-3} + \ldots + c_1 s + c_0)}. \tag{4.77}$$

Calculating its frequency response, separating to real and imaginary part, we get

$$M(\jmath\omega) = -\frac{d_0 c_o + \mathcal{O}(\omega^2)}{\omega^2 \left(c_0^2 + \mathcal{O}(\omega^2)\right)} - \jmath \frac{d_0 c_1 - d_1 c_0 + \mathcal{O}(\omega)}{\omega \left(c_0^2 + \mathcal{O}(\omega^2)\right)}. \tag{4.78}$$

We can neglect the higher order terms in the numerator and denominator, since ω is small. Hence the real part $\Re\{M(\jmath\omega)\} \approx -\frac{d_0 c_o}{\omega^2 c_0^2} = -g_c \frac{1}{\omega^2}$ and the imaginary part $\Im\{M(\jmath\omega)\} \approx \frac{d_0 c_1 - d_1 c_0}{\omega c_0^2} = -g_i \frac{1}{\omega}$, so the approximated open loop frequency response reads

$$\overline{M}(\jmath\omega) = -g_r \frac{1}{\omega^2} - \jmath g_i \frac{1}{\omega}. \tag{4.79}$$

We defined $g_r = \frac{d_0}{c_o}$ and $g_i = \frac{d_0 c_1 - d_1 c_0}{c_0^2}$.

The approximated frequency response of the closed loop is then $\overline{T}_1(\jmath\omega) = \frac{\lambda_1 \overline{M}(\jmath\omega)}{1 + \lambda_1 \overline{M}(\jmath\omega)}$. Its squared modulus is

$$\left|\overline{T}_1(\jmath\omega)\right|^2 = \frac{\lambda_1 \left(g_i^2 \omega^2 + g_r^2\right)}{\left(g_r \lambda_1 - \omega^2\right)^2 + \lambda_1^2 g_i^2 \omega^2}. \tag{4.80}$$

We can calculate the frequency ω_m for which (4.80) attains its maximum. It is

$$\omega_\mathrm{m} = \frac{g_r}{g_i} \sqrt{\sqrt{\frac{2 g_i^2}{g_r} \lambda_1 + 1} - 1}. \tag{4.81}$$

Plugging this frequency for ω to (4.80), we get the maximal modulus as

$$\max_\omega \left|\overline{T}_1(\jmath\omega)\right|^2 \tag{4.82}$$
$$= \frac{g_i^4 \sqrt{g_r + 2 g_i^2 \lambda_1} \lambda_1^2}{g_i^4 \sqrt{g_r + 2 g_i^2 \lambda_1} \lambda_1^2 + (-2 g_r g_i^2 \sqrt{g_r + 2 g_i^2 \lambda_1} + 4 g_i^2 \sqrt{g_r^3}) \lambda_1 - 2 g_r^2 \sqrt{g_r + 2 g_i^2 \lambda_1} + 2 \sqrt{g_r^5}}.$$

Define $\tau = \sqrt{2g_i^2\lambda_1 + g_r}$ and $\tau^2 = 2g_i^2\lambda_1 + g_r$. Then we simplify (4.83) to

$$\begin{aligned}
\max_\omega |\overline{T}_1(\jmath\omega)|^2 &= \frac{g_i^4\lambda_1^2\tau}{g_i^4\lambda_1^2\tau + 2g_r\sqrt{g_r}(2g_i^2\lambda_1 + g_r) - g_r\tau(2g_i^2\lambda_1 + g_r) - g_r^2\tau} \\
&= \frac{g_i^4\lambda_1^2\tau}{g_i^4\lambda_1^2\tau + 2g_r\sqrt{g_r}\tau^2 - g_r\tau^3 - g_r^2\tau} = \frac{g_i^4\lambda_1^2}{g_i^4\lambda_1^2 + 2g_r\sqrt{g_r}\tau - g_r\tau^2 - g_r^2} \\
&= \frac{g_i^4\lambda_1^2}{g_i^4\lambda_1^2 - \left(\sqrt{g_r}\tau - g_r\right)^2} = \frac{g_i^4\lambda_1^2}{\left(g_i^2\lambda_1 + \sqrt{g_r}\tau - g_r\right)\left(g_i^2\lambda_1 - \sqrt{g_r}\tau + g_r\right)} \\
&= \frac{g_i^4\lambda_1^2}{\left(g_i^2\lambda_1 + \sqrt{g_r}\sqrt{2g_i^2\lambda_1 + g_r} - g_r\right)\left(g_i^2\lambda_1 - \sqrt{g_r}\sqrt{2g_i^2\lambda_1 + g_r} + g_r\right)} \\
&= \frac{g_i^4\lambda_1^2}{\left(g_i^2\lambda_1 + g_r\sqrt{1 + \frac{2g_i^2}{g_r}\lambda_1} - g_r\right)\left(g_i^2\lambda_1 - g_r\sqrt{1 + \frac{2g_i^2}{g_r}\lambda_1} + g_r\right)}.
\end{aligned} \tag{4.83}$$

We can use $\sqrt{1+x} = 1 + \frac{1}{2}x - \frac{1}{8}x^2 + \ldots$ to expand $\sqrt{1 + \frac{2g_i^2}{g_r}\lambda_1} = 1 + \frac{g_i^2}{g_r}\lambda_1 - \frac{g_i^4}{2g_r^2}\lambda_1^2 + \ldots \approx 1 + \frac{g_i^2}{g_r}\lambda_1 - \frac{g_i^4}{2g_r^2}$. Plugging this to (4.83) we get

$$\max_\omega |\overline{T}_1(\jmath\omega)|^2 = \frac{2g_r}{2g_i^2\lambda_1 - \frac{g_i^4}{2g_r}\lambda_1^2}, \tag{4.84}$$

from which we can get after neglecting the term with λ_1^2 the final result

$$\max_\omega |\overline{T}_1(\jmath\omega)| \approx \sqrt{\frac{g_r}{g_i^2\lambda_1}} = \Theta(N), \tag{4.85}$$

because the eigenvalue is in order of $1/N^2$.

Simulation of frequency responses of the original system $T_1(s)$ with open loop $M(s)$ and its approximation by $\overline{T}_1(s)$ using the open loop (4.79) is shown in Fig. 4.26. □

4.11.4 Proof of Lemma 4.16

Proof. First factor the open-loop transfer function as $M(s) = \frac{1}{s}M_\mathrm{s}(s)$ with $M_\mathrm{s}(0) < \infty$. Since by assumption the open loop has no pole in CRHP except for one at the origin, we get $|M_\mathrm{s}(\jmath\omega)| \leq \xi < \infty$ for all ω. We prove that there exists $\kappa > 0$ such that $\left\| \frac{\kappa\frac{1}{s}M_\mathrm{s}(s)}{1+\kappa\frac{1}{s}M_\mathrm{s}(s)} \right\|_\infty = 1$.

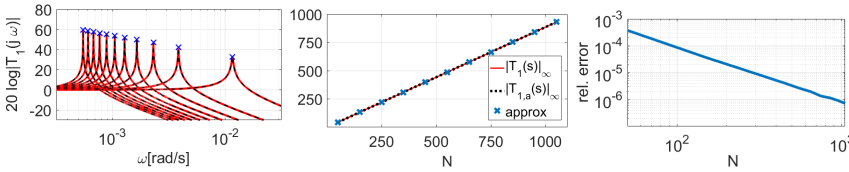

(a) (b) (c)

Figure 4.26: The magnitude frequency responses of $|T_1(\jmath\omega)|$ (red) and $|\overline{T}_1(\jmath\omega)|$ (black) as a function of N for different models is in Fig. 4.26a. The peaks correspond to $N = 50, 150, \ldots, 1050$ (right to left). The original model was $M(s) = \frac{s^2+5s+2}{s^4+8s^3+15s^2}$ and the approximation $\overline{M}(s) = \frac{0.304s+0.133}{s^2}$. It is apparent that responses are almost identical. Fig. 4.26b shows the true and approximated norm of $T_1(s)$. The blue points are the values obtained by (4.85). Fig. 4.26c shows the relative error $\left|\frac{\|T_1(s)\|_\infty - \|\overline{T}_1(s)\|_\infty}{\|T_1(s)\|_\infty}\right|$ of the approximation as a function of N. It decays to zero.

It was shown in Lemma 4.8 b) that in order to achieve $\left\|\frac{\kappa\frac{1}{\jmath\omega}M_s(\jmath\omega)}{1+\kappa\frac{1}{\jmath\omega}M_s(\jmath\omega)}\right\| \leq 1$ for all $\omega \geq 0$, we require that the real part of $\kappa\frac{1}{\jmath\omega}M_s(\jmath\omega)$ is greater than $-\frac{1}{2}$ for all ω. We will show that it is always possible to scale the open-loop transfer function $M(s)$ to achieve that.

We define several functions of ω to capture the frequency response of the open loop. Let $M_s(\jmath\omega) = \frac{\gamma(\omega)+\jmath\delta(\omega)}{\alpha(\omega)+\jmath\beta(\omega)}$, where $\alpha(\omega), \gamma(\omega)$ are real parts of the frequency response of the denominator (resp. numerator) and $\beta(\omega), \delta(\omega)$ are imaginary parts. The frequency response of the open loop then is

$$\begin{aligned}\kappa\frac{1}{\jmath\omega}M_s(\jmath\omega) &= \kappa\frac{-\jmath}{\omega}\frac{\gamma(\omega)+\jmath\delta(\omega)}{\alpha(\omega)+\jmath\beta(\omega)} \\ &= \kappa\frac{-\jmath}{\omega}\frac{\alpha(\omega)\gamma(\omega)+\beta(\omega)\delta(\omega)+\jmath(\alpha(\omega)\delta(\omega)-\beta(\omega)\gamma(\omega))}{\alpha^2(\omega)+\beta^2(\omega)} \\ &= -\kappa\frac{(\alpha(\omega)\delta(\omega)-\beta(\omega)\gamma(\omega))+\jmath(\alpha(\omega)\gamma(\omega)+\beta(\omega)\delta(\omega))}{\omega(\alpha^2(\omega)+\beta^2(\omega))}. \end{aligned} \quad (4.86)$$

Since we expect that $M_s(s)$ has neither poles nor zeros on the imaginary axis, $\beta(0) = \delta(0) = 0$. The real part of (4.86) is

$$\Re\left\{\kappa\frac{1}{\jmath\omega}M_s(\jmath\omega)\right\} = -\kappa\frac{\alpha(\omega)\delta(\omega)-\beta(\omega)\gamma(\omega)}{\omega(\alpha^2(\omega)+\beta^2(\omega))}. \quad (4.87)$$

Note that since $\omega \in \mathbb{R}$, in the denominator the term $\alpha^2(\omega)+\beta^2(\omega) \neq 0$ for any $\omega \neq 0$. Recall that we expect $|M_s(\jmath\omega)| \leq \xi < \infty$ for all ω and note that (4.87)

can be written as

$$-\kappa\frac{1}{\omega}\frac{\alpha(\omega)\delta(\omega)-\beta(\omega)\gamma(\omega)}{\alpha^2(\omega)+\beta^2(\omega)}=-\kappa\frac{1}{\omega}\Im\{M_{\mathrm{s}}(\jmath\omega)\}. \tag{4.88}$$

The term $|\Im\{M_{\mathrm{s}}(\jmath\omega)\}|\leq\xi$ because $|M_{\mathrm{s}}(\jmath\omega)|\leq\xi$. It follows that (4.87) can be unbounded only as $\omega\to 0$. The limit is

$$\lim_{\omega\to 0}\left(-\kappa\frac{\alpha(\omega)\delta(\omega)-\beta(\omega)\gamma(\omega)}{\omega(\alpha^2(\omega)+\beta^2(\omega))}\right)=\frac{0}{0}. \tag{4.89}$$

By using the L'Hospital rule we obtain

$$\lim_{\omega\to 0}\left(-\kappa\frac{\alpha(\omega)\delta(\omega)-\beta(\omega)\gamma(\omega)}{\omega(\alpha^2(\omega)+\beta^2(\omega))}\right)=\frac{\phi_1\psi_0-\phi_0\psi_1}{\psi_0^2}, \tag{4.90}$$

where ψ_0,ψ_1 are coefficients of s^0,s^1, respectively, in the denominator of the open loop $M_{\mathrm{s}}(s)$ and ϕ_0,ϕ_1 are coefficients of s^0,s^1, respectively, in the numerator of the open loop $M_{\mathrm{s}}(s)$. It follows that (4.90) is bounded. Then

$$\left|\kappa\frac{1}{\omega}\frac{\alpha(\omega)\delta(\omega)-\beta(\omega)\gamma(\omega)}{\alpha^2(\omega)+\beta^2(\omega)}\right|\leq\zeta<\infty. \tag{4.91}$$

So the absolute value of the real part of the frequency response of $\kappa\frac{1}{\jmath\omega}M_{\mathrm{s}}(\jmath\omega)$ is bounded. We require that $\Re\{\kappa\frac{1}{\jmath\omega}M_{\mathrm{s}}(\jmath\omega)\}\geq-\frac{1}{2}$. We can calculate κ as

$$\kappa\leq\frac{1}{2\zeta}. \tag{4.92}$$

We have shown that there always exists κ for which for the closed loop holds $\left\|\frac{\kappa\frac{1}{s}M_{\mathrm{s}}(s)}{1+\kappa\frac{1}{s}M_{\mathrm{s}}(s)}\right\|_\infty=1$. □

4.11.5 Proof of Theorem 4.18

Proof. Lemma 4.15 shows that $\|T_1(s)\|_\infty$ grows linearly in N. It also follows from the proof that $\|T_i(s)\|_\infty\leq\|T_1(s)\|_\infty$ for $i>1$ and N sufficiently large. To see this, consider (4.85). By Theorem 3.3 the transfer function $T_{1N}(s)$ can be written as

$$T_{1N}(s)=\prod_{i=1}^{N}T_i(s)=\prod_{i=1}^{N}\frac{\lambda_i b(s)q(s)}{a(s)p(s)+\lambda_i b(s)q(s)}=T_1(s)\prod_{i=2}^{N}T_i(s). \tag{4.93}$$

This follows from the fact that $\vartheta_{1N}=1$ and $\prod_{i=1}^{N}\lambda_i=\det L_{\mathrm{p}}=1$.

Let ω_{m} be the frequency at which $T_1(\jmath\omega)$ attains its maximum. It follows from Lemma 4.8 a) that at this frequency for all transfer functions $T_i(s)$, $i > 1$ holds $|T_i(\jmath\omega_{\mathrm{m}})| \geq 1$ since $\lambda_i \geq \lambda_1$. Hence, from (4.93) we have

$$\|T_{1N}(s)\|_\infty \geq \prod_{i=1}^{N} |T_i(\jmath\omega_{\mathrm{m}})| \geq |T_1(\jmath\omega_{\mathrm{m}})| \geq c_1 N. \tag{4.94}$$

In the second part we show that the norm is upper bounded by $c_2 N$. To do this, we show that $\prod_{i=2}^{N} |T_i(\jmath\omega_{\mathrm{m}})|$ is bounded for frequency ω_{m}. We use the same approximation of the open-loop frequency response as we did in the proof of Lemma 4.15, that is

$$\overline{M}(\jmath\omega) = -\frac{g_r}{\omega^2} - \jmath\frac{g_i}{\omega} \tag{4.95}$$

and the frequency ω_{m} is defined in (4.81). Define $\overline{T}_i(\jmath\omega) = \frac{\lambda_i \overline{M}(\jmath\omega)}{1+\lambda_i \overline{M}(\jmath\omega)}$. The squared frequency response of $\overline{T}_i(\jmath\omega_{\mathrm{m}})$ is using this approximation

$$\left|\overline{T}_i(\jmath\omega_{\mathrm{m}})\right|^2 = \frac{\lambda_i^2 g_i^4 \tau}{(\tau - \sqrt{g_r}) g_i^4 \lambda_i^2 + \sqrt{g_r}(g_i^2 \lambda_i - \sqrt{g_r}\tau + g_r)^2} \tag{4.96}$$

with $\tau = \sqrt{g_r}\sqrt{2\frac{g_i^2}{g_r}\lambda_1 + 1}$. Since λ_1 is small, we approximate $\tau \approx \sqrt{g_r}\left(1 + \frac{g_i^2}{g_r}\lambda_1\right)$. Then

$$\begin{aligned}\left|\overline{T}_i(\jmath\omega_{\mathrm{m}})\right|^2 &= \frac{g_i^6 \lambda_i^2 \lambda_1 + g_i^4 g_r \lambda_i^2}{g_i^6 \lambda_i^2 \lambda_1 + g_i^4 g_r (\lambda_i - \lambda_1)^2} = \frac{\lambda_1 + \frac{g_r}{g_i^2}}{\lambda_1 + \frac{g_r}{g_i^2}(1 - \frac{\lambda_1}{\lambda_i})^2} \approx \frac{\frac{g_r}{g_i^2}}{\frac{g_r}{g_i^2}(1 - \frac{\lambda_1}{\lambda_i})^2} \\ &= \frac{1}{(1 - \frac{\lambda_1}{\lambda_i})^2}, \quad \Rightarrow \left|\overline{T}_i(\jmath\omega_{\mathrm{m}})\right| \approx \frac{1}{1 - \frac{\lambda_1}{\lambda_i}}.\end{aligned} \tag{4.97}$$

We can bound λ_1/λ_i using (4.33) as

$$\frac{\lambda_1}{\lambda_i} \leq \frac{\frac{\pi^2}{(4N+2)^2}}{\frac{(2i-1)^2}{(2N+1)^2}} = \frac{\pi^2}{(4i-2)^2}. \tag{4.98}$$

Then $\left|\overline{T}_i(\jmath\omega_\mathrm{m})\right| \leq 1 + \frac{\pi^2}{(4i-2)^2-\pi^2}$. The product then is

$$\begin{aligned}\prod_{i=2}^{N}|\overline{T}_i(\jmath\omega_\mathrm{m})| &\approx \prod_{i=2}^{N}\frac{1}{1-\frac{\lambda_1}{\lambda_i}} \leq \prod_{i=2}^{N}\left(1+\frac{\pi^2}{(4i-2)^2-\pi^2}\right)\\ &\leq \prod_{i=2}^{N}\left(1+\frac{2}{i^2}\right) \leq \prod_{i=1}^{\infty}\left(1+\frac{2}{i^2}\right).\end{aligned} \tag{4.99}$$

The product can be bounded as ([Melnikov, 2011])

$$\prod_{i=1}^{\infty}\left(1+\frac{2}{i^2}\right) = \frac{\sinh\sqrt{2}\pi}{\sqrt{2}\pi} = c_2. \tag{4.100}$$

It follows that $|T_{1N}(\jmath\omega_\mathrm{m})|$ is bounded as

$$|T_{1N}(\jmath\omega_\mathrm{m})| \approx \prod_{i=1}^{N}\overline{T}_i(\jmath\omega_\mathrm{m}) \leq |T_1(\jmath\omega_\mathrm{m})|\prod_{i=2}^{N}|\overline{T}_i(\jmath\omega_\mathrm{m})| \leq |T_1(\jmath\omega_\mathrm{m})|c_2 \leq c_2 N. \tag{4.101}$$

For other peaks caused by blocks $T_i(s)$ in (4.93) we know that their value is lower than that of $T_1(s)$. Moreover, at higher frequencies the blocks $T_i(s)$ with λ_i very low have they roll-off, hence the frequency response is sufficiently low. So it is the peak of $T_1(s)$ that sets the $\mathcal{H}_\infty$ norm of $T_{1N}(s)$ and this peak scales linearly by (4.94) and (4.101).

Note that the proof of the upper bound is not complete. For a complete proof it would be necessary to prove that the frequency response is bounded for any fixed frequency for any N. Currently, we do not have such a proof. □

4.11.6 Proof of Theorem 4.19

Proof. As in the proof of Lemma 4.11, we will work with the approximate open loop $\overline{M}(s)$ defined in (4.79). Consider the real part of the frequency response $\Re\{\lambda_1\overline{M}(\jmath\omega_\mathrm{m})\}$ with ω_m defined in (4.81). This corresponds to the frequency where the approximate closed loop has its maximum. The real part of the open loop reads

$$\alpha = \Re\{\lambda_1 M(\jmath\omega_m)\} \approx \frac{-g_i^2\lambda_1}{g_r\left(\sqrt{1+\lambda_1\frac{2g_i^2}{g_r}}-1\right)} \approx \frac{-g_i^2\lambda_1}{g_i^2\lambda_1 - \frac{g_i^4}{g_r^2}\lambda_1^2} \leq -1 \text{ for } \lambda_1 \to 0, \tag{4.102}$$

since g_i, g_r are fixed. This is the frequency response of the open loop scaled by the smallest gain possible, λ_1. Hence, for all other open loops $\lambda_i M(\jmath\omega_\mathrm{m})$ it is also less than -1.

The transfer function $T_{NN}(s)$ can be by (4.24) written as

$$T_{NN}(s) = T_{NN}(0)T_1(s)\frac{\lambda_N}{\gamma_1}Z_{1N}(s)\prod_{i=2}^{N-1}\frac{\lambda_i}{\gamma_i}Z_{ii}(s), \tag{4.103}$$

where we defined $Z_{1N}(s) = \frac{a(s)p(s)+\gamma_1 b(s)q(s)}{a(s)p(s)+\lambda_N b(s)q(s)}$. By Cauchy Interlacing Theorem $\gamma_i \geq \lambda_i$. It follows from Lemma 4.8 c) that $\prod_{i=2}^{N-1}\frac{\lambda_i}{\gamma_i}Z_{ii}(\jmath\omega_m) \geq \prod_{i=2}^{N-1}\frac{\lambda_i}{\gamma_i}Z_{ii}(0) = 1$, because $\alpha < -1$. Therefore, we get

$$T_{NN}(\jmath\omega_\mathrm{m}) \geq T_{NN}(0)T_1(\jmath\omega_\mathrm{m})\frac{\lambda_N}{\gamma_1}Z_{1N}(\jmath\omega_\mathrm{m}). \tag{4.104}$$

It follows from Corollary 4.13 that $T_{NN}(0) = N$ and from Lemma 4.15 that $|T_1(\jmath\omega_\mathrm{m})| = \Theta(N)$ (recall that at ω_m the response $T_1(\jmath\omega)$ attains its maximum). Hence, $T_{NN}(0)|T_1(\jmath\omega_\mathrm{m})| = \Theta(N^2)$.

We now prove that $\frac{\lambda_N}{\gamma_1}Z_{1N}(\jmath\omega_\mathrm{m})$ is bounded at ω_m. We will have to work with the approximate model $\overline{M}(s) = -g_r\frac{1}{\omega^2} - \jmath g_i\frac{1}{\omega}$, defined in (4.79), resulting in $\overline{Z}_{1N}(s) = \frac{1+\gamma_1\overline{M}(s)}{1+\lambda_N\overline{M}(s)}$.

After evaluating the $|\frac{\lambda_N}{\gamma_1}\overline{Z}_{1N}(\jmath\omega)|$ at ω_m from (4.81), we get

$$\left|\frac{\lambda_N}{\gamma_1}\overline{Z}_{1N}(\jmath\omega_\mathrm{m})\right|^2 = \frac{\tau + (\frac{\tau}{g_i^2\gamma_1} - g_r)^2}{\tau + (\frac{\tau}{g_i^2\lambda_N} - g_r)^2} \tag{4.105}$$

with $\tau = g_r^2\sqrt{1+\frac{2g_i^2\lambda_1}{g_r}} - g_r^2$. We can approximate the square root as $\sqrt{1+\frac{2g_i^2\lambda_1}{g_r}} = 1 + \frac{g_i^2}{g_r}\lambda_1 - \frac{g_i^4}{2g_r^2}\lambda_1^2 + \ldots$. We keep only $\sqrt{1+\frac{2g_i^2\lambda_1}{g_r}} \approx 1 + \frac{g_i^2}{g_r}\lambda_1$ to get $\tau \approx g_r g_i^2\lambda_1$. Then the modulus simplifies to

$$\left|\frac{\lambda_N}{\gamma_1}\overline{Z}_r(\jmath\omega_\mathrm{m})\right|^2 \approx \frac{\left(\frac{\lambda_1}{\gamma_1}-1\right)^2 + \frac{g_i^2}{g_r}\lambda_1}{\left(\frac{\lambda_1}{\lambda_N}-1\right)^2 + \frac{g_i^2}{g_r}\lambda_1} \leq \frac{\left(\frac{\lambda_1}{\gamma_1}-1\right)^2}{\left(\frac{\lambda_1}{\lambda_N}-1\right)^2 + \frac{g_i^2}{g_r}\lambda_1}. \tag{4.106}$$

Note that for N large, $\lambda_1 \to 0$ and $\lambda_N \to 4$. Then $\frac{g_i^2}{g_r}\lambda_1 \approx 0$ and $\left(\frac{\lambda_1}{\lambda_N}-1\right)^2 +$

$\frac{g_i^2}{g_r}\lambda_1 \approx 1$. We can write

$$\left|\frac{\lambda_N}{\gamma_1}\overline{Z}_{1N}(\jmath\omega_{\mathrm{m}})\right| \approx \left|\frac{\lambda_1}{\gamma_1} - 1\right|. \tag{4.107}$$

Let us show that λ_1 and γ_1 scale similarly with N. Note that γ_1 is an eigenvalue of a principal submatrix of L_{p} with a form

$$\bar{L}_{NN} = \begin{bmatrix} 2 & -1 & 0 & \dots & 0 \\ -1 & 2 & -1 & \dots & 0 \\ \vdots & \vdots & \vdots & \ddots & \vdots \\ 0 & \dots & -1 & 2 & -1 \\ 0 & \dots & 0 & -1 & 2 \end{bmatrix} \in \mathbb{R}^{N-1\times N-1}. \tag{4.108}$$

This corresponds to a path graph with $N-1$ agents where both the first and last vehicle is connected to the leader. The eigenvalues for such a graph are as follows [Parlangeli and Notarstefano, 2012, Prop. 3.3]

$$\gamma_i = 2\left(\cos\frac{i\pi}{N} - 1\right) = 4\sin^2\left(\frac{i\pi}{2N}\right). \tag{4.109}$$

Then it follows that $\lambda_1 = \frac{4\pi^2}{16N^2+16N+4}$ and $\gamma_1 = \frac{4\pi^2}{4N^2}$—we used the same approach as in (4.35). Hence, $\frac{\lambda_1}{\gamma_1} < \frac{1}{4}$. We can get the result that

$$0.75 \leq \left|\frac{\lambda_N}{\gamma_1}Z_{1N}(\jmath\omega_{\mathrm{m}})\right| \leq 1, \tag{4.110}$$

which means the the gain of $\frac{\lambda_N}{\gamma_1}\overline{Z}_{1N}(\jmath\omega_{\mathrm{m}})$ is bounded, regardless of the number of agents. To conclude, we get the lower bound on the norm as

$$\|T_{NN}(s)\|_\infty \geq T_{NN}(\jmath\omega_{\mathrm{m}}) \geq T_{NN}(0)T_1(\jmath\omega_{\mathrm{m}})\frac{\lambda_N}{\gamma_1}Z_{1N}(\jmath\omega_{\mathrm{m}}) \geq \zeta_1 N^2, \quad \zeta_1 = 0.75. \tag{4.111}$$

Now we show that $|T_{NN}(\jmath\omega_{\mathrm{m}})| \leq \zeta_2 N^2$. It follows from (4.110) that $|\frac{\lambda_N}{\gamma_1}Z_{1N}(\jmath\omega_{\mathrm{m}})| \leq 1$. We now show that $\prod_{i=2}^{N-1}|\frac{\lambda_i}{\gamma_i}Z_{ii}(\jmath\omega_{\mathrm{m}})| < \zeta_2$, that is, also this product is

bounded at ω_m. Following the previous reasoning in (4.105), we can write

$$\left|\frac{\lambda_i}{\gamma_i}Z_{ii}(\jmath\omega_\mathrm{m})\right|^2 = \frac{\tau+\left(\frac{\tau}{g_i^2\gamma_i}-g_r\right)^2}{\tau+\left(\frac{\tau}{g_i^2\lambda_i}-g_r\right)^2} \approx \frac{\left(\frac{\lambda_1}{\gamma_i}-1\right)^2}{\left(\frac{\lambda_1}{\lambda_i}-1\right)^2} \Rightarrow \left|\frac{\lambda_i}{\gamma_i}Z_{ii}(\jmath\omega_\mathrm{m})\right| = \frac{1-\frac{\lambda_1}{\gamma_i}}{1-\frac{\lambda_1}{\lambda_i}}. \tag{4.112}$$

We can bound the product $\prod_{i=2}^{N-1}\frac{\lambda_i}{\gamma_i}Z_{ii}(\jmath\omega_\mathrm{m})$ as

$$\begin{aligned}\prod_{i=2}^{N-1}\frac{\lambda_i}{\gamma_i}|Z_{ii}(\jmath\omega_\mathrm{m})| &= \frac{1-\frac{\lambda_1}{\gamma_2}}{1-\frac{\lambda_1}{\lambda_2}}\frac{1-\frac{\lambda_1}{\gamma_3}}{1-\frac{\lambda_1}{\lambda_3}}\cdots\frac{1-\frac{\lambda_1}{\gamma_{N-1}}}{1-\frac{\lambda_1}{\lambda_{N-1}}} \leq \frac{1-\frac{\lambda_1}{\lambda_3}}{1-\frac{\lambda_1}{\lambda_2}}\frac{1-\frac{\lambda_1}{\lambda_4}}{1-\frac{\lambda_1}{\lambda_3}}\cdots\frac{1-\frac{\lambda_1}{\gamma_{N-1}}}{1-\frac{\lambda_1}{\lambda_{N-1}}} \\ &= \frac{1-\frac{\lambda_1}{\gamma_{N-1}}}{1-\frac{\lambda_1}{\lambda_2}} \leq \frac{1}{1-\frac{\lambda_1}{\lambda_2}} \approx \frac{9}{8}.\end{aligned} \tag{4.113}$$

We used the facts that $\lambda_{i+1} > \gamma_i$ and $\frac{\lambda_1}{\lambda_2} \approx \frac{\frac{4\pi^2}{16N^2+16N+4}}{\frac{4\pi^2 9}{16N^2+16N+4}} \approx \frac{1}{9}$ for large N. It follows that

$$\begin{aligned}|T_{NN}(\jmath\omega_\mathrm{m})| &= T_{NN}(0)|T_1(\jmath\omega_\mathrm{m})|\left|\frac{\lambda_N}{\gamma_1}Z_{1N}(\jmath\omega_\mathrm{m})\right|\prod_{i=2}^{N-1}\frac{\lambda_i}{\gamma_i}|Z_{ii}(\jmath\omega_\mathrm{m})| \\ &\leq \frac{9}{8}T_{NN}(0)|T_1(\jmath\omega_\mathrm{m})| \leq \zeta_2 N^2.\end{aligned} \tag{4.114}$$

Combining (4.111) with (4.114) we get the quadratic scaling at ω_m. If we decided to choose $T_i(s)$ instead of $T_1(s)$ in (4.103), the approach would be the same, just the bounds would differ. The lower bound would be bounded as $1 > \zeta_1 > 0.75$ and and the upper bound would be $1 \leq \zeta_2 \leq \frac{9}{8}$. Note that $\|T_1(s)\|_\infty > \|T_i(s)\|_\infty$. That is why we selected $T_1(s)$ for analysis.

A numerical verification that the approximations work is Fig. 4.27.

Note that the proof of the upper bound is not complete. For a complete proof it would be necessary to prove that the frequency response is bounded for any fixed frequency for any N. Currently, we do not have such a proof. □

4.11.7 Proof of Lemma 4.20

Proof. The proof is almost identical to the proof of [Li et al., 2011, Thm. 3]. Note that we work with the reduced Laplacian L_p. Since $y = M(s)e$ and $e = -L_\mathrm{p}y + r$,

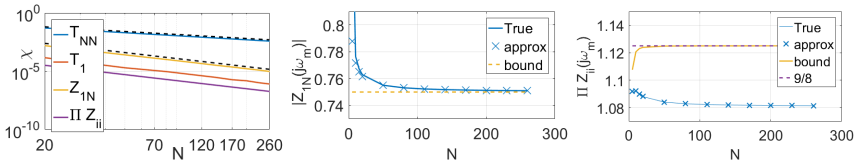

(a) (b) (c)

Figure 4.27: a) Relative error $\chi = \left|\frac{t(\cdot)-p(\cdot)}{t(\cdot)}\right|$, where $t(\cdot)$ is a true value of the quantity, $p(\cdot)$ is the approximated value using our low-frequency approximation in (4.111), (4.107) and (4.113). It is apparent that the approximations work. The error decays to zero linearly for $T_{NN}(s)$ and quadratically for others. b) True value of $\frac{\lambda_N}{\gamma_1} Z_{1N}(j\omega_m)$ at ω_m (frequency at which $T_1(j\omega)$ attains its maximum) with its approximation by (4.107) and lower bound 0.75. c) True value of the product $\prod_{i=2}^{N-1} \frac{\lambda_i}{\gamma_i} |Z_{ii}(j\omega_m)|$ at ω_m with its approximation using (4.112) and bounds (4.113). It is apparent that the bound is not exceeded. The model in all cases was $G(s) = \frac{s^3+7s^2+19s+18}{s^4+8s^3+19s^2}$, $R(s) = \frac{s+3}{s^2+8s+19}$.

we can write

$$y(s) = M(s)\left(-L_p y(s) + r(s)\right), \tag{4.115}$$

from which we get the transfer function matrix $\mathbf{T}(s)$ as

$$y(s) = (I + M(s)L_p)^{-1} M(s) r(s) = \mathbf{T}(s) r(s). \tag{4.116}$$

Let $y = V\hat{y}$ and $r = V\hat{r}$ with $L_p V = V\Lambda$ and $\Lambda = \mathrm{diag}[\lambda_1, \lambda_2, \ldots, \lambda_N]$. Then we can rewrite (4.115) as $V\hat{y}(s) = M(s)\left(-L_p V\hat{y} + r\right)$, from which follows

$$\hat{y}(s) = M(s)\left(-V^{-1}L_p V\hat{y}(s) + V^{-1}r\right) = M(s)\left(-\Lambda\hat{y}(s) + \hat{r}(s)\right). \tag{4.117}$$

We can separate $\hat{y}(s)$ to get

$$\hat{y}(s) = (I + \Lambda M)^{-1} M\hat{r}(s) = \overline{\mathbf{T}}(s)\hat{r}(s). \tag{4.118}$$

The transfer function matrix $\overline{\mathbf{T}}(s) = \mathrm{diag}[F_1(s), F_2(s), \ldots, F_N(s)]$ is block diagonal matrix with blocks

$$F_i(s) = \frac{b(s)q(s)}{a(s)p(s) + \lambda_i b(s)q(s)} = \frac{1}{\lambda_i} T_i(s). \tag{4.119}$$

Note that when (4.116) is transformed to $\hat{r}$ and $\hat{y}$, we get

$$\hat{y}(s) = V^{-1}\mathbf{T}(s)V\hat{r}(s). \tag{4.120}$$

Comparing (4.118) with (4.120) it follows that $\overline{\mathbf{T}}(s) = V^{-1}\mathbf{T}(s)V$. Since the reduced Laplacian L_{p} is symmetric, its matrix of eigenvectors V is a unitary matrix. This means that the norms of the transfer function matrices are equal, i.e., $\|\mathbf{T}(s)\|_\infty = \|\overline{\mathbf{T}}(s)\|_\infty = \max_i \left\| \frac{b(s)q(s)}{a(s)p(s)+\lambda_i b(s)q(s)} \right\|_\infty = \max_i \|F_i(s)\|_\infty$. □

4.11.8 Proof of Theorem 4.22

Proof. Consider $\eta = 1$. We know from Corollary 4.21 that the steady-state gain of $F_1(s) = \frac{b(0)q(0)}{a(0)p(0)+\lambda_1 b(0)q(0)}$ scales quadratically. By Lemma 4.17, for one integrator in the open loop the $\mathcal{H}_\infty$ norm of any $T_i(s) = \lambda_i T_i(s)$ is bounded. Then the scaling of $\|\mathbf{T}(s)\|_\infty$ must be quadratic because of the scaling of the steady-state gain.

For two integrators in the open loop, the peak in the frequency response of $T_1(s) = \lambda_1 \frac{b(s)q(s}{a(s)p(s)+\lambda_1 b(s)q(s)}$ scales linearly (Lem. 4.15). Combining this with the scaling of the steady-state gain we know that

$$\left\| \frac{b(s)q(s)}{a(s)p(s)+\lambda_1 b(s)q(s)} \right\|_\infty = \Theta(N^3). \tag{4.121}$$

It remains to prove that $\left\| \frac{b(s)q(s)}{a(s)p(s)+\lambda_1 b(s)q(s)} \right\|_\infty \geq \left\| \frac{b(s)q(s)}{a(s)p(s)+\lambda_i b(s)q(s)} \right\|_\infty$ for all $\lambda_i > \lambda_1$. It is easy to see from (4.41) that $\left| \frac{b(0)q(0)}{a(0)p(0)+\lambda_1 b(0)q(0)} \right| \geq \left| \frac{b(0)q(0)}{a(0)p(0)+\lambda_i b(0)q(0)} \right|$.

Now we also show that $\|T_1(s)\|_\infty \geq \|T_i(s)\|_\infty$. Let $T_1^N(s)$ be the transfer function $T_1(s)$ for the platoon with N vehicles and $T_1^{N-1}(s)$ be the corresponding transfer function for $N-1$ vehicles. Then by Lemma 4.15 we know that $\|T_1^N(s)\|_\infty > \|T_1^{N-1}(s)\|_\infty$. Let λ_i be the eigenvalues of $L \in \mathbb{R}^{N\times N}$ and μ_i be the eigenvalues of the Laplacian $L \in \mathbb{R}^{N-1\times N-1}$ for a system with $N-1$ vehicles. Then by Cauchy interlacing theorem $\lambda_1 \leq \mu_1 \leq \lambda_2$. Hence, by continuity we have that $\|T_1^{N-1}(s)\|_\infty > \|T_i(s)\|_\infty$ and further $\|T_1(s)\|_\infty \geq \|T_i(s)\|_\infty$ for all $i > 1$. Instability of systems with $\eta \geq 3$ was already discussed in Lemma 4.12. □

4.11.9 Proof of Theorem 4.24

Proof. Before we proceed to the proof, we state one useful result [Horn and Johnson, 1990, Cor. 6.1.6].

Let $A = [a_{ij}] \in \mathbb{R}^{n\times n}$ and let $p_1, \ldots, p_n$ be positive numbers. Consider the matrix $B = P^{-1}AP$ with $P = \mathrm{diag}(p_1, \ldots, p_n)$ and $b_{ij} = [p_j a_{ij}/p_i]$. Then all

eigenvalues of A lie in the union of Gershgorin disks

$$\bigcup_{i=1}^{n} \left\{ z \in \mathbb{C} : |z - a_{ii}| \leq \frac{1}{p_i} \sum_{j=1, j\neq i}^{n} p_j |a_{ij}| \right\}. \tag{4.122}$$

With this result we can get tighter bounds on λ_i by transforming the reduced Laplacian L_p into a *diagonally dominant* form $B = P^{-1} L_\mathrm{p} P$. After the transformation, each row of B reads

$$\left[\ldots \quad 0 \quad -\tfrac{p_{i-1}}{p_i} \quad (1+\epsilon_i) \quad -\tfrac{p_{i+1}}{p_i}\epsilon_i \quad 0 \quad \ldots \right]. \tag{4.123}$$

To make it diagonally dominant, it must hold

$$-\frac{p_{i-1}}{p_i} + (1+\epsilon_i) - \frac{p_{i+1}}{p_i}\epsilon_i \geq 0 \quad \forall i. \tag{4.124}$$

This is a difference inequality with variable p.

We take p as

$$p = \frac{1}{2}\left(1 + \frac{1}{\epsilon_\mathrm{max}}\right), \tag{4.125}$$

which satisfies the inequality. Then P is a diagonal matrix $P = \mathrm{diag}(1, p, p^2, \ldots, p^{N-1})$. Applying this transformation to L_p, we get the ith row

$$\left[\ldots \quad 0 \quad -\tfrac{1}{p} \quad (1+\epsilon_i) \quad -p\epsilon_i \quad 0 \quad \ldots \right]. \tag{4.126}$$

The sum in each row equals the distance $d_i = (1+\epsilon_i) - \frac{1}{p}\epsilon_i - p\epsilon_i$ of Gershgorin's circle from zero and should be positive. After simple calculations, we obtain

$$d_i = -\frac{\epsilon_i}{2}\frac{1-\epsilon_\mathrm{max}}{\epsilon_\mathrm{max}} + \frac{1-\epsilon_\mathrm{max}}{1+\epsilon_\mathrm{max}}. \tag{4.127}$$

Then d_i in the equation above is minimized for $\epsilon = \epsilon_\mathrm{max}$. Therefore, the smallest distance of Gershgorin disks from zero, hence also the lower bound on the eigenvalues is

$$\lambda_\mathrm{min} \geq -\frac{1-\epsilon_\mathrm{max}}{2} + \frac{1-\epsilon_\mathrm{max}}{1+\epsilon_\mathrm{max}} = \frac{(1-\epsilon_\mathrm{max})^2}{2+2\epsilon_\mathrm{max}}. \tag{4.128}$$

Furthermore, it is positive for any $\epsilon_i \leq \epsilon_\mathrm{max}$, making B diagonally dominant. To summarize, we found a bound which does not depend on the matrix size. □

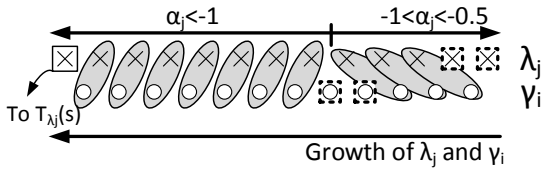

Figure 4.28: Matching of λ_j and γ_i to form $Z_{ij}(s)$. Dashed pairs are the two $Z_{ij}(s)$ for which $|Z_{ij}(\jmath\omega_0)| > 1$ is not guaranteed.

4.11.10 Proof of Theorem 4.28

Proof. In the proof we work with reduced Laplacian L_{p}. Let ω_0 be a frequency at which $|T_{\min}(\jmath\omega_0)| > 1$. The key idea is to form $T_j(s)$ and $Z_{ij}(s)$ from (4.20) as follows:

1. Take each term $a(s)p(s) + \lambda_j b(s)q(s)$ from the denominator of (4.20). Let $\alpha_j + \jmath\beta_j = \lambda_j M(\jmath\omega_0)$. Since $|T_{\min}(\jmath\omega_0)| > 1$, from Lemma 4.8 a) we know that $\alpha_j < -\frac{1}{2}$.

2. If $\alpha_j \leq -1$, then find γ_i such that $\gamma_i \geq \lambda_j$. Form $Z_{ij}(s)$ using such γ_i and λ_j. Then by c) in Lemma 4.8 for such $Z_{ij}(s)$ holds $|Z_{ij}(\jmath\omega_0)| \geq |Z_{ij}(0)|$.

3. If $-1 < \alpha_j \leq -\frac{1}{2}$, then find γ_i such that $\gamma_i \leq \lambda_j$. Form $Z_{ij}(s)$ using these γ_i and λ_j. Then by Lemma 4.8 d) $|Z_{ij}(\jmath\omega_0)| \geq |Z_{ij}(0)|$.

4. Form as much $Z_{ij}(s)$'s as possible using the steps 2) and 3). Use $(\delta_{co} + 1)$ remaining terms $a(s)p(s) + \lambda_j b(s)q(s)$ to form $T_j(s)$.

Lemma 4.6 f) allows us to find $(N - \delta_{co} - 3)$ $Z_{ij}(s)$'s to satisfy either c) or d) in Lemma 4.8—we pair γ_i with λ_{i+2} for $\alpha_j \leq -1$ and γ_i with λ_i for $-1 < \alpha_j \leq 0.5$ (see Fig. 4.28). These $Z_{ij}(s)$'s all have gain greater than their steady-state gain at ω_0. The remaining two $Z_{ij}(s)$'s might have gain lower than their steady-state gain. Since λ_j and γ_i are bounded, there is a lower bound ξ such that $|Z_{ij}(\jmath\omega)| \geq \xi$ for these two.

The transfer function $T_{co}(s)$ given in (4.20) is using such T_j's and Z_{ij}'s written as

$$T_{co}(s) = \vartheta_{co} \prod_{i=1, j\in\mathcal{J}}^{N-\delta_{co}-1} Z_{ij}(s) \prod_{j=1, j\notin\mathcal{J}}^{N} \frac{1}{\lambda_j} \prod_{j=1, j\notin\mathcal{J}}^{N} T_j(s). \tag{4.129}$$

The set $\mathcal{J}$ is the set of λ_j used to form some of Z_{ij}'s. The terms $\vartheta_{co} \prod_{j=1, j\notin\mathcal{J}}^{N} \frac{1}{\lambda_j}$

and steady-state gain of $Z_{ij}(0)$ do not affect the shape of the magnitude frequency response, only its value.

Since $\|T_{\min}(s)\|_\infty > 1$, it follows from a) in Lemma 4.8 that for all transfer functions $T_j(s)$ we have $|T_j(\jmath\omega_0)| > 1$. Due to the lower and upper bounds on eigenvalues, there is a minimum $\zeta > 1$ of modulus frequency response $|T_j(\jmath\omega_0)|$, attained for some λ_j with $\lambda_{\min} \leq \lambda_j \leq \lambda_{\max}$. Then we get the lower bound on the modulus of product of $T_j(s)$ in (4.129) as $\prod_{j=1, j\notin\mathcal{J}}^{N} |T_j(\jmath\omega_0)| \geq \zeta^{\delta_{co}+1}$. Clearly, this part of (4.129) scales exponentially with δ_{co}.

All but two blocks $Z_{ij}(s)$ amplify at ω_0, so $\prod_{i=1}^{N-\delta_{co}-1} |Z_{ij}(\jmath\omega_0)| \geq \xi^2$ (excluding the steady-state gain) and the norm of $T_{co}(s)$ is from (4.129) $\|T_{co}(s)\|_\infty \geq \xi^2\, T_{co}(0)\, \zeta^{\delta_{co}+1}$. □

4.11.11 Proof of Theorem 4.32

Proof. First we prove that if $\|T_{\max}(s)\|_\infty = 1$, then $\|T_{co}(s)\|_\infty = |T_{co}(0)|$. As in the proof of Theorem 4.28, we will form Z_{ij}'s and T_j's in a suitable way. Let $\alpha_j + \jmath\beta_j = \lambda_j M(\jmath\omega_0)$ at some frequency ω_0. Since $\|T_{\max}(s)\|_\infty = 1$, it follows from Lemma 4.8 b) that $|T_j(\jmath\omega_0)| \leq 1\, \forall\omega_0$, $\forall\lambda_j \leq \lambda_{\max}$ and $\alpha_j \geq -\frac{1}{2}$, $\forall\omega_0$.

Using Lemma 4.6 f) we can pair all γ_i with unique λ_j such that $\gamma_i \geq \lambda_j$ to form $Z_{ij}(s)$. Then e) in Lemma 4.8 implies that $|Z_{ij}(\jmath\omega_0)| \leq |Z_{ij}(0)|$ for all i, j. Since $\alpha_j \geq -\frac{1}{2}$ for all ω_0, we have that $\|Z_{ij}(s)\|_\infty = |Z_{ij}(0)|$ for all pairs $\gamma_i \geq \lambda_j$. All remaining terms $T_j(s)$ in (4.129) by Lemma 4.8b) satisfy $|T_j(\jmath\omega_0)| \leq 1$ for all ω_0. Hence, all transfer functions in the product (4.129) have their norm norm less than or equal to one and $\|T_{co}(s)\|_\infty$ is bounded by its steady-state gain.

Now let us go analyze the bidirectional string stability. Consider $o \geq c$ and let r_c be the input at the control node. Then the first transfer function in (4.53) can be written as

$$\begin{aligned}\frac{y_o(s)}{y_{o-1}(s)} &= \frac{r_c(s)T_{c,o}(s)}{r_c(s)T_{c,o-1}(s)} = \frac{T_{c,o}(s)}{T_{c,o-1}(s)} \\ &= \frac{b(s)q(s)\prod_{j=1}^{N-\delta_{co}-1} a(s)p(s) + \gamma_{j,o}\, b(s)q(s)}{\prod_{j=1}^{N-\delta_{co}} a(s)p(s) + \gamma_{j,o-1}\, b(s)q(s)}. \end{aligned} \tag{4.130}$$

Let $\bar{L}_{o-1}$ and $\bar{L}_o$ be the submatrices of L_{p} corresponding to the paths from c to $o-1$ and from c to o, respectively. Their eigenvalues are $\gamma_{j,o-1}$ and $\gamma_{j,o}$, respectively. Because of the fact that $\bar{L}_o$ is a submatrix of $\bar{L}_{o-1}$, the eigenvalues of $\bar{L}_{o-1}$ and $\bar{L}_o$ must interlace in a sense of f) in Lemma 4.6. We can pair $\gamma_{j,o-1}$ and $\gamma_{j,o}$ by Lemma 4.6 f) such that $\gamma_{j,o-1} \leq \gamma_{j,o}$ and form $Z_{ij}(s)$ as above.

Then, $\left\| \frac{a(s)p(s)+\gamma_{j,o}b(s)q(s)}{a(s)p(s)+\gamma_{j,o-1}b(s)q(s)} \right\|_\infty \leq 1 \, \forall j$. Only one term in (4.130) with a form $\frac{b(s)q(s)}{a(s)p(s)+\gamma_{i,o-1}b(s)q(s)}$ remains. Its $\mathcal{H}_\infty$ norm is equal to its steady-state gain by b) in Lemma 4.8. The steady-state gain of $\frac{y_o(s)}{y_{o-1}(s)}$ is one, since by Theorem 4.9 the steady-state gain is identical for all the vehicles behind the control node. Hence, $\|\frac{y_o(s)}{y_{o-1}(s)}\|_\infty \leq 1$ for $c \leq o$.

The other direction ($c \geq o$) has the ratio of outputs with the same structure as (4.130), the only difference is its steady-state gain. It follows from (4.27) that the steady-state gain is

$$\frac{T_{c,o-1}(0)}{T_{c,o}(0)} = \epsilon_{o-1} \frac{\left(1 + \sum_{i=1}^{o-2} \prod_{j=1}^{i} \epsilon_{o-j-1}\right)}{\left(1 + \sum_{i=1}^{o-1} \prod_{j=1}^{i} \epsilon_{o-j}\right)} < 1. \tag{4.131}$$

Since the norm $\|y_{o-1}(s)/y_o(s)\|_\infty$ is at most 1, bidirectional string stability was proved. □

4.11.12 Proof of Theorem 4.33

Proof. Again we work with pinned Laplacian L_{p}. From Theorem 4.32 we know that all elements of the transfer function matrix $\mathbf{T}(s)$ have their $\mathcal{H}_\infty$ norm bounded by their steady-state gains, $\|T_{co}(s)\|_\infty = |T_{co}(0)|$. Since the Laplacian is asymmetric, we can use Corollary 4.26 to get $|T_{co}(0)| \leq \frac{1}{1-\epsilon_{\max}}$. Hence, for the modulus $|\mathbf{T}(\jmath\omega)|$ of each element in $\mathbf{T}(\jmath\omega)$ holds $|T_{co}(\jmath\omega)| \leq \frac{1}{1-\epsilon_{\max}}$.

The norm of the transfer function matrix can be calculated as

$$\|\mathbf{T}(s)\|_\infty = \sup_{\omega \in [0,\infty)} \sigma_{\max}\{\mathbf{T}(\jmath\omega)\}. \tag{4.132}$$

Note that for each matrix $A \in \mathbb{C}$ holds $\sigma_{\max}(A) = \sqrt{\lambda_{\max}(A^{\mathrm{H}}A)}$. Also recall that $\mathrm{tr}(A^{\mathrm{H}}A) = \sum_{i=1}^{N} \lambda_i(A^{\mathrm{H}}A) \geq \lambda_{\max}(A^{\mathrm{H}}A) = \sigma^2_{\max}(A)$. The trace of $\mathbf{T}(\jmath\omega)^{\mathrm{H}}\mathbf{T}(\jmath\omega)$ is $\mathrm{tr}[\mathbf{T}(\jmath\omega)^{\mathrm{H}}\mathbf{T}(\jmath\omega)] = \sum_{c=1}^{N}\sum_{o=1}^{N} (T_{oc}(\jmath\omega))^{\mathrm{H}} T_{co}(\jmath\omega)$. Now using the bound on transfer functions T_{co} we can write

$$\begin{aligned}
\sup_{\omega\in\mathbb{R}} \sigma^2_{\max}(\mathbf{T}(\jmath\omega)) &\leq \sup_{\omega\in\mathbb{R}} \mathrm{tr}[\mathbf{T}(\jmath\omega)^{\mathrm{H}}\mathbf{T}(\jmath\omega)] = \sup_{\omega\in\mathbb{R}} \left(\sum_{c=1}^{N}\sum_{o=1}^{N} (T_{oc}(\jmath\omega))^{\mathrm{H}} T_{co}(\jmath\omega) \right) \\
&\leq \sup_{\omega\in\mathbb{R}} \left(\sum_{c=1}^{N}\sum_{o=1}^{N} |T_{oc}(\jmath\omega)||T_{co}(\jmath\omega)| \right) \leq \sum_{c=1}^{N}\sum_{o=1}^{N} \left(\frac{1}{1-\epsilon_{\max}} \right)^2 \\
&= N^2 \frac{1}{(1-\epsilon_{\max})^2}.
\end{aligned} \tag{4.133}$$

From this we get $\sup_{\omega\in[0,\infty)} \sigma_{\max}\{\mathbf{T}(\jmath\omega)\} \leq N\frac{1}{(1-\epsilon_{\max})}$. The upper bound was proved.

Now we prove the lower bound. Note that $\sup_{\omega\in\mathbb{R}} \sigma_{\max}(\mathbf{T}(\jmath\omega)) \geq \sigma_{\max}(\mathbf{T}(0)) \geq x^{\mathrm{H}}\mathbf{T}(0)x$ for any $x \in \mathbb{C}^N$. Let us use $x = \frac{1}{\sqrt{N}}\mathbf{1}$. Then we get

$$\sigma_{\max}(\mathbf{T}(0)) \geq \frac{1}{N}\mathbf{1}^{\mathrm{T}}\mathbf{T}(0)\mathbf{1} = \frac{1}{N}\sum_{c=1}^{N}\sum_{o=1}^{N} T_{co}(0) \geq \frac{1}{N}\sum_{o=1}^{N}\sum_{c=o}^{N} T_{co}(0). \quad (4.134)$$

Note that by Theorem 4.9 $|T_{c,c}(0)| = |T_{c,i}(0)|$ for all $i \geq c$ and also $|T_{co}(0)| = \vartheta_{co}\left(1 + \sum_{i=1}^{c-1}\prod_{j=1}^{i}\epsilon_{c-j}\right) \geq 1$ since $\vartheta_{co} = 1$ for $o \geq c$. Plugging this to (4.134) yields

$$\sigma_{\max}(\mathbf{T}(0)) \geq \frac{1}{N}\sum_{o=1}^{N}\sum_{c=o}^{N} T_{co}(0) \geq \frac{1}{N}\sum_{o=1}^{N}\sum_{c=o}^{N} 1 = \frac{1}{N}\frac{N}{2}(N+1) = \frac{N+1}{2}. \quad (4.135)$$

Thus, also the lower bound scales linearly with N, which proves the result. □

5 Platoons with different Laplacians

Recalling the results of previous chapter, we know that there is basically no good controller for a platoon with vehicles having two integrators in the open loop when only proportional asymmetry is used. It might seem that allowing only one integrator in the open loop might be a solution. However, this requires permanent communication of the leader's velocity or distances growing with velocity (time headway).

Let us start this chapter with a simple quiz. Have a look at Fig. 5.1. All the figures show responses of the platoon with the same vehicles, only the communication topology uses different weights. Therefore, the communication topology is the same, only the Laplacian is different. One of the controllers is an LQ-optimal distributed controller, it has a good convergence time and bounded steady-state gain. Which of the communication topologies would you think satisfies the aforementioned qualities? Without reading the previous chapter probably no one would guess that this is the top right figure, which apparently has the worst performance. The bottom right figure, on the other hand, has quite a good response. Surprisingly enough, almost nothing is known about the performance of such system. A system with such a communication structure appeared in the literature only recently and not many of its properties are known.

Let us now describe the individual communication topologies and introduce the notation used in this chapter. The top left figure is a standard symmetric bidirectional control with $\epsilon_i = 1, \forall i$, called SPSV. The abbreviation SPSV stands for "Symmetric position, symmetric velocity" coupling. The top right figure is an inversely optimal asymmetric bidirectional control, abbreviated as APAV (asymmetric position, asymmetric velocity), with $\epsilon_i = 0.5$. The bottom left figure is a standard predecessor following, abbreviated as PF. The bottom right figure shows a response of a controller which uses different asymmetry in position and

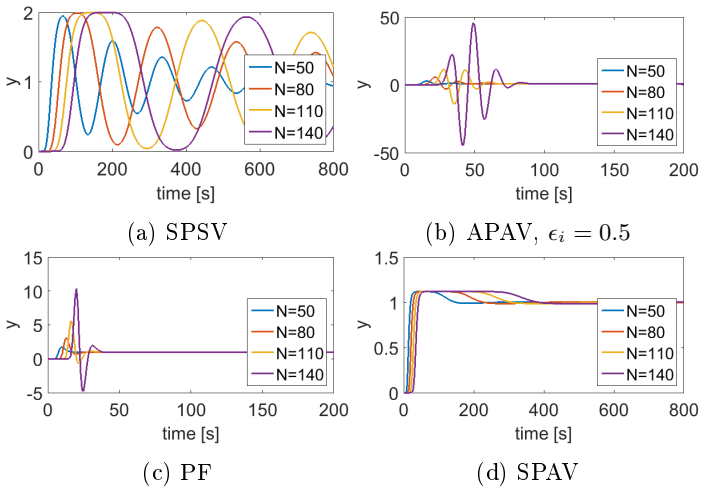

(a) SPSV

(b) APAV, $\epsilon_i = 0.5$

(c) PF

(d) SPAV

Figure 5.1: Architecture comparison for a model $R(s) = 7.6s + 2.2$, $G(s) = \frac{1}{s^2}$ for different N. The position of the last agent in the platoon is shown. The figures show response to the step in the leader's position. The controller used is inversely optimal for asymmetric control with matrices $Q_2 = I_2, R_2 = 30$. Note different scales in both axes.

different asymmetry in velocity. In fact, the coupling in position is symmetric and in velocity asymmetric, hence the name "Symmetric position, asymmetric velocity"—SPAV.

The SPAV system is an instance of the distributed control system which uses multiple Laplacians—the model is of the form (2.23). An asymmetric Laplacian is used for a coupling in velocity, while a symmetric Laplacian is used for a coupling in position. As was written in the introduction to distributed control, it is very hard to analyze such systems, since the block diagonalization similar to [Fax and Murray, 2004] is not possible. Nevertheless, the performance of such systems can be superior to the performance of the systems with only one Laplacian.

In this chapter we will first introduce some results derived by prof. J.J.P. Veerman and his collaborators. Their work was the first to calculate some properties of the system having two integrators and two Laplacians. They considered double-integrator models with different coupling in position and velocity. We will review their results here, since they will be needed later on. Subsequently, we derive conditions on the communication topology—the output state must use symmetric coupling in order to guarantee good scaling. Then we extend the work by [Cantos and Veerman, 2014] to a third-order system and provide

an optimization procedure. To our best knowledge, this is one of the first optimizations for vehicular platoons which allows simultaneous calculation of the controller parameters and communication weights.

The results of this chapter appeared as the journal publication [Herman et al., 2016d] and the conference paper [Herman et al., 2015c].

5.1 Path and circular graph

Every real platoon has a path graph topology (possibly with a coupling to the leader for each vehicle). The leader is not influenced by the in-platoon vehicles. On the other hand, some properties of the standard platoon can be derived from the graph having circular topology. In this case, the leader becomes coupled to the last vehicle and vice-versa. It is the relation between path and circular communication topology which allowed J.J.P. Veerman and his collaborators to derive some properties of the transients in platoons which have different coupling in position and velocity. A system having a circular communication topology is much easier to analyze than the system with a path-graph topology.

In this introductory section, we will not give the precise definitions of the terms used here. They will be shown later on. For instance, the path system is defined in equation (5.38), while circular system is defined in (5.42).

5.1.1 Assumptions

Here we review the basic assumptions, which will allow us to infer properties of the path system from the properties of the circular system. The solution in [Cantos and Veerman, 2014] is based on two main conjectures relating the path and circular systems. Although we cannot prove them, we use them here as well. The final justification of both conjectures is in the match of the predicted and simulated values, as shown in Sec. 5.4.1. The first one states that a local behavior of both systems is identical.

Assumption 5.1. *If the path formation (5.38) is stable and flock stable, then the behavior of a circular system is the same as in the path system for vehicles reasonably far from the boundaries.*

Flock stability is formally defined in Definition 5.8. It means that the distance between the leader and the last vehicle scales less than exponentially in N. Assumption 5.1 allows to use properties derived for the circular graph (which is much easier to analyze) in the path graph. It means that far away from the boundaries, a signal will propagate the same way in a system with a path-graph

interconnection structure as it does in the system with a circular topology.

A similar assumption has been made by others (see [Bamieh et al., 2002, 2012; D'Andrea and Dullerud, 2003]) to simplify the analysis and make the system spatially invariant. In fact, in solid-state physics this idea is known as *periodic boundary conditions* and goes back to the beginning of the 20th century (see [Ashcroft and Mermin, 1976]).

As in previous chapter, we want to guarantee good scaling of the transients in platoon. We definitely do not want transients to scale exponentially. Better-than-exponential scaling is captured by the term *flock stability* (see Def. 5.8). In order to investigate flock stability in the path system using properties of a circular system, we need an additional assumption about relations of the two interconnections.

Assumption 5.2. *If the circular formation is asymptotically unstable, then the path formation is either asymptotically unstable or flock unstable.*

The explanation in [Cantos et al., 2014, Def. 3.2] is that the path system has non-normal eigenspaces which makes the bad effects (instability) more pronounced. To this explanation we can add an additional one based on the travelling wave concept in distributed control [Martinec et al., 2014]. Asymptotic instability can be caused by the travelling wave which is amplified as it travels in the formation. The amplification will happen far from boundaries also in the path system. This results either in an asymptotic instability or in a flock instability (if the boundaries attenuate the signal sufficiently) of the path system.

Both assumptions are illustrated in Fig. 5.2 for a system having agents of the third order. It shows the initial-condition responses (the position of the vehicle with index 35 is $y_{35}(0) = 2$, for the others $y_i(0) = 0$ for $i \neq 35$ and $\Delta_{\text{ref}} = 0$) of the circular and path system. The model is $M(s) = \frac{g_v s + g_y}{s^3 + a s^2}$ and asymmetry $\rho_v = \rho_y = 0.33$ (see (5.4) for explanation of these parameters). There is the same asymmetry in position and in velocity. As can be seen, the signal gets amplified as it propagates from one agent to the other. On the other hand, individual agent's response goes to zero, until the amplified travelling wave gets back to the agent after propagating through all other agents (see the sharp growth at time 70 in Fig. 5.2a). The initial responses of the path and circular systems are the same—both amplify the signal. However, in the circular graph it results in asymptotic instability (the signal travels around the circle infinitely many times), while the path graph is stabilized thanks to boundary conditions.

As we want to prevent flock instability, based on Assumption 5.2, we have to guarantee asymptotic stability of the circular system. This is the content of the next section.

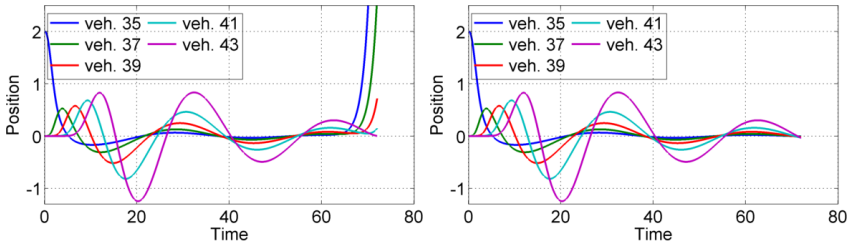

(a) Circular system. (b) Path system.

Figure 5.2: Signal propagation in an initial-condition response. a) response of an asymptotically unstable circular system, b) response of a flock unstable path system. In both cases $N = 70, a = 3, g_y = 2, g_v = 3, \rho_v = \rho_y = 0.33$.

5.2 Necessary conditions for stability of circular system

Based on the previous section, analysis of stability of the circular system might be also useful in analysis of the path system (Assumptions 5.1 and 5.2). In this section we find necessary conditions for stability of a system in which multiple Laplacians are used and the communication topology is a circular graph for each state. The results here hold for general models and as in previous chapter the distinguishing factor is the number of integrators in the open loop. After we derive the stability conditions for the circular system, we will in the next section analyze properties of the path system.

It was shown in [Cantos et al., 2014] that the circular system must have symmetric coupling in position in order to achieve asymptotic stability. They considered double integrators. This brings about the question: what happens when we have a different open-loop model having two integrators? Is it still necessary to have symmetric coupling in the output state? When there are three integrators, is it possible to stabilize the system using symmetric coupling in the output state and its derivative? In this section we answer these questions by deriving necessary stability conditions.

The results of this section were published in [Herman et al., 2015c].

5.2.1 System model

We consider $N + 1$ identical agents which exchange information about their states over a communication graph with a *circular topology*. The coupling can be asymmetric and each state can use different asymmetry.

All agents have identical SISO models of higher order—the order n of the agent can be arbitrary. We assume that the agent is modelled in a controller canonical form

$$\dot{x}_i = Ax_i + Be_i \tag{5.1}$$

with matrices $A \in \mathbb{R}^{n\times n}, B \in \mathbb{R}^{n\times 1}$. The state vector of the ith ($i = 0, 1, \ldots, N$) agent is given as $x_i = [x_{i,0}, x_{i,1}, x_{i,2}, \ldots, x_{i,n-1}]^{\mathrm{T}}$. Usually, the first two states are position and velocity, i.e. $x_{i,0} = y_i$ and $x_{i,1} = v_i$, respectively. The matrices are given as

$$A = \begin{bmatrix} 0 & 1 & 0 & \ldots & 0 \\ 0 & 0 & 1 & \ldots & 0 \\ \vdots & \vdots & \vdots & \ddots & \vdots \\ -p_0 & -p_1 & -p_2 & \ldots & -p_{n-1} \end{bmatrix}, B = \begin{bmatrix} 0 \\ 0 \\ \vdots \\ 1 \end{bmatrix}. \tag{5.2}$$

The characteristic polynomial of the open loop is clearly

$$p(s) = s^n + p_{n-1}s^{n-1} + p_{n-2}s^{n-2} + p_{n-3}s^{n-3} + \ldots + p_0. \tag{5.3}$$

We assume there are η integrators in the open loop, therefore $p_i = 0$ for $i = 0, \ldots, \eta - 1$. The most common cases are one, two or three integrators. We will call the state $x_{i,0}$ the output state (typically the position y_i). Except for the poles at the origin, the open-loop model is supposed to be stable.

Remark 5.3. *The agent's model can be a combination of a plant (vehicle) model and a dynamic controller. We assume in this case that (5.1) models an open loop of the system—controller in series with plant—composed together. It can be the controller-canonical realization of the transfer function $M(s)$. Although in principle the agents can exchange all states, the dynamic controller may still be necessary to satisfy the internal model principle, see Lemma 2.11. For instance, in vehicular formations with a nearest-neighbor interaction, two integrators in the open loop are necessary for leader tracking.*

The agent can measure relative states to the neighbors (distance, relative velocity etc.) or can use communication to obtain information about the states of neighboring agents. Each state can use different asymmetry of the interaction. We assume that $m \leq n$ states are exchanged and those are the states $x_{i,0}, x_{i,1}, x_{i,2}, \ldots, x_{i,m-1}$—the output state (position) and its $m-1$ derivatives. We will use index i to denote the index of the agent while index j is used to index the state of an individual agent. Thus, $x_{i,j}$ is the jth state of the ith agent.

The control law for each agent is given as

$$e_i = \sum_{j=0}^{m-1} g_j(1-\rho_j)(x_{i-1,j} - x_{i,j}) - \rho_j g_j(x_{i,j} - x_{i+1,j}). \tag{5.4}$$

The terms g_j are the coupling gains for the state j and ρ_j is the *asymmetry of coupling* of the jth state. If $\rho_j = 0.5$, then the coupling of the state is symmetric, if $\rho_j = 0$ the agent looks only ahead and if $\rho_j = 1$ it looks only behind. The control law is a weighted error to the neighbor's states.

Remark 5.4. *Here we have to apologize to the reader of the thesis, because a different type of asymmetry is introduced. ρ is used instead of ϵ. It emphasizes that ϵ was the same for all states, while ρ_j is different for each state j. Here the symmetry is $\rho = 0.5$, while in previous chapter it was $\epsilon = 1$. Although Laplacian defined using ρ can be recalculated to the Laplacian with ϵ_i, we will in this chapter stick to ρ. The reason is that all the derivations and also the optimization are prepared using this notation.*

Since we work with a circular communication topology, the Laplacians describing the interconnections are given as the following circulant matrices

$$L_j = \begin{bmatrix} 1 & -\rho_j & 0 & 0 & \dots & -(1-\rho_j) \\ -(1-\rho_j) & 1 & -\rho_j & 0 & \dots & 0 \\ 0 & -(1-\rho_j) & 1 & -\rho_j & \dots & 0 \\ \vdots & \vdots & \vdots & \vdots & \ddots & \vdots \\ -\rho_j & 0 & \dots & 0 & -(1-\rho_j) & 1 \end{bmatrix} \in \mathbb{R}^{N+1 \times N+1} \tag{5.5}$$

with $j = 0, 1, \dots, m-1$.

The eigenvalues of the Laplacian L_j are given as [Cantos and Veerman, 2014]

$$\lambda_j(\theta) \quad = \quad [1 - \cos\theta + \jmath(1-2\rho_j)\sin\theta] \tag{5.6}$$

with $\theta = \frac{2\pi k}{N+1}$, $k = 0, 1, \dots, N$ and $\jmath = \sqrt{-1}$. Since we are interested in behavior of formations with large number of agents, we will treat the eigenvalues as a continuous function of $\theta \in [0, 2\pi]$. The eigenvalues of L_j are complex unless $\rho_j = 0.5$.

After the coupling of all the states is incorporated, the overall state space model

has a form

$$\dot{x} = A_c\, x + B_c\, e. \tag{5.7}$$

The state vector is given as a stacked vector $x = [x_{0,0}, x_{1,0}, \dots x_{N,0}, x_{1,1}, x_{2,1}, \dots, x_{N,1}, \dots, x_{1,n-1}, x_{2,n-1}, \dots, x_{N,n-1}]^{\mathrm{T}}$, that is, first are the states $x_{i,0}$ for all $N+1$ vehicles (positions), then the states $x_{i,1}$ (velocities) for all vehicles, etc. The matrices are

$$A_c = \begin{bmatrix} 0 & I & 0 & \dots & 0 \\ 0 & 0 & I & \dots & 0 \\ \vdots & \vdots & \vdots & \ddots & \vdots \\ -\hat{P}_0 & -\hat{P}_1 & -\hat{P}_2 & \dots & -\hat{P}_{n-1} \end{bmatrix}, B_c = \begin{bmatrix} 0 \\ 0 \\ \vdots \\ I \end{bmatrix}, \tag{5.8}$$

$A_c \in \mathbb{R}^{(N+1)n \times (N+1)n}$ and $B_c \in \mathbb{R}^{(N+1)n}$. We introduced the matrices $\hat{P}_j = Ip_j + g_j L_j$. If we do not want to use coupling at the jth state, we can set $g_j = 0$, therefore $g_j = 0$ for $j \geq m$.

5.2.2 Stability analysis

We calculate the eigenvalues ν of A_c as $A_c w = \nu w$. In vector form with $w = [w_0^{\mathrm{T}}, w_1^{\mathrm{T}}, \dots, w_N^{\mathrm{T}}]^{\mathrm{T}}$,

$$\begin{bmatrix} 0 & I & \dots & 0 \\ 0 & 0 & \dots & 0 \\ \vdots & \vdots & \ddots & \vdots \\ -\hat{P}_0 & -\hat{P}_1 & \dots & -\hat{P}_{n-1} \end{bmatrix} \begin{bmatrix} w_0 \\ w_1 \\ \dots \\ w_{n-1} \end{bmatrix} = \nu \begin{bmatrix} w_0 \\ w_1 \\ \dots \\ w_{n-1} \end{bmatrix}. \tag{5.9}$$

It follows that $w_j = \nu w_{j-1}$. The last row gives us

$$-\hat{P}_0 w_0 - \hat{P}_1 w_0 \nu - \dots - \hat{P}_{n-1} w_0 \nu^{n-1} = w_0 \nu^n. \tag{5.10}$$

Then w_0 must be an eigenvector of all matrices $\hat{P}_j$, from which we get that it is also an eigenvector of L_j. All circular matrices are simultaneously diagonalizable by discrete Fourier transform, that is, the eigenvectors w_j of L_j have elements

$$(w_j)_k = e^{\jmath\theta k}. \tag{5.11}$$

Hence,

$$\hat{P}_j w_0 = (Ip_j + g_j L_j) w_0 = (p_j + g_j \lambda_j(\theta)) w_j. \tag{5.12}$$

From (5.10) we can get $N+1$ characteristic equations of A_c of the form

$$\begin{aligned}\nu^n + (p_{n-1} + g_{n-1}\lambda_{n-1}(\theta))\nu^{n-1} + \dots \\ +(p_1 + g_1\lambda_1(\theta))\nu + p_0 + g_0\lambda_0(\theta) = 0.\end{aligned} \tag{5.13}$$

Plugging the eigenvalues λ_j from (5.6), we get

$$\begin{aligned}\nu^n + (p_{n-1} + g_{n-1}[1 - \cos\theta + \jmath(1-2\rho_{n-1})\sin\theta])\nu^{n-1} \\ + \dots + (p_1 + g_1[1 - \cos\theta + \jmath(1-2\rho_1)\sin\theta])\nu \\ + p_0 + g_0[1 - \cos\theta + \jmath(1-2\rho_0)\sin\theta] = 0.\end{aligned} \tag{5.14}$$

This is a complex-coefficient characteristic polynomial. Note that this decomposition to $N+1$ characteristic equations is similar to the block diagonalization of Lemma 2.6.

Let $\beta_j = 1 - 2\rho_j$. We can expand the eigenvalues (5.6) of Laplacian L_j in a Taylor series around $\phi = 0$ as

$$\lambda_j(\theta) = \jmath\beta_j\theta + \frac{1}{2}\theta^2 - \frac{\jmath}{6}\beta_j\theta^3 \dots \tag{5.15}$$

5.2.3 Conditions on interconnection

Now we analyze the conditions for stability of the matrix A_c in (5.7) when the number of vehicles gets very high, $N \to \infty$. We are not interested in finding the stability conditions for one particular model of the vehicle. Instead, we would like to see what are the requirements on the communication topology.

Let us first analyze the necessary conditions for stability when the polynomial (5.14) is only real.

Lemma 5.5. *A necessary condition for asymptotic stability of (5.7) is that the following real-coefficient polynomials*

$$\nu^n + (p_{n-1} + 2g_{n-1})\nu^{n-1} + \dots + (p_1 + 2g_1)\nu + p_0 + 2g_0 = 0, \tag{5.16}$$

$$\nu^n + p_{n-1}\nu^{n-1} + \dots + p_1\nu + p_0 = 0 \tag{5.17}$$

are stable.

Proof. Set $\theta = \pi$ in (5.14) to get (5.16) and $\theta = 0$ to get (5.17). □ □

If (5.17) is not asymptotically stable (due to poles at origin), then the formation will drift away, but still the agents might synchronize. The equation is a con-

sequence of the zero eigenvalue of Laplacian. So for synchronization purposes, stability of (5.17) does not have to be required (this is so-called cooperative stability).

Since for stability the roots of (5.17) must be in the left half-plane, all the curves $\nu(\phi)$, $\phi \in [0, 2\pi]$ start in the left-half plane. The only exception are the poles at origin (there are η poles at the origin) in (5.17). In order to guarantee stability of A_c, the curves must not leave closed left half-plane. That is, they must not cross the imaginary axis.

The following theorem shows that symmetric coupling in the output state $x_{i,0}$ is a necessary condition for stability when there are two integrators in the open loop. Moreover, systems with three integrators cannot be stabilized for N large enough.

Theorem 5.6. *Let η be the number of integrators in the agent model (5.2). Then as $N \to \infty$, the circular system (5.7)*

1. *is unstable if $\eta = 2$ and $\rho_0 \neq 0.5$.*
2. *is unstable if $\eta > 2$.*
3. *is unstable if the agent model (5.2) has eigenvalues in open right half-plane.*

If $\eta = 1$, stability depends on the system and tuning of the parameters.

Proof. Since by Lemma 5.5 $n - \eta$ roots of (5.17) lie in the open left half-plane and η of them are at the origin, we will be interested in the behavior close to the origin. Let us investigate what are the roots of (5.14) as $\theta \to 0$. Since θ is small, we can keep only two lowest order terms (to keep both real and imaginary parts) of the Taylor expansion in (5.15), i.e., $\lambda_j(\theta) \approx \jmath\beta_j\theta + \frac{1}{2}\theta^2$. The polynomial (5.14) is then

$$\begin{aligned} q(\nu) \approx \nu^n + \left(p_{n-1} + g_{n-1}\left[\jmath\beta_{n-1}\theta + \frac{1}{2}\theta^2\right]\right)\nu^{n-1} \\ + \ldots + \left(p_1 + g_1\left[\jmath\beta_1\theta + \frac{1}{2}\theta^2\right]\right)\nu + p_0 + g_0\left[\jmath\beta_0\theta + \frac{1}{2}\theta^2\right] = 0. \end{aligned} \tag{5.18}$$

We can decompose it to three polynomials as

$$q(\nu) = q_1(\nu) + \frac{1}{2}\theta^2 q_2(\nu) + \jmath\theta q_3(\nu), \tag{5.19}$$

where the polynomials are defined as

$$q_1(\nu) = p(\nu) = \nu^n + p_{n-1}\nu^{n-1} + \ldots + p_1\nu_1 + p_0, \tag{5.20}$$
$$q_2(\nu) = g_{n-1}\nu^{n-1} + g_{n-2}\nu^{n-2} + \ldots g_1\nu + g_0, \tag{5.21}$$
$$q_3(\nu) = g_{n-1}\beta_{n-1}\nu^{n-1} + g_{n-2}\beta_{n-2}\nu^{n-2} + \ldots + g_0\beta_0. \tag{5.22}$$

We can convert the complex-coefficient polynomial $q(\nu)$ in (5.18) to the real-coefficient polynomial $\hat{q}(\nu)$ by

$$\hat{q}(\nu) = q(\nu)\bar{q}(\nu), \tag{5.23}$$

where $\bar{q}(\nu)$ has all coefficients as complex conjugates of those in $q(\nu)$. Then we can write

$$\begin{aligned}\hat{q}(\nu) &= \left[q_1(\nu) + \frac{1}{2}\theta^2 q_2(\nu) + \jmath\theta q_3(\nu)\right]\left[q_1(\nu) + \frac{1}{2}\theta^2 q_2(\nu) - \jmath\theta q_3(\nu)\right] \\ &= \left[q_1(\nu) + \frac{1}{2}\theta^2 q_2(\nu)\right]^2 + [\theta q_3(\nu)]^2 \\ &= q_1^2(\nu) + \theta^2 q_1(\nu)q_2(\nu) + \frac{1}{4}\theta^4 q_2^2(\nu) + \theta^2 q_3^2(\nu).\end{aligned} \tag{5.24}$$

The polynomial $\hat{q}(\nu)$ is stable if and only if $q(\nu)$ is stable. Since θ is small, the terms with θ^4 can be neglected in (5.24). Then equation (5.24) has a form

$$\hat{q}(\nu) \approx q_1^2(\nu) + \theta^2\left[q_1(\nu)q_2(\nu) + q_3^2(\nu)\right]. \tag{5.25}$$

This can be viewed a closed-loop polynomial of the system $M_{\text{rl}}(\nu)$ defined as

$$M_{\text{rl}}(\nu) = \theta^2\frac{q_1(\nu)q_2(\nu) + q_3^2(\nu)}{q_1^2(\nu)}. \tag{5.26}$$

The term θ^2 acts as a gain in the closed loop. The closed-loop system $\theta^2 M_{\text{rl}}(\nu)/(1+\theta^2 M_{\text{rl}}(\nu))$ is stable if and only if $\hat{q}(\nu)$ is stable for all θ^2. Recall that there are η integrators in the open loop of the system and $p_i = 0$ for $i = 0, \ldots, \eta - 1$. Then ν^η can be factored out from q_1 to get $q_1(\nu) = \nu^\eta\hat{q}_1(\nu)$, where $\hat{q}_1(\nu)$ has a nonzero absolute term. $M_{\text{rl}}(\nu)$ then reads

$$M_{\text{rl}}(\nu) = \theta^2\frac{\nu^\eta\hat{q}_1(\nu)q_2(\nu) + q_3^2(\nu)}{\nu^{2\eta}\hat{q}_1^2(\nu)}. \tag{5.27}$$

Such a system has 2η poles at the origin. By the root-locus rules [Dorf and Bishop, 2008, p. 418], when we close the loop these poles will start to move on the trajectories in a complex plane separated by angles $2\pi/(2\eta)$. Therefore, if there are more than 2 poles at the origin, at least one branch will go to the right

half-plane. Thus, the system will be unstable for small θ^2. In order to cancel the unwanted poles at the origin and keep at most two of them, we require that there are at least $2\eta - 2$ zeros at the origin in the numerator of $M(\nu)$.

If $\eta = 2$, then we need two zeros at the origin. That is, we must be able to factor ν^2 out of the numerator of (5.27). Such a term is already present in $\nu^\eta \hat{q}_1(\nu) q_2(\nu)$. To make sure that ν^2 can also be factored out of $q_3^2(\nu)$, we require that the absolute term in $q_3(\nu)$ is zero. This is achieved from (5.22) by setting $\beta_0 = 0$, which means $\rho_0 = 0.5$. Then we obtain two zeros at the origin, as required. If the output state uses non-symmetric coupling, we cannot have two zeros at the origin and the system (5.7) is unstable. The root locus for one particular system is shown in Fig. 5.3a for symmetric output state and in Fig. 5.3b for asymmetric output state.

If $\eta > 2$ we require that there are $2\eta - 2$ zeros at the origin. Since the numerator is $\nu^\eta \hat{q}_1(\nu) q_2(\nu) + q_3^2(\nu)$, we can affect only the lowest η coefficients of the numerator to be zero, because both $\hat{q}_1(\nu)$ and $q_2(\nu)$ have a nonzero absolute term which cannot be changed by the interconnection. But for $\eta > 2$ we have that $\eta < 2\eta - 2$ and we cannot have sufficient number of zeros. The system (5.7) is therefore unstable.

Regarding c): for θ very low, the roots of (5.14) will be close to roots of (5.17), which are by assumption unstable. Hence, the roots will also be unstable. □

The stability conclusion is the same as for the symmetric circular system, where we also cannot have more than two integrators ([Barooah and Hespanha, 2005]). The symmetric coupling in the output state holds for all models and all orders of the system. Thus, the results of [Cantos and Veerman, 2014; Herman et al., 2016d] with symmetric coupling in positions are special cases of this theorem.

If the necessary conditions of Lemma 5.5 and Theorem 5.6 are satisfied, then we can use the imaginary axis as a guardian map.

Lemma 5.7. *The system (5.7) is asymptotically stable if the following equation*

$$\begin{aligned}(\jmath\omega)^n + (p_{n-1} + g_{n-1}[1 - \cos\theta + \jmath(1 - 2\rho_{n-1})\sin\theta])(\jmath\omega)^{n-1} \\ + \ldots + (p_1 + g_1[1 - \cos\theta + \jmath(1 - 2\rho_1)\sin\theta])(\jmath\omega) \\ + p_0 + g_0[1 - \cos\theta + \jmath(1 - 2\rho_0)\sin\theta] = 0.\end{aligned} \tag{5.28}$$

has no solution for all $\omega \in \mathbb{R}$.

Proof. As discussed above, by Lemma 5.5 all curves $\nu(\theta)$ start in the left half plane or at the origin. Suppose that the necessary conditions following from

Theorem 5.6 are satisfied. When the curves $\nu(\theta)$ do not cross the imaginary axis, the system (5.7) is stable. Therefore, there must not exist a solution to (5.14) which has purely imaginary roots. That is why when $\jmath\omega$ is plugged for ν to (5.14), it must not have a solution. This fact is captured by (5.28). □

5.2.4 Simulations

In this section we verify our results numerically for a particular system. Suppose that the model of the vehicle is a double integrator with a viscous friction (velocity feedback), given in a transfer function as $G(s) = \frac{1}{s^2+0.5s}$. Its output is the vehicle's position y_i. For such a model we designed a controller $R(s) = \frac{14.3s^2+14.3s+3}{s^2+3s}$. The controller connected in series with the vehicle model form the open loop $M(s) = R(s)G(s)$. The open loop has 2 integrators, hence it satisfies Internal Model Principle for tracking of a ramp signal, caused by the platoon's leader moving with a constant velocity.

The open loop can be modelled in a controller-canonical form as

$$A = \begin{bmatrix} 0 & 1 & 0 & 0 \\ 0 & 0 & 1 & 0 \\ 0 & 0 & 0 & 1 \\ 0 & 0 & -1.5 & -3.5 \end{bmatrix}, B = \begin{bmatrix} 0 \\ 0 \\ 0 \\ 1 \end{bmatrix}, C = \begin{bmatrix} 3 & 14.3 & 14.3 & 0 \end{bmatrix}. \tag{5.29}$$

The state vector is $[y, v, c_1, c_2]^{\mathrm{T}}$ with the states being position, velocity, controller state 1 and controller state 2, respectively. We will use the terms in the matrix C as coupling coefficients, i. e., $g_0 = 3, g_1 = 14.3$ and $g_2 = 14.3$. That is, position, velocity and output controller state are used for control.

The overall system has a form

$$A_c = \begin{bmatrix} 0 & I & 0 & 0 \\ 0 & 0 & I & 0 \\ 0 & 0 & 0 & I \\ -3L_y & -14.3L_v & -14.3L_c - 1.5I & -3.5I \end{bmatrix}, B_c = \begin{bmatrix} 0 \\ 0 \\ 0 \\ I \end{bmatrix}. \tag{5.30}$$

The Laplacians have a form of (5.5) with asymmetries ρ_y, ρ_v, ρ_c for L_y, L_v, L_c, respectively. We will vary the asymmetries to illustrate the stability and instability. The characteristic equation (5.14) has now a form

$$\nu^4+3.5\nu^3+(1.5+14.3\lambda_c(\theta))\nu^2+14.3\lambda_v(\theta)\nu+3\lambda_y(\theta) = 0. \tag{5.31}$$

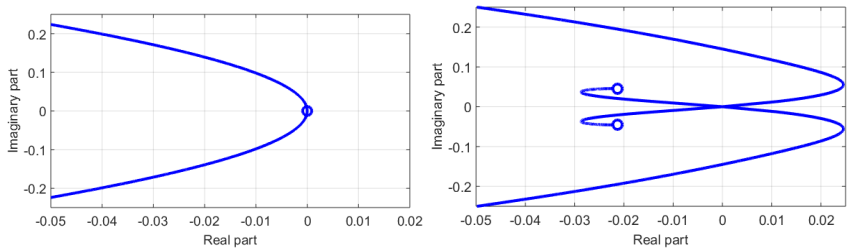

(a) Symmetric position (b) Asymmetric position

Figure 5.3: Root locus plots for $M_{\mathrm{rl}}(s)$ from the proof of Theorem 5.6.

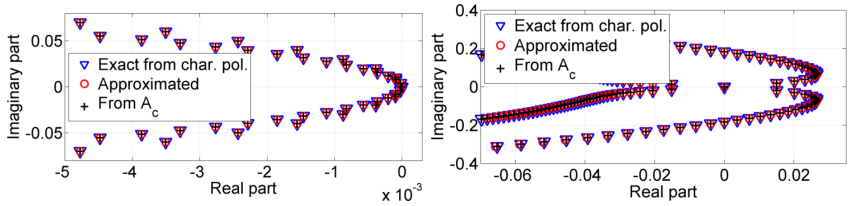

(a) Symmetric position: $\rho_y = 0.5, \rho_v =$ $0.45, \rho_c = 0.35$ (b) Asymmetric position: $\rho_y =$ $0.48, \rho_v = 0.45, \rho_c = 0.35$

Figure 5.4: Eigenvalue locations for $N = 1000$ calculated using different formulas. ∇ - calculation based on (5.14), o - calculation based on (5.18) and + shows eigenvalues of A_c. Note different scales of axes.

First we illustrate the root-locus approach used in the proof of Theorem 5.6. The transfer function is $M_{\mathrm{rl}}(s) = \frac{q_1(s)q_2(s)+q_3^2(s)}{q_1^2(s)}$. In this case, the polynomials are $q_1(s) = s^4 + 3.5s^3 + 1.5s^2, q_2(s) = 14.3s^2 + 14.3s + 3$ and $q_3(s) = (1 - 2\rho_c)14.3s^2 + (1 - 2\rho_v)14.3s + (1 - 2\rho_y)3$. Fig. 5.3 shows a plot of root-locus of $M_{\mathrm{rl}}(s)$ for: a) $\rho_y = 0.5, \rho_v = 0.45, \rho_c = 0.35$ (symmetry in position) and b) $\rho_y = 0.48, \rho_v = 0.45, \rho_c = 0.35$ (small asymmetry in position). It is clear that for the asymmetric position the roots lie in the right half-plane, so the system (5.30) gets unstable. When there is a symmetry in position and an asymmetry in other states, stability is achieved.

Fig. 5.4 illustrates that the eigenvalues ν_i of the second-order Taylor series approximation (5.18) match those calculated using exact formula (5.14) and also those obtained as the eigenvalues of A_c. The figure also confirms Theorem 5.6, since the system with the asymmetric coupling in the position is asymptotically unstable—the eigenvalues are in the right half-plane.

For three integrators in the open loop it is impossible to design an interaction

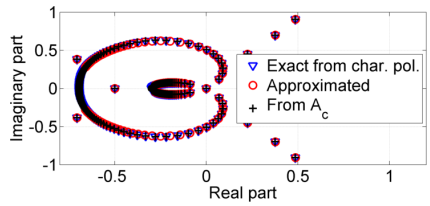

Figure 5.5: Eigenvalues for $N = 100$ for a system with three integrators (5.32). $\bigtriangledown$ - calculation based on (5.14), o - calculation based on (5.18) and $+$ shows eigenvalues of A_c.

achieving asymptotic stability. Let us show it using the following model

$$A_c = \begin{bmatrix} 0 & I & 0 & 0 \\ 0 & 0 & I & 0 \\ 0 & 0 & 0 & I \\ -3L_y & -14.3L_v & -14.3L_c & -3.5I \end{bmatrix}, B_c = \begin{bmatrix} 0 \\ 0 \\ 0 \\ I \end{bmatrix} \tag{5.32}$$

with $\rho_y = 0.5, \rho_v = 0.5$ and $\rho_c = 0.3$, that is, the only asymmetry is in the controller state. The eigenvalues are shown in Fig. 5.5. As expected, such a system is unstable.

5.3 Platoon with third-order vehicles

Having the necessary conditions on stability of the circular system, we can go back to platoons. In this section we will consider a vehicle model which has friction. This requires an integral action in the controller. Thus, the model is of the third order. We will analyze the properties of such platoons and propose an optimization procedure for controller parameter tuning.

The results here are based on the papers [Cantos and Veerman, 2014; Cantos et al., 2014]. We will use the approach presented there and also some results. Basically, this section shows that the approach there is applicable to more complicated systems as well. After deriving the transient properties, we propose an optimization procedure for controller design.

5.3.1 System model

We assume $N+1$ identical vehicles travelling on a line, indexed as $0, \ldots, N$. The first vehicle with index 0 is a leader which is driven independently of the the rest of the formation. Unlike standard double integrator models [Bamieh et al., 2012; Tangerman et al., 2012; Cantos et al., 2014], real systems have a friction, i. e., there is a feedback from velocity, which eventually makes the vehicle to stop. The vehicle model is

$$\ddot{y}_i = -av_i + F_i, \tag{5.33}$$

where y_i is the position of the ith vehicle, $v_i = \dot{y}_i$ is its velocity, $a \in \mathbb{R}$ is the viscous friction coefficient and F_i is the input to the vehicle, which is usually the force acting on it.

In order to enable the vehicles in the platoon to track the leader moving with a constant velocity, we need to satisfy the Internal Model Principle (Lemma 2.11) which in our case means the presence of two integrators in the open-loop model of each vehicle. Since one integrator is already present in the vehicle model ($\dot{y}_i = v_i$), it suffices to add an integral action into the controller of each vehicle. The controller is given as

$$\dot{\bar{c}}_i = e_i \tag{5.34}$$

with e_i defined in (5.35) and $\bar{c}_i$ is the state of the integrator in the controller. The input to the vehicle is then $F_i = \bar{c}_i$.

Each vehicle uses only the information obtained from its nearest neighbors — the vehicle in front of it and behind. The goal of the vehicle is to keep a prescribed spacing to them, i.e., $y_{i-1} - y_i \to \Delta_{\text{ref}}$ with Δ_{ref} being the desired distance between the neighboring vehicles. The controller input e_i comes from the relative spacing and velocity errors as

$$\begin{aligned} e_i = g_y\Big[(1-\rho_y)(y_{i-1} - y_i - \Delta_{\text{ref}}) - \rho_y(y_i - y_{i+1} - \Delta_{\text{ref}})\Big] \\ + g_v\Big[(1-\rho_v)(v_{i-1} - v_i) - \rho_v(v_i - v_{i+1})\Big], \end{aligned} \tag{5.35}$$

where the position asymmetry is labeled as ρ_y, velocity asymmetry as ρ_v and $g_y, g_v \in \mathbb{R}$ are weights of position and velocity errors. The coupling in position is symmetric if $\rho_y = 0.5$ and asymmetric otherwise (the same for ρ_v).

To simplify the analysis, we introduce error variables $z_i = y_i - y_0 + \Delta_{\text{ref}0,i}$ with $\Delta_{\text{ref}0,i}$ being the reference distance between the leader and the ith vehicle. This implies $z_{i-1} - z_i = y_{i-1} - y_i - \Delta_{\text{ref}}$ and $\dot{z}_{i-1} - \dot{z}_i = \dot{y}_{i-1} - \dot{y}_i$. The single vehicle

model combined with the controller then has a form

$$\dddot{z}_i = -a\ddot{z}_i + \bar{c}, \quad \dot{\bar{c}}_i = e_i. \tag{5.36}$$

We use a minor state transformation $c_i = \bar{c}_i - av_i$ to obtain a controller-canonical form of the individual-vehicle model

$$\begin{pmatrix} \dot{z}_i \\ \ddot{z}_i \\ \dot{c}_i \end{pmatrix} = \begin{pmatrix} \dot{z}_i \\ \ddot{z}_i \\ \dddot{z}_i \end{pmatrix} = \begin{pmatrix} 0 & 1 & 0 \\ 0 & 0 & 1 \\ 0 & 0 & -a \end{pmatrix} \begin{pmatrix} z_i \\ \dot{z}_i \\ \ddot{z}_i \end{pmatrix} + \begin{pmatrix} 0 \\ 0 \\ 1 \end{pmatrix} e_i. \tag{5.37}$$

In a vector form we write the overall system of $N+1$ vehicles (including the leader) as

$$\frac{d}{dt}\begin{pmatrix} z \\ \dot{z} \\ \ddot{z} \end{pmatrix} = A_c \begin{pmatrix} z \\ \dot{z} \\ \ddot{z} \end{pmatrix} \equiv \begin{pmatrix} 0 & I & 0 \\ 0 & 0 & I \\ -g_y L_y & -g_v L_v & -aI \end{pmatrix} \begin{pmatrix} z \\ \dot{z} \\ \ddot{z} \end{pmatrix}, \tag{5.38}$$

where $z = [z_0, \ldots, z_N]^{\mathrm{T}}$. Let us call the system (5.38) *a path system*, since the communication topology is a weighted path graph. The Laplacians $L_y, L_v \in \mathbb{R}^{N+1 \times N+1}$ of the path graph are defined as

$$L_y = \begin{pmatrix} 0 & 0 & 0 & 0 & \ldots & 0 \\ -(1-\rho_y) & 1 & -\rho_y & 0 & \ldots & 0 \\ 0 & -(1-\rho_y) & 1 & -\rho_y & \ldots & 0 \\ \vdots & \vdots & \vdots & \vdots & \ddots & \vdots \\ 0 & 0 & 0 & \ldots & -1 & 1 \end{pmatrix}, \tag{5.39}$$

$$L_v = \begin{pmatrix} 0 & 0 & 0 & 0 & \ldots & 0 \\ -(1-\rho_v) & 1 & -\rho_v & 0 & \ldots & 0 \\ 0 & -(1-\rho_v) & 1 & -\rho_v & \ldots & 0 \\ \vdots & \vdots & \vdots & \vdots & \ddots & \vdots \\ 0 & 0 & 0 & \ldots & -1 & 1 \end{pmatrix}. \tag{5.40}$$

The last vehicle has no follower, so it uses only front spacing and velocity errors. This type of boundary condition is called regular boundary condition [Cantos and Veerman, 2014]. The second boundary condition is that the leader is driven

independently of the platoon (zeros in the first rows of L_y, L_v).

We assume that initially the system in (5.38) is at stand-still and then the leader starts to move with unit velocity:

$$\begin{aligned} z_i(t) &= 0 \text{ for } i = 1, \dots, N,\ t < 0, \\ y_0(t) &= 0,\ t < 0,\ \ y_0(t) = t,\ t \geq 0. \end{aligned} \tag{5.41}$$

5.3.2 Review of previous work

This chapter builds on the results of works [Cantos et al., 2014; Cantos and Veerman, 2014]. Both papers deal with a signal propagation in systems with nearest-neighbor interaction. The vehicle model is a double integrator, i.e., $\ddot{z}_i = e_i$ with e_i given by (5.35).

The work [Cantos et al., 2014] analyzes a system with a circular topology. We call such system a *circular system*. The interaction between the leader and the vehicle N is added. The most important condition for stability of this circular system is that $\rho_y = 0.5$ [Cantos et al., 2014, Prop. 3.5]—there must be a symmetric coupling in the position. This was generalized in Theorem 5.6. For stable circular systems it is shown in [Cantos et al., 2014, Thm. 4.8] that an external input or a disturbance causes two signals to propagate in the system in opposite directions and with different velocities. These so-called signal velocities are calculated from the phase velocities [Cantos et al., 2014, Lem. 4.4]. We will use the same ideas in this chapter (Sec. 5.3.5) to describe a stable system in terms of traveling waves.

The paper [Cantos and Veerman, 2014] studies transients in path systems. Its main result is the description of the transient in the path graph using two travelling waves, attenuated at the boundaries [Cantos and Veerman, 2014, Thm. 3.5]. The connection of the circular system from [Cantos et al., 2014] to the path system (which is the one we are really interested in) was conjectured in [Cantos and Veerman, 2014] as follows: the asymptotic instability of the circular system should imply either flock or asymptotic instability of the path system. Flock stability is defined as follows.

Definition 5.8 (Flock stability, [Cantos and Veerman, 2014])**.** *The system is called flock stable if it is asymptotically stable and if* $\sup_{t\in\mathbb{R}} |z_0(t) - z_N(t)|$ *grows sub-exponentially in* N *for the conditions (5.41).*

5.3.3 Analysis of the circular system

If $\rho_y \neq \rho_v$ in the path system in (5.38), there are two different Laplacians L_y and L_v which are not simultaneously diagonalizable. This prevents many convenient approaches to guarantee stability such as a synchronization region [Zhang et al., 2011] or LMI-based criterion [Massioni and Verhaegen, 2009]. Thus, stability and performance analysis of the path system become very difficult.

To overcome this limitation, we invoke the Assumptions 5.1 and 5.2 to extract some properties of the circular system and apply them in the analysis of the path system. So we assume in this section that the communication structure is the circular graph with Laplacians $\hat{L}_y, \hat{L}_v$. These Laplacians are circulant matrices, which are *simultaneously diagonalizable*. Note that we investigate the circular system only in order to learn something about the path system—the circular system is *not of practical interest* by itself.

5.3.4 Stability of the circular system

When we assume the circular interaction topology, the state-space model has a form

$$\frac{d}{dt}\begin{pmatrix} z \\ \dot{z} \\ \ddot{z} \end{pmatrix} = \hat{A}_c \begin{pmatrix} z \\ \dot{z} \\ \ddot{z} \end{pmatrix} \equiv \begin{pmatrix} 0 & I & 0 \\ 0 & 0 & I \\ -g_y\hat{L}_y & -g_v\hat{L}_v & -aI \end{pmatrix} \begin{pmatrix} z \\ \dot{z} \\ \ddot{z} \end{pmatrix}. \tag{5.42}$$

The Laplacians $\hat{L}_y, \hat{L}_v$

$$\hat{L}_y = \begin{pmatrix} 1 & -\rho_y & 0 & \dots & -(1-\rho_y) \\ -(1-\rho_y) & 1 & -\rho_y & \dots & 0 \\ \vdots & \vdots & \vdots & \ddots & \vdots \\ -\rho_y & 0 & \dots & -(1-\rho_y) & 1 \end{pmatrix}, \tag{5.43}$$

$$\hat{L}_v = \begin{pmatrix} 1 & -\rho_v & 0 & \dots & -(1-\rho_v) \\ -(1-\rho_v) & 1 & -\rho_v & \dots & 0 \\ \vdots & \vdots & \vdots & \ddots & \vdots \\ -\rho_v & 0 & \dots & -(1-\rho_v) & 1 \end{pmatrix}. \tag{5.44}$$

As discussed before, they are simultaneously diagonalizable by the discrete

Fourier transform. So let w_m be the m-th eigenvector of $\hat{L}$, that is the vector whose j-th component satisfies $(w_m)_j = e^{\jmath\theta j} \equiv e^{\jmath \frac{2\pi m}{N+1} j}, \quad j = 0, 1, \ldots, N$ with $\theta = 2\pi m/(N+1)$ and $\jmath = \sqrt{-1}$. By [Cantos et al., 2014], we calculate the eigenvalues λ_y of $\hat{L}_y$ and λ_v of $\hat{L}_v$ as

$$\begin{aligned} \lambda_y(\theta) &= 1 - \cos\theta + \jmath(1-2\rho_y)\sin\theta, \\ \lambda_v(\theta) &= 1 - \cos\theta + \jmath(1-2\rho_v)\sin\theta. \end{aligned} \tag{5.45}$$

Let us denote $\psi_y = 1 - 2\rho_y$, $\psi_v = 1 - 2\rho_v$. We can expand the eigenvalues λ_y and λ_v in the Taylor series

$$\lambda_y(\theta) = \jmath\psi_y\theta + \frac{1}{2}\theta^2 - \frac{\jmath}{6}\psi_y\theta^3 \ldots, \tag{5.46}$$

$$\lambda_v(\theta) = \jmath\psi_v\theta + \frac{1}{2}\theta^2 - \frac{\jmath}{6}\psi_v\theta^3 \ldots \tag{5.47}$$

We now calculate three eigenvalues $\nu_{m,i}$, $i = 1, 2, 3$ of $\hat{A}_c$ associated with w_m for each m. For simplicity of notation we drop the subscripts of ν except from when ambiguity seems possible. Similarly to (5.13), we calculate the eigenvalue equation as

$$\nu^3 + a\nu^2 + g_v\lambda_v(\theta)\nu + g_y\lambda_y(\theta) = 0. \tag{5.48}$$

Substituting the expressions for $\lambda_y(\theta)$ and $\lambda_v(\theta)$, we get

$$\begin{aligned} \nu^3 + a\nu^2 + g_v[1 - \cos\theta + \jmath(1-2\rho_v)\sin\theta]\nu \\ + g_y[1 - \cos\theta + \jmath(1-2\rho_y)\sin\theta] = 0. \end{aligned} \tag{5.49}$$

By letting θ equal 0 or π we get real polynomials

$$\nu^3 + a\nu^2 = 0, \tag{5.50}$$

$$\nu^3 + a\nu^2 + 2g_v\nu + 2g_y = 0. \tag{5.51}$$

The equation (5.51) implies via Routh-Hurwitz criterion a simple necessary conditions for stability.

Lemma 5.9. *The necessary conditions for the stability of (5.42) for all N are $a > 0$, $g_y > 0$ and $g_v > 0$ and $a > g_y/g_v$.*

The next theorem guarantees stability of an arbitrarily large system with a circular topology.

Theorem 5.10. *All non-trivial eigenvalues of (5.42) have negative real part if*

and only if all of the below hold:

$$\begin{aligned} &\text{I.}: \quad a > 0 \wedge g_y > 0 \wedge g_v > 0 \wedge a > g_y/g_v, \\ &\text{II.}: \quad \rho_y = 1/2, \\ &\text{III.}: \quad 1 - 2\rho_v \in \left(-\frac{ag_v - g_y}{\sqrt{2{g_v}^3}}, \frac{ag_v - g_y}{\sqrt{2{g_v}^3}} \right). \end{aligned} \tag{5.52}$$

Proof. Let us call the statement "Circular system (5.42) is stable" as S. The necessity of condition I. follows from Lemma 5.9 and the necessity of II. follows from Theorem 5.6. We will use them to prove that given I. and II., then III. is false is equivalent to S is false.

We know from (5.50) that $-a$ is a solution of (5.49) and that it lies in the left half-plane. By continuity of roots of polynomials all the solutions of (5.49) must lie on a curve $\nu(\theta)$ starting at $-a$. To have unstable roots on the curve $\nu(\theta)$, the curve must cross the imaginary axis for some $\theta \in (0, 2\pi)$. Then there must be purely imaginary solutions $\jmath\omega$ (ω real) to (5.49). Substitute $\jmath\omega$ for ν into (5.49) to get

$$-\jmath\omega^3 - a\omega^2 + [\jmath(1-\cos\theta) - \psi_v \sin\theta] g_v \omega + g_y(1-\cos\theta) = 0. \tag{5.53}$$

The real and imaginary parts of (5.53) are, respectively:

$$-a\omega^2 - g_v \psi_v \omega \sin\theta + g_y(1-\cos\theta) = 0, \tag{5.54}$$

$$-\omega(\omega^2 - g_v(1-\cos\theta)) = 0. \tag{5.55}$$

So S is false if both of the last equations hold (i.e., (5.53) has a solution). The equation (5.55) holds for $\omega = 0$ or $\omega^2 = g_v(1-\cos\theta)$, where $\omega = 0$ gives only the 'trivial' eigenvalue (namely $\theta = 0$). Plugging the other solution $\omega^2 = g_v(1-\cos\theta)$ into (5.54) gives:

$$\psi_v = \pm \frac{ag_v - g_y}{\sqrt{2{g_v}^3}} \frac{\sqrt{2(1-\cos\theta)}}{\sin\theta}. \tag{5.56}$$

The factor $\frac{\sqrt{2(1-\cos\theta)}}{\sin\theta}$ maps the unit circle onto $[-\infty, -1] \cup [1, \infty]$. So for $|\psi_v| \geq \frac{ag_v - g_y}{\sqrt{2|g_v|^3}}$ there exists θ for which equation (5.53) is satisfied, the system then has purely imaginary roots and therefore the system can be unstable. If $|\psi_v| < \frac{ag_v - g_y}{\sqrt{2|g_v|^3}}$, then no imaginary solution exists and whole curve $\nu(\theta)$ lies in the stable half-plane. □

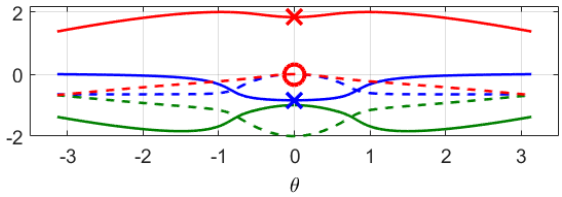

Figure 5.6: Phase velocities calculated by (5.57) in *vehicles/s* (solid) and the corresponding damping (dashed) as a function of θ. There are three waves for each θ, two with negative velocity (blue and green) and one with positive (red). The phase velocities in green have all high damping, so they do not affect the signal velocity. The signal velocities from (5.60) are shown by red (c_+) and blue (c_-) crosses, the corresponding damping by a red circle. $N = 500, a = 2, g_y = 6.2, g_v = 10, \rho_v = 0.4$.

5.3.5 Signal properties

Similarly to [Cantos et al., 2014], we would like to obtain the signal velocity in our circular system (5.42). By [Cantos et al., 2014, Lem. 4.4], the phase velocity $c_{m,i}$ and its damping $\alpha_{m,i}$ for a mode associated with a given $\theta = 2\pi m/(N+1)$ can be calculated as

$$c_{m,i} = -\Im\{\nu_{m,i}\}/\theta, \quad \alpha_{m,i} = \Re\{\nu_{m,i}\},\ i = 1, 2, 3. \tag{5.57}$$

We are interested in modes with very low damping, since they travel in the system with slow decay—they give us the signal velocity. Thus, we want to find the eigenvalues $\nu(\theta)$ with small real parts. They are those corresponding to $\theta \to 0$. To find them, first expand $\nu(\theta)$ as

$$\nu(\theta) = \jmath n_1\theta + \frac{1}{2}n_2\theta^2 + \frac{\jmath}{6}n_3\theta^3 \dots. \tag{5.58}$$

We substitute the expansions (5.46), (5.47) and (5.58) into (5.49). Notice that the expansion (5.58) works because the terms depending on θ cancel in (5.49). We collect terms of order θ^2, and θ^3, etc. The coefficients of these orders must be zero and that will determine n_i. The first non-trivial equation is the coefficient of θ^2. It reads: $\mathcal{O}(2) : an_1^2 + g_v\psi_v n_1 - \frac{1}{2}g_y = 0$. We calculate n_1 as

$$n_1 = \frac{-g_v\psi_v \pm \sqrt{2ag_y + {g_v}^2\psi_v^2}}{2a}. \tag{5.59}$$

Since for θ small by (5.58) and (5.57) $\Im\{\nu(\theta)\} \approx n_1\theta$, the coefficient $-n_1$ determines the signal velocities.

Lemma 5.11. *The signal velocities are given as*

$$c_{\pm} = \frac{g_v \psi_v \pm \sqrt{{g_v}^2 \psi_v^2 + 2 a g_y}}{2a}, \tag{5.60}$$

where $c_+ > 0$ *and* $c_- < 0$ *(velocity in vehicles/second).*

By the stability conditions we mentioned, (5.60) gives one positive real and one negative real solution (red and blue crosses in Fig. 5.6). The wave with the positive velocity c_+ propagates in the direction with growing vehicle index and the wave with c_- the other way.

5.4 Transients in the path system

We have obtained enough properties of the circular system to derive the transients of the original *path system* (5.38). The transient we analyze is when the platoon is in steady state and the leader starts to move with a unit velocity (5.41).

We have Theorem 5.10 guaranteeing stability of the circular system which by Assumption 5.2 allows for flock stability of the path system. The signal velocity in (5.60) should remain the same in the path system—Assumption 5.1. The boundary conditions are the same as in [Cantos and Veerman, 2014]—the leader driven independently of the platoon and the agent N having no follower. For stable systems (in both senses), the orbit of the last agent can be characterized by the following quantities (see Fig. 5.7): half-period T is the smallest $t > 0$ such that $z_N(t) - z_0(t) = 0$ and the amplitude A_i of the ith oscillation is $A_i = \max_{t \in [(i-1)T, iT]} |z_0 - z_N|$. We can now restate [Cantos and Veerman, 2014, Thm. 3.5] for our system with friction.

Theorem 5.12. *If Assumptions 5.1 and 5.2 hold and the path system (5.38) is asymptotically stable, if the parameter values satisfy the conditions in Theorem 5.10 and as* N *tends to infinity, the system (5.38) will behave as a wave equation with boundary conditions. The signal velocities are given by (5.60). In particular, if from an equilibrium position at rest, the leader starts to move with a unit velocity at* $t = 0$*, then the characteristics of the orbit of* $z_0(t) - z_N(t)$ *are:*

$$A_1 = \frac{N}{|c_+|}, \tag{5.61}$$

$$|A_{k+1}/A_k| = |c_-|/|c_+|, \tag{5.62}$$

$$T = N \left| \frac{1}{|c_+|} + \frac{1}{|c_-|} \right|. \tag{5.63}$$

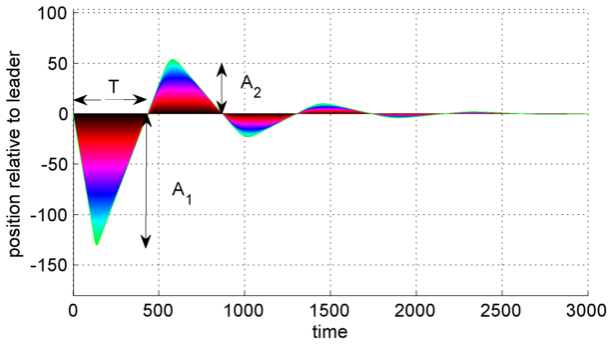

Figure 5.7: Spacing error to the leader $z_0 - z_i$ with optimized controller (see Sec. 5.4.2 and 5.4.3). $N = 250, a = 2, g_y = 6.2, g_v = 10$ and $\rho_v = 0.4$.

The proof of [Cantos and Veerman, 2014, Thm. 3.5] uses only boundary conditions and wave velocities, hence it remains valid for our case as well. Note that when the leader starts moving, this causes first a wave with velocity c_+, which then reflects at agent N as a wave with velocity c_-. Notice that we want $|c_-|/|c_+|$ to be less than 1 to avoid exponential growth of the amplitudes. Since g_v and a must be positive, we want to keep $\psi_v > 0$, i.e., $\rho_v < 1/2$ and the agent pays more attention to the front velocity error.

Remark 5.13. *The theorem has as a condition that the path system must be asymptotically stable. Indeed, it does not follow from any statement in this section that the path system is proven to be stable. Unfortunately, so far we have no conditions for stability of the path system. From simulations it seems that when the circular system is stable for any N, then the path system is stable as well. But we have no proof for that. Thus, we have to test stability of the path system for a given number of vehicles, for instance by looking at the eigenvalues.*

5.4.1 Simulation verification

Fig. 5.8 numerically validates Theorem 5.12 by calculating the relative error between the predicted and measured values as a function of N. Let χ be a given quantity of interest in Thm. 5.12 — either A_i, A_{i+1}/A_i or T. Let χ_{pred} be the value predicted by (5.61), (5.62) or (5.63), respectively, and χ_{meas} be the value measured from the numerical simulations of a finite platoon. The error is calculated as

$$\vartheta = \log\left(\frac{\chi_{\text{pred}}}{\chi_{\text{meas}}} - 1\right), \tag{5.64}$$

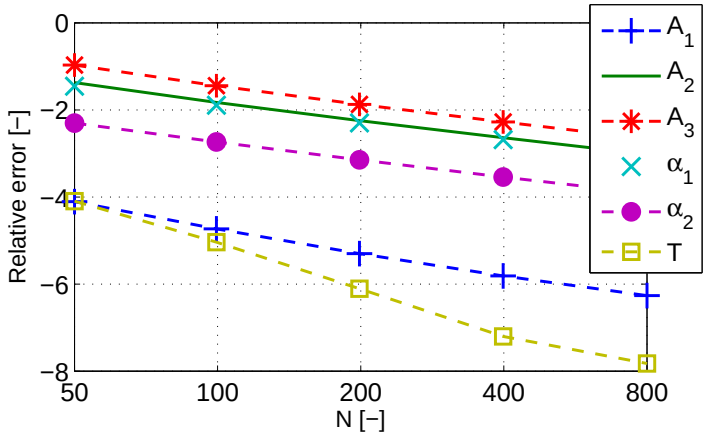

Figure 5.8: The numerical verification of (5.61), (5.62) and (5.63). The relative errors are carried out with (5.64) for $g_y = 6.2$, $g_v = 10$, $a = 2$, $\rho_y = 0.5$ and $\rho_v = 0.4$. The α_1 and α_2 are the attenuation coefficients from (5.62) for A_2/A_1 and A_3/A_2, respectively.

We can see that the relative error of each predicted parameter decreases exponentially with the increasing number of vehicles in the platoon. This confirms the asymptotic formulas in Theorem 5.12 and also Assumptions 5.1 and 5.2.

The numerical simulations in Fig. 5.9 show that a platoon with a controller tuned symmetrically (the left panel, SPSV—symmetric position, symmetric velocity) has a very long transient. The transient is shortened for the case of the asymmetric controller (the middle panel, APAV—asymmetric position, asymmetric velocity), however, the overshoot of such a platoon is extremely large, which is a consequence of Theorem 5.6 and Assumption 5.2—the circular system is unstable, hence the path system is flock unstable at best. When we set the asymmetry only in the velocity (right, SPAV—symmetric position, asymmetric velocity), then both the transient and the overshoot are reasonable.

A better transient can often be achieved just by increasing the control effort. We will show that when symmetric coupling in position is used, the control effort for the response to leader's step in velocity is the same regardless of the number of agents. Fig. 5.10 shows control efforts for different control architectures. It can be seen that the maximal control effort remains bounded for SPSV and SPAV, while it grows exponentially for APAV. The maximal control effort of the first vehicle is identical for all N, while the control effort of the last vehicle decays for SPAV and SPSV and grows exponentially for APAV. Hence, SPAV architecture achieves better transient with almost the same maximal control effort as SPSV.

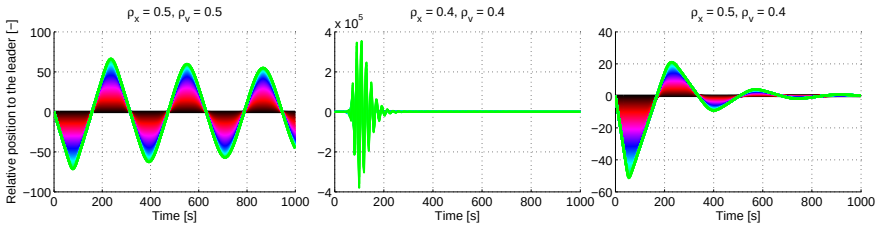

Figure 5.9: The numerical simulations comparing the responses of three different control strategies for $N = 100$, when the leader changes its velocity from 0 to 1. The figure shows the relative positions to the leader $z_0(t) - z_i(t)$ of all the vehicles for three different combinations of ρ_y and ρ_v. For all three cases were $g_y = 6.2$, $g_v = 10$ and $a = 2$.

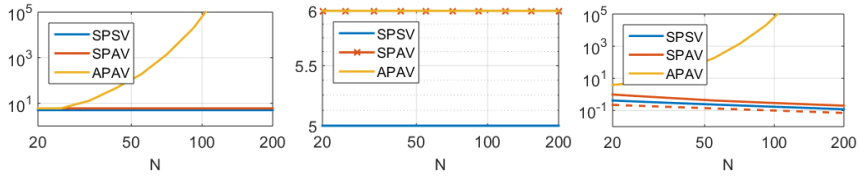

(a) Max. cont. effort (b) Max. eff. of $i = 1$ (c) Max. eff. of $i = N$

Figure 5.10: Maximal control efforts for the leader's step in velocity. a) Maximal control effort among all agents, b) maximal control effort of the first vehicle and c) maximal control effort of the last vehicle. SPSV: $\rho_y = \rho_v = 0.5$, SPAV: $\rho_y = 0.5, \rho_v = 0.4$, APAV: $\rho_y = \rho_v = 0.4$. Note logarithmic coordinates in a) and c). The dashed line in c) is $1/\sqrt{N}$, hence the maximal control effort of the last vehicle decays with rate this rate.

What is most surprising is the comparison of the convergence time—the time T_f it took the system to achieve $z_i(t) < 0.03$ for all i and $t > T_\mathrm{f}$. As follows from Fig. 5.11, the settling time in SPSV scales quadratically, while both in SPAV and APAV it scales only linearly. That is, for the same maximal control effort, SPAV has qualitatively different settling time than SPSV! At the same time, for approximately 4 times shorter settling time in case of APAV the price to pay is to have extremely large overshoots and control effort. Thus, SPAV is the best solution among the cases shown. On the other hand, we admit that the controller used was optimized for SPAV, see the next section.

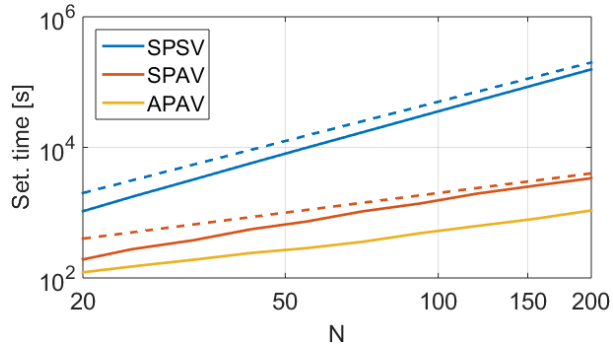

Figure 5.11: Settling time of the three architectures as a function of N. The blue dashed line is $10N^2$ and red is $20N$. Note logarithmic coordinates.

5.4.2 Optimization of controller parameters

The previous section gave us signal velocities and amplitudes of the transient, which depend on the gains g_y and g_v and the velocity asymmetry ρ_v. In this section we give an approach how to select these three parameters. We assume that the friction a is given by the vehicle model and cannot be affected by the designer.

We propose the following method for "optimal" (due to asymptotic formulas) gain and asymmetry selection. It is based on minimizing the absolute value of the spacing error of all vehicles in the formation, denoted as E, when the leader starts to move from the stand-still. Therefore, the optimization has a form

$$\min_{g_y,g_v,\psi_v} E = \min_{g_y,g_v,\psi_v} \sum_{i=1}^{N} \int_0^\infty |\tilde{z}_i(t)|dt, \tag{5.65}$$

where the error is given by $\tilde{z}_i(t) = z_0(t) - z_i(t)$. Clearly, $\tilde{z}_0 = 0$. E is minimized over g_y, g_v, ψ_v.

Theorem 5.12 tells us that the system behaves as a wave equation with boundaries. After a unit change of leader's velocity, first the signal spreads from the leader to vehicle N with velocity c_+ and then it reflects back with velocity c_-. The graph of the response of the last vehicle in the formation must then be almost triangular, as shown in Fig. 5.7. The error of the first oscillation for the last vehicle (before $\tilde{z}_N$ gets back to zero for the first time) is

$$E_{N,1} = \int_0^T |\tilde{z}_N(t)|dt \approx \frac{1}{2}TA_1. \tag{5.66}$$

To get the error of the other vehicles we assume that the maximal value of the error of ith vehicle is given by $\frac{A}{N}i$ (the peaks are uniformly spaced from 0 to A_1 with distance $\frac{A_1}{N}$). Then the shape of the error is almost a trapezoid with one base of length T and the other with $(N-i)\left(\frac{1}{|c_+|}+\frac{1}{|c_-|}\right) = T - \frac{i}{N}T = T\left(1-\frac{i}{N}\right)$. The absolute value of the error of the ith vehicle in the first oscillation is approximately the area of the trapezoid

$$E_{i,1} = \int_0^T |\tilde{z}_i(t)| \approx \frac{A_1}{N} iT\left(1-\frac{i}{2N}\right). \tag{5.67}$$

We have approximated the first oscillations. The errors of the others are calculated in a similar same way, i.e. the period is again T and the amplitude is obtained using (5.62). The total absolute value of the error of the ith vehicle is $E_i = \int_0^\infty |\tilde{z}_i(t)|dt$, which is using the trapezoidal approximation given as the sum of areas of all oscillations

$$\begin{aligned} E_i &= \int_0^\infty |\tilde{z}_i(t)|dt = \sum_{j=1}^{\infty} E_{i,j} \approx \sum_{j=1}^{\infty} \frac{A_j}{N} iT\left(1-\frac{i}{2N}\right) \\ &= \frac{A_1}{N} iT\left(1-\frac{i}{2N}\right)\frac{1}{1-\frac{|c_-|}{|c_+|}}. \end{aligned} \tag{5.68}$$

We used (5.62) to quantify the amplitude of the jth oscillation and then the sum of geometric series since $\frac{|c_-|}{|c_+|} < 1$.

Our criterion (5.65) captures the sum of E_i of all agents. It can be calculated as

$$E = \sum_{i=1}^{N} E_i \approx \sum_{i=1}^{N} \frac{A_1}{N} iT\left(1-\frac{i}{2N}\right)\frac{1}{1-\frac{|c_-|}{|c_+|}} = A_1 \frac{1}{1-\frac{|c_-|}{|c_+|}} TC = JC. \tag{5.69}$$

with $C = \sum_{i=1}^{N} \frac{i}{N}\left(1-\frac{i}{2N}\right)$ being a constant which cannot be changed by optimization. Thus, it suffices to minimize J. After plugging from (5.63) and (5.62), it has a form

$$J = \frac{A_1 T}{1-\frac{|c_-|}{|c_+|}} = \left(\frac{|c_-|+|c_+|}{|c_+||c_-|}\right)\frac{N^2}{|c_+|-|c_-|} = \hat{J}N^2. \tag{5.70}$$

The number of agents is not part of the optimization and does not affect the minimum. Plugging for the signal velocities from (5.60) we evaluate the sums and products as $|c_-|+|c_+| = (\sqrt{{g_v}^2\psi_v^2 + 2ag_y})/a$, $|c_-|-|c_+| = (g_v\psi_v)/a$, $|c_-||c_+| =$

$g_y/(2a)$. With these terms the criterion (5.70) becomes

$$\hat{J} = \frac{\sqrt{{g_v}^2\psi_v^2 + 2ag_y}}{g_v\psi_v}\frac{2a}{g_y} = \sqrt{\frac{1}{{g_y}^2} + \frac{2a}{{g_v}^2\psi_v^2 g_y}}2a. \tag{5.71}$$

Since a is a given constant and the square root is a monotone function, we get the final optimization problem

$$\begin{aligned} \min \quad & \frac{1}{{g_y}^2} + \frac{2a}{{g_v}^2\psi_v^2 g_y}, \\ & \text{s.t. stability conditions in (5.52).} \end{aligned} \tag{5.72}$$

The final criterion is a function only of the parameters g_y, g_v and ψ_v, which the platoon designer can affect.

Scaling of the absolute error

The total error (5.65) can be written using (5.69) and (5.70)

$$E \approx JC = \hat{J}N^2 \sum_{i=1}^{N} \frac{i}{N}\left(1 - \frac{i}{2N}\right). \tag{5.73}$$

Lemma 5.14. *The error E in (5.65) scales cubically with N as*

$$E(N) \approx \frac{\hat{J}}{12}N(N+1)(4N-1). \tag{5.74}$$

Proof. The proof is a simple manipulation of (5.73).

$$\begin{aligned} E \approx \hat{J}N^2 \sum_{i=1}^{N} \frac{i}{N}\left(1 - \frac{i}{2N}\right) = \hat{J}N^2 \sum_{i=1}^{N} \frac{2Ni - i^2}{2N^2} = \frac{\hat{J}}{2}\left[2N\sum_{i=1}^{N} i - \sum_{i=1}^{N} i^2\right] \\ = \frac{\hat{J}}{2}\left(2N\frac{N(N+1)}{2} - \frac{N(N+1)(2N+1)}{6}\right) = \frac{\hat{J}}{12}N(N+1)(4N-1). \end{aligned} \tag{5.75}$$

□

The scaling of E of different architectures with N calculated from simulations is in Fig. 5.12. It is clear that the error is the smallest for asymmetry only in velocity and also that the error of asymmetric control with identical asymmetries scales exponentially in N, which confirms flock instability ($\rho_y \neq 0.5$). Also the predicted value (5.74) matches the simulated one.

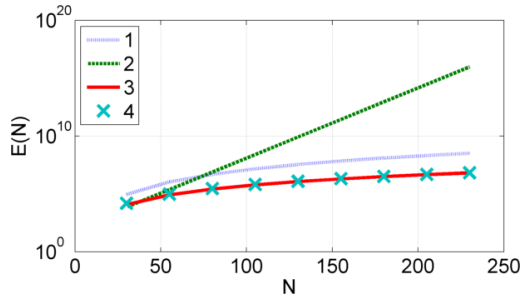

Figure 5.12: Logarithm of $E(N)$ for different architectures—SPSV with $\rho_y = \rho_v = 0.5$ (line 1), APAV with $\rho_y = \rho_v = 0.4$ (line 2) and SPAV with $\rho_y = 0.5, \rho_v = 0.4$ (line 3). Line 4 shows estimate using (5.74). Other parameters were $g_y = 6.2, g_v = 10, a = 2$.

5.4.3 Optimization results

We used the function *fmincon* in Matlab to carry out the optimization of the nonlinear criterion (5.72), subject to nonlinear stability constraints in (5.52). The optimization terminated quickly and successfully and as it seems from Fig. 5.13, the global minimum was reached. The code used for simulations in the whole chapter can be obtained at [Herman et al., 2015a].

As follows from (5.72), the optimization procedure tried to increase the gains g_y and g_v to decrease the criterion. Therefore we specified upper bounds on g_y, g_v to limit the controller effort. The optimization was conducted for a given friction $a = 2$ and we got the values $g_y = 6.2, g_v = 10$ and $\rho_v = 0.4$. The upper bounds for both gains g_y, g_v were set to 10. To stay away from the flock stability boundary, we changed the flock stability criterion in Thm. 5.10 to

$$\psi_v = 1 - 2\rho_v \in \left(-\frac{ag_v - g_y}{\sqrt{2{g_v}^3}} + \varepsilon,\ \frac{ag_v - g_y}{\sqrt{2{g_v}^3}} - \varepsilon \right), \tag{5.76}$$

with $\varepsilon = 0.1$. The response is shown in Fig. 5.7 and 5.9c.

5.4.4 Robustness evaluation

The optimization results should be verified to give robust results. The simplest way to achieve robustness is to add some nonzero term ε to each of the stability criteria (5.52), similarly to (5.76). Then the system is not allowed to operate on the flock stability boundary.

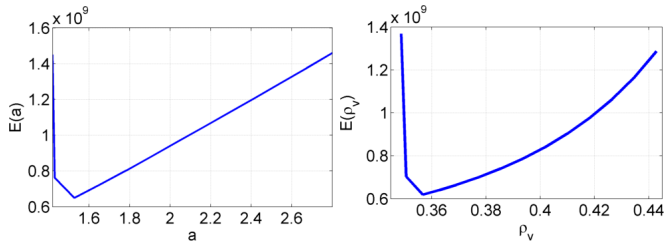

(a) Sens. to change in a. (b) Sens. to change in ρ_v.

Figure 5.13: Sensitivities to different parameters. The plots show value of E in (5.65) calculated from simulations.

The most important parameter of the system is the friction a. This might change during the operation of the system and also might not be exactly known apriori. Using the values $g_y = 6.2, g_v = 10, \rho_v = 0.4, N = 1200$, we simulated the response of the system for friction range $a \in [1.4, 2.8]$ and calculated the norm of the error using (5.65). Fig. 5.13a shows how the norm changes with friction. We see that the change is approximately linear in friction and the system has a good performance for a wide range of a. The sharp growth for low friction caused by a flock instability confirms the Assumption 5.2. The stability criterion of a circular system in Thm. 5.10 is violated for $a \leq 1.514$ since $\psi_v = 1 - 2\rho_v > \left(\frac{ag_v - g_y}{\sqrt{2|g_v|^3}}\right)$, making the system flock unstable. As $N \to \infty$, the sharp growth appears exactly at the critical point $a = 1.514$.

The Figure 5.13b shows how the error norm changes as a function of $\rho_v \in [0.34, 0.44]$ with the optimal value $\rho_v{}^* = 0.37$ (other parameters are $g_y = 8.3, g_v = 10$, $a = 2, N = 1200$). These are the values with $\varepsilon = 0$ in (5.76). It is clear that the value $\rho_v{}^*$ is almost the minimum of the function $E(\rho_v)$. The better performance for lower (non-optimal) $\rho_v \leq \rho_v{}^*$ is due to asymptotic formulas used. When the number of vehicles increases, the minimum will get closer to $\rho_v{}^*$. Due to the sharp growth for $\rho_v < 0.36$ we recommend using $\rho_v = 0.40$ to achieve robustness, as obtained using (5.76) with $\varepsilon = 0.1$. Then we get also $g_y = 6.2$, as above.

5.5 General models

We have necessary stability results for any system with circular topology and a complete analysis of a particular system—the third-order model having two integrators in the open loop. Unfortunately, we have no universal result, similar to those in the previous chapter. To the author's best knowledge, there is no

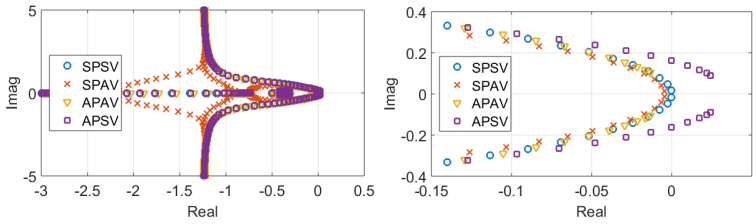

Figure 5.14: Eigenvalues of different systems for $N = 100$. Right—a detail around the origin.

result available so far.

In this section we will compare various characteristics of the platoon for the fourth-order model (5.29). We will keep the same open loops, only the asymmetries in individual states will be different. We will abbreviate the different cases as follows:

- SPSV (Symmetric Position, Symmetric Velocity):$\rho_x = 0.5, \rho_v = 0.5, \rho_c = 0.5$,
- SPAV (Symmetric Position, Asymmetric Velocity): $\rho_x = 0.5, \rho_v = 0.45, \rho_c = 0.35$,
- APAV (Asymmetric Position, Asymmetric Velocity): $\rho_x = 0.45, \rho_v = 0.45, \rho_c = 0.45$,
- APSV (Asymmetric Position, Symmetric Velocity): $\rho_x = 0.45, \rho_v = 0.5, \rho_c = 0.5$.

Let us start with the eigenvalues of the systems. They are shown in Fig. 5.14. The eigenvalues of SPSV and APAV lie on the root-locus curve. APAV and APSV achieve uniform boundedness of the eigenvalues. The most important fact following from the figure is that the APSV case has eigenvalues in the right half-plane, making the system unstable. Due to this fact we will not show any other property for the APSV case.

The comparison of transients for different asymmetries is shown in Fig. 5.15. It shows the response of the formation to the conditions in (5.41). It is clear that the completely symmetric interaction (Fig. 5.15a) has a very long transient. Contrary, when the coupling in all states is asymmetric (Fig. 5.15b), the transient has a very high overshoot—the flock instability appears, because of the asymmetry in position. The symmetric coupling in position and asymmetric coupling in the other states (Fig. 5.15c) shows a very good transient with a low overshoot. The simulations therefore confirm the Assumption 5.2 even for the fourth-order system. It also suggests that the partial asymmetry can substantially improve the transient for this fourth-order model. Thus, it seems that the property of necessity of symmetric coupling in position is valid in general for

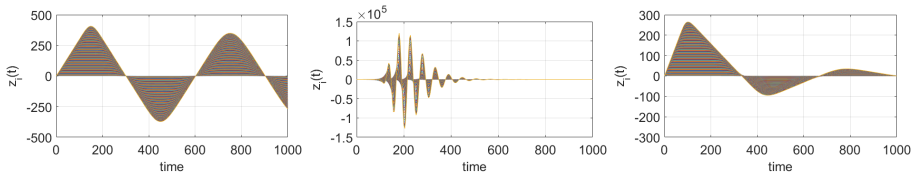

(a) SPSV (b) APAV (c) SPAV

Figure 5.15: Comparison of different asymmetries for $N = 150$. Note different scales in the y-axis.

systems with two integrators in the open loop. This would extend the results of papers by [Hao et al., 2012; Cantos and Veerman, 2014; Herman et al., 2016d] to more general models.

The following transient measures are evaluated for the conditions (5.41). Scaling of settling time is shown in logarithmic coordinates in Fig. 5.16a. Clearly, the SPAV and APAV both have comparable settling time (approx. linear), while SPSV scales quadratically. The maximal control effort (Fig. 5.16b) is bounded for SPSV and SPAV, while it scales exponentially in APAV. The maximal distance to the leader $\max_{i,t} z_i(t)$ (Fig. 5.16c) of SPSV and SPAV grows linearly in N (this follows from 5.61 and logically, it takes the signal some time to reach the last vehicle), but APAV scales exponentially.

Other important characteristic is the scaling of the $\mathcal{H}_\infty$ norm of the transfer function matrix. It is shown in Fig. 5.16d. Based on the figure, SPSV scales cubically (Theorem 4.22), SPAV grows only quadratically (we have no proof for this) and APAV again exponentially (Theorem 4.28). The most important fact is that SPAV achieved quadratic scaling, which is qualitatively identical to the scaling of SPSV with only integrator in the open loop (Theorem 4.21) which requires communicating the leader's velocity. That is, by introducing different asymmetries, we can qualitatively achieve the same scaling, which for identical asymmetries was possible only with communication.

A more thorough comparison of the scaling of the $\mathcal{H}_\infty$ norm of the transfer function matrix $\mathbf{T}(s)$ is in Fig. 5.17. There we illustrate scaling of the norm for the system (5.29), which has two integrators in the open loop, and a system with one integrator in the open loop, given as

$$A_c = \begin{bmatrix} 0 & I & 0 & 0 \\ 0 & 0 & I & 0 \\ 0 & 0 & 0 & I \\ -3L_y & -14.3L_v - 0.5I & -14.3L_c - 1.5I & -3.5I \end{bmatrix}, B_c = \begin{bmatrix} 0 \\ 0 \\ 0 \\ I \end{bmatrix}. \qquad (5.77)$$

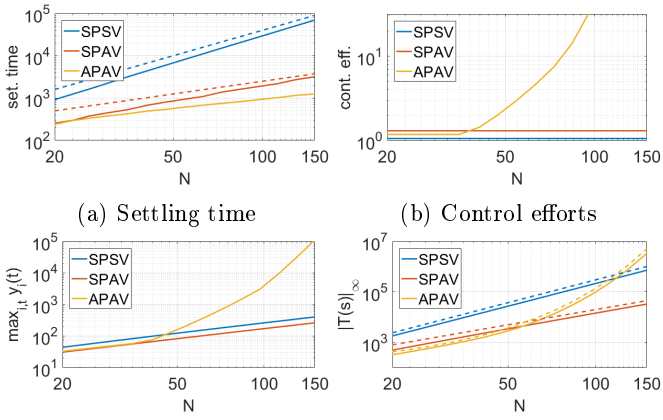

(a) Settling time (b) Control efforts

(c) Maximal overshoot (d) $\mathcal{H}_\infty$ norms of $\mathbf{T}(s)$

Figure 5.16: Various transient characteristics for different couplings in logarithmic coordinates. a) Settling time: the dashed lines show $30N$ (red) and $4N^2$ (blue). b) Scaling of maximal control effort among all vehicles and for any t. APAV scales exponentially. c) Maximal overshoot taken as $\max_{i,t} z_i(t)$, d) $\mathcal{H}_\infty$ norms of the transfer function matrix. The dashed lines are $0.3N^3$ (blue), $2N^2$ (red) and $100 \cdot 1.075^N$ (yellow).

It is clear that SPSV-1 and SPAV-2 are qualitatively the same (norm of SPAV-2 is slightly larger), but SPAV-2 does not require any communication with the leader. The best scaling is achieved for asymmetric control with one integrator, APAV-1.

5.5.1 Local string stability

There is one very strong result presented in the paper [Martinec et al., 2016b]. The paper analyzes a local string stability in a path-graph topology. In order to achieve the local string stability, the paper proves the fact that for a system having two integrators in the open loop it is necessary to have a symmetric coupling in the output state. The paper considers even a more general setup than discussed here: the front spacing error can be processed by a different controller than the rear spacing error. So instead of having different weights, even a different number of states can be present. The main result of the paper is that when there is not a symmetric coupling in position, the wave propagating in the system as a result of disturbance or initial conditions is amplified. The reason is that the $\mathcal{H}_\infty$ norm of the wave transfer function (2.48) is greater than

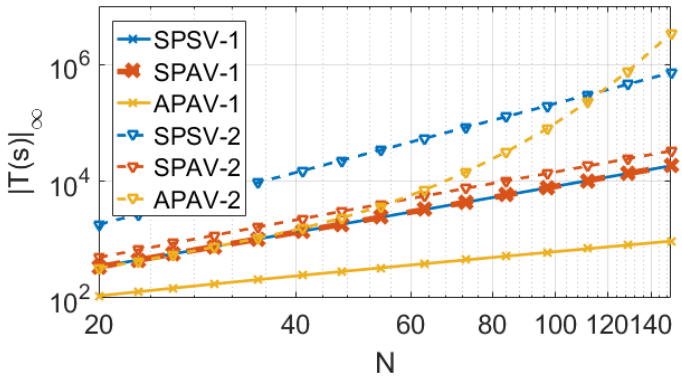

Figure 5.17: $\mathcal{H}_\infty$ norm comparison for systems (5.77), labeled as XPXV-1 and having one integrator, and with open loop (5.29), labeled XPXV-2 and having two integrators in the open loop.

one, i.e., $\|G(s)\|_\infty > 1$. This fact was named local string instability. Moreover, due to the local nature of waves in the system, the results holds for more general graphs as well.

However, no results were given for a system having three integrators in the open loop. That is why the author of this thesis believes that Theorem 5.6 still makes sense.

5.6 Open problems

As we stated in the introduction to this chapter, the research in vehicle platoons with different Laplacians is still at its beginning. Therefore, there is a lot of open problems. To the best knowledge of the author, the only works dealing with different Laplacians are [Hao et al., 2012; Cantos and Veerman, 2014; Cantos et al., 2014; Herman et al., 2015c, 2016d,a].

The most important research direction is stability. As follows from Theorem 5.12, we do not even have a stability condition for a path graph with the third-order agents. For second-order agents, quite thorough stability conditions are shown in [Herman et al., 2016a]. However, even there are some conjectures. It seems that whenever there is a greater asymmetry in position than in velocity, the system will become unstable if the number of vehicles is large enough. On the other hand, when there are larger asymmetries in other states than in position, probably the system will be stable. There are no proofs even for such simple systems, so it would be very useful to find some general conditions.

Except for stability, analysis of transient properties is also very important. As follows from the simulations in this chapter, SPAV control is superior to SPSV and APAV. Nevertheless, the tests were done only numerically and there might exist a case when it is not true. Most probably, the approach used in this chapter for transient analysis would work also for higher-order systems. But it has to be repeated for every single vehicle model.

Scaling of various norms for general models is definitely worth of research. First step into this is done in [Herman et al., 2016a] for double-integrator models. The paper analyzes $\mathcal{L}_2$ norms of deviations as a result of disturbance. It is shown there that SPSV has quadratic scaling, while SPAV only linear. But no generalization is available so far.

After we obtain some qualitative and quantitative descriptions of the platoon with multiple Laplacians, some controller design procedure should be provided. In this chapter we provide it for the third-order model, but still many conditions are taken from circular, not path system. What about general models? How do we select the individual asymmetries? This remains to be answered. But for sure, the controller design should be able to find the controller parameters along with the asymmetries for individual states. Separate design of the Laplacian and controller parameters makes no sense due to qualitatively different scaling.

Partial asymmetry might also help in other types of graphs, which do not use only nearest-neighbor interaction. First steps into this field is in [Herbrych et al., 2015], where next-nearest-neighbor interaction is investigated. The most interesting result there is a reflectionless wave, which shortens the transient a lot. This is a type of behavior which cannot appear in simple nearest-neighbor platoons. Since asymmetry in velocity shortens the transient in platoons, it should do the same in general graphs.

5.7 Conclusion

In this chapter we considered a novel approach to fixed-distance platoons, in which different Laplacians are used for different states. Such a system is very rarely considered in the distributed-control literature. The analysis in this chapter is based on the ideas by J.J.P. Veerman about the similarity of certain properties of path and circular systems. It was shown that a symmetric coupling in the output state is a necessary condition for stability of the circular system. Based on the reasonable assumptions, we can transfer the same condition to the path systems. Then we analyzed transients in a vehicular platoon with third-order vehicles.

We have shown that when there is a symmetric coupling in position and asym-

metric in velocity, much better transients can be achieved than are achievable with proportional asymmetry. This comes at no price: the implementation is no more difficult than that of symmetric bidirectional control and the maximal control effort is identical. The only difficulty is the analysis of the system, since a block diagonalization is not possible. Numerical examples illustrating superiority of SPAV to any other fully distributed control were shown. It follows that SPAV control achieves in some sense qualitatively similar as the symmetric control with communicated leader's velocity. Hence, it seems that it is the best strategy which does not require communication.

There is one important message of this chapter: one should never optimize with respect to the Laplacian. The Laplacian is never given, it is only the communication topology which might restrict the designer. The particular elements in the Laplacian should be given along with the controller parameters. We have proposed such a procedure.

6 Conclusion

The thesis dealt with scaling in vehicle platoons. It analyzed platoons in which a vehicle can measure (or obtain) states of its nearest neighbors—the car ahead (its predecessor) and the car behind (its successor). The coupling can be asymmetric, that is, the vehicle pays more attention (greater weight) to the front spacing and velocity error than to the rear one. Even different asymmetries in position and velocity can be used. Such a control is called asymmetric bidirectional control.

In order to obtain some scaling properties, it was first necessary to derive a general structure of a transfer function in a network system of SISO agents. The communication topology was a directed graph. The agents were assumed to be identical and they used output feedback and only one Laplacian. A transfer function between an input of one node (called the control node) and an output of another node (called the output node) was analyzed. It was shown that the transfer function can be expressed in a convenient product form. The terms in the numerator and the denominator have the same structure—they have a form of a denominator polynomial of the closed loop of a single agent. The "gains" in these terms are given by poles and zeros of the single-integrator systems. It follows from the product form that for at least one integrator in the open loop the steady-state gain does not depend on the agent model. A result on a minimal dimension of the controllable subspace of a network system is given.

Next, asymmetric vehicle platoons with proportional asymmetry were analyzed. Proportional asymmetry means that only one Laplacian (identical for all states) is used for coupling. In this case the analysis is simpler, since the Laplacian has only real eigenvalues and a convenient block-diagonalization procedure can be used. Various characteristics were investigated: steady-state gain, possibility of stabilization, transient time and in particular scaling of $\mathcal{H}_\infty$ norm of transfer functions. The results are not limited to any particular model, the analysis works

for an arbitrary model of the vehicle. It was shown that the most important distinguishing factor in scaling is the number of integrators in the open loop. For one integrator the scaling can be good, while for two and more the scaling is very bad. The results contain many cases previously discussed in the literature.

First, a symmetric bidirectional control was analyzed. It was shown that platoons with symmetric control suffer from very slow transients, because the eigenvalues get arbitrarily close to the origin. The $\mathcal{H}_\infty$ norms of various transfer functions in the platoon scale linearly for one integrator, quadratically for two integrators and the norm of the transfer function matrix scales cubically in the number of vehicles.

When asymmetry is allowed, the Laplacian has uniform bounds on eigenvalues. This in turn means that the platoon will not get arbitrarily slow with increasing number of vehicles. It was proved that such platoons have bounded steady-state gains and might be even inversely optimal. However, when there are at least two integrators in the open loop, exponential scaling of the $\mathcal{H}_\infty$ norm must occur and there is no linear controller which would prevent that. The same holds when the vehicles have unstable open loop. If the vehicles are allowed to know the leader's velocity, then only one integrator in the open loop is sufficient for tracking. With one integrator in the open loop, even bidirectional string stability is achievable. A sufficient condition is provided to achieve it and this condition can be used for controller design for a platoon of arbitrary size. The reason is that this condition requires only a single-agent model. Moreover, there always exists a string-stable predecessor following strategy when the open loop has only one integrator. The best possible scaling of the $\mathcal{H}_\infty$ norm of the transfer function matrix of the platoon is linear, achieved with asymmetric control and one integrator in the open loop.

The scaling results both for symmetric and asymmetric platoons show inherent limitations of platoon control, imposed by the communication topology. The reason is that the results hold for arbitrary open-loop models. Just by slightly changing the weights in the Laplacian, a qualitatively different behavior is obtained. It seems that the weights in the communication topology are more important than the agent model.

Time-headway spacing policy behaves as a system with one integrator in the open loop, so the benefit for changing the desired distance with velocity is in much better scaling.

Since it was apparent that for two integrators in the open loop there is no good controller with proportional asymmetry, an investigation of the effects of different asymmetries in position and velocity was started. Analysis of such systems is very difficult, because the system cannot be block diagonalized as in the case of

identical asymmetries. That is, no general result was obtained.

The conjectures of Peter Veerman from Portland State University were used for analysis. They are based on a relation of the path system to the circular system. Using these conjectures, it was possible to prove that for two integrators in the open loop the system must use symmetric coupling in position in order to prevent exponentially increasing transients. For more than two integrators this cannot be achieved. However, symmetric coupling in position does not disapprove using asymmetry in other states, particularly in velocity.

A thorough analysis of a platoon where vehicles have second-order model with a viscous friction, controlled by a PI controller, is provided. For such third-order systems, properties of a response to the step in leader's velocity were derived. It was shown that the behavior of the platoon is similar to the wave equation where the two waves have different velocities. Having the transient properties, an optimization procedure was proposed which optimizes the controller parameters along with asymmetry in velocity. This optimization procedure thus takes into account both the controller and the communication topology.

From numerical simulations it follows that for two integrators in the open loop, a control with symmetric coupling in position but asymmetric in velocity is the best among the cases considered in this thesis. It has a similar convergence time as the completely asymmetric control and still keeps a bounded control effort as the symmetric control does. Moreover, its $\mathcal{H}_\infty$ norm scales the same way as it does when the leader's velocity is available. Hence, although using just local information, it can compete with a control law having centralized information. In addition, this partially asymmetric control law is no more complicated than control laws with identical asymmetry. Since the analysis of this control law is very difficult, there are still many open problems to be solved. But definitely it seems as a promising solution.

6.1 Contribution of the author

Basically all theorems and lemmas, which do not have a direct reference to the literature, are derived by the author of the thesis, with minor exceptions in Chapter 5, where the ideas are often by prof. Peter Veerman.

The results of Chapter 3 were originally inspired by [Briegel et al., 2011], but their results were extended to higher-order dynamics and directed graphs. The product form is an original work of the author, as well as the relation to the single-integrator case. The remark on minimal dimension of controllable subspace is probably also new result. Theorem 3.10 was independently discovered by [Abad Torres and Roy, 2013], but the author got to know this result after he

published the paper [Herman et al., 2014b]. Moreover, the way of the proof is different. On the contrary, the paper by [Torres and Roy, 2015] was inspired by [Herman et al., 2014b], but it uses state-space techniques. Currently, a paper [Herman et al., 2016c] which summarizes the results in Chapter 3 is submitted.

The investigation of scaling of the $\mathcal{H}_\infty$ norm in vehicular platoons was mainly inspired by [Tangerman et al., 2012; Hao and Barooah, 2012; Bamieh et al., 2012], which worked only for double-integrator models. The result that the scaling depends on the number of integrators was inspired by Seiler's result for two integrators in the open loop [Seiler et al., 2004]. However, the author is not aware of any paper dealing with scaling in general asymmetric or symmetric platoons. So except for scaling of the predecessor following, all the results in Chapter 4 are the original work of the author. This can be justified by the fact that exponential scaling of the norm asymmetric platoons was presented as [Herman et al., 2014a], published as [Herman et al., 2015b] and its extension is conditionally accepted as [Herman et al., 2016b].

The comprehensive overview of scaling shown in Table 4.2 is presented for the first time in this thesis. The property of uniform bound on eigenvalues of platoon appeared for the first time in [Hao and Barooah, 2012; Tangerman et al., 2012]. Here the author generalized it to arbitrary asymmetric platoons. The conditions that the type of scaling can be judged just by looking at the single-agent transfer function corresponding to some eigenvalue of the Laplacian is also unique in author's work. The result on inverse optimality of asymmetric platoons is new in this thesis and was submitted as [Herman, 2016a].

The results in Chapter 5 are based on cooperation with Peter Veerman, so many ideas in the chapter are identical to his papers. Namely, the relation between the circular system and the path system is his idea and we only used it in our joint paper [Herman et al., 2016d]. The same holds for the approach for signal velocity, the use of boundary conditions and in general on the transient description. It was our joint work to extend P. Veerman's work to the third-order vehicles, but the tools used are those derived by Peter Veerman. On the other hand, the general proof of necessity of symmetric coupling in position in circular systems is the work of the author, presented as [Herman et al., 2015c]. Also the optimization procedure for controller-parameter design was derived by the author of the thesis.

The author continued the investigation of different asymmetries in cooperation with Steffi Knorn and Anders Ahlén from Uppsala. Together they derived scaling of the effect of the disturbance on the distances between cars for double-integrator systems. It was submitted as [Herman et al., 2016a]. This is probably the first paper which without any conjecture analytically proves better scaling of symmetric control in position and asymmetric in velocity.

6.2 Fulfillment of the goals

Here it is stated where the goals of the thesis were, in the opinion of the author, satisfied.

1. **Transfer functions in distributed control.** This is mainly dealt with in Chapter 3, where the structure of a transfer function in distributed control is discussed. The product form of a transfer function is derived and the structure of a higher-order dynamics is related to a single-integrator dynamics.

2. **Properties of asymmetric bidirectional control.** This is accomplished in Chapter 4, where asymmetric bidirectional platoons with proportional asymmetry are considered. Almost all the properties were obtained using separation of the properties of the Laplacian and the single-agent model. The main results are summarized in Tables 4.2 and 4.3.

3. **Conditions when asymmetry/symmetry is beneficial.** This is again the content of Chapter 4. Asymmetric control achieves a uniform bound on eigenvalues of the platoon, it has a bounded steady-state gain and can be tuned to be inversely optimal. It can even stabilize a formation of unstable vehicles. For one integrator in the open loop asymmetric control is a better solution than symmetric. However, for two integrators in the open loop, the exponential scaling does not allow asymmetry to be used. Symmetric control in this case offers better (but still bad) polynomial scaling. For two integrators in the open loop, it seems that symmetry in position and asymmetry in other states is a good solution.

4. **Scaling of $\mathcal{H}_\infty$ norm.** The scaling of $\mathcal{H}_\infty$ norm is presented in Table 4.2. The results are general, depending only on the topology and on the number of integrators in the open loop. The results shown are the best achievable given the topology and agent model.

5. **Conditions for string-stable platoon.** This task is fulfilled in Section 4.6, where a condition on string stability is presented. This condition can be satisfied only when the vehicles have only one integrator in the open loop. In this case predecessor following controller can always be designed.

6. **Different asymmetry.** This is done in Chapter 5. Unlike in previous statements, the results in Chapter 5 hold for a particular model only. Wave properties and some conditions on stability are shown. The controller parameters are obtained using optimization. It follows from the results in the chapter that symmetry in position and asymmetry in velocity (and possibly other states) seems to be a very good solution for control of platoons with vehicles having two integrators in the open loop. It does not require communication at all.

Bibliography

Abad Torres, J. and Roy, S. (2013). Connecting Network Graph Structure to Linear-System Zero Structure. In *American Control Conference (ACC) 2013*, 6114–6119.

Abad Torres, J. and Roy, S. (2014). Graph-theoretic characterisations of zeros for the input–output dynamics of complex network processes. *International Journal of Control*, 87(5), 940–950.

Abad Torres, J. and Roy, S. (2014). Stabilization and Destabilization of Network Processes by Sparse Remote Feedback : Graph-Theoretic Approach. In *American Control Conference (ACC), 2014*, 3984–3989. Portland, Oregon, USA.

Abad Torres, J. and Roy, S. (2015). Graph-theoretic analysis of network input-output processes: Zero structure and its implications on remote feedback control. *Automatica*, 61, 73–79.

Agaev, R. and Chebotarev, P. (2005). On the spectra of nonsymmetric Laplacian matrices. *Linear Algebra and its Applications*, 399(02), 157–168.

Alam, A., Gattami, A., and Johansson, K.H. (2010). An experimental study on the fuel reduction potential of heavy duty vehicle platooning. *13th International IEEE Conference on Intelligent Transportation Systems*, 306–311.

Alam, A., Mårtensson, J., and Johansson, K.H. (2015). Control Engineering Practice Experimental evaluation of decentralized cooperative cruise control for heavy-duty vehicle platooning. *Control Engineering Practice*, 38, 11–25.

Arcak, M. (2007). Passivity as a Design Tool for Group Coordination. *IEEE Transactions on Automatic Control*, 52(8), 1380–1390.

Ashcroft, N.W. and Mermin, N.D. (1976). *Solid State Physics*. Cengage Learning.

Bamieh, B., Paganini, F., and Dahleh, M. (2002). Distributed control of spatially invariant systems. *IEEE Transactions on Automatic Control*, 47(7), 1091–1107.

Bamieh, B. (2014). Complexity and Performance in Large-Scale and Distributed Systems Networked / Cooperative / Distributed Control. In *European Control Conference (ECC) - plenary talk*, June. Strasbourgh. Available at http://www.ecc14.eu/plenary-talks.html.

Bamieh, B., Jovanović, M.R., Mitra, P., and Patterson, S. (2012). Coherence in Large-Scale Networks: Dimension-Dependent Limitations of Local Feedback. *IEEE Transactions on Automatic Control*, 57(9), 2235–2249.

Barooah, P. and Hespanha, J.P. (2005). Error Amplification and Disturbance Propagation in Vehicle Strings with Decentralized Linear Control. In *Proceedings of the 44th IEEE Conference on Decision and Control*, 4964–4969. IEEE.

Barooah, P., Mehta, P.G., and Hespanha, J.P. (2009). Mistuning-Based Control Design to Improve Closed-Loop Stability Margin of Vehicular Platoons. *IEEE Transactions on Automatic Control*, 54(9), 2100–2113.

Bergenhem, C., Pettersson, H., Coelingh, E., Englund, C., Shladover, S., and Tsugawa, S. (2012). Overview of platooning systems. In *19th ITS World Congress*.

Biggs, N. (1974). *Algebraic graph theory*. Cambridge University Press, cambridge edition.

Briegel, B., Zelazo, D., Burger, M., and Allgower, F. (2011). On the zeros of consensus networks. In *IEEE Conference on Decision and Control and European Control Conference*, 1890–1895. IEEE.

Cantos, C.E. and Veerman, J.J.P. (2014). Transients in the Synchronization of Oscillator Arrays. *Arxiv preprint*, arXiv:1308, 1–11.

Cantos, C.E., Veerman, J.J.P., and Hammond, D.K. (2014). Signal Velocity in Oscillator Arrays. *Arxiv preprint*, arXiv:1307, 1–18.

Chan, E., Gilhead, P., Jelínek, P., Krejčí, P., and Robinson, T. (2012). Cooperative control of SARTRE automated platoon vehicles. *Proceedings of the 19th ITS World Conference*, 1–9.

Chang, K.S., Li, W., Shaikhbahai, A., Assaderaghi, F., and Varaiya, P. (1991a). A preliminary implementation for vehicle platoon control system. In *American Control Conference*, 3078–3083. Boston.

Chang, K., Li, W., Devlin, P., Shaikhbahai, a., Varaiya, P., Hedrick, J., McMahon, D., Narendran, V., Swaroop, D., and Olds, J. (1991b). Experimentation with a vehicle platoon control system. *Vehicle Navigation and Information Systems Conference, 1991*, 2, 1117–1125.

Chapman, A. and Mesbahi, M. (2013). On strong structural controllability of networked systems: A constrained matching approach. In *2013 American Control Conference*, 6126–6131. IEEE, Washington DC.

Chebotarev, P. and Agaev, R. (2002). Forest matrices around the Laplacian matrix. *Linear Algebra and its Applications*, 356(1-3), 253–274.

Chebotarev, P. and Agaev, R. (2014). The Forest Consensus Theorem. *IEEE Transactions on Automatic Control*, 59(9), 2475–2479.

Chopra, N. and Spong, M. (2006). Passivity-Based Control of Multi-Agent Systems. In S. Kawamura and M. Svinin (eds.), *Advances in robot control*, 107–134. Springer Berlin Heidelberg, Berlin, Heidelberg.

Clark, A., Alomair, B., Bushnell, L., and Poovendran, R. (2014). Input selection for performance and controllability of structured linear descriptor systems. *arXiv preprint*, 1–28.

Coelingh, E. and Solyom, S. (2012). All aboard the robotic road train. *IEEE Spectrum*, 49(11), 34–39.

da Fonseca, C. and Veerman, J. (2009). On the spectra of certain directed paths. *Applied Mathematics Letters*, 22(9), 1351–1355.

D'Andrea, R. and Dullerud, G. (2003). Distributed control design for spatially interconnected systems. *IEEE Transactions on Automatic Control*, 48(9), 1478–1495.

Darbha, S. (2003). On the synthesis of controllers for continuous time LTI systems that achieve a non-negative impulse response. *Automatica*, 39(1), 159–165.

Dorf, R.C. and Bishop, R.H. (2008). *Modern Control Systems*. Pearson Education, Upper Saddle River.

ETPC (2016). European Truck Platooning Challenge. Available at https://www.eutruckplatooning.com/home/default.aspx.

Eyre, J., Yanakiev, D., and Kanellakopoulos, I. (1998). A Simplified Framework for String Stability Analysis of Automated Vehicles. *Vehicle System Dynamics*, 30(5), 375–405.

Fallat, S.M. and Johnson, C.R. (2011). *Totally Nonnegative Matrices*. Princeton University Press.

Fax, J. and Murray, R. (2004). Information Flow and Cooperative Control of Vehicle Formations. *IEEE Transactions on Automatic Control*, 49(9), 1465–1476.

Fiedler, M. (1973). Algebraic Conectivity of Graphs. *Czechoslovak Mathematical Journal*, 23(2), 298–305.

Fitch, K. and Leonard, N.E. (2013). Information centrality and optimal leader selection in noisy networks. In *52nd IEEE Conference on Decision and Control*, 7510–7515. IEEE.

Fradkov, A. and Junussov, I. (2011). Synchronization of linear object networks by output feedback. In *IEEE Conference on Decision and Control and European Control Conference*, 8188–8192. IEEE, Orlando, Florida, USA.

Godsil, C. and Royle, G. (2001). *Algebraic graph theory*. Springer Verlag New York.

Hao, H. and Barooah, P. (2012). On Achieving Size-Independent Stability Margin of Vehicular Lattice Formations With Distributed Control. *IEEE Transactions on Automatic Control*, 57(10), 2688–2694.

Hao, H. and Barooah, P. (2013). Stability and robustness of large platoons of vehicles with double-integrator models and nearest neighbor interaction. *International Journal of Robust and Nonlinear Control*, 23(18), 2097–2122.

Hao, H., Barooah, P., and Mehta, P.G. (2011). Stability Margin Scaling Laws for Distributed Formation Control as a Function of Network Structure. *IEEE Transactions on Automatic Control*, 56(4), 923–929.

Hao, H., Yin, H., and Kan, Z. (2012). On the robustness of large 1-D network of double integrator agents. In *2012 American Control Conference (ACC)*, 6059–6064. IEEE.

Hedrick, J., Tomizuka, M., and Varaiya, P. (1994). Control issues in automated highway systems. *IEEE Control Systems*, 14(6), 21–32.

Hengster-Movric, K. and Lewis, F.L. (2014). Cooperative Optimal Control for Multi-Agent Systems on Directed Graph Topologies. *IEEE Transactions on Automatic Control*, 59(3), 769–774.

Hengster-Movric, K., Lewis, F.L., and Sebek, M. (2015a). Distributed static output-feedback control for state synchronization in networks of identical LTI systems. *Automatica*, 53, 282–290.

Hengster-Movric, K., Lewis, F.L., Šebek, M., and Vyhlídal, T. (2015b). Cooperative synchronization control for agents with control delays: A synchronizing region approach. *Journal of the Franklin Institute*, 352(5), 2002–2028.

Hengster-Movric, K., You, K., Lewis, F., and Xie, L. (2012). Synchronization of discrete-time multi-agent systems on graphs using Riccati design. *Automatica*, 49(2), 414–423.

Herbrych, J., Chazirakis, a.G., Christakis, N., and Veerman, J.J.P. (2015). Dynamics of locally coupled oscillators with next-nearest-neighbor interaction. *arXiv preprint 1506.07381*.

Herman, I. (2016a). Optimal distributed control with application to asymmetric vehicular platoons. In *submitted to 55th IEEE Conference on Decision and Control*, 1, 1–6.

Herman, I. (2016b). Scaling of H-infinity Norm in Symmetric Bidirectional Platoons. In *submitted to 6th IFAC Workshop on Distributed Estimation and Control in Networked Systems (NecSys)*, 1–6. Tokyo, Japan.

Herman, I., Knorn, S., and Ahlén, A. (2016a). Disturbance scaling in bidirectional vehicle platoons with different asymmetry in position and velocity coupling. *submitted to Automatica, arXiv preprint 1604.00868*.

Herman, I., Martinec, D., Cantos, C., and Veerman, J.J.P. (2015a). Code for simulations. Available at: https://www.mathworks.com/matlabcentral/fileexchange/52493.

Herman, I., Martinec, D., Hurák, Z., and Šebek, M. (2013). PDdE-based analysis of vehicular platoons with spatio-temporal decoupling. In *4th IFAC Workshop on Distributed Estimation and Control in Networked Systems (NecSys)*, 144–151. Koblenz, Germany.

Herman, I., Martinec, D., Hurak, Z., and Sebek, M. (2014a). Harmonic instability of asymmetric bidirectional control of a vehicular platoon. In *2014 American Control Conference*, 5396–5401. IEEE, Portland, Oregon, USA.

Herman, I., Martinec, D., Hurak, Z., and Sebek, M. (2015b). Nonzero Bound on Fiedler Eigenvalue Causes Exponential Growth of H-Infinity Norm of Vehicular Platoon. *IEEE Transactions on Automatic Control*, 60(8), 2248–2253.

Herman, I., Martinec, D., Hurák, Z., and Sebek, M. (2016b). Scaling in bidirectional platoons with dynamic controllers and proportional asymmetry. *conditionally accepted to IEEE Transactions on Automatic Control*, PP, 1–6.

Herman, I., Martinec, D., and Sebek, M. (2014b). Zeros of Transfer Functions in Network Control with Higher-Order Dynamics. In *19th IFAC World Congress*, 9177–9182. Cape Town, South Africa.

Herman, I., Martinec, D., and Sebek, M. (2016c). Transfer functions in consensus systems with higher-order dynamics and external input. *arXiv preprint:1512.05222*, 1–13.

Herman, I., Martinec, D., and Veerman, J. (2016d). Transients of platoons with asymmetric and different Laplacians. *Systems & Control Letters*, 91, 28–35.

Herman, I., Martinec, D., Veerman, J., and Sebek, M. (2015c). Stability of a circular system with multiple asymmetric Laplacians. In *5th IFAC Workshop on Distributed Estimation and Control in Networked Systems (NecSys)*, volume 48, 162–167.

Horn, R.A. and Johnson, C.R. (1990). *Matrix analysis*. Cambridge University Press, Cambridge.

Horn, R.A. and Johnson, C.R. (1999). *Topics in Matrix Analysis*. Cambridge University Press.

Horowitz, R. and Varaiya, P. (2000). Control design of an automated highway system. *Proceedings of the IEEE*, 88(7), 913–925.

Hurák, Z. (2015). *Traveling waves and scattering in control of chains*. Habilitation. Available at: http://aa4cc.dce.fel.cvut.cz/content/traveling-waves-and-scattering-control-chains.

Jia, D. and Ngoduy, D. (2016). Platoon based cooperative driving model with consideration of realistic inter-vehicle communication q. *Transportation Research Part C*, 68, 245–264.

Jovanovic, M.R. (2010). On the optimality of localised distributed controllers. *International Journal of Systems, Control and Communications*, 2(1/2/3), 82.

Jovanović, M.R., Fowler, J.M., Bamieh, B., and D'Andrea, R. (2008). On the peaking phenomenon in the control of vehicular platoons. *Systems & Control Letters*, 57(7), 528–537.

Junussov, I. (2014). Static consensus in passifiable linear networks. *arXiv preprint 1402.7274*, 0034, 1–13.

Knorn, S., Donaire, A., Agüero, J.C., and Middleton, R.H. (2014). Passivity-based control for multi-vehicle systems subject to string constraints. *Automatica*, 50(12), 3224–3230.

Knorn, S., Donaire, A., Agüero, J.C., and Middleton, R.H. (2015). Scalability of bidirectional vehicle strings with static and dynamic measurement errors. *Automatica*, 62, 208–212.

Kotte, J., Huang, Q., and Zlocki, A. (2012). Impact of platooning on traffic efficiency. *Proceedings of the 19th ITS World Congress*, EU(00273), 1–8.

Lewis, F.L. and Syrmos, V.L. (1995). *Optimal control*. Wiley, 2nd edition.

Lewis, F.L., Zhang, H., Hengster-Movric, K., and Das, A. (2014). *Cooperative Control of Multi-Agent Systems*. Springer.

Li, Z., Ren, W., Liu, X., and Fu, M. (2013a). Consensus of Multi-Agent Systems With General Linear and Lipschitz Nonlinear Dynamics Using Distributed Adaptive Protocols. *IEEE Transactions on Automatic Control*, 58(7), 1786–1791.

Li, Z., Duan, Z., and Chen, G. (2011). On Hinf and H2 performance regions of multi-agent systems. *Automatica*, 47(4), 797–803.

Li, Z., Duan, Z., Chen, G., and Huang, L. (2010). Consensus of Multiagent Systems and Synchronization of Complex Networks: A Unified Viewpoint. *IEEE Transactions on Circuits and Systems I: Regular Papers*, 57(1), 213–224.

Li, Z., Duan, Z., Xie, L., and Liu, X. (2012). Distributed robust control of linear multi-agent systems with parameter uncertainties. *International Journal of Control*, 85(8), 1039–1050.

Li, Z., Ren, W., Liu, X., and Xie, L. (2013b). Distributed consensus of linear multi-agent systems with adaptive dynamic protocols. *Automatica*, 49(7), 1986–1995.

Li, Z., Wen, G., Duan, Z., and Ren, W. (2015). Designing Fully Distributed Consensus Protocols for Linear Multi-Agent Systems With Directed Graphs. *IEEE Transactions on Automatic Control*, 60(4), 1152–1157.

Lin, F., Fardad, M., and Jovanovic, M.R. (2012a). Performance of leader-follower networks in directed trees and lattices. In *2012 IEEE 51st IEEE Conference on Decision and Control (CDC)*, 734–739. IEEE, Maui, Hawaii, USA.

Lin, F., Fardad, M., Jovanović, M.R., and Jovanovic, M.R. (2012b). Optimal control of vehicular formations with nearest neighbor interactions. *IEEE Transactions on Automatic Control*, 57(9), 2203–2218.

Lovisari, E., Garin, F., and Zampieri, S. (2013). Resistance-based performance analysis of the consensus algorithm over geometric graphs. *SIAM Journal on Control and Optimization*, 51(5), 3918–3945.

Lunze, J. (2012). Synchronization of Heterogeneous Agents. *IEEE Transactions on Automatic Control*, 57(11), 2885–2890.

Martinec, D., Herman, I., Hurák, Z., and Šebek, M. (2014). Wave-absorbing vehicular platoon controller. *European Journal of Control*, 20(5), 237–248.

Martinec, D., Herman, I., and Šebek, M. (2015). Travelling waves in a multi-agent system with general graph topology. In *5th IFAC Workshop on Distributed Estimation and Control in Networked Systems (NecSys)*, volume 48, 82–87. IFAC.

Martinec, D., Herman, I., and Šebek, M. (2016a). A travelling wave approach to a multi-agent system with a path-graph topology. *arXiv preprint 1410.0474*.

Martinec, D., Herman, I., and Šebek, M. (2016b). On the necessity of symmetric positional coupling for string stability. *ArXiv preprint 1603.06970*, 1–9.

Massioni, P. and Verhaegen, M. (2009). Distributed Control for Identical Dynamically Coupled Systems: A Decomposition Approach. *IEEE Transactions on Automatic Control*, 54(1), 124–135.

Melnikov, Y.A. (2011). Green's Functions and Infinite Products: Bridging the Divide. 17–42. Birkhäuser Boston, Boston.

Mesbahi, M. and Egerstedt, M. (2010). *Graph Theoretic Methods in Multiagent Networks*. Princeton University Press, princeton edition.

Middleton, R.H. and Braslavsky, J.H. (2010). String Instability in Classes of Linear Time Invariant Formation Control With Limited Communication Range. *Automatic Control, IEEE Transactions on*, 55(7), 1519–1530.

Milanés, V., Shladover, S.E., Spring, J., Nowakowski, C., Kawazoe, H., and Nakamura, M. (2014). Cooperative adaptive cruise control in real traffic situations. *Inteligent Transportation Systems, IEEE Transactions on*, 15(1), 296–305.

Naus, G., Vugts, R., Ploeg, J., van de Molengraft, R., and Steinbuch, M. (2010a). Cooperative adaptive cruise control, design and experiments. In *American Control Conference 2010*, 1, 6145–6150.

Naus, G.J.L., Vugts, R.P.A., Ploeg, J., van de Molengraft, M.R.J.G., and Steinbuch, M. (2010b). String-Stable CACC Design and Experimental Validation: A Frequency-Domain Approach. *IEEE Transactions on Vehicular Technology*, 59(9), 115.

O'Connor, W.J. (2007). Wave-Based Analysis and Control of Lump-Modeled Flexible Robots. *IEEE Transactions on Robotics*, 23(2), 342–352.

O'Connor, W.J. (2011). Wave-like modelling of cascaded, lumped, flexible systems with an arbitrarily moving boundary. *Journal of Sound and Vibration*, 330(13), 3070–3083.

O'Connor, W.J. and McKeown, D.J. (2008). A new approach to modal analysis of uniform chain systems. *Journal of Sound and Vibration*, 311(3-5), 623–632.

Olfati-Saber, R., Fax, J.A., and Murray, R.M. (2007). Consensus and Cooperation in Networked Multi-Agent Systems. *Proceedings of the IEEE*, 95(1), 215–233.

Öncü, S., van de Wouw, N., Heemels, W.P.M.H., and Nijmeijer, H. (2012). String Stability of Interconnected Vehicles Under Communication Constraints. In *IEEE Conference on Decision and Control 2012*, 2459–2464.

Özban, A.Y. (2006). A new refined form of Jordan's inequality and its applications. *Applied Mathematics Letters*, 19(2), 155–160.

Parlangeli, G. and Notarstefano, G. (2012). On the Reachability and Observability of Path and Cycle Graphs. *IEEE Transactions on Automatic Control*, 57(3), 743–748.

Patterson, S. and Bamieh, B. (2014). Consensus and Coherence in Fractal Networks. *IEEE Transactions on Control of Network Systems*, 1(4), 338–348.

Peters, A., Middleton, R.H., and Mason, O. (2013). Leader tracking in homogeneous vehicle platoons with broadcast delays. *Automatica*, (1992).

Pirani, M. and Sundaram, S. (2014). Spectral properties of the grounded Laplacian matrix with applications to consensus in the presence of stubborn agents. In *2014 American Control Conference*, 2160–2165. IEEE, Portland, Oregon, USA.

Pirani, M. and Sundaram, S. (2015). On the Smallest Eigenvalue of Grounded Laplacian Matrices. *IEEE Transactions on Automatic Control*, 61(2), 509–514.

Ploeg, J., Semsar-Kazerooni, E., Lijster, G., van de Wouw, N., and Nijmeijer, H. (2015). Graceful degradation of cooperative adaptive cruise control. *IEEE Transactions on Intelligent Transportation Systems*, 16(1), 488–497.

Ploeg, J., van de Wouw, N., and Nijmeijer, H. (2014). Lp String Stability of Cascaded Systems: Application to Vehicle Platooning. *IEEE Transactions on Control Systems Technology*, 22(2), 786–793.

Qu, Z. (2009). *Cooperative Control of Dynamical Systems: Applications to Autonomous Vehicles*. Springer-Verlag London, London.

Rajamani, R. and Shladover, S. (2001). An experimental comparative study of autonomous and co-operative vehicle-follower control systems. *Transportation Research Part C: Emerging Technologies*, 9(1), 15–31.

Rajamani, R., Tan, H.S., Law, B.K., and Zhang, W.B. (2000). Demonstration of integrated longitudinal and lateral control for the operation of automated vehicles in platoons. *IEEE Transactions on Control Systems Technology*, 8(4), 695–708.

Ren, W. and Beard, R. (2008). *Distributed Consensus in Multi-vehicle Cooperative Control*. Springer-Verlag London, 1st edition.

Sebek, M. and Hurak, Z. (2011). 2-D Polynomial Approach to Control of Leader Following Vehicular Platoons. In *Preprints of the 18th IFAC World Congress*, 6017–6022.

Seiler, P., Pant, A., and Hedrick, K. (2004). Disturbance Propagation in Vehicle Strings. *IEEE Transactions on Automatic Control*, 49(10), 1835–1841.

Shi, G., Sou, K.C., Sandberg, H., and Johansson, K.H. (2014). A graph-theoretic approach on optimizing informed-node selection in multi-agent tracking control. *Physica D: Nonlinear Phenomena*, 267, 104–111.

Sirota, L. and Halevi, Y. (2014). Wave Based Vibration Control of Membranes. In *American Control Conference (ACC), 2014*, volume 2729, 2729–2734. Portland, Oregon, USA.

Sirota, L. and Halevi, Y. (2015). Fractional order control of the two-dimensional wave equation. *Automatica*, 59, 152–163.

Swaroop, D. and Hedrick, J. (1996). String stability of interconnected systems. *Automatic Control, IEEE Transactions on*, 41(3), 349–357.

Tangerman, F.M., Veerman, J.J.P., and Stosic, B.D. (2012). Asymmetric decentralized flocks. *IEEE Transactions on Automatic Control*, 57(11), 2844–2853.

Torres, J.A. and Roy, S. (2015). A two-layer transformation for characterizing the zeros of a network input-output dynamics. In *2015 54th IEEE Conference on Decision and Control (CDC)*, 902–907. IEEE, Osaka, Japan.

Treiber, M. and Kesting, A. (2013). *Traffic Flow Dynamics*. Springer-Verlag Berlin Heidelberg.

Trentelman, H.L., Takaba, K., and Monshizadeh, N. (2013). Robust Synchronization of Uncertain Linear Multi-Agent Systems. *IEEE Transactions on Automatic Control*, 58(6), 1511–1523.

Varaiya, P. (1993). Smart cars on smart roads. Problems of control. *IEEE Transactions on Automatic Control*, 38(2), 195–207.

Veerman, J.J.P., Stošić, B., and Olvera, A. (2007). Spatial instabilities and size limitations of flocks. *Networks and Heterogeneous Media*, 2(4), 647–660.

Wieland, P., Sepulchre, R., and Allgöwer, F. (2011). An internal model principle is necessary and sufficient for linear output synchronization. *Automatica*, 47(5), 1068–1074.

Wu, C.W. and Chua, L.O. (1995). Application of Kronecker products to the analysis of systems with uniform linear coupling. *IEEE Transactions on Circuits and Systems I: Fundamental Theory and Applications*, 42(10), 775–778.

Yadlapalli, S.K., Darbha, S., and Rajagopal, K.R. (2006). Information flow and its relation to the stability of the motion of vehicles in a rigid formation. *Automatic Control, IEEE Transactions on*, 51(8), 1315–1319.

Zamani, M., Helmke, U., and Anderson, B.D. (2015). Zeros of networked systems with time-invariant interconnections. *Automatica*, 61, 97–105.

Zelazo, D. and Mesbahi, M. (2011). Edge Agreement: Graph-Theoretic Performance Bounds and Passivity Analysis. *IEEE Transactions on Automatic Control*, 56(3), 544–555.

Zhang, H., Lewis, F.L., and Das, A. (2011). Optimal Design for Synchronization of Cooperative Systems: State Feedback, Observer and Output Feedback. *IEEE Transactions on Automatic Control*, 56(8), 1948–1952.

Zhang, H., Lewis, F.L., and Qu, Z. (2012). Lyapunov, Adaptive, and Optimal Design Techniques for Cooperative Systems on Directed Communication Graphs. *IEEE Transactions on Industrial Electronics*, 59(7), 3026–3041.

Zhang, S., Cao, M., and Camlibel, M.K. (2014). Upper and lower bounds for controllable subspaces of networks of diffusively coupled agents. *IEEE Transactions on Automatic Control*, 59(3), 745–750.

Zhou, K., Doyle, J.C., and Glover, K. (1996). *Robust and Optimal Control*. Prentice Hall.

Author's publications

Related to the thesis

Published journal papers

[1] I. Herman, D. Martinec, Z. Hurák, and M. Sebek, "Nonzero Bound on Fiedler Eigenvalue Causes Exponential Growth of H-Infinity Norm of Vehicular Platoon,"*IEEE Transactions on Automatic Control*, vol. 60, no. 8, pp. 2248–2253, Aug. 2015.
co-authorship 50 %

[2] I. Herman, D. Martinec, and J. J. P. Veerman, "Transients of platoons with asymmetric and different Laplacians," *Systems & Control Letters*, vol. 91, pp. 28–35, May 2016.
co-authorship 33 %

Conditionally accepted journal papers

[3] I. Herman, D. Martinec, Z. Hurák, and M. Sebek, "Scaling in bidirectional platoons with dynamic controllers and proportional asymmetry," *IEEE Transactions on Automatic Control*, pp. 1–6, arXiv preprint 1410.3944, 2016.
co-authorship 50 %

Submitted journal papers

[4] I. Herman, S. Knorn, and A. Ahlén, "Disturbance scaling in bidirectional vehicle platoons with different asymmetry in position and velocity coupling," submitted to *Automatica*, arXiv preprint 1604.00868, pp. 1–13, 2016.
co-authorship 33 %

[5] I. Herman, D. Martinec, and M. Sebek, "Transfer functions in consensus sys-

tems with higher-order dynamics and external input," submitted to *European Journal of Control*, pp. 1–13, arXiv preprint 1512.05222, 2016.
co-authorship 70 %

Published conference papers

[6] I. Herman, D. Martinec, Z. Hurák, and M. Sebek, "Harmonic instability of asymmetric bidirectional control of a vehicular platoon," in *American Control Conference (2014)*, 2014, pp. 5396–5401.
co-authorship 25 %

[7] I. Herman, D. Martinec, and M. Sebek, "Zeros of Transfer Functions in Network Control with Higher-Order Dynamics," in *19th IFAC World Congress 2014*, 2014, pp. 9177–9182.
co-authorship 33 %

[8] I. Herman, D. Martinec, J. J. P. Veerman, and M. Sebek, "Stability of a Circular System with Multiple Asymmetric Laplacians," in *5th IFAC Workshop on Estimation and Control of Networked Systems (NecSys)*, 2015, pp. 161–167.
co-authorship 25 %

[9] I. Herman, D. Martinec, Z. Hurák, and M. Sebek, "PDdE-based analysis of vehicular platoons with spatio-temporal decoupling," in *4th IFAC Workshop on Distributed Estimation and Control in Networked Systems (NecSys)*, 2013, pp. 144–151.
co-authorship 25 %

[10] I. Herman, D. Martinec, Z. Hurák, and M. Sebek, "Equalization of intervehicular distances in platoons on a circular track," in *Process Control Conference (PC)*, 2013, pp. 47–52.
co-authorship 25 %

Submitted conference papers

[11] I. Herman, "Optimal distributed control with application to asymmetric vehicular platoons," in *IEEE Conference on Decision and Control(2016)*, 2016, pp. 1–6.
co-authorship 100 %

[12] I. Herman, "Scaling of H-infinity Norm in Symmetric Bidirectional Platoons," in *6th IFAC Workshop on Distributed Estimation and Control in Networked Systems (NecSys)*, 2016, pp. 1–6.
co-authorship 100 %

Not related to the thesis

Published journal papers

[13] D. Martinec, I. Herman, Z. Hurák, and M. Sebek, "Wave-absorbing vehicular platoon controller," *European Journal of Control*, vol. 20, no. 5, pp. 237–248, Sep. 2014.
co-authorship 30 %

[14] P. Vaclavek, P. Blaha, and I. Herman, "AC Drives Observability Analysis," *IEEE Transactions on Industrial Electronics*, vol. 60, no. 8, pp. 3047–3059, Aug. 2013.
co-authorship 33 %

Conditionally accepted journal papers

[15] D. Martinec, I. Herman, and M. Sebek, "On the necessity of symmetric positional coupling for string stability," *IEEE Transactions on Control of Network Systems*, pp. 1–9, arXiv preprint 1603.06970, Mar. 2016.
co-authorship 30 %

Submitted journal papers

[16] D. Martinec, I. Herman, and M. Sebek, "A travelling wave approach to a multi-agent system with a path-graph topology," submitted to *Systems & Control Letters*, pp. 1–9, arXiv preprint 1410.0474, 2016.
co-authorship 30 %

Published conference papers

[17] I. Herman and P. Vaclavek, "Load torque and moment of inertia observability analysis for alternating current drive sensorless control," in *IECON 2012 - 38th Annual Conference on IEEE Industrial Electronics Society*, 2012, pp. 1864–1869.
co-authorship 50 %

[18] D. Martinec, I. Herman, Z. Hurák and M. Sebek, "Refinement of a bidirectional platooning controller by wave absorption at the leader," in *European Control Conference (ECC)*, 2014, pp. 2845–2850.
co-authorship 25 %

[19] D. Martinec, M. Hromčík, I. Herman, T. Vyhlídal, and M. Sebek, "On zero-

vibration signal shapers and a wave-absorbing controller for a chain of multi-agent dynamical systems," in *European Control Conference (ECC)*, 2015, no. 13, pp. 1025–1030.
co-authorship 20 %

[20] Dan, Martinec, I. Herman, M. Sebek, "Two-Sided Wave-Absorbing Control of a Heterogenous Vehicular Platoon," in *19th IFAC World congress 2014*, 2014, no. 1968, pp. 8091–8096.
co-authorship 33 %

[21] D. Martinec, I. Herman, and M. Sebek, "Travelling waves in a multi-agent system with general graph topology," in *5th IFAC Workshop on Distributed Estimation and Control in Networked Systems (NecSys)*, 2015, vol. 48, no. 22, pp. 82–87.
co-authorship 33 %